Elucidating the intestinal response to ischemia-reperfusion

Elucidating the intestinal response to ischemia-reperfusion

From molecular profiling in humans, to disease modeling in organoids

The work described in this thesis was performed at the Department of Surgery, within the framework of NUTRIM School of Nutrition and Translational Research in Metabolism.

ISBN: 978-94-6423-613-2

Cover design: Wendy Schoneveld | www.wenzid.nl
Lay-out: Mirjam Kip
Printed by: Ridderprint | www.ridderprint.nl

Elucidating the intestinal response to ischemia-reperfusion

From molecular profiling in humans, to disease modeling in organoids

PROEFSCHRIFT

Ter verkrijging van de graad van doctor aan de Universiteit Maastricht,
op gezag van de Rector Magnificus, Prof. dr. Rianne M. Letschert
volgens het besluit van het College van Decanen,
in het openbaar te verdedigen
op donderdag 10 februari 2022 om 13.00 uur

door

Anna Maria Kip

geboren op 20 december 1989
te Limbricht

Promotor

Prof. dr. S.W.M. Olde Damink

Copromotor

Dr. K. Lenaerts

Beoordelingscommissie

Prof. dr. D.M.A.E. Jonkers (voorzitter)
Prof. dr. T. Cramer (RWTH University Hospital Aachen, Germany)
Prof. dr. C. Libert (VIB, Universiteit Gent, Belgium)
Prof. dr. E. Mariman
Prof. dr. P.J. Peters

CONTENTS

CHAPTER 1

General introduction

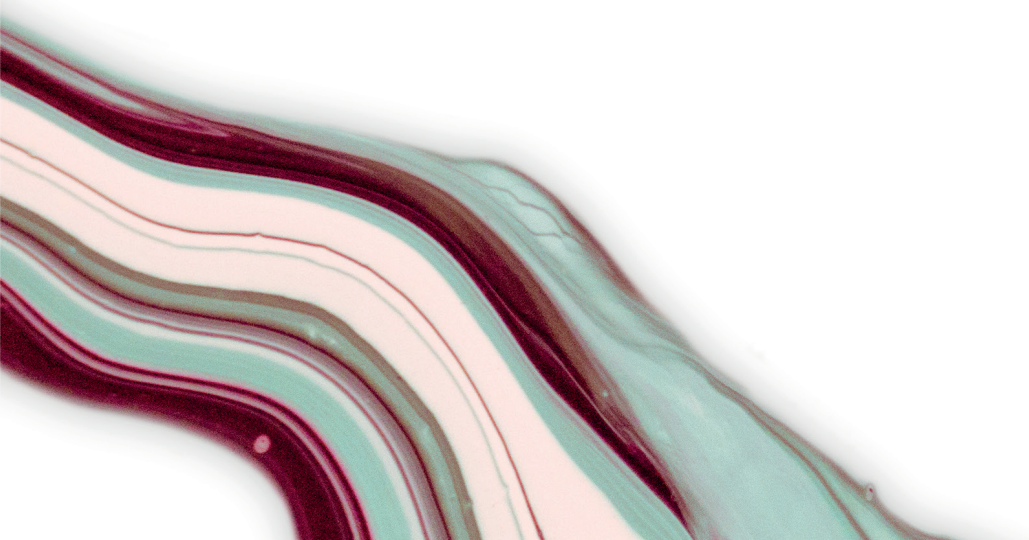

GENERAL INTRODUCTION

Intestinal ischemia-reperfusion

Intestinal ischemia-reperfusion (IR) is a potentially life-threatening phenomenon that occurs in a variety of physiological and pathological conditions. The intestinal mucosa experiences profound fluctuations in the blood flow as part of normal physiology, e.g. intestinal perfusion is enhanced following meal ingestion and is considerably reduced during physical exercise[1,2]. IR injury is the result of severe impairment of intestinal perfusion due to occlusion or severe hypoperfusion of the mesenteric vessels. Occlusive causes include mesenteric venous thrombosis or arterial embolism. Systemic hypovolemia, for example as a result of major surgery, trauma, hemorrhagic shock or sepsis, leads to redistribution of blood to the vital organs, e.g. heart and brain, and thus hypoperfusion of the intestine[3-5]. In addition, it is well appreciated that intestinal ischemia occurs secondary to inflammation, which plays a crucial role in the pathophysiology of inflammatory bowel disease[1,6]. Finally, IR injury is an inevitable consequence of intestinal transplantation.

Acute mesenteric ischemia is a serious condition, which can progress towards bowel necrosis and a severe inflammatory response. In the Netherlands, the incidence of acute mesenteric ischemia is estimated at 13 per 100,000 people per year[7]. With its high overall mortality rates of about 60 to 80%[3-5], this condition accounts for 1400 to 1800 deaths per year. The high mortality could partly be attributed to a delay in diagnosis. The difficulty in recognizing acute mesenteric ischemia at an early stage is due to its non-specific clinical presentation and lack of accurate diagnostic markers. In addition, the lack of effective therapeutic options contributes to continued high morbidity and mortality rates of intestinal ischemia[8-10]. Rapid restoration of perfusion to the ischemic intestine is crucial, yet associated with an exacerbation of tissue injury and an inflammatory response. Therapeutic strategies aimed at attenuation of reperfusion injury are needed to improve patient outcome.

In the past decades, several therapeutic strategies have been proposed based on their protective effects against IR injury in animal models, including ischemic preconditioning, antioxidants and anticomplement therapy[11]. However, there is no clinical evidence of beneficial effects of such therapies and hence these have not been implemented in clinical practice[3,4,12]. Importantly, the development of human experimental IR models has substantially advanced our understanding of the pathophysiology of IR in man in the last decade. The human small intestinal IR model is one of the models used in this thesis. Furthermore, human small intestinal organoids are used to investigate underlying mechanisms of IR-induced epithelial injury and test potential therapies.

The cascade of events contributing to IR injury

The cascade of events that contribute to ischemia and reperfusion injury has been investigated in animal and *in vitro* models of IR injury in different organs and is depicted in **Figure 1** (reviewed in[13]). Low oxygen levels during ischemia force cells to switch to anaerobic metabolism, which is less efficient and produces lactic acid, resulting in ATP depletion and a reduced intracellular pH. As a consequence, alterations in ion exchange – H^+/Na^+ exchange to buffer accumulation of H^+ ions, inactivation of ATPases e.g. Na^{+}/K^+ ATPase, reduction of active Ca^{2+} efflux, and limited Ca^{2+} re-uptake

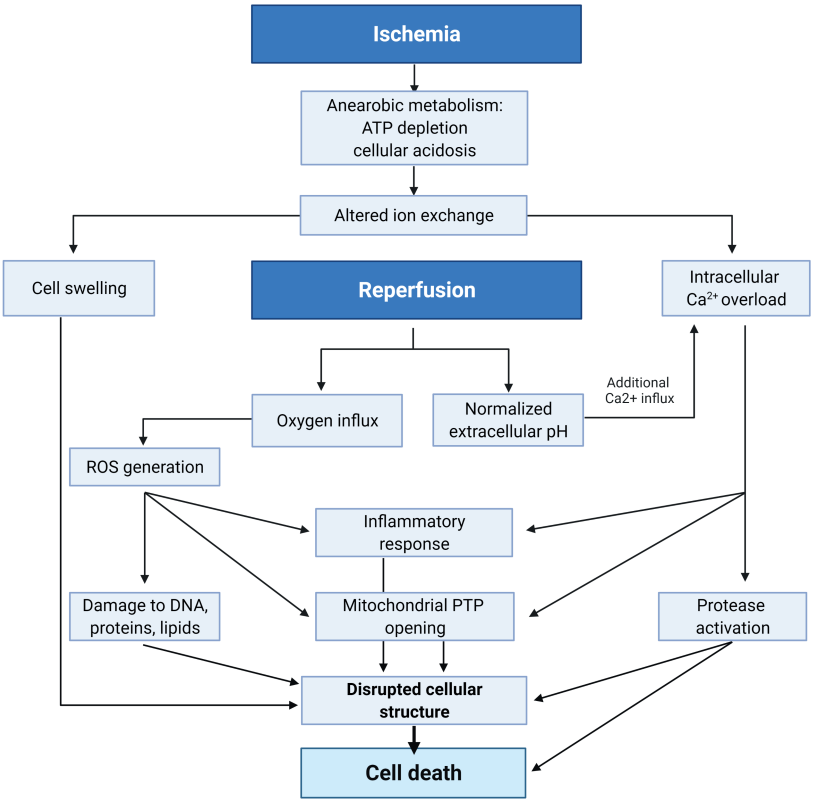

Figure 1. The cascade of events that contribute to ischemia and reperfusion injury. *During ischemia, cells are forced to switch to anaerobic metabolism, which results in ATP depletion and cellular acidosis. Subsequent alterations in ion exchange lead to intracellular Ca^{2+} overload and cell swelling. The oxygen influx upon reperfusion induces the production of ROS, which damages DNA, proteins and lipids, triggers opening of the mitochondrial permeability transition pore (mPTP) and activates an inflammatory response. Additionally, intracellular Ca^{2+} massively increases during reperfusion, which drives further opening of the mPTP, pathological activation of Ca^{2+}-dependent proteases and inflammatory signaling. All these events may eventually contribute to cell death following IR. Modified from Kalogeris et al.[13]. Figure created with BioRender.com*

into the ER – result in an intracellular calcium overload[13,14]. Simultaneously, a disrupted mitochondrial architecture and reduced mitochondrial membrane potential further impairs ATP production. In addition, some events do not directly contribute to ischemic injury, but exacerbate damage upon reperfusion, for example the accumulation of xanthine oxidase (XO), an enzyme that generates reactive oxygen species (ROS) and requires oxygen to be activated[15].

The reintroduction of oxygen upon reperfusion initiates a complex cascade of events. While aerobic ATP generation and extracellular pH are restored, oxygen influx rapidly results in XO-driven ROS generation[15]. Elevated levels of ROS quickly damage lipids, proteins and DNA, induce opening of the mitochondrial permeability transition pore (mPTP), and activate inflammatory responses that exacerbate injury[14]. In addition, as a consequence of restored extracellular pH, the influx of calcium is stimulated which means the intracellular Ca^{2+} levels are greatly enhanced during reperfusion. The

massive calcium overload drives several events that contribute to cell death. Uptake of Ca^{2+} into the mitochondrial matrix can trigger further opening of the mPTP[16]. Also, elevated Ca^{2+} levels activate pathological activation of Ca^{2+}-dependent proteases[17], resulting in the degradation of intracellular proteins. Finally, via the generation of danger signals that bind inflammasomes, Ca^{2+} overload indirectly mediates the production of inflammatory cytokines[14]. All aforementioned events can contribute to cell death following IR in general. Moreover, in the colonized intestine, the subsequent disruption of the epithelial barrier has serious consequences that exacerbate inflammation and damage.

The intestinal epithelial barrier

Organization of the intestinal epithelium

The intestinal epithelium has two main functions: absorption of nutrients and protection against the external environment. Two important features that protect the intestinal epithelium from continuous external hazards are the crypt-villus structure and the continuous regeneration of the epithelium[18]. The intestinal epithelium is organized into crypt-villus structures. The villi are fingerlike protrusions into the intestinal lumen that markedly enlarge the surface area and improve the absorptive capacity of the epithelium. The villus epithelium consists of mature cells with a short lifespan of 3-5 days[19], which minimizes exposure to environmental threats that could lead to a breach in the epithelial lining. Villi are surrounded by multiple invaginations, the crypts, which are better protected against the harmful environment. Stem cells, located in the bottom of the crypt, give rise to transit amplifying (TA) cells which rapidly proliferate and finally differentiate into mature epithelial cells. The epithelial layer is composed of different types of specialized cells, which can be divided in the absorptive and secretory lineage. The absorptive enterocytes are the most abundant cell type (up to 80%); the secretory lineage comprises Paneth cells, goblet cells, enteroendocrine cells and tuft cells (**Figure 2**). While Paneth cells move downward and reside in the crypt base, where they alternate with stem cells, the other mature cell types emerge from the crypt and migrate towards the villus tip where they undergo apoptosis and are shed into the lumen[20].

Epithelial barrier function

The epithelial cells are connected by tight junctions, adherence junctions and desmosomes to form a tight physical barrier, that is selectively permeable to allow absorption of nutrients, electrolytes and water, yet at the same time prevents the entry of harmful intraluminal toxins, antigens and microorganisms[21]. The physical barrier and several biochemical and immunological players cooperate to establish a multi-layered defense system to maintain homeostasis at the luminal interface (**Figure 2**).

The first line of defense is the mucus layer covering the epithelium. The mucus layer provides a physical barrier, spatially segregating the gut microbiota and their toxins from the epithelial lining. In addition, antimicrobial peptides in the mucus layer provide a biochemical barrier[22]. To this end, two types of specialized epithelial cells play an important role. Goblet cells are responsible for the production and secretion of mucins that form this protective mucus layer[23,24]. Paneth cells secrete a variety of antimicrobial peptides, including lysozyme and α-defensin, which not only protect the

stem cells in the crypt, but also mix with mucus to provide protection against bacterial invasion along the whole epithelium[25-27]. The cellular layer, sealed with adhesive complexes, forms another line of defense. In addition to forming a physical barrier, enterocytes contribute to mucosal innate immunity via expression of pattern-recognition receptors (PRRs) that sense microbial signals[28]. Finally, the lamina propria, a thin layer of connective tissue underneath the epithelial layer, is populated with leukocytes, including macrophages and dendritic cells, and serves an important role in immune defense.

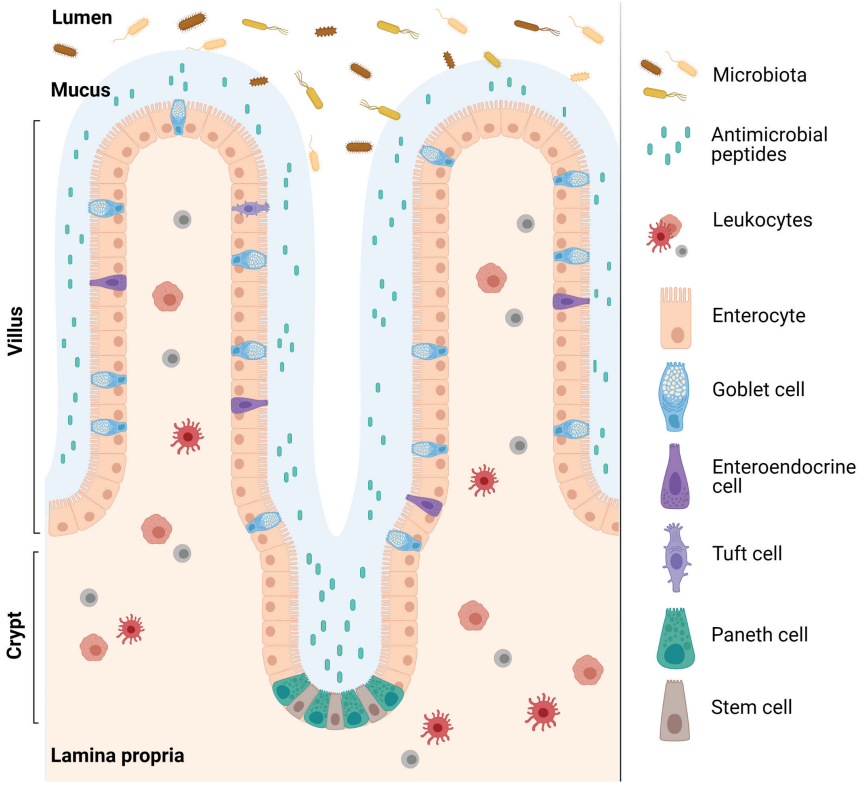

Figure 2. The intestinal epithelial barrier. *The intestinal epithelial barrier consists of multiple layers of defense to maintain homeostasis. 1) The mucus layer acts as a physical barrier, which is strengthened by antimicrobial peptides. 2) A single layer of tightly connected intestinal epithelial cells forms the next physical barrier. 3) Paneth cells in the crypt secrete antimicrobial peptides, and factors that support stem cells. 4) The stem cells are responsible for continuous renewal of the intestinal epithelium. 5) The lamina propria underneath the epithelium is populated with leukocytes (e.g. macrophages, dendritic cells, and lymphocytes) and provides innate immune defense as well as immunological memory. Figure created with BioRender.com*

Damage to the intestinal epithelial barrier

Impairment of one or more layers of defense, e.g. changes in mucus composition, disruption of epithelial cells or tight junctions, or loss of Paneth cells, affect the integrity of the intestinal barrier. When epithelial barrier integrity is compromised, harmful luminal contents may translocate to

the sterile inner mucosa, which may cause a severe inflammatory response. Induction of a local inflammatory response is essential to clear invading microbes and their products, and prevent systemic infection[29]. Intestinal epithelial cells and innate immune cells sense microbial signals, called microbe-associated molecular patterns (MAMPs), which provokes the onset of inflammation[30]. These MAMPs are expressed by both commensal microbiota and pathogens. In addition, damaged cells release intracellular components, such as heat-shock proteins and nucleic acids. These non-microbial stimuli, the so-called damage-associated molecular patterns (DAMPs), can interact with immune cells via PRRs and elicit inflammation as well[31]. Despite the beneficial effects of local inflammation in case of epithelial barrier breach, inflammation can also exacerbate tissue damage which may lead to uncontrolled chronic inflammation.

Epithelial barrier breach in clinical conditions

Disruption of the epithelial barrier plays a critical role in various intestinal pathologies, including inflammatory bowel disease[32,33] and celiac disease[34]. In addition, environmental conditions such as ischemia and reperfusion can threaten barrier integrity. IR of the human intestine has been shown to impair the physical as well as immunological epithelial barrier and cause local inflammation (see paragraph '*Insights on intestinal IR in man*').

Restoring the injured epithelium: importance of the stem cell niche

The intestinal epithelium has an exceptional ability to recover from acute injury and rapidly regenerate. The stem cells in the crypt bottom, the so-called crypt-base columnar stem cells (CBCs), are the drivers of both homeostatic renewal of the epithelium and injury-induced regeneration[35]. Importantly, the crypt bottom has developed into a highly protective environment, in which stem cells are supported and damage is minimized[18]. Within this niche, Paneth cells are interspersed with stem cells and are indispensable for stem cell maintenance. Paneth cells provide essential paracrine signals, such as Wnt ligands, epidermal growth factor (EGF) and Notch ligands, to maintain the stem cells[36]. Additionally, as mentioned before, Paneth cells secrete antimicrobial peptides that protect the niche. Besides the epithelial component, the mesenchyme is an important player in the intestinal stem cell niche. Mesenchymal cells - including fibroblasts, myofibroblasts, endothelial cells, smooth muscle cells and neural cells - provide key signals that regulate stem cells, e.g. Wnt ligands, R-spondins, bone morphogenetic proteins (BMPs) and BMP inhibitors[18]. The complex coordination of these signals derived from both epithelial and mesenchymal cells regulate stem cell activity and control the balance between proliferation and differentiation into the secretory or absorptive lineage. Besides the active CBCs, a reserve pool of 'damage-responsive' stem cells have been described. These stem cells maintain in a quiescent state, are relatively resistant to injury and are thought to play a crucial role in injury-induced epithelial regeneration if CBC stem cells are lost[35].

A human experimental model to study intestinal IR injury

A decade ago, an experimental model was developed to study ischemia and reperfusion injury and subsequent repair in human small intestine[37]. Patients undergoing abdominal surgery with small intestinal reconstruction, for example pancreatico-duodenectomy, were included in the study. As part of the surgical procedure, a healthy segment of proximal jejunum is resected. This allowed the

use of this segment for *in vivo* modeling of IR in the human small intestine within the time window of the surgical procedure. The experimental procedure is described in detail by Derikx et al.[37]. In short, a jejunal segment of approximately 6 cm, containing a central mesenteric arteriole and venule, is isolated by transection at both ends. Ischemia was induced by placing atraumatic vascular clamps over the mesentery. After a variable period of ischemia, 2 cm of the isolated segment is dissected using a cutting stapler, and immediately thereafter the clamps are removed to initiate reperfusion. Tissue samples are collected at short (30 min) and prolonged (120 min) reperfusion time points. Finally, a jejunal sample not exposed IR is collected at the end of the procedure, serving as internal control. In addition, at every time-point, blood is sampled from the venule draining the isolated intestinal segment, and from the arterial line which is placed as part of routine intraoperative monitoring. Tissue and blood were collected according to a standardized protocol, which provided a robust model with reproducible results. This model has significantly improved our understanding of the pathophysiology of varying periods of ischemia followed by reperfusion. The main findings are discussed next.

Insights on intestinal IR in man

The intestine appears to be relatively resistant to short periods of ischemia. After 30 min of ischemia, the damaged epithelial cells at the villus tips get detached from their basement membrane, resulting in the appearance of subepithelial spaces[38]. This, however, did not directly lead to disruption of the epithelial lining. Early during reperfusion, the detached epithelial sheets are pulled together through the accumulation of myosin at the basal side of the epithelial cells, a phenomenon known as zipper-like epithelial constriction[39]. This mechanism prevented actual barrier breach and allowed closure of the epithelial lining while being protected from exposure to harmful luminal content. After 120 min of reperfusion, the contracted sheets were shed into the lumen and the epithelial lining was restored[39]. In addition, a massive inflammatory response stays out[40]. The mechanisms could explain how the gut can tolerate mild reductions in intestinal perfusion as observed for example during physical exercise.

The protective mechanisms are not sufficient after longer periods of ischemia (>45 min). Prolonged IR leads to disruption of the intestinal barrier and induction of inflammation. Disruption of the epithelial lining is already apparent after ischemia and continues during reperfusion[41]. Apoptosis occurs initially at the villus tips and progresses towards the crypt with increasing duration of ischemic periods. As a consequence, epithelial damage (DAMPs) and exposure to luminal microbes (MAMPS) elicit an inflammatory response, which is characterized by influx of neutrophils and activation of complement[41]. This local inflammation is accompanied by an increase in pro-inflammatory cytokines. In addition, while the intestinal crypt remained unaffected by short ischemic periods, prolonged IR triggered apoptosis of Paneth cells[42], which impairs immunological barrier function. Paneth cells directly respond to microbial threats, by actively sensing their presence and in response releasing antimicrobial peptides[43]. It is suggested that Paneth cells have a crucial function in limiting bacterial translocation and preventing systemic inflammation[42].

The fact that the mature enterocytes at the villus tips are more susceptible to IR, can be explained by the oxygen gradient along the crypt-villus axis presenting a decreasing oxygen tension

towards the villus tip[44]. Also, as the villus-tip enterocytes are at the end of their lifespan, they are physiologically in a pro-apoptotic state[45].

Human small intestinal organoids

The *in vivo* model for human intestinal IR is incredibly useful to study its pathophysiology, however, it is not suitable for in-depth mechanistic studies and testing of therapeutic targets. For that, an *in vitro* model that offers improved translation to *in vivo* IR is urgently needed. In this thesis we generate small intestinal organoids from human origin, and we subject them to hypoxia and reoxygenation as a model to study IR injury *in vitro*.

Organoids are three-dimensional near-physiological, self-renewing cultures that are derived from primary tissue and exhibit similar architecture and functionality as the tissue of origin[46,47]. The purely epithelial structures are cultured in a basement membrane extract, which facilitates self-organization into structures that reflect aspects of the original tissue. Since the development of the murine intestinal organoid model in 2009 by Sato et al.[48], the organoid model has attracted a lot of attention as an *in vitro* tool to study epithelial biology, e.g. stem cell/niche function and tissue renewal. Next to studying basic biology, numerous clinical applications have been described, including disease modeling (e.g. cancer, infectious diseases and hereditary diseases)[49-52], personalized cancer therapy[53] and regenerative medicine[54].

Organoids represent an important bridge between *in vitro* tumor-derived cell lines and *in vivo* models. They are more physiologically relevant than traditional monolayer cell culture and, on the other hand, far more easily manipulated compared to *in vivo* models. The fact that organoids lack

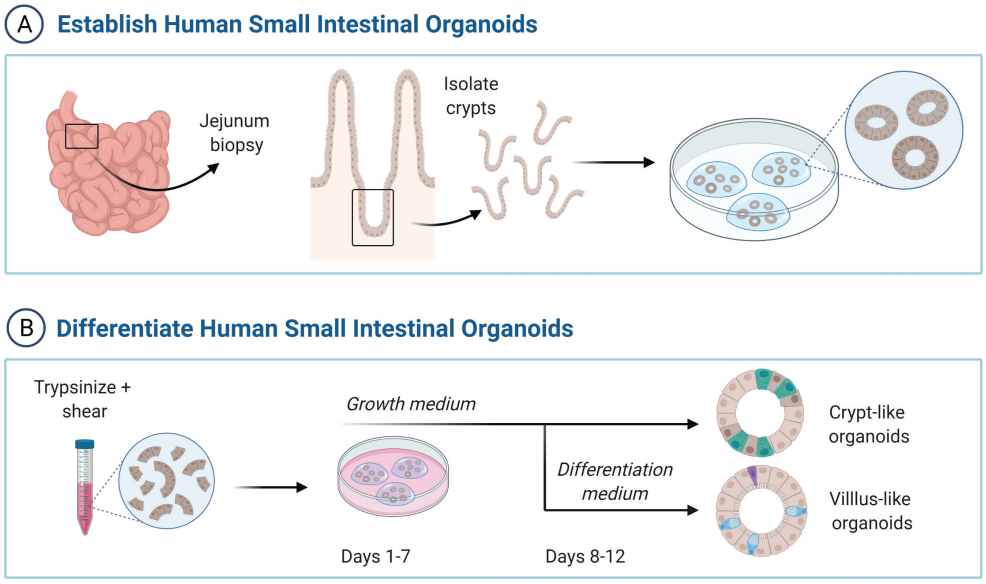

Figure 3. Human small intestinal organoid model. ***a****) Establishment of small intestinal organoids from a human jejunal biopsy.* ***b****) After passaging, intestinal organoids can be grown as proliferating crypt-like organoids or differentiated into villus-like organoids.*

mesenchymal, stromal and immune cells enables investigation of epithelial damage and regeneration without confounding environmental influences. Another advantage is that longer reoxygenation times can be studied, in contrast to the human model which is restricted by surgery time.

For the establishment of organoids lines, a small fragment of healthy jejunum, which is residual tissue from a surgical procedure, is used. From this tissue, the intestinal crypts containing adult stem cells and Paneth cells, are isolated and embedded in basement membrane extract (**Figure 3a**). The crypts grow into organoids that consist of a polarized epithelial layer, with the apical side oriented towards a central lumen. Organoids are genetically and phenotypically stable[55] and harbor stem cells that give rise to all mature epithelial cells, i.e. absorptive enterocytes, Paneth cells, goblet cells and enteroendocrine cells. To support establishment, expansion, long-term culture and further differentiation, the organoid culture medium is supplemented with several growth factors.

Stem cell fate determination is tightly regulated by four signaling pathways: Wnt, Notch, EGF and BMP signaling[56]. Wnt signaling is crucial for stem cell maintenance and the key driver of proliferation. Notch helps to maintain the undifferentiated state of both stem cells and TA cells and controls differentiation fate (secretory versus absorptive), and EGF promotes proliferation. In contrast, BMP signaling is active in the villus and its inhibition is crucial in the stem cell niche[56]. Activators of Wnt signaling (Wnt3A and R-spondin), EGF, and BMP inhibitor Noggin are needed for stem cell expansion *in vitro*, and key components of the organoid culture medium[48,57]. Supplementation with nicotinamide, gastrin, small molecule inhibitor of Alk and inhibitor of p38 improves culture efficiency and is required for long-term culture of human small intestinal organoids[57]. However, while this growth factor cocktail supports stem cells and stimulates proliferation, differentiation into mature absorptive or secretory cell types is suppressed. Withdrawal of certain growth factors from the medium will induce a differentiated phenotype of human intestinal organoids which allows the study of villus-like organoids[50,51] (**Figure 3b**).

AIMS AND OUTLINE OF THE THESIS

Intestinal IR is a potentially fatal condition, and mortality rates have not improved in the last decades. Further unraveling the pathophysiology is crucial in order to improve patient outcome. In this thesis, we study the consequences of intestinal IR injury in a clinical setting (**chapter 2**) and we use omics approaches to gain more insight in the molecular mechanisms underlying intestinal IR injury in the human experimental IR model (**chapter 3** and **5**). In addition, we aim to develop a near-physiological organoid model to study intestinal IR *in vitro* (**chapter 4**) and use this model to further investigate processes that are found to be regulated during IR (**chapter 5** and **6**).

In **chapter 2**, we study the consequences of intestinal IR injury in a clinical setting, namely during intestinal transplantation. Organ transplantation is inevitably accompanied by IR injury, which has a negative impact on transplant outcome. As Paneth cells play a crucial role in innate epithelial immunity, their loss may increase vulnerability of the graft to rejection. In this retrospective study, we investigate Paneth cell alterations following IR injury in intestinal transplantation, and the correlation with clinical outcome.

To improve our understanding of the biological processes involved in IR injury, it is of great value to unravel dynamic changes in the intestinal proteome in response to IR. In **chapter 3**, three complementary approaches are used to study changes in protein abundance, phosphorylation and localization in human intestine exposed to ischemia and reperfusion: Liquid Chromatography-Mass Spectrometry (LC-MS/MS) proteomics, LC-MS/MS-based phosphoproteomics, and Matrix-Assisted Laser Desorption/Ionization-Mass Spectrometry Imaging (MALDI MSI).

Chapter 4 describes the use of human small intestinal organoids to model IR *in vitro* by exposure to hypoxia-reoxygenation. We aim to characterize different organoid phenotypes, i.e. crypt-like and villus-like organoids, as well as to decipher protein dynamics and molecular mechanisms of IR injury in crypt- and villus-like organoids separately. To this end, we use a mass spectrometry-based proteomics approach.

In **chapter 5**, we decipher the transcriptional landscape of the human intestinal response to IR, and identified unfolded protein stress as one of the top regulated processes during reperfusion. This led us to further investigate the unfolded protein response in IR pathophysiology and its potential as a therapeutic target in IR injury, using the human intestinal organoid model.

Proteomics analysis of the hypoxia-reoxygenation response in chapter 4 points to occurrence of mitophagy in crypt-like organoids, yet no indications were found in villus-like organoids. This interesting finding gave rise to study mitochondrial damage and signs of mitophagy in response to hypoxia-reoxygenation in crypt- and villus organoids in **chapter 6** of this thesis.

Finally, **chapter 7** presents an integrated view of the main findings of this thesis and discusses implications for future research.

REFERENCES

1 Colgan, S. P. & Taylor, C. T. Hypoxia: an alarm signal during intestinal inflammation. *Nat Rev Gastroenterol Hepatol* **7**, 281-287 (2010).

2 van Wijck, K. *et al.* Exercise-induced splanchnic hypoperfusion results in gut dysfunction in healthy men. *PloS one* **6**, e22366 (2011).

3 Bala, M. *et al.* Acute mesenteric ischemia: guidelines of the World Society of Emergency Surgery. *World journal of emergency surgery : WJES* **12**, 38 (2017).

4 American Gastroenterological Association Medical Position Statement: guidelines on intestinal ischemia. *Gastroenterology* **118**, 951-953 (2000).

5 Oldenburg, W. A., Lau, L. L., Rodenberg, T. J., Edmonds, H. J. & Burger, C. D. Acute mesenteric ischemia: a clinical review. *Archives of internal medicine* **164**, 1054-1062 (2004).

6 Ibrahim, C. B., Aroniadis, O. C. & Brandt, L. J. On the role of ischemia in the pathogenesis of IBD: a review. *Inflamm Bowel Dis* **16**, 696-702 (2010).

7 Blauw, J. T. M., Geelkerken, R. H. & Kolkman, J. J. Mesenteriaal ischemie, een multidisciplinaire uitdaging. *FocusVasculair* **1** (2016).

8 Kassahun, W. T., Schulz, T., Richter, O. & Hauss, J. Unchanged high mortality rates from acute occlusive intestinal ischemia: six year review. *Langenbeck's archives of surgery* **393**, 163-171 (2008).

9 Mastoraki, A. *et al.* Mesenteric ischemia: Pathogenesis and challenging diagnostic and therapeutic modalities. *World journal of gastrointestinal pathophysiology* **7**, 125-130 (2016).

10 Kougias, P. *et al.* Determinants of mortality and treatment outcome following surgical interventions for acute mesenteric ischemia. *Journal of vascular surgery* **46**, 467-474 (2007).

11 Mallick, I. H., Yang, W., Winslet, M. C. & Seifalian, A. M. Ischemia-reperfusion injury of the intestine and protective strategies against injury. *Dig Dis Sci* **49**, 1359-1377 (2004).

12 Tilsed, J. V. *et al.* ESTES guidelines: acute mesenteric ischaemia. *Eur J Trauma Emerg Surg* **42**, 253-270 (2016).

13 Kalogeris, T., Baines, C. P., Krenz, M. & Korthuis, R. J. Ischemia/Reperfusion. *Compr Physiol* **7**, 113-170 (2016).

14 Kalogeris, T., Baines, C. P., Krenz, M. & Korthuis, R. J. Cell biology of ischemia/reperfusion injury. *Int Rev Cell Mol Biol* **298**, 229-317 (2012).

15 Raedschelders, K., Ansley, D. M. & Chen, D. D. The cellular and molecular origin of reactive oxygen species generation during myocardial ischemia and reperfusion. *Pharmacol Ther* **133**, 230-255 (2012).

16 Baines, C. P. The mitochondrial permeability transition pore and ischemia-reperfusion injury. *Basic Res Cardiol* **104**, 181-188 (2009).

17 Croall, D. E. & Ersfeld, K. The calpains: modular designs and functional diversity. *Genome Biol* **8**, 218 (2007).

18 Gehart, H. & Clevers, H. Tales from the crypt: new insights into intestinal stem cells. *Nat Rev Gastroenterol Hepatol* **16**, 19-34 (2019).

19 Darwich, A. S., Aslam, U., Ashcroft, D. M. & Rostami-Hodjegan, A. Meta-analysis of the turnover of intestinal epithelia in preclinical animal species and humans. *Drug Metab Dispos* **42**, 2016-2022 (2014).

20 van der Flier, L. G. & Clevers, H. Stem cells, self-renewal, and differentiation in the intestinal epithelium. *Annu Rev Physiol* **71**, 241-260 (2009).

21 Chelakkot, C., Ghim, J. & Ryu, S. H. Mechanisms regulating intestinal barrier integrity and its pathological implications. *Exp Mol Med* **50**, 1-9 (2018).

22 Deplancke, B. & Gaskins, H. R. Microbial modulation of innate defense: goblet cells and the intestinal mucus layer. *Am J Clin Nutr* **73**, 1131s-1141s (2001).

23 Birchenough, G. M., Johansson, M. E., Gustafsson, J. K., Bergström, J. H. & Hansson, G. C. New developments in goblet cell mucus secretion and function. *Mucosal Immunol* **8**, 712-719 (2015).

24 Specian, R. D. & Oliver, M. G. Functional biology of intestinal goblet cells. *Am J Physiol* **260**, C183-193 (1991).

25 Allaire, J. M. *et al.* The Intestinal Epithelium: Central Coordinator of Mucosal Immunity. *Trends Immunol* **39**, 677-696 (2018).

26 Bevins, C. L. & Salzman, N. H. Paneth cells, antimicrobial peptides and maintenance of intestinal homeostasis. *Nature reviews. Microbiology* **9**, 356-368 (2011).

27 Gassler, N. Paneth cells in intestinal physiology and pathophysiology. *World journal of gastrointestinal pathophysiology* **8**, 150-160 (2017).

28 Sansonetti, P. J. War and peace at mucosal surfaces. *Nat Rev Immunol* **4**, 953-964 (2004).

29 Thoo, L., Noti, M. & Krebs, P. Keep calm: the intestinal barrier at the interface of peace and war. *Cell Death Dis* **10**, 849 (2019).

30 Artis, D. Epithelial-cell recognition of commensal bacteria and maintenance of immune homeostasis in the gut. *Nat Rev Immunol* **8**, 411-420 (2008).

31 Chen, G. Y. & Nuñez, G. Sterile inflammation: sensing and reacting to damage. *Nat Rev Immunol* **10**, 826-837 (2010).

32 Turner, J. R. Intestinal mucosal barrier function in health and disease. *Nat Rev Immunol* **9**, 799-809 (2009).

33 Clayburgh, D. R., Shen, L. & Turner, J. R. A porous defense: the leaky epithelial barrier in intestinal disease. *Laboratory Investigation* **84**, 282-291 (2004).

34 Visser, J., Rozing, J., Sapone, A., Lammers, K. & Fasano, A. Tight junctions, intestinal permeability, and autoimmunity: celiac disease and type 1 diabetes paradigms. *Ann N Y Acad Sci* **1165**, 195-205 (2009).

35 Barker, N. Adult intestinal stem cells: critical drivers of epithelial homeostasis and regeneration. *Nat Rev Mol Cell Biol* **15**, 19-33 (2014).

36 Clevers, H. C. & Bevins, C. L. Paneth cells: maestros of the small intestinal crypts. *Annu Rev Physiol* **75**, 289-311 (2013).

37 Derikx, J. P. *et al.* A new model to study intestinal ischemia-reperfusion damage in man. *The Journal of surgical research* **166**, 222-226 (2011).

38 Derikx, J. P. *et al.* Rapid reversal of human intestinal ischemia-reperfusion induced damage by shedding of injured enterocytes and reepithelialisation. *PloS one* **3**, e3428 (2008).

39 Grootjans, J. *et al.* Rapid lamina propria retraction and zipper-like constriction of the epithelium preserves the epithelial lining in human small intestine exposed to ischaemia-reperfusion. *The Journal of pathology* **224**, 411-419 (2011).

40 Matthijsen, R. A. *et al.* Enterocyte shedding and epithelial lining repair following ischemia of the human small intestine attenuate inflammation. *PloS one* **4**, e7045 (2009).

41 Grootjans, J. *et al.* Human intestinal ischemia-reperfusion-induced inflammation characterized: experiences from a new translational model. *Am J Pathol* **176**, 2283-2291 (2010).

42 Grootjans, J. *et al.* Level of Activation of the Unfolded Protein Response Correlates With Paneth Cell Apoptosis in Human Small Intestine Exposed to Ischemia/Reperfusion. *Gastroenterology* **140**, 529-539000 (2011).

43 Vaishnava, S., Behrendt, C. L., Ismail, A. S., Eckmann, L. & Hooper, L. V. Paneth cells directly sense gut commensals and maintain homeostasis at the intestinal host-microbial interface. *Proceedings of the National Academy of Sciences of the United States of America* **105**, 20858-20863 (2008).

44 Blikslager, A. T. Life in the gut without oxygen: adaptive mechanisms and inflammatory bowel disease. *Gastroenterology* **134**, 346-348 (2008).

45 Bullen, T. F. *et al.* Characterization of epithelial cell shedding from human small intestine. *Lab Invest* **86**, 1052-1063 (2006).
46 Fatehullah, A., Tan, S. H. & Barker, N. Organoids as an in vitro model of human development and disease. *Nat Cell Biol* **18**, 246-254 (2016).
47 Clevers, H. Modeling Development and Disease with Organoids. *Cell* **165**, 1586-1597 (2016).
48 Sato, T. *et al.* Single Lgr5 stem cells build crypt-villus structures in vitro without a mesenchymal niche. *Nature* **459**, 262-265 (2009).
49 Dutta, D., Heo, I. & Clevers, H. Disease Modeling in Stem Cell-Derived 3D Organoid Systems. *Trends Mol Med* **23**, 393-410 (2017).
50 Foulke-Abel, J. *et al.* Human Enteroids as a Model of Upper Small Intestinal Ion Transport Physiology and Pathophysiology. *Gastroenterology* **150**, 638-649.e638 (2016).
51 Saxena, K. *et al.* Human Intestinal Enteroids: a New Model To Study Human Rotavirus Infection, Host Restriction, and Pathophysiology. *J Virol* **90**, 43-56 (2016).
52 Onozato, D. *et al.* Application of Human Induced Pluripotent Stem Cell-Derived Intestinal Organoids as a Model of Epithelial Damage and Fibrosis in Inflammatory Bowel Disease. *Biol Pharm Bull* **43**, 1088-1095 (2020).
53 Ooft, S. N. *et al.* Patient-derived organoids can predict response to chemotherapy in metastatic colorectal cancer patients. *Sci Transl Med* **11** (2019).
54 Leushacke, M. & Barker, N. Ex vivo culture of the intestinal epithelium: strategies and applications. *Gut* **63**, 1345-1354 (2014).
55 Sato, T. & Clevers, H. Growing self-organizing mini-guts from a single intestinal stem cell: mechanism and applications. *Science* **340**, 1190-1194 (2013).
56 Clevers, H. The intestinal crypt, a prototype stem cell compartment. *Cell* **154**, 274-284 (2013).
57 Sato, T. *et al.* Long-term expansion of epithelial organoids from human colon, adenoma, adenocarcinoma, and Barrett's epithelium. *Gastroenterology* **141**, 1762-1772 (2011).

CHAPTER 2

Paneth cell alterations during ischemia-reperfusion, follow-up, and graft rejection after intestinal transplantation

*Anna M Kip, *Laurens J Ceulemans, Inca HR Hundscheid, Emilio Canovai, Hermien Hartog, Rachel M Brown, Olivier Corcos, Francisca Joly, Gert De Hertogh, Girish Gupte, Cornelis HC Dejong, Steven WM Olde Damink, Jacques Pirenne, Darius Mirza, Kaatje Lenaerts
*Shared first authorship

Transplantation 104, 1952-1958 (2020)

ABSTRACT

Ischemia-reperfusion (IR) injury is inevitable during intestinal transplantation (ITx) and executes a key role in the evolution towards rejection. Paneth cells (PC) are crucial for epithelial immune defense and highly vulnerable to IR injury. We investigated the effect of ITx on PC after reperfusion (T0), during follow-up, and rejection. Moreover, we investigated whether PC loss was associated with impaired graft homeostasis. Endoscopic biopsies, collected according to center-protocol and at rejection episodes, were retrospectively included (n=28 ITx, n=119 biopsies). Biopsies were immunohistochemically co-stained for PC (lysozyme) and apoptosis, and PC/crypt and lysozyme intensity were scored. We observed a decrease in PC/crypt and lysozyme intensity in the first week after ITx (W1) compared to T0. There was a tendency towards a larger decline in PC/crypt (p=0.08) and lysozyme intensity (p=0.08) in W1 in patients who later developed rejection compared to patients without rejection. Follow-up biopsies showed that the PC number recovered, whereas lysozyme intensity remained reduced. This persisting innate immune defect may contribute to the well-known vulnerability of the intestine to infection. There was no clear evidence that PC were affected throughout rejection. This study revealed a transient fall in PC numbers in the early post-ITx period, but a permanent reduction in lysozyme intensity following ITx. Further research is needed to determine the potential clinical impact of PC impairment after ITx.

INTRODUCTION

Intestinal transplantation (ITx) is a life-saving treatment for patients suffering from functional or anatomical short bowel syndrome and complicated intestinal failure[1]. Among all solid-organ transplantations, the intestine remains immunologically and biologically the most challenging and most vulnerable to acute rejection. Despite improved surgical and clinical expertise and improved immunosuppression therapy[2], acute cellular rejection is still a frequent (50%) and life-threatening complication after ITx[3].

Ischemia-reperfusion (IR) injury, an inevitable consequence of transplantation, is known to contribute to the cascade leading to allograft rejection. IR injury triggers innate immunity and may thereby enhance the alloimmune response towards the graft and promote rejection[4]. In colonized organs, IR-induced tissue damage is accompanied by bacterial translocation. Translocation of endotoxin occurs directly after reperfusion of the intestinal graft as well as during rejection. This represents another 'danger' signal stimulating alloreactivity and sensitizing the graft towards rejection[5-9]. In other solid-organ transplants, IR injury is associated with an increased number of rejection episodes and impairs both acute and long-term graft function[10,11].

IR of the human small intestine triggers apoptosis of Paneth cells (PCs) in the crypt epithelium[12]. PCs are crucial for the maintenance of intestinal bacterial homeostasis and contribute to innate epithelial immunity. PCs respond to bacterial presence and secrete antimicrobial products, including lysozyme and alpha-defensin, thereby controlling homeostasis between colonizing microbiota and the host[13,14]. PC loss has been associated with increased bacterial translocation and intestinal inflammation in Crohn's disease and a human model of intestinal IR[12,15]. This might suggest that bacterial translocation after graft reperfusion, and consequently the greater vulnerability to rejection[5], could be (partly) due to IR-induced PC loss. We hypothesized that IR induces PC apoptosis shortly after ITx, which impairs graft homeostasis in the short and long term.

Next to the supposed effect of IR, PCs may also play a role in the process of graft rejection. Several diseases associated with intestinal inflammation, such as Crohn's disease and graft-versus-host disease, show PC loss and reduced production of antimicrobial peptides[16-19]. We hypothesized that PCs also play a role in the pathophysiology of graft rejection. In this regard, two previous studies have reported no difference in PC number and antimicrobial peptide expression during rejection in ITx patients compared to healthy volunteers[20] or stable grafts[21]. However, whether PC impairment precedes rejection, indicating a role in initiation of the rejection process, and/or whether PC are targeted by the rejection process, is unknown.

In this study we aimed to investigate 1) the change in PC numbers and lysozyme intensity in the early reperfusion phase after ITx and at multiple follow-up time points up to 5 years post-ITx; 2) the association between the extent of PC impairment in the early post-ITx period and clinical outcomes; and 3) PC loss and lysozyme intensity throughout acute graft rejection episodes.

MATERIALS AND METHODS

Patients and biopsies

The study retrospectively included 28 pediatric patients who underwent ITx between 2003 and 2012 at the Birmingham Children's Hospital, United Kingdom. The study was approved by the research ethics committee (10/H1207/67) and informed consent was obtained. Patient characteristics and clinical information are presented in **Table 1**. Induction immunosuppressive therapy was identical for all patients (tacrolimus/steroid/basiliximab), whereas maintenance immunosuppressive therapy varied between patients (**Table 1**). Rejection episodes were treated with high-dose steroids, increase of maintenance immunosuppression and – if refractory – by thymoglobulin.

Archived biopsy samples, collected as part of the graft monitoring protocol or when clinically indicated, for example, during rejection, were used for analysis. After graft reperfusion (up to 30 min), a tissue specimen of the terminal ileum was collected intraoperatively (T0). According to the monitoring protocol, mucosal biopsies from the terminal ileum were obtained regularly early after ITx and with increasing time intervals (2-3 times in the first week, weekly during the first month, monthly during the first year, and yearly thereafter). In this study, biopsies were grouped as shown in **Figure 1a**. Additional biopsies were obtained during acute rejection. For evaluation of rejection, samples were grouped in biopsies obtained prior to rejection (Pre-Rej), at diagnosis (Rej1), later during rejection (Rej2, day 2-14), and after recovery of rejection (first biopsy with normal histology, Post-Rej). The Pre-Rej biopsy was included in case a routine biopsy was available up to 9 days before rejection.

Immunohistochemistry and scoring of PC/crypt and lysozyme intensity

Formalin-fixed paraffin-embedded tissue sections were immunohistochemically stained for the detection of lysozyme (PC) and M30 (apoptosis) as previously described[12]. All samples from one patient were stained in the same batch to prevent batch-dependent variability within one patient. The same control sample of human small intestine was included in every batch for inter-batch difference evaluation in staining intensity. Immunostained tissue sections were scored for the number of lysozyme-positive cells per crypt (PC/crypt) and M30-positive lysozyme-positive cells (apoptotic PC) in whole biopsy sections or – for larger tissue specimens – in 10 representative microscopic fields (200x magnification). Samples containing ≤ 5 crypts were excluded. In addition, lysozyme staining intensity was graded using a 5-point scale from very weak (1) to very intense (5). All scorings were performed by two independent observers in a blinded way. Interobserver reliability was good, with an intraclass correlation coefficient of 0.80 (95%; CI: 0.75-0.85) for PC count, and 0.89 (95%; CI: 0.86-0.92) for lysozyme intensity scores.

Histological grading of IR injury and rejection

T0 and W1 samples were H&E-stained and scored for IR injury according to Park/Chiu by an experienced pathologist (G.D.H.). Park/Chiu scores progression of injury from the villi tips to the crypts and into deeper layers of the intestinal wall in 8 grades, in which a higher grade reflects more damage[22]. Grading of rejection biopsies was based on clinical reporting by a small specialist team of three pathologists. Biopsies were graded using a standard scale: no, mild, moderate, or severe acute cellular rejection[23].

Statistical analysis

Statistical analysis was performed using IBM SPSS 22.0 and GraphPad Prism 6 software. Intraclass correlation coefficient and 95% confidence intervals were calculated based on a mean-rating (K=2), consistency, 2-way mixed-effects model. Linear mixed model analysis was used to examine statistical significance of changes in PC/crypt and lysozyme intensity over time following ITx (covariance structure: heterogeneous compound symmetry) and throughout rejection (compound symmetry). Wilcoxon matched-paired signed rank test was performed to compare Park-Chiu scores. The relation between Park-Chiu and PC scores was analyzed using Spearman correlation analysis. Mann-Whitney test was used to compare PC scores in clinical outcome groups (rejection versus no rejection). All p-values are two-sided. P-values <0.05 were considered statistically significant.

Table 1. Patient characteristics and clinical information

	Median (range)	N patients
Recipient characteristics		
Age, months	54 (11-194)	
Gender [M/F], n		16/12
Weight, kg	15 (6-52)	
Type of Itx, n		
Isolated/combined/MMV/MV		12/12/3/1
Donor characteristics		
Age, months	96 (12-480)	
Gender [M/F], n		11/15
Weight, kg	24 (11-70)	
Surgical variables		
Cold ischemia time, minutes	380 (221-740)	
Warm ischemia time, minutes	33 (10-53)	
Operating time, minutes	381 (250-739)	
Post-surgery		
ICU stay, days	2.5 (1-145)	
In-hospital stay, days	55.5 (25-115)	
Maintenance Immunosuppression, n		
TAC+ST		20
TAC+ST+RAPA		3
TAC+ST+MMF		4
Outcome		
Mortality, n (%)		7 (25%)
Reason of death, n		
Infection		3
Rejection		2
Thrombosis of graft		1
Technical complications		1
Graft loss, n (%)		10 (35,7%)
Episodes of rejection, n		6/11/5/4/2
0/1/2/3/4		
Early rejection (< 3 months), n (%)		15 (54%)

Combined, small intestine and liver; MVV, modified multivisceral; MV, multivisceral; TAC, tacrolimus; ST, steroid; BAS, basiliximab; ATG, anti-thymocyte globulin; RAPA, rapamycin; MMF, mycophenolate mofetil

RESULTS

PCs are affected after intestinal transplantation

To investigate whether PCs were affected after ITx, changes in PC/crypt and lysozyme intensity were evaluated, as well as the presence of apoptotic PCs. In T0 samples collected shortly after reperfusion, apoptotic cells were abundant in the villi tips, but no apoptotic PC could be detected (data not shown). Interestingly, both the PC/crypt (**Figure 1b**) and the lysozyme intensity (**Figure 1c**) were significantly reduced in the first follow-up biopsy (W1) compared to T0 ($p<0.001$). Also, a strong positive correlation was observed between PC/crypt and lysozyme intensity score at T0 ($r=0.70$, $p=0.003$) and W1 ($r=0.76$, $p=0.001$). PC/crypt remained reduced at W2 and M1 compared to T0 ($p<0.001$ and $p<0.05$ respectively), but restored thereafter gradually to numbers comparable to T0. In contrast, lysozyme intensity continued to be reduced at all time points after ITx compared with T0 (**Figure 1c**). Evaluation of consecutive time points shows intra-individual as well as inter-individual variation, especially for lysozyme intensity, as illustrated in **Figure 1d**.

PC number and lysozyme intensity do not correlate with histologically graded IR injury

To investigate whether the observed PC and lysozyme loss could be related to IR injury, the extent of IR injury was graded in T0 (median 2, interquartile range = 2-5) and W1 (median 2, interquartile range = 1-6) samples based on the Park-Chiu scoring. Park Chiu scores did not significantly improve in W1 compared to T0 ($p=0.60$). However, five out of 11 patients showed decreased and thus improved Park-Chiu scores, whereas for the other six patients no improvement was observed at W1. The change in Park-Chiu (ΔW1-T0) did not correlate with a change in PC/crypt and lysozyme intensity (ΔW1-T0). Also, there was no correlation between IR injury and PC/crypt or lysozyme intensity at T0 and W1 (**Figure S1**). In addition, no relation could be found between cold or warm ischemia time and PC/crypt or lysozyme intensity at T0, W1 or ΔW1-T0.

Relation between PC (antimicrobial) loss and clinical outcome

To evaluate whether PC impairment in the early post-ITx period was associated with later occurrence of acute rejection, two groups were compared: patients who later developed rejection (n=8) and patients without graft rejection (n=3). At T0 and W1, the PC/crypt and lysozyme intensity did not differ between the groups (**Figure 1e, f**). However, there was a tendency towards a larger decline in PC/crypt ($p=0.085$) and lysozyme intensity ($p=0.079$) in the first follow-up biopsy relative to T0 (ΔW1-T0) in the rejection group compared to the no-rejection group (n=8 and n=3 respectively for paired analysis) (**Figure 1e, f**). In this patient cohort, no relation could be found between the extent of PC loss or decrease in lysozyme intensity in the first week post-ITx (ΔW1-T0), and other clinical outcomes: ICU time, graft loss, and mortality. In addition, there was no association between PC/crypt or lysozyme intensity at T0 or W1, and these clinical outcomes.

PC alterations throughout rejection

Independent acute rejection episodes were graded as mild (n=18), moderate (n=4), or severe (n=6). Both early rejections (n=21), defined as episodes occurring within 3 months post-ITx, and late rejection episodes (n=7) were included in the analysis. For overall evaluation of PC impairment throughout

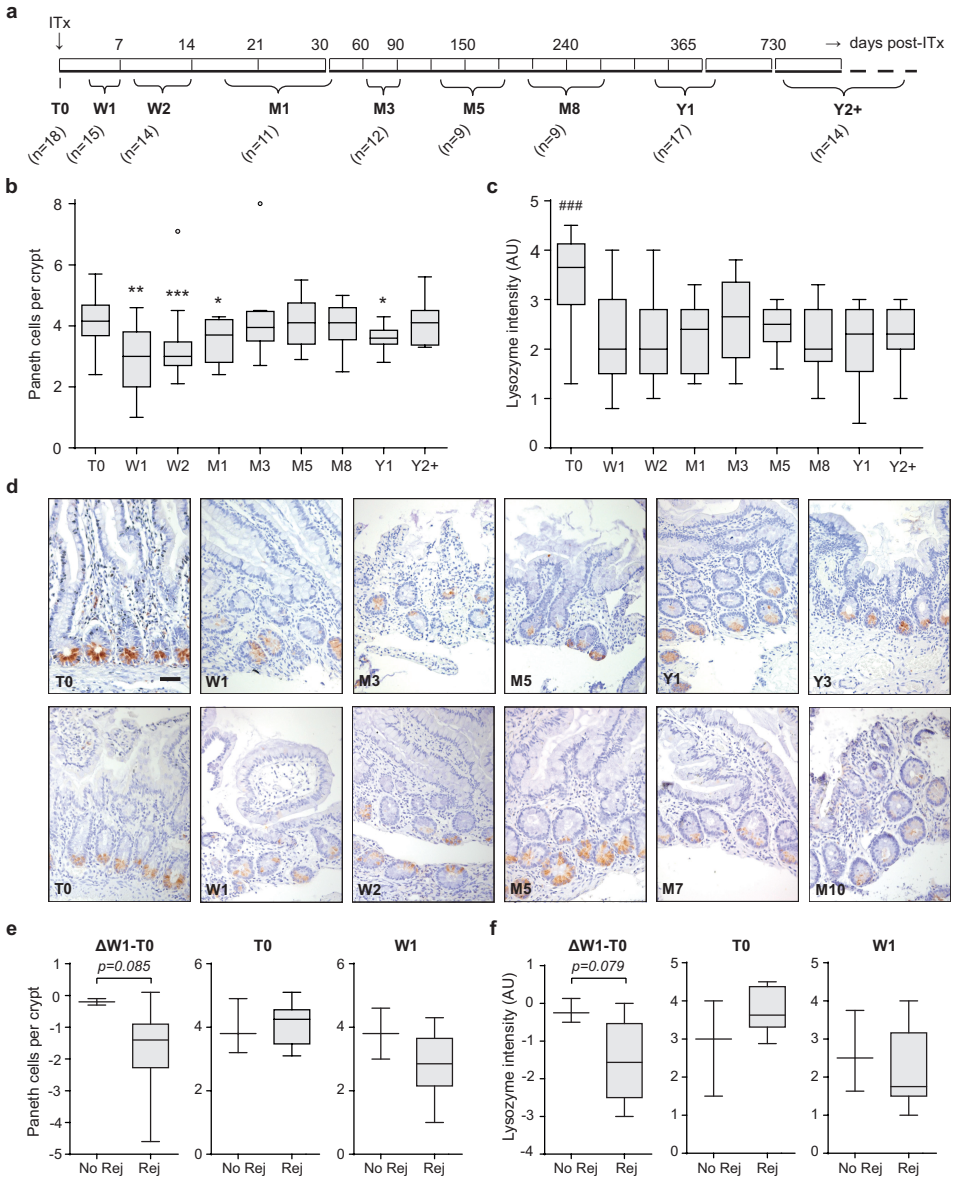

Figure 1. Paneth cells per crypt and lysozyme staining intensity after intestinal transplantation. ***a****) Timeline of biopsies collected following monitoring protocol. Biopsies were grouped in time points: T0 (after reperfusion, n=18); W1 (day 3-7, n=15); W2 (day 8-14, n=14); M1 (day 17-46, n=11); M3 (day 60-98, n=12); M5 (day 125-178, n=9); M8 (day 197-277, n=9); Y1 (day 311-446, n=17); Y2+ (2-5 years post-ITx, n=14)* ***b****) PC/ crypt and* ***c****) lysozyme staining intensity in PCs in biopsies collected after ITx as part of the monitoring protocol. Data are displayed in Tukey Boxplot; dots indicate outliers. *p<0.05, **p<0.01, ***p<0.001 compared with T0. ###p<0.001 compared to all other time-points.* ***d****) Representative lysozyme staining on consecutive post-ITx biopsies from two patients. Scale bar represents 100 µm.* ***e****) PC/crypt and* ***f)*** *lysozyme intensity in patient group with rejections (n=8) and patients without rejections (n=3) at T0, W1 (3-5 days post-ITx) and ΔW1-T0. Patients with both T0 and W1 biopsies available were included in analysis. Data are displayed in Tukey Boxplot.*

rejection (n=28), samples were grouped as shown in **Figure 2a**. We observed no differences in PC/crypt (**Figure 2b**) or lysozyme intensity (**Figure 2c**) between Pre-Rej, Rej1, Rej2 and Post-Rej. Although overall no significant differences were detected, examination of individual rejection episodes showed notable differences in PC changes between patients (**Figure 2d**). These inter-individual differences could not be explained by severity or timing of rejection, as no difference was observed between high- and low-grade rejection or between early and late episodes.

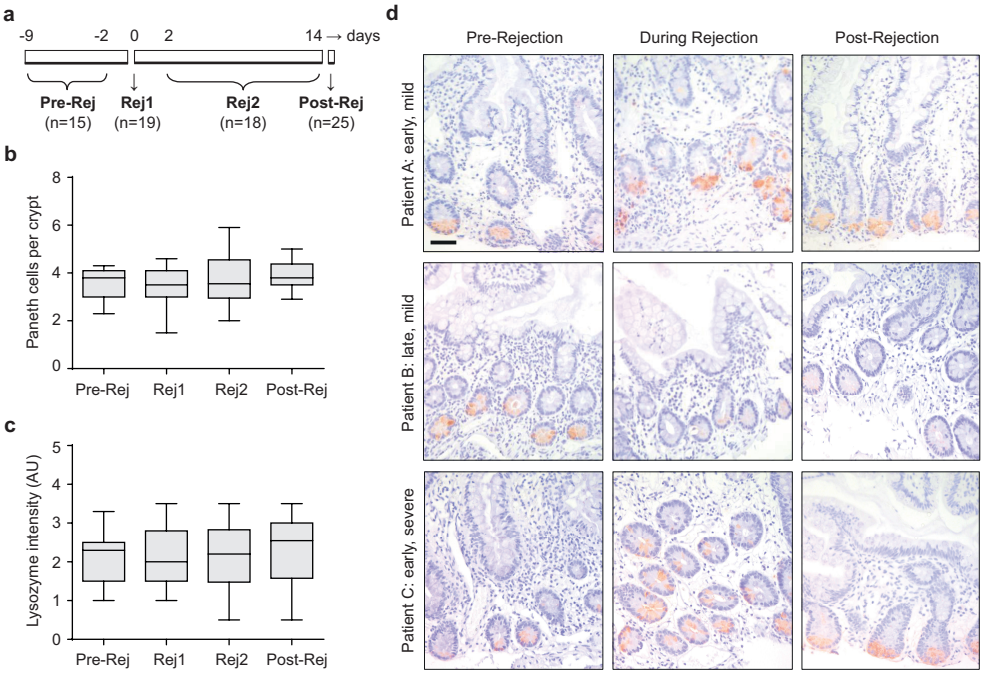

Figure 2. Paneth cells per crypt and lysozyme staining intensity throughout rejection episodes. a*) Timeline of biopsies collected throughout rejection episodes. Samples were grouped in Pre-Rej (up to 9 days prior to rejection, n=15), Rej1 (at diagnosis of acute rejection, n=19), Rej2 (later during acute rejection, n=18), and Post-Rej (after recovery of rejection, n=24),* ***b****) PC/crypt and* ***c****) lysozyme staining intensity in PC. Data are displayed in a Tukey Box-and-whisker plot.* ***d****) Lysozyme stainings in biopsies prior to, during and after rejection episodes from three different patients. Grade (mild, severe) and timing (early, late) of rejection episodes are indicated. Scale bar represents 100 µm.*

DISCUSSION

IR injury is inevitable during ITx and known to induce apoptosis of PCs, key elements in innate epithelial immunity. This study focused on PC loss and antimicrobials after ITx, and the relation between PC impairment in the early post-ITx period and long-term graft homeostasis. In addition, we studied the PC alterations in the course of graft rejection.

In contrast to what we expected based on the study by Grootjans et al., in which significant numbers of apoptotic PC were present after 45 minutes of ischemia followed by short reperfusion in human jejunum[12], no apoptotic PCs could be detected shortly after reperfusion of the intestinal graft. This observation is in line with the relatively low Park-Chiu scores in T0 biopsies, and both indicate mild IR injury following ITx. A shorter warm ischemia time in the ITx cohort (33 minutes versus 45 minutes in the human IR model[12]) and the fact that ileum is less susceptible to IR injury than jejunum could explain the mild IR injury and absence of PC apoptosis. In addition, organ preservation solution and topical cooling may have a protective effect on the graft and alleviate IR injury. It is also important to consider we cannot rule out that the apoptotic event might have been missed due to timing of the T0 sample.

Despite absence of PC apoptosis very early after reperfusion, the reduction in PC numbers in the first follow-up biopsy indicates that PC are effectively lost in the subsequent days post-transplantation. Because PC count did not correlate with Park-Chiu scores, it is likely that PC loss was not directly related to IR injury. Other post-operative factors (e.g. ICU stay, immunosuppression) or immune factors may also play a role. The reduced lysozyme intensity and PC number in the first months after ITx might, in part, account for the increased susceptibility of the graft to rejection and infection in this early period. The observation that PC numbers gradually recuperate, suggests a normalization of mucosal homeostasis of the graft in the longer term.

Interestingly, in the current study we also show a permanent reduction in lysozyme intensity after ITx. Deficiencies of antimicrobial proteins have been described in several pathologies associated with intestinal inflammation, such as Crohn's disease, obesity, and graft-versus-host-disease[17,18,24]. Furthermore, Fishbein et al. have reported a decrease in expression of antimicrobial peptides in the intestinal graft of ITx recipients with NOD2 Crohn's disease-associated polymorphism[25]. The NOD2 status of our patient cohort could not be determined for ethical restrictions. In addition, it is likely that immunosuppressive therapy has an effect on lysozyme expression in ITx patients. Indeed, immunosuppressive drugs (like calcineurin-inhibitors) have been shown to alter gene expression of antimicrobial peptides in mouse ileum, as well as microbiota composition[26].

On the other hand, changes in microbiota composition in ITx patients[27] may also be a consequence of reduced intensity of antimicrobial peptides. We speculate that the observed persistent reduction in lysozyme intensity in ITx patients may facilitate colonization by opportunistic pathogens, and thereby partially account for the well-established susceptibility of the grafted intestine to infectious enteritis. In addition, failure of antimicrobial defense combined with a hostile microbiota stimulates the immune response, and may, therefore, albeit indirectly increase vulnerability to rejection. Indeed, decreased expression of antimicrobial peptides in ITx patients with NOD2 polymorphisms has been shown to be a significant risk factor for graft rejection[25].

The relation between PC loss shortly after ITx and rejection in the long-term could be investigated only in a limited number of patients because of missing T0 and W1 samples. Although sample size was small and statistical significance was not reached, there was a trend showing a larger decline in PC number and lysozyme intensity (ΔW1-T0) in the patients who developed rejections compared

to the no-rejection group. These data suggest that the decline at W1 relative to T0, rather than PC (antimicrobial) scores at T0 or W1, may predict rejection. However, this observation should be confirmed in a larger ITx cohort.

One of the histological hallmarks of acute rejection following ITx is an increased number of apoptotic bodies in the crypt epithelium[23,28]. Our results showed no PC apoptosis during rejection or PC loss compared to biopsies obtained prior to and after rejection, which suggests that PC are not (further) affected by the rejection process in ITx patients. Likewise, a previous study by Fishbein et al. reported no change in PC number before and during early mild-graded rejection[21]. This is in stark contrast to graft-versus-host disease following allogeneic hematopoietic cell transplantation, where PCs have been shown to be highly affected, and the PC number correlated with clinical severity[16]. When comparing mild and severe acute rejection in our ITx cohort, no differences in PC number and lysozyme intensity were found, which is in line with observations by Pucci Molineris et al.[20]. The inexplicable variation between rejection events suggests that acute rejection is a complex process, in which the interplay of multiple factors influences the PC and antimicrobial immune defense.

Only pediatric patient samples were examined and it cannot be assumed that results are necessarily applicable to adults. Although PC are immune competent at birth[29], the gut microbiome is still developing in young children[30] which might have an effect on PC function. Nevertheless, Pucci Molineris et al. reported no differences between the pediatric and adult cohort when examining PC during rejection after ITx[20].

Because of the relatively small number of ITx cases per center, it remains challenging to perform large ITx studies, especially when using tissue samples. Given the retrospective nature of this study, a considerable amount of biopsies was not available for research. Also, some biopsies were not sufficient to give reliable results and were therefore excluded from the analysis. Small sample size impeded thorough statistical analysis of the association between PC impairment and clinical outcome, as well as in-depth analysis of PC alterations during acute rejection and comparing mild and severe rejections. In addition, infection episodes could not be studied due to the respective nature of the study.

This study provides new insights on PC alterations in the early reperfusion phase following ITx. Analysis of multiple follow-up biopsies in the same patients, gave valuable insight in the biology of the graft. We report a loss of PCs and lysozyme intensity in the early post-ITx period, but an association with IR injury could not be demonstrated. While PC numbers gradually restored, there was a permanent decline in lysozyme intensity in ITx patients. Further research in a larger cohort is needed to determine the potential impact of PC impairment on rejection and infection after ITx.

REFERENCES

1 Abu-Elmagd, K. The concept of gut rehabilitation and the future of visceral transplantation. *Nature reviews. Gastroenterology & hepatology* **12**, 108-120 (2015).

2 Ceulemans, L. J. *et al.* The Leuven Immunomodulatory Protocol Promotes T-Regulatory Cells and Substantially Prolongs Survival After First Intestinal Transplantation. *Am J Transplant* **16**, 2973-2985 (2016).

3 Grant, D. *et al.* Intestinal Transplant Registry Report: Global Activity and Trends. *Am J Transplant* **15**, 210-219 (2015).

4 Chong, A. S. & Alegre, M. L. The impact of infection and tissue damage in solid-organ transplantation. *Nat Rev Immunol* **12**, 459-471 (2012).

5 Kawai, M., Kitade, H., Koshiba, T., Waer, M. & Pirenne, J. Intestinal ischemia reperfusion and lipopolysaccharide transform a tolerogenic signal into a sensitizing signal and trigger rejection. *Transplantation* **87**, 1464-1467 (2009).

6 Lenaerts, K. *et al.* New insights in intestinal ischemia–reperfusion injury. *Current Opinion in Organ Transplantation* **18**, 298-303 (2013).

7 Alegre, M. L. *et al.* Antagonistic effect of toll-like receptor signaling and bacterial infections on transplantation tolerance. *Transplantation* **87**, S77-79 (2009).

8 Matzinger, P. The danger model: a renewed sense of self. *Science (New York, N.Y.)* **296**, 301-305 (2002).

9 Beebe, D. S. *et al.* Endotoxemia during small bowel transplantation in pigs. *Transplantation proceedings* **27**, 593-594 (1995).

10 Lutz, J., Thurmel, K. & Heemann, U. Anti-inflammatory treatment strategies for ischemia/reperfusion injury in transplantation. *J Inflamm (Lond)* **7**, 27 (2010).

11 Gueler, F., Gwinner, W., Schwarz, A. & Haller, H. Long-term effects of acute ischemia and reperfusion injury. *Kidney international* **66**, 523-527 (2004).

12 Grootjans, J. *et al.* Level of activation of the unfolded protein response correlates with Paneth cell apoptosis in human small intestine exposed to ischemia/reperfusion. *Gastroenterology* **140**, 529-539 (2011).

13 Vaishnava, S., Behrendt, C. L., Ismail, A. S., Eckmann, L. & Hooper, L. V. Paneth cells directly sense gut commensals and maintain homeostasis at the intestinal host-microbial interface. *Proc Natl Acad Sci U S A* **105**, 20858-20863 (2008).

14 Bevins, C. L. & Salzman, N. H. Paneth cells, antimicrobial peptides and maintenance of intestinal homeostasis. *Nat Rev Microbiol* **9**, 356-368 (2011).

15 Kaser, A. & Blumberg, R. S. Paneth cells and inflammation dance together in Crohn's disease. *Cell Res* **18**, 1160-1162 (2008).

16 Levine, J. E. *et al.* Low Paneth cell numbers at onset of gastrointestinal graft-versus-host disease identify patients at high risk for nonrelapse mortality. *Blood* **122**, 1505-1509 (2013).

17 Wehkamp, J. *et al.* Reduced Paneth cell alpha-defensins in ileal Crohn's disease. *Proc Natl Acad Sci U S A* **102**, 18129-18134 (2005).

18 Eriguchi, Y. *et al.* Graft-versus-host disease disrupts intestinal microbial ecology by inhibiting Paneth cell production of alpha-defensins. *Blood* **120**, 223-231 (2012).

19 Zhao, D. *et al.* Survival signal REG3alpha prevents crypt apoptosis to control acute gastrointestinal graft-versus-host disease. *The Journal of clinical investigation* **128**, 4970-4979 (2018).

20 Pucci Molineris, M. *et al.* Paneth and intestinal stem cells preserve their functional integrity during worsening of acute cellular rejection in small bowel transplantation. *Am J Transplant* **18**, 1007-1015 (2018).

21 Fishbein, T. M. *et al.* Rejection reversibly alters enteroendocrine cell renewal in the transplanted small intestine. *Am J Transplant* **9**, 1620-1628 (2009).
22 Quaedackers, J. S. *et al.* An evaluation of methods for grading histologic injury following ischemia/reperfusion of the small bowel. *Transplantation proceedings* **32**, 1307-1310 (2000).
23 Ruiz, P. *et al.* Histological criteria for the identification of acute cellular rejection in human small bowel allografts: results of the pathology workshop at the VIII International Small Bowel Transplant Symposium. *Transplantation proceedings* **36**, 335-337 (2004).
24 Hodin, C. M. *et al.* Reduced Paneth cell antimicrobial protein levels correlate with activation of the unfolded protein response in the gut of obese individuals. *The Journal of pathology* **225**, 276-284 (2011).
25 Fishbein, T. *et al.* NOD2-expressing bone marrow-derived cells appear to regulate epithelial innate immunity of the transplanted human small intestine. *Gut* **57**, 323-330 (2008).
26 Tourret, J. *et al.* Immunosuppressive Treatment Alters Secretion of Ileal Antimicrobial Peptides and Gut Microbiota, and Favors Subsequent Colonization by Uropathogenic Escherichia coli. *Transplantation* **101**, 74-82 (2017).
27 Hartman, A. L. *et al.* Human gut microbiome adopts an alternative state following small bowel transplantation. *Proc Natl Acad Sci U S A* **106**, 17187-17192 (2009).
28 Fishbein, T. M., Liu, J., Wang, L., Li, Y. & Boros, P. Increased apoptosis is specific for acute rejection in rat small bowel transplant. *The Journal of surgical research* **119**, 51-55 (2004).
29 Heida, F. H. *et al.* Paneth cells in the developing gut: when do they arise and when are they immune competent? *Pediatric research* **80**, 306-310 (2016).
30 Ringel-Kulka, T. *et al.* Intestinal microbiota in healthy U.S. young children and adults--a high throughput microarray analysis. *PloS one* **8**, e64315 (2013).

SUPPLEMENTARY INFORMATION

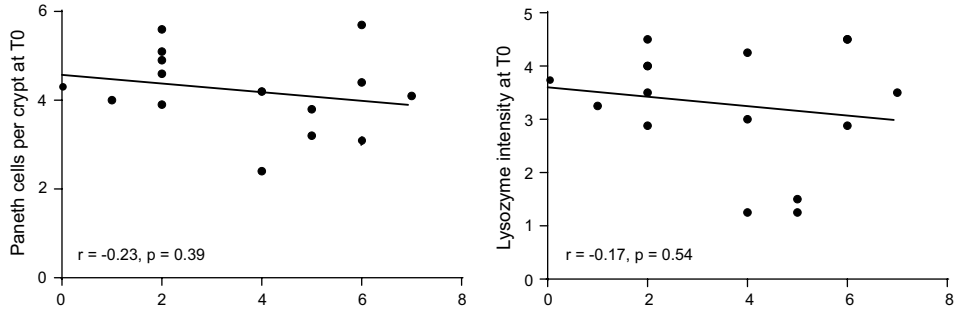

Figure S1. No correlation between Paneth cell impairment and IR injury after ITx*. Scatter plots illustrate there is no correlation between Park-Chiu scores and Paneth cell number (r= -0.23, p=0.39) or lysozyme intensity (r= -0.17, p=0.54) at T0.*

CHAPTER 3

Combined quantitative (phospho)proteomics and mass spectrometry imaging reveal temporal and spatial protein changes in human intestinal ischemia-reperfusion

Anna M. Kip, Juan Manuel Valverde, Maarten Altelaar, Ron M.A. Heeren, Inca H.R. Hundscheid, Cornelis H.C. Dejong, Steven W.M. Olde Damink, Benjamin Balluff, Kaatje Lenaerts

J Proteome Res. (2021) In press

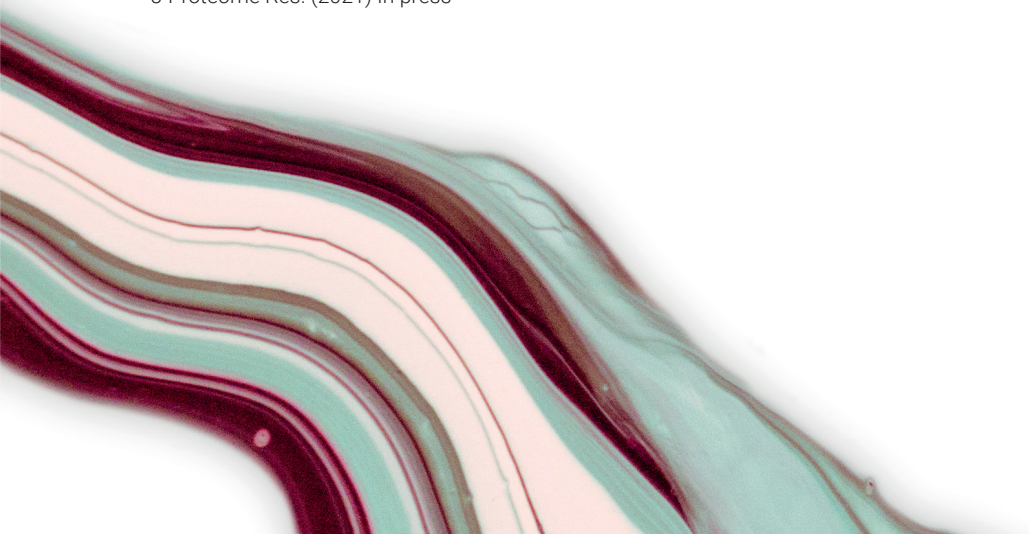

ABSTRACT

Intestinal ischemia–reperfusion (IR) injury is a severe clinical condition, and unraveling its pathophysiology is crucial to improve therapeutic strategies and reduce the high morbidity and mortality rates. Here, we studied the dynamic proteome and phosphoproteome in the human intestine during ischemia and reperfusion, using liquid chromatography-tandem mass spectrometry (LC-MS/MS) analysis to gain quantitative information of thousands of proteins and phosphorylation sites, as well as mass spectrometry imaging (MSI) to obtain spatial information. We identified a significant decrease in abundance of proteins related to intestinal absorption, microvillus, and cell junction, whereas proteins involved in innate immunity, in particular the complement cascade, and extracellular matrix organization increased in abundance after IR. Differentially phosphorylated proteins were involved in RNA splicing events and cytoskeletal and cell junction organization. In addition, our analysis points to mitogen-activated protein kinase (MAPK) and cyclin-dependent kinase (CDK) families to be active kinases during IR. Finally, matrix-assisted laser desorption/ionization time-of-flight (MALDI-TOF) MSI presented peptide alterations in abundance and distribution, which resulted, in combination with Fourier-transform ion cyclotron resonance (FTICR) MSI and LC-MS/MS, in the annotation of proteins related to RNA splicing, the complement cascade, and extracellular matrix organization. This study expanded our understanding of the molecular changes that occur during IR in the human intestine and highlights the value of the complementary use of different MS-based methodologies.

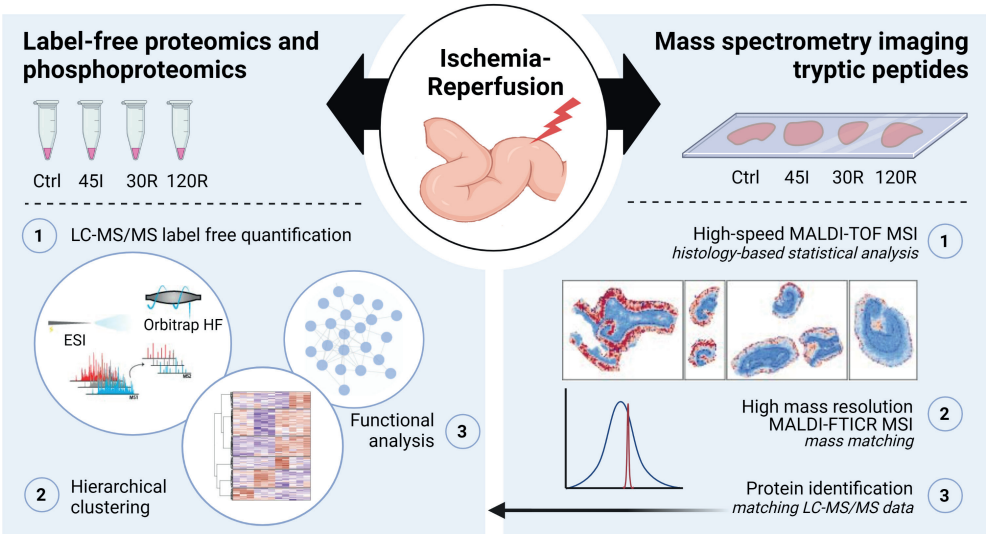

INTRODUCTION

Intestinal ischemia–reperfusion (IR) is a clinical phenomenon carrying high morbidity and mortality and can occur in various conditions. Based on etiology, intestinal ischemia is classified into chronic ischemia, e.g. due to atherosclerosis, and acute ischemia. The latter is further divided into occlusive disease, caused by the obstruction of the mesenteric blood flow, or nonocclusive disease, caused by hypoperfusion, for example, due to major surgical procedures, trauma, hemorrhagic shock, or sepsis[1-3]. The lack of oxygen during ischemia obviously leads to cell injury and hence rapid reperfusion is crucial. However, reperfusion can also aggravate injury as the sudden oxygen supply to the ischemic intestine initiates a cascade of events, including Ca^{2}+ influx and the production of reactive oxygen species (ROS), which damages cellular structures and activates an inflammatory response[4]. The intestinal epithelium serves as an important barrier that protects the body from the hostile luminal environment. Disruption of this barrier, which can be caused by IR injury, allows entry of harmful luminal microorganisms and toxins into the sterile inner mucosa, which may cause a severe inflammatory response. Observations from a human experimental model of intestinal IR showed that the intestine was relatively resistant to short periods of ischemia[5,6], whereas prolonged ischemia (>45 min) followed by reperfusion disrupted the epithelial lining and induced inflammation[7]. Cell death occurs initially at the villi tips and progresses toward the crypt with increasing duration of the ischemic period[7,8]. Severe IR can eventually lead to bowel necrosis and severe systemic inflammation. The high mortality rates (60–80%) of acute intestinal ischemia[1-3] can be attributed to the difficulty to diagnose acute mesenteric ischemia at an early stage, as well as the lack of effective therapeutic options[9-11]. Further unraveling the molecular mechanisms underlying ischemia–reperfusion is crucial to improve therapeutic strategies and patient outcomes.

Identification of changes in (local) protein abundance that occur following ischemia and during reperfusion in the human experimental model is of great interest for understanding the biological processes involved in IR injury and tissue repair. As many cellular functions are regulated by the dynamic phosphorylation of proteins, we were interested in investigating changes in protein phosphorylation as well. Furthermore, given the aforementioned differences in function and susceptibility to IR across the layers and cell types of the intestinal wall, spatial information of protein changes is of particular interest in the context of intestinal IR injury.

Liquid chromatography coupled to mass spectrometry (LC-MS)-based proteomics has emerged as an important tool to study cell biology and disease mechanisms and enables untargeted identification and quantification of several thousand proteins[12]. A multistep process, including protein extraction, digestion, and separation by LC, is currently used to obtain this thorough protein coverage and accuracy. However, with homogenization of the tissue during sample preparation, spatial information on protein distribution gets lost. A powerful technology to complement LC-MS-based proteomics is matrix-assisted laser desorption/ionization (MALDI) mass spectrometry imaging (MSI) of tissue sections. MALDI MSI allows analyzing hundreds of molecules simultaneously, providing spatial distribution and local abundance of these molecules in biological tissues in a label-free manner.

Combining MALDI MSI with the histological information of these tissue enables a histology-driven analysis. Intact proteins can be detected by MSI; however, their detection is limited by low ionization efficiency that limits sensitivity in the high mass range of the instrumentation. Recent studies have shown imaging of proteins up to 200 kDa[13,14]. MSI of trypsinized proteins can therefore – at least theoretically – increase the coverage of the proteome beyond this sensitivity limit. Moreover, the on-tissue digestion approach allows better integration of MSI data with liquid chromatography-tandem mass spectrometry (LC-MS/ MS) of the same or an adjacent tissue section to enable the identification of the observed local peptide signals, especially when using high-mass resolution MSI instrumentation[15,16]. However, these high-mass resolution MSI methods are limited by a long acquisition time and consequently suffer from a low throughput. This issue can be overcome by the use of highspeed MALDI-time-of-flight (TOF) MSI complemented by high-mass resolution MSI data[17], which is the approach that we applied in our study.

The main objective of this study is to analyze the dynamic proteome and phosphoproteome in the human intestine exposed to ischemia and reperfusion. To this end, we used two complementary MS-based technologies: LC-MS/MS (phospho)proteomics to gain in-depth quantitative information and MALDI MSI of tryptic peptides to obtain spatial information and study location-specific protein changes.

MATERIALS AND METHODS

Patients and experimental procedure

Human intestinal tissues exposed to ischemia and reperfusion were obtained using a controlled *in vivo* experimental model. The study was approved by the Medical Ethical Committee of the Maastricht University Medical Center+ and written informed consent was obtained from all patients. Nine patients (sex 3M/6F; median age 66 years, range 43–84 years) undergoing pancreatoduodenectomy were included in the study. The experimental procedure was performed as described previously[5]. In short, a 6 cm jejunal segment, which is routinely resected as part of the surgical procedure, was isolated and subjected to ischemia by placing vascular clamps across the mesentery. After 45 min, one-third of the ischemic segment was resected (45I). Next, clamps were removed to start reperfusion. Another segment of isolated jejunum was removed after 30 min (30R) and 120 min of reperfusion (120R). Finally, a jejunal segment that was not exposed to IR but underwent similar surgical handling was resected (control, Ctrl). Jejunal tissue samples were immediately snap-frozen and stored at −80 °C.

LC-MS/MS analysis

Cell lysis and protein digestion

Tissue samples were treated with sodium deoxycholate (SDC) 1% to induce cell lysis. The buffer also contained 10 mM tris(2-carboxyethyl)-phosphine hydrochloride (TCEP), 40 mM chloroacetamide, 100 mM TRIS pH 8.0, further supplemented with a protease inhibitor (cOmplete

mini ethylenediaminetetraacetic acid (EDTA)-free; Roche, Basel, Switzerland) and a phosphatase inhibitor (PhosSTOP, Roche). The samples were sonicated with a Bioruptor Plus (Diagenode, Liege, Belgium) for 15 cycles of 30 s. The protein amount in each sample was quantified by a Bradford protein assay. Next, proteins were digested overnight at 37 °C with Lys-C (FUJIFILM Wako pure chemical corporation, Osaka, Japan) and trypsin (SigmaAldrich, Zwijndrecht, The Netherlands), with enzyme to protein ratios of 1:75 and 1:50, respectively. SDC was precipitated by the addition of 2% formic acid (FA), and peptides were desalted using Sep Pak C18 cartridges (Waters Corporation, Milford, Massachusetts) to subsequently be dried down and stored at −80 °C.

Phosphopeptide enrichment

Phosphopeptides were enriched by Ti(IV)-IMAC; 500 µg of beads were packed into microtip columns and washed with methanol and a loading buffer made of 80% acetonitrile (ACN) and 6% trifluoroacetic acid (TFA). Then, 200 µg of peptides per sample was dissolved in loading buffer and subsequently loaded into the columns. Peptides were washed with 50% ACN/0.5% TFA in 200 mM NaCl, followed by a second wash with 50% ACN/0.1% TFA. Phosphopeptides were eluted with 10% ammonia and 80% ACN/2% FA directly into 10% FA. The samples were dried down and stored at −80 °C until LC-MS/MS analysis. A detailed description of this protocol was published elsewhere[18].

Data acquisition by LC-MS/MS

The samples were analyzed using a UHPLC 1290 system (Agilent, Santa Clara, California) coupled to an Orbitrap Q Exactive HF (Thermo Fisher Scientific, Waltham, Massachusetts). The nanoflow rate (~300 nL/min) was achieved by passively splitting the flow using an external valve[19]. Peptides were first trapped into a precolumn (an inner diameter [ID] of 100 µm and 2 cm length; packed in-house with 3 µm C18 ReproSil particles [Dr. Maisch GmbH]) and eluted into an analytical column (ID of 75 µm and 50 cm length; packed in-house with 2.7 µm Poroshell EC-C18 particles [Agilent]). We used a two-system buffer consisting of solvent A (0.1% FA in water) and B (0.1% FA in 80% ACN). Peptides were trapped for 5 min at a 5 µL/min flow rate with solvent A before switching to a nanoflow of ~300 nL/min. For the measurement of the full proteome, we used a 155 min gradient from 10 to 36% of solvent B. On the other hand, for the phosphoproteome, we used a 95 min gradient from 8 to 32% of solvent B. Both methods included a wash with 100% solvent B for 5 min followed by a column equilibration with 100% solvent A during the last 10 min.

The mass spectrometer was operated in a data-dependent acquisition mode. For the proteome analysis, full scan MS was acquired from *m/z* 375–1600 with a 60,000 resolution at *m/z* 200. The accumulation target value was set to 3×10^6 ions with a maximum injection time of 20 ms. Up to 15 of the most intense precursor ions were isolated (*m/z* 1.4 window) for fragmentation using high energy collision-induced dissociation (HCD) with a normalized collision energy of 27. For MS2 scans, an accumulation target value of 1×10^5 ions, a maximum injection time of 50 ms, and a dynamic exclusion time of 24 s were selected. Scans were acquired from *m/z* 200–2000 with a 30,000 resolution at *m/z* 200. For the phosphoproteome, the same settings were used with the exception of the dynamic exclusion window, which was set to 16 s. The electrospray voltage was set to 1.9 kV during the measurement of all samples.

Data processing

Raw files were processed with MaxQuant (version 1.6.17.0) using a false discovery rate (FDR) <0.01. The default settings were used, with the following exceptions: variable modifications, specifically methionine oxidation, protein N-term acetylation and serine, threonine and tyrosine phosphorylation were selected. Cysteine carbamidomethylation was selected as a fixed modification. Label-free quantification was performed and we enabled the 'match between runs' option with the default values. Database search was conducted against the human reviewed Swiss-Prot database (October, 2020).

The results were uploaded to Perseus (version 1.6.0.2) for subsequent analysis. For the proteome only proteins identified by more than one unique peptide were considered, and for the phosphoproteome only phosphosites with a localization probability score >0.75 were kept for further analysis. Decoys and potential contaminants were removed. The intensities were log 2 transformed and normalized by median subtraction. Finally, all values were filtered to keep only those proteins (or phosphosites) that were detected in a minimum of two out of three replicates for at least one condition. Missing values were replaced using a normal distribution applying a downshift of 1.8 times the standard deviation of the dataset and a width of 0.3 times the standard deviation.

An analysis of variance (ANOVA) test ($p<0.05$) was used to keep only significantly changing proteins (or phosphosites) among the different conditions. Z-scored intensities were visualized using the Complex Heatmap package in R, applying a combination of k-means and hierarchical clustering. K-means clusters were set to 4 and 6 for proteome and phosphoproteome, respectively. This number was chosen based on the gap statistic method, which estimates the optimal number of groups for a given dataset[20]. Next, we used the Pearson correlation distance with average linkage for clustering. Gene ontology (GO) analysis was done using the STRING web tool[21]; enriched GO terms were filtered to keep only those with $p<0.01$, fold enrichment (Log 10[observed/expected]) >5, and a minimum of five proteins per term. The list of terms was further condensed by the removal of redundant terms using the Revigo web tool[22].

Sequence logos for motif analysis were obtained implementing previously described algorithms in R[23]. Briefly, each sequence logo displays over- and underrepresented residues in each position of the sequence window centered on the phosphorylated residue. Calculations are based on the frequency change between a foreground (phosphosites from each cluster) and a background (all detected phosphosites). For kinase enrichment analysis, we used the online tool KEA2 to look for phosphosites previously linked to effector kinases[24]. In addition, we applied post-translational modification signature enrichment analysis (PTM-SEA), which looks for the enrichment of phosphosite-specific "signatures" related to specific kinases, signaling pathways, or perturbations previously reported in the literature[25].

MALDI MSI analysis

Tissue preparation for MALDI MSI analysis

Fresh frozen tissues were sectioned at 10 µm thickness at −20 °C using a cryostat (Leica, Leica CM1860, Leica Biosystems) and thaw-mounted onto clean indium tin oxide (ITO)-coated glass slides (Delta Technologies LTD, Loveland). A within-subjects experimental design was pursued, i.e., all four

different tissue sections (Ctrl, 45I, 30R, and 120R) from one patient were always mounted on the same ITO slide. Mounted tissue sections were dried in a vacuum desiccator for 20 min, followed by three 2-min washes in 100% ethanol and then two 5 min washes in water. Fresh ethanol/water was used in every wash, and sections were not dried between steps. Antigen retrieval was performed in a 10 mM citric acid buffer (Sigma-Aldrich) (pH 6.0) for 20 min using the Antigen Retriever 2100 (Aptum Biologics, Rownhams, U.K.). Sections were allowed to cool down for 20 min, rinsed with water, and dried in a vacuum desiccator. Prior to trypsin digestion, 1 µL of 1 mg/ mL cytochrome c (from equine heart, Sigma-Aldrich) was applied on the slide, away from the tissue, to evaluate digestion efficacy. Water-dissolved porcine trypsin (20 µg/mL) was sprayed onto the tissue samples using a SunCollect pneumatic sprayer device (Sunchrom GmbH, Friedrichsdorf, Germany) in 15 layers (flow rate: 10 µL/ min, speed: 900 mm/min, track spacing: 1 mm, spray head distance: 25 mm). Afterward, the samples were incubated at 37 °C for 17 h in an airtight box containing 50% methanol. Finally, slides were coated with 5 mg/mL α-cyano-4-hydroxycinnamic acid (Sigma-Aldrich) in 50% acetonitrile and 0.2% trifluoroacetic acid using the SunCollect sprayer device. The matrix was applied in a series of seven layers with the increasing flow rate starting at 10 µL/ min followed by 20, 30, and 40 µL/min for all subsequent layers (speed: 1390 mm/min, track spacing: 2 mm, spray head distance: 25 mm). Prior to matrix application, slides were scanned (Super Coolscan 5000 ED, Nikon) to obtain high-quality optical images.

MALDI MSI data acquisition

High-speed MALDI-TOF MSI analysis was performed on a RapifleX MALDI Tissuetyper (Bruker Daltonics GmbH, Bremen, Germany) equipped with a 10 kHz Nd:YAG (355 nm) laser. The instrument was operated in a positive ionization reflectron mode, and peptide spectra were acquired in a mass range *m/z* 620–3000 with a spatial raster of 50 µm and 500 averaged laser shots per pixel. An experimental mass resolution of 15,000 was achieved at *m/z* 1000. High mass resolution MALDI-Fourier-transform ion cyclotron resonance (FTICR) MSI experiments were performed with a Solarix 9.4 T (Bruker Daltonics), achieving an experimental mass resolution of 200,000 at *m/z* 1000. MSI data were acquired within a mass range of *m/z* 800–3000 (1×10^6 data points) in a positive ionization mode with a transient time of 2.94 s. The spatial raster width was 70 µm. At each pixel, 600 shots were accumulated with a laser frequency of 500 Hz. Data acquisition was controlled using ftmsControl and FlexImaging 4.1 (Bruker Daltonics). All MSI measurements were preceded by an instrument calibration using Red phosphorus. MALDI-TOF analysis was performed on 36 tissue samples from nine patients. MALDI-FTICR MSI measurements were performed on selected samples (four conditions from one patient) to improve the identification of the proteins behind the relevant peptides obtained from TOF analysis.

Histological staining and tissue annotation

After MSI analysis, the matrix was removed by submersion in 70% ethanol and tissues were stained with hematoxylin and eosin (H&E). Optical images of H&E-stained tissues were obtained with a MIRAX desk scanner (Sysmex, Etten-Leur, The Netherlands). The MSI images were coregistered with the corresponding histological images in the FlexImaging software (v5.0, Bruker Daltonics), which allows the annotation of the histological regions of interest: mucosa, submucosa, and muscle layers.

MSI data pre-processing

MALDI-TOF MSI data were recalibrated using FlexAnalysis v3.4 (Bruker Daltonics). Cubic-enhanced calibration function was performed with a 500 ppm peak assignment tolerance and using *m/z* 868.5, 1138.6, 1562.8, 2115.2, 2567.3, and 2869.3 as calibrants. A total of 36 (nine patients with four conditions each) MALDI-TOF MSI datasets were imported into SCiLS 2019c (Bruker Daltonics), where mass spectra were normalized to their total ion count. Peak picking was performed on the overall mean spectrum in mMass[26] using the following settings: 35 precision baseline correction, deisotoping with an isotope mass tolerance of *m/z* 0.1, isotope intensity tolerance of 50%, and a signal to noise (S/N) ratio of 7. The peak list was then imported back into SCiLS to create a data matrix containing every annotated region and sample the maximum intensity in each peak interval (*m/z* ±0.2).

The average spectra of the MALDI-FTICR MSI datasets were recalibrated in mMass with linear correction using the tryptic peptides of histone H2A (*m/z* 944.5312; pos. 22–30 "AGLQFPVGR") and histone H4 (*m/z* 1325.7535; pos. 25– 36 "DNIQGITKPAIR") and known trypsin autolysis products at *m/z* 842.5094 (pos. 108–115 "VATVSLPR") and *m/z* 1045.5637 (pos. 98–107 "LSSPATLNSR"). Peak picking on those recalibrated spectra was performed in MATLAB R2018 (Mathworks, Natick, Massachusetts) using the following settings: TopHat filter (window: 30 dp) for baseline correction, Gaussian smoothing (window: 20 dp), a minimum intensity for peak picking of 500, deisotoping with an isotope mass tolerance of 0.02 *m/z* and isotope intensity tolerance of 50%.

Statistical analysis MALDI-TOF MSI data

An outlier detection was performed based on a cytochrome c spot applied onto every slide prior to trypsin digestion. For this, peak picking was limited to known peptides of cytochrome c, which resulted in the consideration of four signals (HKTGPNLHGLFGR, *m/z* 1433.77; HKTGPNLHGLFGRK, *m/z* 1561.87; TGPNLHGLFGRK, *m/z* 1296.72; TGPNLHGLFGR, *m/z* 1168.62). Using these four features, principal component analysis (PCA) was performed on the average intensity in the cytochrome c spot from each slide (N=9) in SCiLS. Any measurement outside the 95% confidence ellipse in the PC1–PC2 score plot was considered an outlier.

The data matrix from the included patients was exported for statistical analysis in R (v3.5.1). Trypsin-related peaks were determined by Pearson correlation >0.9 to the *m/z* 842.5 and excluded from analysis (removal of six peaks). Statistically significant differences in peak intensities between the conditions (Ctrl, 45I, 30R, 120R) were tested for each histological layer separately (mucosa, submucosa, muscle). The intensities for every peak were compared using a repeated measurements ANOVA. P-values were corrected for multiple testing by Benjamini–Hochberg and p-values <0.01 were considered statistically significant. As several tissue sections lacked the muscle layer, statistical analysis could not be performed for the muscle layer.

Protein identification strategy

MALDI-FTICR MSI experiments were performed on selected samples to obtain high mass-resolution data of tryptic peptides, which was used to identify the proteins behind the significantly changed peptides from MALDI-TOF MSI statistics. These significantly changed *m/z* values were matched with

a tolerance of ±80 ppm to the peaks in the MALDI-FTICR MSI measurements. Next, these accurate peptide masses were matched with the masses of the (phospho)peptides detected using LC-MS/MS and corresponding identified protein with a tolerance of ±6 ppm. As there is no alkylation and reduction step in the MSI workflow, the peptide masses of the LC-MS/MS were adapted by subtracting the mass shift (*m/z* 57.02146) caused by the formation of S-carboxyamidomethylcysteine for every cysteine in the peptide.

The matching and identification process was performed using four FTICR MSI datasets (data was obtained from one patient across all four conditions). The annotation of a protein was accepted if mass matching from TOF to FTICR (with ±80 ppm tolerance) and FTICR to LC-MS/MS (with ±5 ppm tolerance) resulted in one matching protein ID and this in at least three out of the four FTICR datasets. In cases where two FTICR peaks were detected in the analogous mass range in the TOF spectrum, the most intense FTICR peak (>10 fold higher) within this window was selected for mass matching with the LC-MS/MS data

Data availability

The mass spectrometry proteomics and phosphoproteomics datasets have been deposited to the ProteomeXchange Consortium via the PRIDE[27] partner repository with the data set identifier PDX026076.

RESULTS

Changes in protein expression and protein phosphorylation during IR of the human intestine were studied by combining a quantitative MS-based (phospho)proteomics approach with imaging MS. The dynamic (phospho)proteome during IR was investigated by analyzing tissue samples collected after 45 min of ischemia (45I), 30 and 120 min of reperfusion (30R and 120R), and in control tissue (Ctrl). A schematic of the experimental design and data analysis workflow are depicted in **Figure 1**.

Proteomics

LC-MS/MS analysis resulted in the identification and quantification of 2562 proteins. The correlation between biological replicates was high (Pearson r>0.9), with the exception of one 30R sample (r<0.85), which was therefore excluded from further analysis (**Figure S1**). Cluster analysis of the complete proteome showed that the two main clusters were represented by 45I and Ctrl samples, on the one hand, and 30R and 120R samples, on the other hand (**Figure S2**). Analysis of dynamic changes in the proteome revealed that the abundance of 239 proteins was significantly altered during IR (**Table S1**). Hierarchical clustering of these differentially expressed proteins resulted in four main clusters reflecting distinct temporal expression profiles (**Figure 2a**) and clearly distinguished the proteins decreasing (clusters 1 and 2) and proteins increasing in abundance (clusters 3 and 4) during reperfusion.

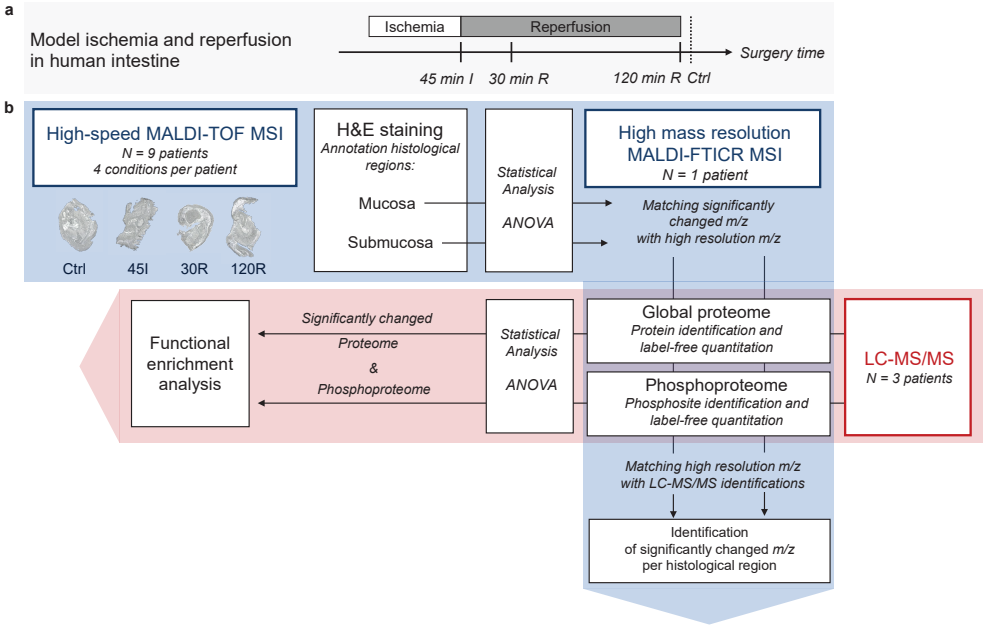

Figure 1. Experimental design and data analysis workflow. ***a****) Experimental model of ischemia-reperfusion in human intestine, with tissue collection after 45 min of ischemia (45I), 30 min of reperfusion (30R) and 120 min of reperfusion (120R), and tissue not exposed to ischemia-reperfusion (Ctrl).* ***b****) Mass spectrometry and data analysis workflow. The red area shows the workflow of LC-MS/MS measurement and subsequent data analysis. The blue area shows the MS imaging (MSI) measurements.*

Functional enrichment analysis of the dynamic proteome

To gain global functional insight into the changing proteome during IR, we performed GO term enrichment analysis of differentially expressed proteins. These proteins were predominantly involved in processes such as intestinal absorption and digestion, cell junction organization, and innate immune responses (**Figure 2b**). In line with this observation, overrepresented cellular component GO terms included brush border and microvillus, actin filament, and cell–cell contact zone. Proteins in cluster 1 of the changing proteome, showing a decrease in abundance at 30R, which restored at 120R, were related to various processes such as protein translation, including EIF2S2, EIF4EBP1, EIF5B, and the cellular response to stress, such as HSPA4, TNIK, Nup50, and LAMTOR1.

Protein abundances in cluster 2 decreased during reperfusion (**Figure 2c**) and were significantly enriched for GO terms related to intestinal digestion/absorption, microvillus, and cell junction (**Table S2**). Moreover, network analysis of the total changing proteome showed interactions of proteins involved in these GO terms. The majority of interacting proteins in these networks exhibited the same temporal profile (cluster 2; **Figure 2d**, blue fill). Proteins involved in digestion and absorption included IFABP, LCT, ANPEP, NAALADL1, and SLC5A1 (**Figure 2d**, left). Proteins associated with microvillus organization included actin-bundling proteins such as VIL1, ESPN, and PLS1, motor protein MYO1A, anchoring protein EZR, and microvillus–microvillus adhesion molecules CDHR2 and MYO7B. Other

proteins playing a role in actin filament organization were COBL and MAP7. In addition, various proteins playing an important role in cell–cell junction organization were decreased, such as CDH1, CDH17, CDHR5, CDHR2, AFDN, NECTIN-1, F11R, EpCAM, and CD2AP and CGN (**Figure 2d**, right; **Table S1**).

Cluster 3 showed an opposite expression profile with increased protein levels during reperfusion. Overrepresented GO terms in this cluster were predominantly associated with the innate immune response, in particular the complement pathway (**Figure 2c**). Both regulatory and effector proteins of the complement cascade were significantly increased at reperfusion and included C3, C5, C6, C8B, PROS1, and F2, which were all among the top 20 proteins showing the highest fold change amongst conditions, and exhibited very similar temporal profiles. In addition, various proteins in cluster 3 were involved in an extracellular matrix organization, including COL15A1, COL18A1, FBN1, NID2, ITGA, and JAM3. One of the protein interaction networks, resulting from network analysis of the complete changing proteome, contained mostly proteins of cluster 3 and showed interactions of complement proteins and proteins related to extracellular matrix organization (**Figure 2e**, red fill).

Proteins in cluster 4 gradually increased in abundance during ischemia and reperfusion and were involved in a variety of biological processes without a clear overrepresentation, and included the metabolism of amino acids, metabolism of nucleotides, post-translational protein modification, and cellular response to stress. Interesting proteins in this cluster include CYGB, SQSTM1, and CASP1.

In addition to the protein interaction networks that could be linked to clusters 2 and 3, another network showed interactions of proteins located in all four clusters and thus showing distinct temporal profiles (**Figure S3**). These proteins were associated with the cellular response to stress, protein, and RNA metabolism.

Phosphoproteomics

LC-MS/MS analysis resulted in the identification and quantification of 1802 phosphosites derived from 1214 proteins (whole phosphoproteome). The observed distribution of phosphosites was 90% phosphoserine, 9.8% phosphothreonine, and 0.2% phosphotyrosine (**Figure S4a**). The majority of these phosphosites had a high localization probability score, indicative of accurate localization of the phosphorylated residue in the peptide backbone (**Figure S4b**). In total, 305 phosphosites on 162 proteins showed a significant change during IR (dynamic phosphoproteome) (**Table S3**).

Prediction of the kinases responsible for detected phosphorylation

A kinase enrichment analysis for all detected phosphosites was performed to get an overview of which kinases were potentially active during IR. Here, 279 detected phosphosites were mapped to putative effector kinases (**Figure S4c**). Some of these kinases, such as GSK3B and casein kinase II, are constitutively active and participate in a myriad of cellular processes. We also predicted the activity of cyclin-dependent kinases (CDK), namely, CDK1 and CDK2, both involved in cell cycle control. Finally, we detected putative targets of the mitogen-activated protein (MAP) kinases MAPK9 (JNK2) and MAPK10 (JNK3), part of the JNK signaling pathway, and MAPK14 (p38α), part of the p38 MAP kinase pathway, which are both activated in response to cellular stress. The full list of targets related to each of these kinases are listed in **Table S4**.

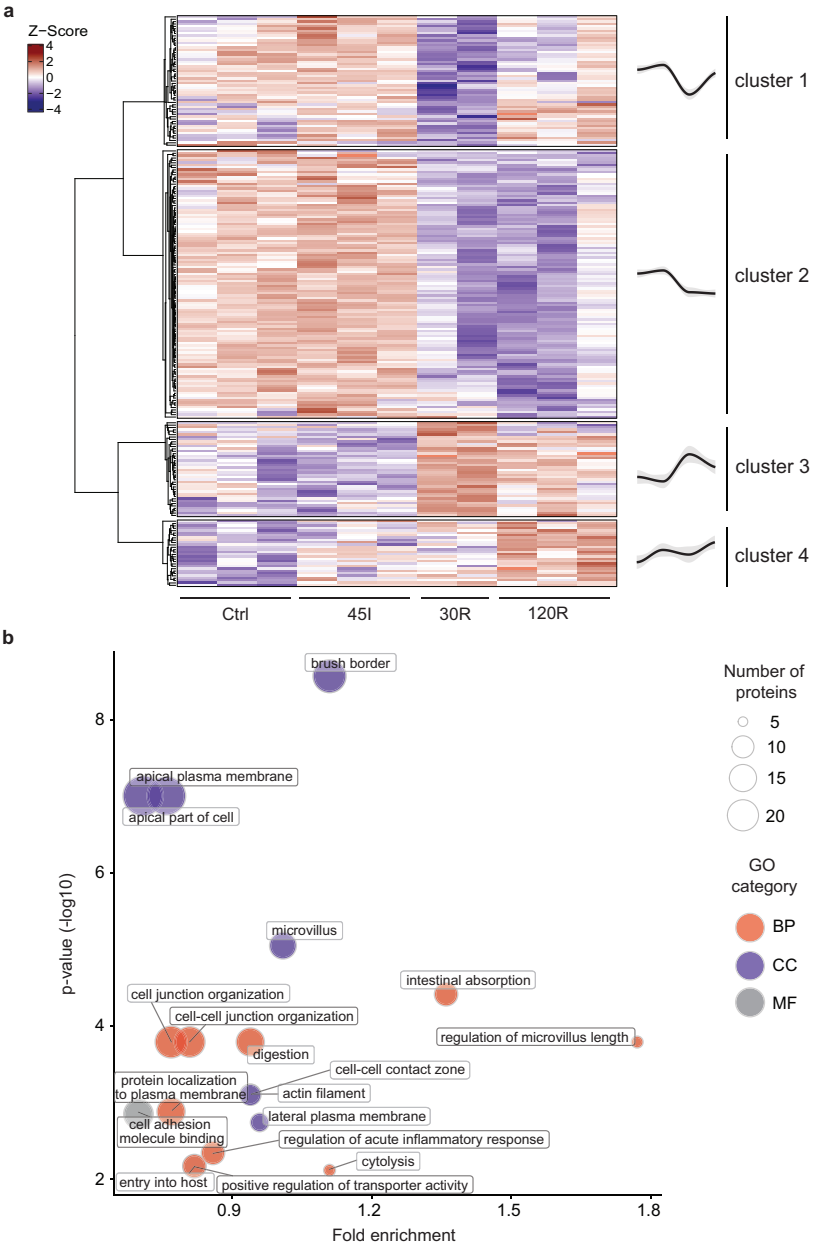

Figure 2. The dynamic proteome during ischemia-reperfusion in the human intestine. ***a***) *Heatmap visualizing clustering of differentially expressed proteins. Hierarchical clustering was based on Z-scores of the log2 values of differentially expressed proteins. The ANOVA test was perfromed and p<0.05 was considered statistically significant. Average temporal profiles are shown for every cluster (a grey area represents CI).* ***b***) *Functional enrichment analysis of differentially expressed proteins. Overrepresented Gene Ontology (GO) terms are shown (p<0.05). GO term fold enrichment (log10[observed/expected]) is plotted against p-value (-log10). The size of the dot correlates with the number of proteins linked to that GO term, as indicated in the legend. Red, GO biological processes; blue, GO cellular component, grey, GO molecular function.*

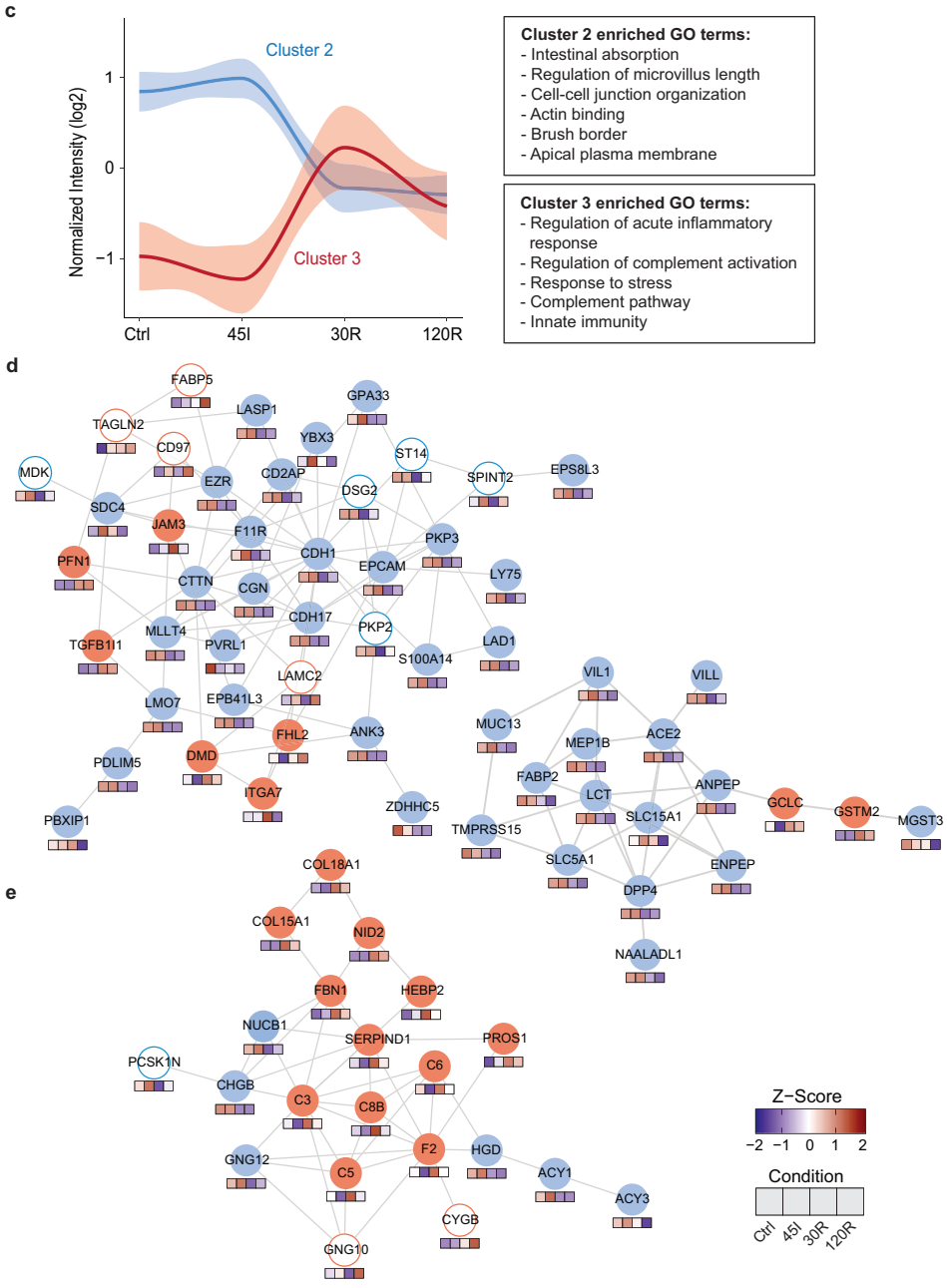

Figure 2 continued. ***c****) Dynamic profile for proteins in cluster 2 (blue) and 3 (red) is shown, as well as corresponding overrepresented GO terms.* ***d, e****) Protein networks showing interacting proteins. Networks were generated using STRING. The color of the circle indicates the temporal profile (cluster) of the protein. Blue line, cluster 1; blue fill, cluster 2; red fill, cluster 3, red line, cluster 4. Color cubes below each protein indicate the Z-score intensity in Ctrl, 45I, 30R and 120R respectively. The majority of proteins in the networks in panel d are located in cluster 2 (blue fill). The majority of proteins in the network in panel e are located in cluster 3 (red fill).*

Kinase enrichment analysis focused on the 305 significantly regulated phosphosites (**Table S3**) and mapped 47 phosphosites to potential effector kinases (**Figure S4d**). Notably, putative substrates of several MAP kinases, like MAPK9 (JNK2), MAPK3 (ERK1), MAPK13 (p38δ), and MAPK8 (JNK1) were present. Dynamic phosphosites linked to casein kinase II and CDKs were detected as well. The full list of phosphosites and predicted effector kinases can be found in **Table S5**.

Clustering and motif enrichment of the dynamic phosphoproteome

Hierarchical clustering of altered phosphosites resulted in six distinct groups and revealed a highly dynamic regulation of protein phosphorylation during the course of ischemia and reperfusion (**Figure 3a**). In contrast to the global proteome, phosphorylation changes occur rapidly, already following ischemia. Kinases recognize their substrate partly through certain sequence motifs near the phosphorylation site, and some of these motifs are associated with specific kinases. Motif analysis revealed differences in its composition amongst clusters (**Figure S5**). First, we observed that proline-directed phosphorylation comprised almost half of the significantly changed phosphosites (144 out of 305). These were spread across all six clusters. Amongst the non-proline-directed motifs, the clusters 1, 2, 5, and 6 showed predominantly acidic motifs characterized by the presence of aspartic and glutamic acid. Cluster 3 showed basic residues upstream of the phosphorylation site, and cluster 4 was mostly comprised of proline-directed phosphosites. These results show how the activity of different kinases changes during the different stages of IR injury.

Functional enrichment analysis of the proteins with significantly regulated phosphorylation

In general, differentially phosphorylated proteins were involved in the regulation of mRNA processing and RNA splicing, supramolecular fiber organization/cytoskeleton, and cell junction organization (**Figure 3b**). Related molecular functions – e.g., RNA polymerase binding and actin binding – and cellular components – e.g., spliceosomal complex, actin cytoskeleton, and adherence junction – were overrepresented as well. In contrast to the changing proteome, the GO analysis per cluster revealed that differentially phosphorylated proteins related to the same biological process appeared in different clusters (**Table S6**). Moreover, changing phosphosites from the same protein were represented in different clusters, for instance, phosphosites on MISP (clusters 2–5) or SRRM2 (clusters 1, 3, 5) (**Table S3**).

Next, similar to the proteome data, we explored the connectivity and association of dynamically phosphorylated proteins. The network analysis showed that many of the phosphorylated proteins were related to either cell junctions or RNA splicing, forming discrete networks of highly interconnected proteins (**Figure 3c**). This highlights that proteins related to these two biological processes are highly regulated by phosphorylation during IR.

Altered phosphorylation of RNA splicing factors was observed for various serine/arginine proteins, including SRRM2, SRRM1, and SRSF2 (**Figure 3d**). In addition, several heterogeneous nuclear ribonucleoproteins were found to show changes in phosphorylation and included HNRNPK and HNRNPC (**Figure 3d**). Differentially phosphorylated proteins related to cell junction organization included cadherin-associated CTNND1, scaffolding proteins such as ZO-1 (TJP1), and other proteins contributing to cell adhesion and related cytoskeleton organization, including CTTN, DSP, and

SYNPO2 (**Figure 3d**). Phosphorylated proteins associated with supramolecular fiber organization included STMN1 and ESPN.

Exploration of specific phosphosites with known functionality

After focusing on the proteins that displayed dynamic phosphorylation during IR, we next explored our data for phosphosites with a previously studied functionality. By applying PTM-SEA to all of the phosphosites detected, various signatures were found to be regulated during IR injury (**Figure S4e**). Overall, control and ischemic samples showed a lower expression of phosphosites related to the growth factor response (e.g., EGF treatment and ERK2/MAPK1 signature) and cell division (e.g., CDK1 and CDK2 signatures), with the lowest intensities observed during ischemia. In contrast, 30 min reperfusion presented a high intensity of phosphosites related to growth factor stimulus. A similar trend was observed for CDK targets, which were highly phosphorylated during the reperfusion conditions when compared to the control and ischemic samples.

When looking at the individual trend of biologically relevant phosphosites belonging to these signatures, we encountered phosphorylation on transcription factor ATF2, namely, T69 and T71, to be upregulated upon ischemia, peaking at 30 min reperfusion and dropping at 120 min (**Figure 3d**). On the other hand, phosphorylation on the ribosomal protein RPS6, a known marker of active translation, increased drastically at 30 min reperfusion. Potential targets of MAP kinases and CDKs were upregulated during reperfusion times, such as S405 and S418 of CTTN and S25 and S38 of STMN1 (**Figure 3d**). The latter two proteins are related to cytoskeleton organization.

Proteins showing regulated phosphosites as well as significant alterations in abundance

When looking at the overlap between the proteome and the phosphoproteome, we found that twenty-two of the differentially phosphorylated proteins were also found to be significantly changed in abundance at the protein level. Among these overlapping proteins, a major part (16/22) was located in cluster 2 of the changing proteome, and hence these proteins showed a decrease in abundance during reperfusion and the majority was related to cell junction and cytoskeleton (e.g., CDHR5, CTTN, CGN, MYO7B, and ESPN) and digestion/absorption (e.g., LCT, SLC9A3R). For these 16 proteins, almost half of the phosphorylation changes occurred already at 45I (27 changing phosphosites in clusters 1, 2, 5, and 6 versus 29 altered phosphosites in clusters 3 and 4), indicating that alterations in phosphorylation preceded a decrease in their abundance.

On-tissue imaging of tryptic peptides using MALDI-TOF MSI

Next to IR-induced proteomic changes in whole tissues, we explored histological region-specific protein changes. Highspeed MALDI-TOF MSI enabling bottom-up tissue proteomics experiments were performed on a total of 36 tissue sections belonging to nine patients (four experimental conditions per patient: Ctrl, 45I, 30R, 120R). Prior to imaging proteins underwent tryptic on-tissue proteolysis. As digestion efficiency greatly influences signal intensities of tryptic peptides, a spot of cytochrome *c* was added to each slide as a quality control[28], and its digestion profile was used to detect outliers. Based on PCA analysis of the average cytochrome c mass spectrum, one out of nine patient datasets was excluded from analysis (**Figure S6**). **Figure 4a** shows the average peptide spectrum across all control tissues.

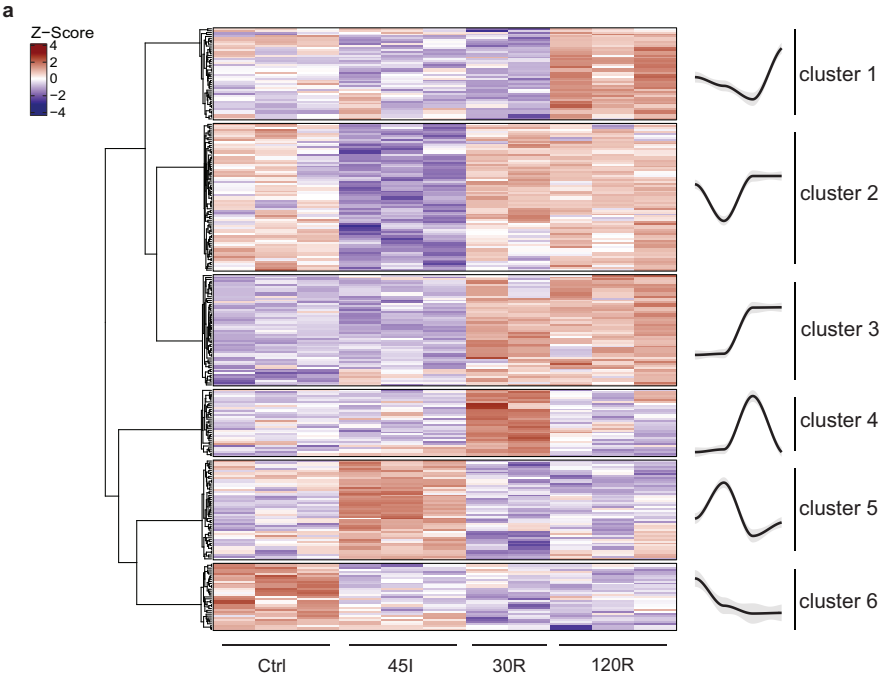
a
Z−Score
4
2
0
−2
−4
cluster 1
cluster 2
cluster 3
cluster 4
cluster 5
cluster 6
Ctrl
45I
30R
120R

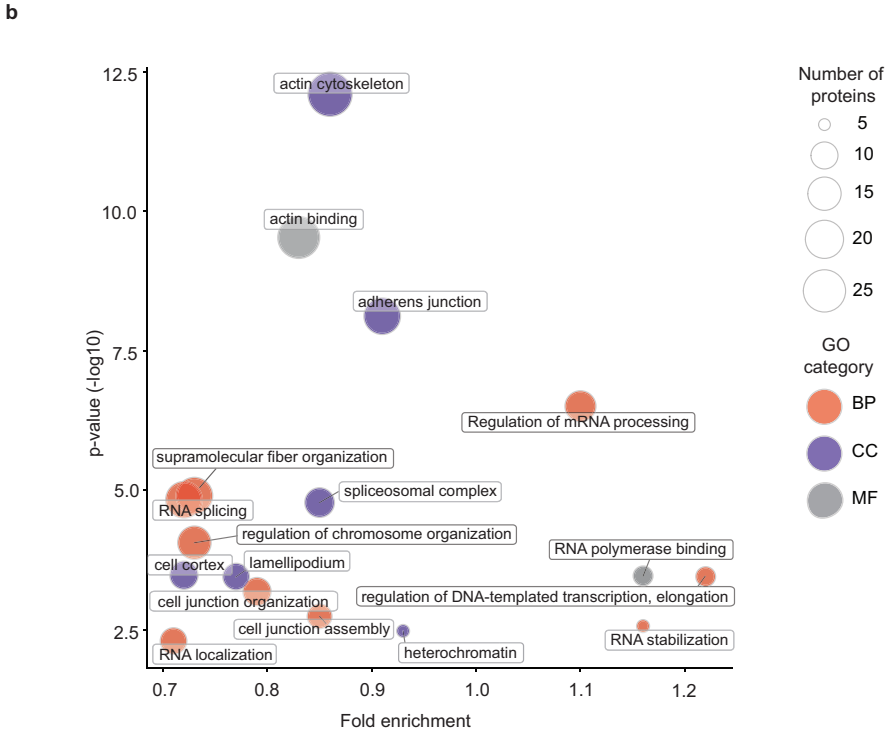
b
12.5
10.0
7.5
5.0
2.5
p-value (-log10)
0.7
0.8
0.9
1.0
1.1
1.2
Fold enrichment
actin cytoskeleton
actin binding
adherens junction
Regulation of mRNA processing
supramolecular fiber organization
RNA splicing
spliceosomal complex
regulation of chromosome organization
cell cortex
lamellipodium
cell junction organization
cell junction assembly
RNA localization
heterochromatin
RNA polymerase binding
regulation of DNA-templated transcription, elongation
RNA stabilization
Number of proteins
5
10
15
20
25
GO category
BP
CC
MF

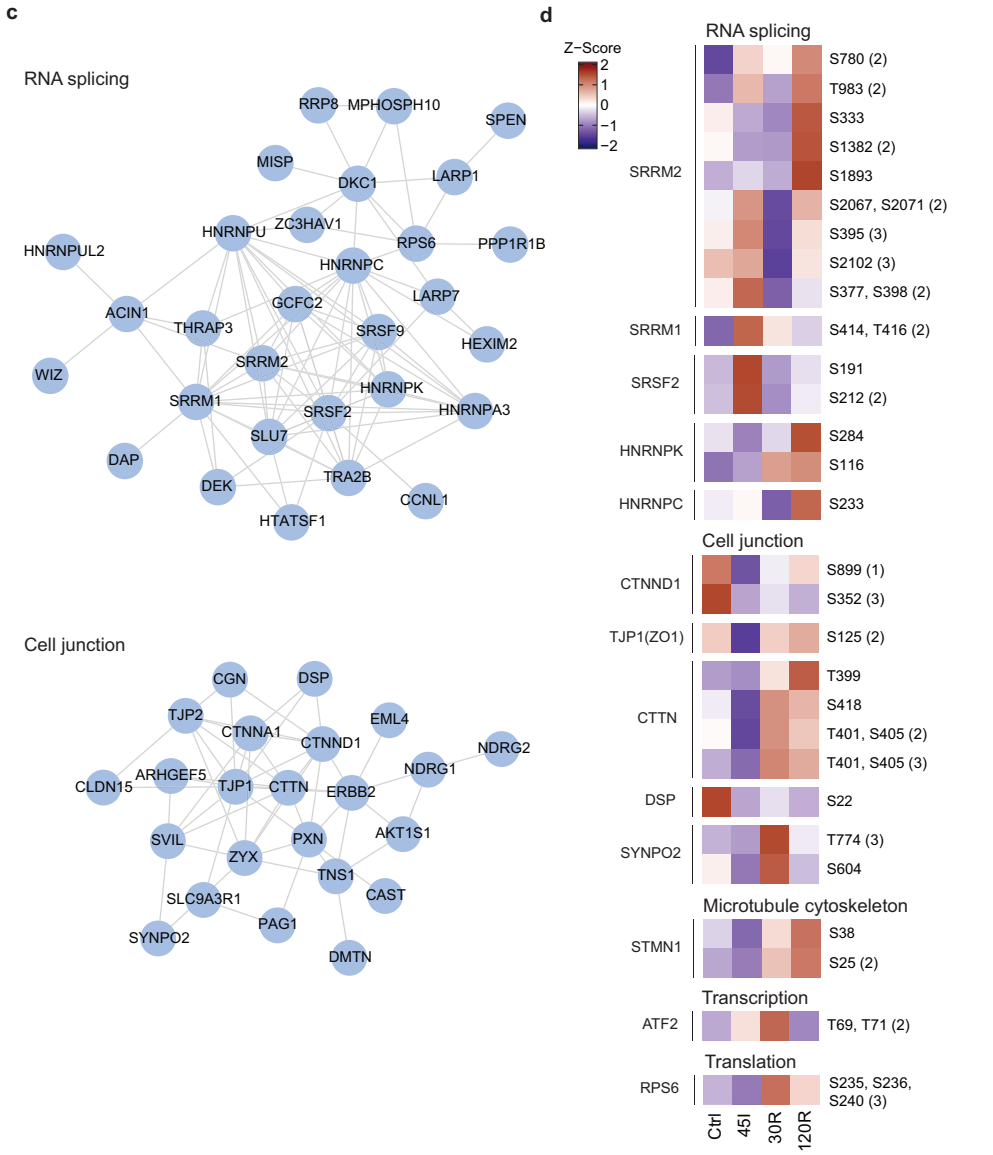

Figure 3. The dynamic phosphoproteome during ischemia-reperfusion in the human intestine. ***a****) Heatmap visualizing clustering of changing phosphosites, and average temporal profiles for every cluster (grey area represents CI). Hierarchical clustering was based on Z scores of the log2 values of differentially expressed proteins. The ANOVA test was performed and p<0.05 was considered statistically significant.* ***b****) Functional enrichment analysis of differentially phosphorylated proteins. Overrepresented Gene Ontology (GO) terms are shown (p<0.05). The size of the dot correlates with the number of proteins linked to that GO term, as indicated in the legend. Red, GO biological processes; blue, GO cellular component, grey, GO molecular function.* ***c****) Networks of highly interconnected phosphoproteins related to overrepresented terms of RNA splicing and cell junction.* ***d****) Heat maps of single phosphosites related to different biological processes. Showing the Z scores of the averaged log2 intensities for each condition.*

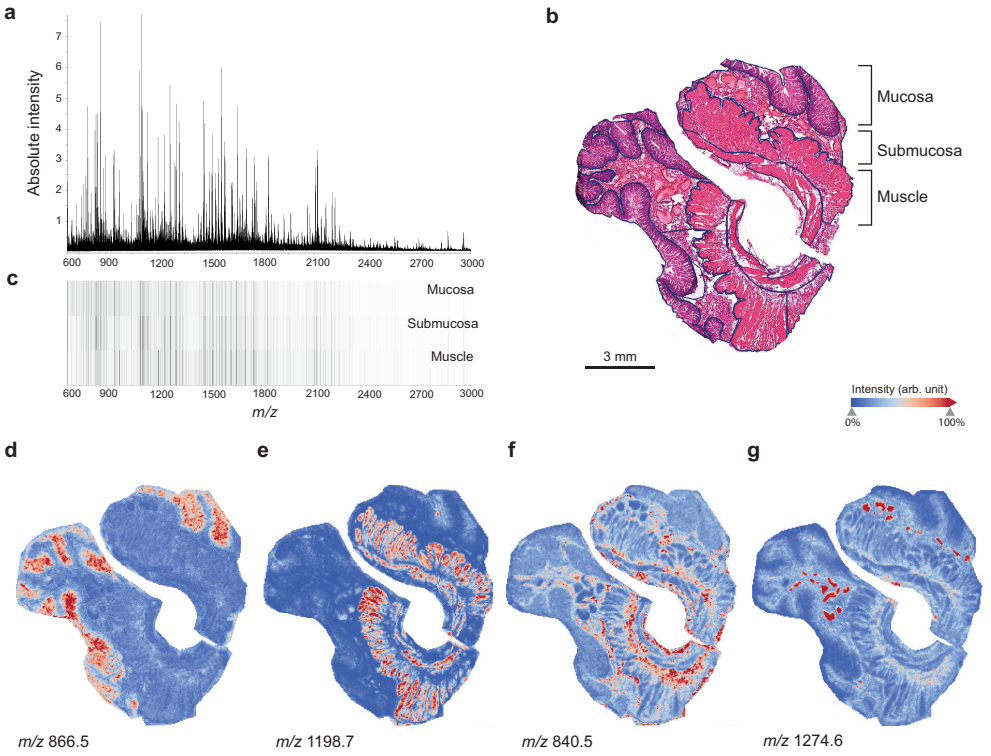

Figure 4. MALDI MSI of distinct histological structures in human small intestine. ***a****) Average mass spectrum of whole tissues (Ctrl).* ***b****) H&E staining showing annotation of histological layers mucosa, submucosa and muscle. See also Figure S7 for region annotations in all tissues.* ***c****) Heatmap visualizing intensity differences for average mass spectra obtained from mucosa, submucosa and muscle layer of the small intestine. Individual peptide images of m/z values with specific localization in* ***d****) mucosa (m/z 886.5 ± 0.2Da),* ***e****) muscle (m/z 1198.7 ± 0.2Da),* ***f****) submucosa (m/z 840.5 ± 0.2Da), and* ***g****) blood vessels (m/z 1274.6 ± 0.2Da).*

MALDI-TOF MSI of distinct histological structures in human small intestine

We first compared peptide distributions with the tissue's histology to evaluate the potential of MALDI MSI to detect region-specific IR-induced protein changes. After MALDI MSI, tissue sections were H&E-stained, and optical scans were coregistered to the MSI images. Histological regions were annotated in the H&E images (**Figure 4b** and **Figure S7**) and heat maps of average mass spectra acquired from mucosa, submucosa, and muscle regions showed distinct peptide profiles for the different histological regions (**Figure 4c**). In addition, individual peptide images showed specific localization in distinct intestinal tissue structures. For example, *m/z* 866.5 was located in the mucosa region (**Figure 4d**) and *m/z* 1198.7 in muscle (**Figure 4e**). In addition, *m/z* 840.5 was found to be associated with connective tissues of the submucosa layer but also surrounding muscle tissue (**Figure 4f**), and *m/z* 1274.6 was specifically located in blood vessels (**Figure 4g**). To identify region-specific IR-induced protein changes, we performed subsequent analysis for each histological layer separately. Since 10 out of 32 tissues did not contain muscle in the analyzed section (**Figure S7**), statistical analysis could not be performed for the muscle layer.

IR-induced changes in mucosa and submucosa

In the context of IR injury, we are particularly interested in the mucosa layer as this is the most susceptible to damage. PCA analysis of mucosa regions revealed the highest similarity between Ctrl and 45I conditions, on the one hand, and reperfusion conditions (30R, 120R) on the other hand (**Figure 5a**), which is congruent with the clustering of the LC-MS/MS proteomics data. Peak picking resulted in 319 peptide signals to be included for statistical analysis, of which 154 *m/z* values were found to be significantly changing in intensity during IR (**Table S7**). In general, signal intensities were either gradually correlated or anticorrelated to the IR sequence (Ctrl-45I-30R-120R). Remarkably, a

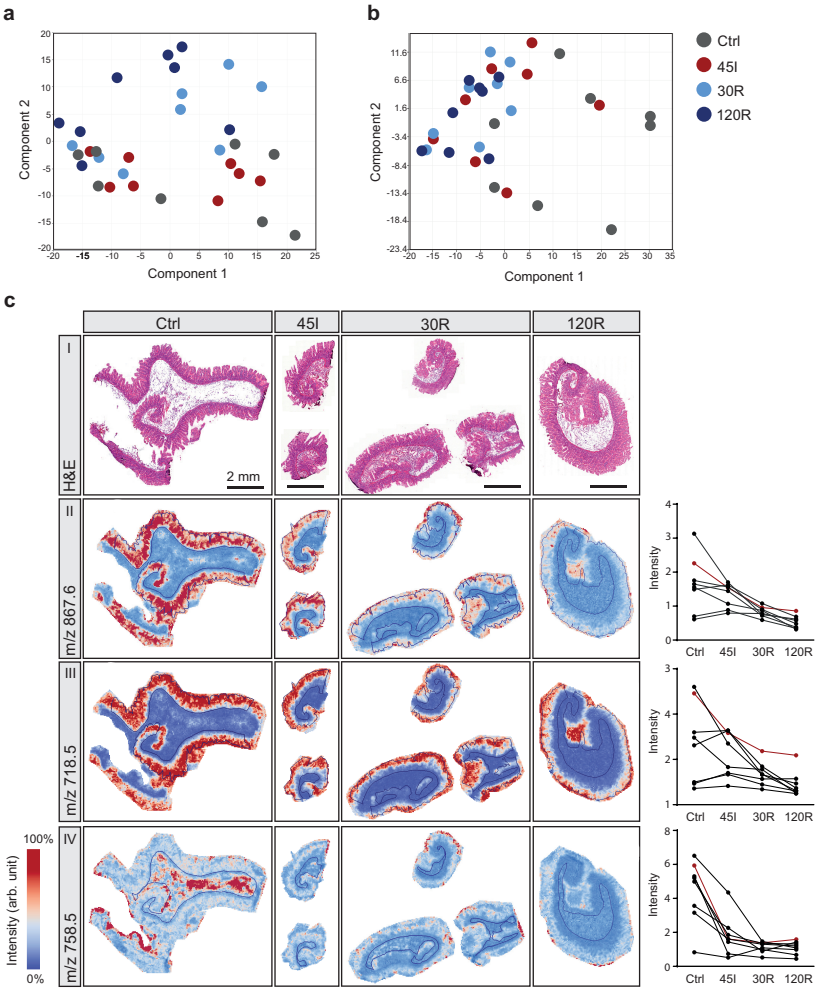

Figure 5. Region-specific changes in response to ischemia-reperfusion. *Principle component analysis of* ***a****) mucosa regions and* ***b****) submucosa regions.* ***c****) H&E staining (I) and peptide images showing high fold change peptides in the mucosa (II,III) and submucosa (IV). Corresponding graphs show intensity data for all patients (presented peptide images correspond to a red line in the graph). See also Figure S8 and Figure S9 for peptide images from all samples.*

decreasing intensity gradient was observed predominantly for peptides in the lower mass range (*m/z* <1500), whereas peptides in the higher mass range (*m/z* >1500) showed an increasing intensity gradient (**Table S7**). Images of the peptides with the 10 highest fold changes showed mucosa-specific localization and a decreasing abundance during IR in most of the patients (**Figure 5c-II**, all tissues in **Figure S8a-d**). Two of these were among the top 10 peaks with the highest intensity (**Figure S8c, d**). Interestingly, some peptides show a distribution shift from the whole mucosa in Ctrl toward the villus tips after 120R, as shown in **Figure 5c-III** (**Figure S8a**). The peaks with an increasing intensity gradient appeared to be mostly low-intensity peptides, expressed in all histological layers.

PCA analysis of submucosa regions resulted in a slightly different grouping of samples compared to the mucosa (**Figure 5b**). In total, 185 peptide signals were found to be significantly changed between IR conditions, and all showed a decreasing intensity gradient (**Table S8**). Looking at peptides exhibiting a high fold change, only a few showed specific localization in the submucosa layer (**Figure 5c-IV**, all tissues in **Figure S9a, b**). Images of high-intensity peptides better represented submucosa-specific peptide changes (**Figure S9c, d**).

Protein identification of relevant peptides obtained from MALDI-TOF MSI analysis

To link the MALDI-TOF MSI data (R=15,000 at *m/z* 1000) of peptides to the LC-MS/MS protein identifications, we used MALDI-FTICR MSI measurements (R=200,000 at *m/z* 1000) as an intermediate step to obtain more accurate mass descriptions of the peptides of interest. With regard to the mucosa, 75 out of 154 significantly changing *m/z* values from TOF-MSI could be matched to one or more peaks in the high mass resolution FTICR data. Matching these accurate *m/z* values to the LC-MS/MS (phospho)-proteome data enabled annotation of 10 proteins (**Table S9**). Performing the same analysis for the submucosa data resulted in 96 matched FTICR *m/z* values and in the annotation of 11 proteins (**Table S9**). None of the annotations were based on matched phosphopeptides. We next highlight a selection of proteins of interest, showing layer-specific localization (peptide images can be found in **Figure S10**).

Remarkably, among annotated proteins significantly changing in the mucosa, three proteins (ELAV1, SNRNP70, and HNRNPC) were associated with mRNA splicing and processing. Peptide signals belonging to these proteins were mucosa-specific and had the highest intensity in the control sample, which decreased during the IR sequence (**Figures 6-II** and **Figure S10a-c**). Images of complement C5 showed localization specifically in the mucosa layer. The decreasing intensity during IR was accompanied by a distribution shift toward the villus tips (**Figure 6-III**) and expression in villus debris in reperfusion samples (**Figure S10d**). Interestingly, for complement C7, a decreasing intensity ($p<0.01$) in submucosa was accompanied by an increase in the mucosa layer ($p=0.02$). Peptide images confirm this distribution shift (**Figures 6-IV** and **Figure S10e**). The collagen-α-2(I) chain, a structural constituent of the extracellular matrix, exhibited a significant downregulation in the submucosa (**Figures 6-V** and **Figure S10f**).

Imaging MS and quantitative MS-based proteomics are complementary methods

When comparing imaging MS with LC-MS/MS proteomics results, only two (Nup50, complement C5) of the 22 annotated proteins overlapped with the list of significantly changed proteins based on LC-

MS/MS analysis. Nevertheless, the proteins found to be changed in MSI experiments were involved in processes that were overrepresented among differentially expressed proteins in LC-MS/MS analysis. **Figure 7** summarizes and connects the most important results of this study.

Overrepresented processes in the changing proteome (blue), phosphoproteome (red), or both (blue-red) are highlighted, and images of significantly changed peptides and corresponding annotated proteins are shown with arrows pointing toward the corresponding process (red, mucosa; blue, submucosa). The overview shows that the applied methods complement each other; insight into the different regulated processes in the global (phospho)proteome is accompanied by partially overlapping spatial information provided by MSI.

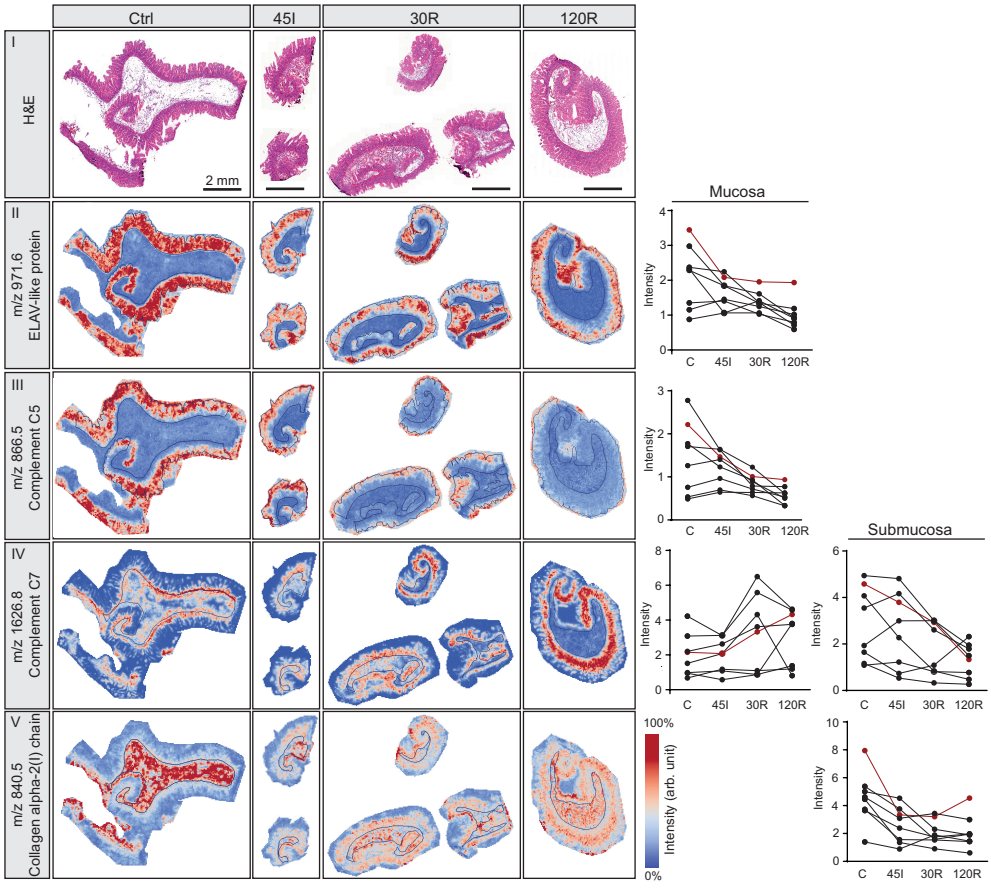

Figure 6. Selection of annotated proteins using MALDI-TOF MSI in combination with FTICR and LC-MS/MS. *H&E staining (I) and peptide images from one patient are shown for indicated m/z values, which were identified as ELAV-like protein (II), complement C5 (III), complement C7 (IV) and collagen alpha2(I)chain (V). Graphs show intensities for all patients in mucosa (left) and/or submucosa (right) in case the m/z was differentially expressed in the respective layer. Corresponding graphs show intensity data for all patients (presented peptide images correspond to a red line in the graph). See also Figure S10 for peptide images from all patient samples.*

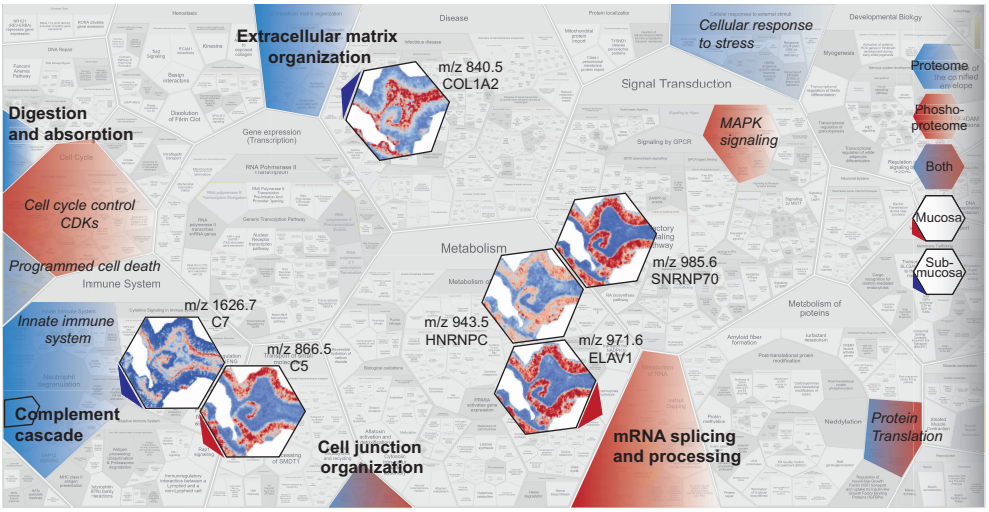

Figure 7. Summary of MS-based proteome and phosphoproteome functional analysis and imaging MS data showing that these methods complement as well as support each other. *Overview summarizing regulated processes during IR based on the dynamic proteome (blue) and phosphoproteome (red) or both (blue-red). Processes that were shown to be significantly enriched are indicated in bold. Peptide images show significantly changing proteins, specifically located in the mucosa (red arrow) or submucosa (blue arrow). These proteins were related to indicated processes (arrow). The overview image was adjusted from ReacFoam format (Reactome.org). C5, complement 5; C7, complement 7; SNRNP70, small nuclear ribonucleoprotein U1 subunit 70; HNRNPC, heterogeneous nuclear ribonucleoprotein C; ELAV1, ELAV like protein 1; and COL1A1, collagen 1 alpha2 (I) chain.*

DISCUSSION

Here, we present a comprehensive study of the proteome and phosphoproteome in combination with MALDI MSI to unravel protein alterations during IR of the human intestine. LC-MS/MS-based (phospho)proteomics resulted in the identification and quantification of thousands of proteins and phosphosites, and enabled thorough functional enrichment and interaction network analyses. We showed that proteins related to the intestinal absorption, microvillus structure and cell junction were decreased in abundance after IR, whereas proteins involved in innate immunity were increased in abundance. Phosphoproteome analysis revealed regulation of RNA splicing events and cytoskeletal/cell junction organization, and suggested MAPK and CDK families to be active kinases during IR. In addition, MALDI MSI enabled the identification of mucosa-specific protein changes as well as alterations in protein distribution, for instance a shift in localization of complement C5 during the course of IR.

Functional interpretation of the dynamic proteome in intestinal IR

Functional enrichment analysis of the dynamic proteome during IR revealed that proteins showing a decrease in abundance during reperfusion were overrepresented for GO terms related to microvilllus/cell junction/cytoskeleton. Proteins showing an increase during reperfusion were related to the innate

immune response. Functional interpretation of the changing proteome will be discussed per cluster.

The downregulation of various translation initiation factors (EIF2S2, EIF4EBP1, EIF5B) suggests that protein translation is inhibited in the early reperfusion phase. Inhibition of translation initiation is one of the cytoprotective mechanisms of the unfolded protein response[29], which is induced in response to proteotoxic stress in the ER, and known to play an important role in IR injury[8]. Interestingly, we observed a decrease in abundance of HspA4, a member of the Hsp70 family, which act as chaperones and is known to be induced in response to proteotoxic stress and protect cells from its harmful effects[30]. We speculate that acute IR-induced/oxidative stress depleted Hsp70 protein at 30R, which was rapidly recovered by IR stress-induced transcription of Hsp70s[31]. Another stress-response related protein showing decreased abundance was Nup50, which has a direct role in nuclear transport and is known to be sensitive to different stressors including oxidative stress[32]. A reduction in TNIK, which acts as a critical activator of Wnt targets[33], suggests that this kinase may play a role in the inhibition of proliferation during IR-induced cellular stress.

The decreased abundance of proteins involved in intestinal digestion/absorption and related to microvillus and cell junction organization likely reflects the loss of villus tips as a consequence of reperfusion injury. This group of proteins included many structural proteins of intestinal microvilli, but also brush border enzymes and transporters for nutrient absorption. Our group has previously described how IR-induced destruction of the intestinal epithelium led to contraction of the epithelial sheets and shedding of the damaged villus tips which resulted in reduced length of the villi[6]. Reorganization of the actin cytoskeleton and accumulation of F-actin at the basal side of enterocytes enabled this protective mechanism. The actin cytoskeleton is tightly anchored to the lateral membranes by cell-cell junction complexes. This interaction between the cytoskeleton and cell junction is crucial for the integrity of epithelial barrier and changes in organization of either one affects the other and may contribute to gut barrier disruption[34], which is known to occur in inflamed and injured intestine[35] and cardiac IR[36]. A decreased abundance of cytosolic IFABP protein in the villus is a well-known consequence of intestinal IR[5]. The loss of enterocyte membrane integrity results in the release of IFABP into the circulation and has been shown to be a useful serological biomarker for intestinal IR injury[37-39].

Functional enrichment analysis of the cluster of proteins exhibiting increased expression during reperfusion (cluster 3), strongly indicates activation of the innate immune response upon reperfusion of the ischemically damaged intestine, and points in particular to a crucial role of the complement system, as also demonstrated by the presented network of interconnected proteins in this cluster. Activation of the complement system has been well-documented in animal models of intestinal IR[40-43]. In addition, our group has previously reported complement activation after IR in human intestine[7]. In that study, high amounts of complement activation product C3c were detected in the luminal debris of shed enterocytes but not in mucosal tissue, whereas native C3 was present in the tissue[7]. Interestingly, our MSI data show that C5 expression shifted toward the villus tips and that C5 was almost absent in the mucosal tissue itself during reperfusion. The decrease of complement C5 in the mucosa layer seems contradictory to the quantitative proteomics data, showing an overall increase in complement proteins. This discrepancy may be explained by homogenization of whole tissue, including the luminal debris that may contains complement proteins, for proteomics analysis.

Images of C7, on the other hand, showed increasing abundance in the mucosa layer together with a decrease in submucosal expression. It should be noted that we cannot verdict on actual complement activation, as our proteomics analysis could not distinguish the native and active forms of complement factors. Our findings shed new light on the importance of the complement system in IR of the human intestine and could give rise to further studies investigating the activation of complement and its role in human intestinal IR. To date, the potentially protective effects of complement inhibition during intestinal IR have been investigated in animal models only[41-43]. Moreover, these data underline the strength of combining LC-MS/MS data giving robust and reliable quantitative data and MS images exposing changes in protein localization. An alternative spatial proteomics approach that could be very useful to identify and quantify peptides in a specific tissue area, is laser capture microdissection of the area of interest followed by LC-MS/MS analysis[44, 45].

Furthermore, both LC-MS/MS and MSI approaches point to changing ECM organization during IR, which is in accordance with our previous proteomics analysis of hypoxia-reoxygenation in a human intestinal organoid model[46]. Interestingly, network analysis indicated interconnection of proteins directly related to innate immunity and ECM proteins. Unbalanced ECM remodeling, and associated altered expression of ECM proteins, are a well-known feature in inflammatory bowel disease (IBD)[47]. Immune activation and inflammation are known to induce both the degradation and synthesis of the ECM. The interplay between inflammation and the ECM is a dynamic process, in which ECM alterations can also actively promote inflammation and contribute to disease progression in IBD[48]. The observed alterations in the expression of ECM proteins, both quantitatively and in peptide images, may reflect remodeling of the ECM as a result of IR-induced inflammation.

The small cluster of proteins that gradually increased during IR (cluster 4) contained proteins involved in a variety of processes. Cytoglobin, which has an important role in oxygen transport, was significantly increasing during IR and has been shown to be protective against IR injury in other organs[49, 50]. Interestingly, the increase in caspase-1 protein may point to the promotion of pyroptosis, a pro-inflammatory form of programmed cell death, which is initiated by caspase-1, and has recently been shown to play a role in murine intestinal IR injury[51].

The dynamic phosphoproteome

Protein phosphorylation and its regulation by kinases and phosphatases play a key role in the regulation of cellular functions, and changes in phosphorylation can be a cause as well as a consequence of a variety of diseases[52]. By analyzing our data with a combination of phosphosite- and protein-centric approaches, we identified dynamic protein phosphorylation events that regulate specific biological processes, and hence are expected to play an important role in the cellular response to IR.

Hierarchical clustering accompanied with motif analysis per cluster revealed the dynamic nature of protein phosphorylation during IR. The majority of phosphosites are proline directed, which suggests that they are potential targets of a variety of kinases, from CDKs to MAP kinases[53, 54]. In the case of IR, it is very likely that many of the regulated phosphosites are targets of MAP kinases such as JNK and p38, which are activated by cellular stress and thus their targets are expected to locate to clusters showing upregulation after IR (cluster 1, 3, 4, 5). Indeed, phosphosites of STMN1 (S25, S38), ATF2 (T69, T71) and CTTN (S405, S418), which are proposed targets of either JNK or p38 (Table S5),

locate to clusters 3 and 4, which contain phosphosites that appear upregulated during reperfusion. Proline-directed phosphosites could also be targets of MAP kinases related to growth and survival, like ERK1/ERK2. We found that phosphorylation of ERK2 on T185 and Y187, which are indicative of kinase activation[55], were located in cluster 4, which suggests that ERK2 is highly active shortly after reperfusion. Cluster 5, which exhibits upregulated phosphosites at 45I, is predominantly comprised of non-proline directed phosphosites, which suggests that other kinases than MAPK are likely to be active during ischemia. Overall, the differences in dynamics and motif composition amongst clusters suggests that protein phosphorylation response to IR is complex and comprises different effector kinases acting at different stages.

Phosphorylation dynamics and its relation with signaling pathways

We further examined which kinases may be responsible for the protein phosphorylations by analyzing how phosphosite dynamics relate to signatures of specific kinases or signaling pathways. As expected, we observed that most potential MAPK and CDK targets tend to decrease during ischemic conditions, followed by a drastic increase during reperfusion. However, when looking into specific phosphosites with known biological function, we highlighted some examples displaying interesting trends. One of these is the phosphorylation of ATF2, a transcription factor regulating cell growth and survival, on T69 and T71, which are known targets of MAP kinases in response to both cellular stress and growth factors[56]. Both phosphosites showed increased intensity upon ischemia and peaked at 30R, which equals induction of ATF2 transcription activity[57-59]. This is in line with previously reported increased ATF2 binding activity in renal IR[60]. It is conceivable that stress responsive MAP kinases (JNK and/or p38) induce phosphorylation during ischemia, which is subsequently boosted by other MAP kinase activity (e.g. ERK1/ERK2) in response to growth factors upon reperfusion[61].

In addition, we identified protein phosphorylation events known to regulate protein translation, namely S235 and S236 phosphorylation on RPS6, an important ribosomal protein that is regulated by kinases responsive to growth factors[62, 63]. As these phosphosites on RPS6 promote assembly of the preinitiation complex[64], our data indicate translation seemed to be inhibited during ischemia and resumed upon reperfusion. The latter supports our findings in the proteome data, where proteins involved in translation appeared to decrease in abundance early in reperfusion and then recover after 120R.

Functional interpretation of changes in the phosphoproteome

Through GO enrichment analysis, we found that most of the phosphorylation-regulated proteins were involved in RNA splicing and cell junction/cytoskeleton organization. This is consistent with a previous phosphoproteome study in a swine model for cardiac IR, reporting that the majority of phosphoprotein alterations were involved in RNA processing and cell junction[65].

Pre-mRNA splicing is executed by the spliceosome. The phosphorylation state of splicing factors is crucial for the correct regulation of their function and organization, and for the formation of the spliceosome complex[66]. Splicing factors exhibited increasing as well as decreasing phosphorylation (cluster 1 and 5), suggesting that both phosphorylation and dephosphorylation events play a role in the regulation of RNA splicing, which has been shown previously[67]. In addition to the role in constitutive

splicing, phosphorylation acts as a major player in the regulation of alternative splicing[68], a process that 95% of human genes undergo, and is considered an important mechanism in pathological cellular processes[69]. Accumulating evidence indicates that pre-mRNA splicing plays an essential role in the adaptation to hypoxic stress[70-72]. Hypoxia-induced alternative splicing, for example of VEGF, Bcl-x, BNIP3 and CAIX, changes gene expression patterns in order to enhance proliferation and survival[71]. This may explain the ischemia-induced changes in phosphorylation of splicing-related proteins in our model. Furthermore, stress-activated MAP kinases such as JNK and p38, which are activated during IR, can indirectly modulate splicing by phosphorylation of selected splicing factors[73]. In addition to the phosphorylation changes in splicing factors, MSI results showed a locally decreased mucosal intensity of peptides annotated as spliceosome component SNRNP70 and RNA binding proteins ELAV1 and HNRNPC which play a role in RNA splicing. This further supports regulation of splicing events during IR.

A substantial part of phosphorylation-regulated proteins was related to cell junction and cytoskeletal organization. In contrast to the decrease in abundance of these proteins following reperfusion, changes in phosphorylation exhibited various temporal profiles, including phosphosites that were regulated immediately after ischemia. Regulation of cell junction proteins by phosphorylation plays an important role in the assembly and disassembly of adherence junctions[74]. The latter are known to interact with the actin cytoskeleton of adjacent cells, suggesting that the dynamic phosphorylation of junctional and cytoskeletal proteins during IR likely affects its organization and integrity. Interestingly, we detected some specific phosphosites with a known function in the regulation of cytoskeleton organization, which showed an increase during reperfusion. Cortactin (CTTN) phosphorylation on S405 and S418 is associated with cytoskeleton reorganization[75, 76], and STMN1 phosphosites S16, S25 and S38 are linked to polymerization of the microtubule cytoskeleton[77]. Together, these findings suggest that increased phosphorylation of junctional proteins upon reperfusion may be related to the reorganization of the cytoskeleton during IR of the human intestine[6].

MSI data interpretation and limitations

The clustering of control and ischemia samples on the one hand and reperfusion samples on the other hand, was comparable for MSI and proteome data. However, the fact that for MSI the peptides in the lower mass range exhibited a decreasing gradient, and those in the higher mass range an increasing intensity gradient may suggest that enzymatic digestion efficiency was affected negatively by ischemia and an increasing reperfusion time. While these results have to be interpreted with care, we can speculate that IR-induced changes in endogenous proteolytic enzymes may affect digestion efficiency. This is supported by animal studies which have shown that during IR, pancreatic enzymes from the intestinal lumen leak into the intestinal wall, resulting in self-digestion[78, 79].

Where LC-MS/MS proteomics is a well-established and robust technology, MSI methodologies are evolving rapidly. One of the existing challenges of tryptic peptide MSI is the identification of the corresponding proteins. Here, we assigned MSI-detected peptides to protein data from LC-MS/MS analysis of the same tissue samples. A trade-off between speed, sensitivity and mass resolution made us decide to use MALDI-TOF MSI for the screening of the 36 tissue samples and to perform additional MALDI-FTICR measurements only as an intermediate step to aid in the identification

process because of their higher mass accuracy. When compared to phospho- and global proteomics, MSI identification results were sparse. There are several explanations for this. First, the number of peptide signals is relatively low in MSI analysis due to the mass resolution of the TOF system and the lack of an additional dimension of separation. This low mass resolution was also the major limiting factor for the identification of the peptide signals since about 30% of the TOF peaks could be further resolved into at least two peptide signals in the FTICR spectrum. We therefore assume that the use of high-resolution MALDI MSI for all tissue sections would have significantly increased the number of identified (phospho)peptides, although it is more time-consuming. Another factor that limits identification is the use of different ionization methods (ESI for LC-MS/MS versus MALDI in MSI), which inherently limits the overlap between the detected peptides. Despite these detrimental factors, the proteins annotated to significantly changing peptides with our MSI analysis were related to the same processes that were shown to be altered in our quantitative proteomics analysis, supporting the coherence between the different types of data used. For further studies, MSI- and/or morphology guided laser microdissection could be performed and analyzed by LC-MS/MS[44].

Conclusion

Altogether, we identified IR-induced alterations in abundance, phosphorylation and distribution of proteins, which expanded our understanding of the molecular events that occur during IR in the human intestine. In addition, the study highlights the strength of the complementary use of different MS-based methodologies.

ACKNOWLEDGEMENTS

This work was funded by NUTRIM, Maastricht University Medical Center+ (NUTRIM Graduate Program grant to Anna M. Kip), NWO (Aspasia grant 015.010.046 to Kaatje Lenaerts), NWO (project 184.034.019), and was part of the Netherlands X-omics Initiative. Juan Manuel Valverde was supported by scholarships from the Ministry of Science and Technology of Costa Rica (MICITT) and the University of Costa Rica (UCR). We thank the surgical team of Maastricht University Medical Center+ for their excellent surgical assistance. Table of Contents graphic was created with BioRender.com.

REFERENCES

1 American Gastroenterological Association Medical Position Statement: guidelines on intestinal ischemia. *Gastroenterology* **118**, 951-953 (2000).

2 Bala, M. *et al.* Acute mesenteric ischemia: guidelines of the World Society of Emergency Surgery. *World journal of emergency surgery : WJES* **12**, 38 (2017).

3 Oldenburg, W. A., Lau, L. L., Rodenberg, T. J., Edmonds, H. J. & Burger, C. D. Acute mesenteric ischemia: a clinical review. *Archives of internal medicine* **164**, 1054-1062 (2004).

4 Kalogeris, T., Baines, C. P., Krenz, M. & Korthuis, R. J. Ischemia/Reperfusion. *Compr Physiol* **7**, 113-170 (2016).

5 Derikx, J. P. *et al.* Rapid reversal of human intestinal ischemia-reperfusion induced damage by shedding of injured enterocytes and reepithelialisation. *PloS one* **3**, e3428 (2008).

6 Grootjans, J. *et al.* Rapid lamina propria retraction and zipper-like constriction of the epithelium preserves the epithelial lining in human small intestine exposed to ischaemia-reperfusion. *J Pathol* **224**, 411-419 (2011).

7 Grootjans, J. *et al.* Human intestinal ischemia-reperfusion-induced inflammation characterized: experiences from a new translational model. *The American journal of pathology* **176**, 2283-2291 (2010).

8 Grootjans, J. *et al.* Level of activation of the unfolded protein response correlates with Paneth cell apoptosis in human small intestine exposed to ischemia/reperfusion. *Gastroenterology* **140**, 529-539. e523 (2011).

9 Kassahun, W. T., Schulz, T., Richter, O. & Hauss, J. Unchanged high mortality rates from acute occlusive intestinal ischemia: six year review. *Langenbeck's archives of surgery* **393**, 163-171 (2008).

10 Mastoraki, A. *et al.* Mesenteric ischemia: Pathogenesis and challenging diagnostic and therapeutic modalities. *World journal of gastrointestinal pathophysiology* **7**, 125-130 (2016).

11 Kougias, P. *et al.* Determinants of mortality and treatment outcome following surgical interventions for acute mesenteric ischemia. *Journal of vascular surgery* **46**, 467-474 (2007).

12 Altelaar, A. F., Munoz, J. & Heck, A. J. Next-generation proteomics: towards an integrative view of proteome dynamics. *Nat Rev Genet* **14**, 35-48 (2013).

13 Liu, H. *et al.* A Caffeic Acid Matrix Improves In Situ Detection and Imaging of Proteins with High Molecular Weight Close to 200,000 Da in Tissues by Matrix-Assisted Laser Desorption/Ionization Mass Spectrometry Imaging. *Analytical chemistry* **93**, 11920-11928 (2021).

14 Han, J. *et al.* Imaging of protein distribution in tissues using mass spectrometry: An interdisciplinary challenge. *TrAC Trends in Analytical Chemistry* **112**, 13-28 (2019).

15 Huber, K. *et al.* Approaching cellular resolution and reliable identification in mass spectrometry imaging of tryptic peptides. *Analytical and bioanalytical chemistry* **410**, 5825-5837 (2018).

16 Schober, Y., Schramm, T., Spengler, B. & Rompp, A. Protein identification by accurate mass matrix-assisted laser desorption/ionization imaging of tryptic peptides. *Rapid communications in mass spectrometry : RCM* **25**, 2475-2483 (2011).

17 Spraggins, J. M. *et al.* Next-generation technologies for spatial proteomics: Integrating ultra-high speed MALDI-TOF and high mass resolution MALDI FTICR imaging mass spectrometry for protein analysis. *Proteomics* **16**, 1678-1689 (2016).

18 Zhou, H. *et al.* Robust phosphoproteome enrichment using monodisperse microsphere-based immobilized titanium (IV) ion affinity chromatography. *Nat Protoc* **8**, 461-480 (2013).

19 Meiring, H. D., van der Heeft, E., ten Hove, G. J. & de Jong, A. P. J. M. Nanoscale LC-MS(n): technical design and applications to peptide and protein analysis. *J Sep Sci* **25**, 557-568 (2002).

20 Tibshirani, R., Walther, G. & Hastie, T. Estimating the number of clusters in a data set via the gap statistic. *Journal of the Royal Statistical Society: Series B (Statistical Methodology)* **63**, 411-423 (2001).

21 Szklarczyk, D. *et al.* STRING v11: protein-protein association networks with increased coverage, supporting functional discovery in genome-wide experimental datasets. *Nucleic Acids Res* **47**, D607-d613 (2019).

22 Supek, F., Bošnjak, M., Škunca, N. & Šmuc, T. REVIGO summarizes and visualizes long lists of gene ontology terms. *PloS one* **6**, e21800 (2011).

23 Vacic, V., Iakoucheva, L. M. & Radivojac, P. Two Sample Logo: a graphical representation of the differences between two sets of sequence alignments. *Bioinformatics* **22**, 1536-1537 (2006).

24 Lachmann, A. & Ma'ayan, A. KEA: kinase enrichment analysis. *Bioinformatics* **25**, 684-686 (2009).

25 Krug, K. *et al.* A Curated Resource for Phosphosite-specific Signature Analysis*[S]. *Molecular & Cellular Proteomics* **18**, 576-593 (2019).

26 Strohalm, M., Hassman, M., Kosata, B. & Kodicek, M. mMass data miner: an open source alternative for mass spectrometric data analysis. *Rapid communications in mass spectrometry : RCM* **22**, 905-908 (2008).

27 Perez-Riverol, Y. *et al.* The PRIDE database and related tools and resources in 2019: improving support for quantification data. *Nucleic Acids Res* **47**, D442-d450 (2019).

28 Vos, D. R. N. *et al.* Strategies for managing multi-patient 3D mass spectrometry imaging data. *J Proteomics* **193**, 184-191 (2019).

29 Pavitt, G. D. & Ron, D. New insights into translational regulation in the endoplasmic reticulum unfolded protein response. *Cold Spring Harb Perspect Biol* **4**, a012278 (2012).

30 Rosenzweig, R., Nillegoda, N. B., Mayer, M. P. & Bukau, B. The Hsp70 chaperone network. *Nature Reviews Molecular Cell Biology* **20**, 665-680 (2019).

31 Kip, A. M. *et al.* Temporal transcript profiling identifies a role for unfolded protein stress in human gut ischemia-reperfusion injury. *Cell Mol Gastroenterol Hepatol.*, http://doi.org/10.1016/j.jcmgh.2021.1011.1001 (in press).

32 Kodiha, M., Chu, A., Matusiewicz, N. & Stochaj, U. Multiple mechanisms promote the inhibition of classical nuclear import upon exposure to severe oxidative stress. *Cell Death Differ* **11**, 862-874 (2004).

33 Mahmoudi, T. *et al.* The kinase TNIK is an essential activator of Wnt target genes. *Embo j* **28**, 3329-3340 (2009).

34 Delacour, D., Salomon, J., Robine, S. & Louvard, D. Plasticity of the brush border - the yin and yang of intestinal homeostasis. *Nat Rev Gastroenterol Hepatol* **13**, 161-174 (2016).

35 Lechuga, S. & Ivanov, A. I. Disruption of the epithelial barrier during intestinal inflammation: Quest for new molecules and mechanisms. *Biochimica et Biophysica Acta (BBA) - Molecular Cell Research* **1864**, 1183-1194 (2017).

36 Tansey, E. E. *et al.* Reduction and redistribution of gap and adherens junction proteins after ischemia and reperfusion. *Ann Thorac Surg* **82**, 1472-1479 (2006).

37 Kanda, T. *et al.* Intestinal fatty acid-binding protein as a sensitive marker of intestinal ischemia. *Dig Dis Sci* **37**, 1362-1367 (1992).

38 Kanda, T. *et al.* Diagnosis of ischemic small bowel disease by measurement of serum intestinal fatty acid-binding protein in patients with acute abdomen: a multicenter, observer-blinded validation study. *J Gastroenterol* **46**, 492-500 (2011).

39 Schellekens, D. H. *et al.* Plasma intestinal fatty acid-binding protein levels correlate with morphologic epithelial intestinal damage in a human translational ischemia-reperfusion model. *J Clin Gastroenterol* **48**, 253-260 (2014).

40 Arumugam, T. V., Shiels, I. A., Woodruff, T. M., Granger, D. N. & Taylor, S. M. The role of the complement system in ischemia-reperfusion injury. *Shock* **21**, 401-409 (2004).

41 Wada, K., Montalto, M. C. & Stahl, G. L. Inhibition of complement C5 reduces local and remote organ injury after intestinal ischemia/reperfusion in the rat. *Gastroenterology* **120**, 126-133 (2001).

42 Fleming, S. D. *et al.* C5a causes limited, polymorphonuclear cell-independent, mesenteric ischemia/reperfusion-induced injury. *Clin Immunol* **108**, 263-273 (2003).

43 Arumugam, T. V. *et al.* Protective effect of a new C5a receptor antagonist against ischemia-reperfusion injury in the rat small intestine. *J Surg Res* **103**, 260-267 (2002).

44 Dewez, F. *et al.* MS Imaging-Guided Microproteomics for Spatial Omics on a Single Instrument. *Proteomics* **20**, e1900369 (2020).

45 Mezger, S. T. P., Mingels, A. M. A., Bekers, O., Heeren, R. M. A. & Cillero-Pastor, B. Mass Spectrometry Spatial-Omics on a Single Conductive Slide. *Analytical chemistry* **93**, 2527-2533 (2021).

46 Kip, A. M. *et al.* Proteomics analysis of human intestinal organoids during hypoxia and reoxygenation as a model to study ischemia-reperfusion injury. *Cell Death Dis* **12**, 95 (2021).

47 Mortensen, J. H. *et al.* The intestinal tissue homeostasis - the role of extracellular matrix remodeling in inflammatory bowel disease. *Expert Rev Gastroenterol Hepatol* **13**, 977-993 (2019).

48 Petrey, A. C. & de la Motte, C. A. The extracellular matrix in IBD: a dynamic mediator of inflammation. *Curr Opin Gastroenterol* **33**, 234-238 (2017).

49 Tian, S. F. *et al.* Mechanisms of neuroprotection from hypoxia-ischemia (HI) brain injury by up-regulation of cytoglobin (CYGB) in a neonatal rat model. *J Biol Chem* **288**, 15988-16003 (2013).

50 Nishi, H. *et al.* Cytoglobin, a novel member of the globin family, protects kidney fibroblasts against oxidative stress under ischemic conditions. *The American journal of pathology* **178**, 128-139 (2011).

51 Jia, Y. *et al.* Metformin protects against intestinal ischemia-reperfusion injury and cell pyroptosis via TXNIP-NLRP3-GSDMD pathway. *Redox Biol* **32**, 101534 (2020).

52 Cohen, P. The role of protein phosphorylation in human health and disease. The Sir Hans Krebs Medal Lecture. *Eur J Biochem* **268**, 5001-5010 (2001).

53 Malumbres, M. Cyclin-dependent kinases. *Genome Biology* **15**, 122 (2014).

54 Chen, Z. *et al.* MAP kinases. *Chemical reviews* **101**, 2449-2476 (2001).

55 Roskoski, R., Jr. ERK1/2 MAP kinases: structure, function, and regulation. *Pharmacol Res* **66**, 105-143 (2012).

56 Morton, S., Davis, R. J. & Cohen, P. Signalling pathways involved in multisite phosphorylation of the transcription factor ATF-2. *FEBS Lett* **572**, 177-183 (2004).

57 Gupta, S., Campbell, D., Dérijard, B. & Davis, R. J. Transcription factor ATF2 regulation by the JNK signal transduction pathway. *Science* **267**, 389-393 (1995).

58 Livingstone, C., Patel, G. & Jones, N. ATF-2 contains a phosphorylation-dependent transcriptional activation domain. *Embo j* **14**, 1785-1797 (1995).

59 van Dam, H. *et al.* ATF-2 is preferentially activated by stress-activated protein kinases to mediate c-jun induction in response to genotoxic agents. *Embo j* **14**, 1798-1811 (1995).

60 Morooka, H., Bonventre, J. V., Pombo, C. M., Kyriakis, J. M. & Force, T. Ischemia and reperfusion enhance ATF-2 and c-Jun binding to cAMP response elements and to an AP-1 binding site from the c-jun promoter. *J Biol Chem* **270**, 30084-30092 (1995).

61 Ouwens, D. M. *et al.* Growth factors can activate ATF2 via a two-step mechanism: phosphorylation of Thr71 through the Ras-MEK-ERK pathway and of Thr69 through RalGDS-Src-p38. *Embo j* **21**, 3782-3793 (2002).

62 Ferrari, S., Bandi, H. R., Hofsteenge, J., Bussian, B. M. & Thomas, G. Mitogen-activated 70K S6 kinase. Identification of in vitro 40 S ribosomal S6 phosphorylation sites. *J Biol Chem* **266**, 22770-22775 (1991).

63 Bandi, H. R., Ferrari, S., Krieg, J., Meyer, H. E. & Thomas, G. Identification of 40 S ribosomal protein S6 phosphorylation sites in Swiss mouse 3T3 fibroblasts stimulated with serum. *J Biol Chem* **268**, 4530-4533 (1993).

64 Roux, P. P. *et al.* RAS/ERK signaling promotes site-specific ribosomal protein S6 phosphorylation via RSK and stimulates cap-dependent translation. *J Biol Chem* **282**, 14056-14064 (2007).

65 Ledee, D. *et al.* Quantitative cardiac phosphoproteomics profiling during ischemia-reperfusion in an immature swine model. *Am J Physiol Heart Circ Physiol* **313**, H125-h137 (2017).

66 Misteli, T. RNA splicing: What has phosphorylation got to do with it? *Curr Biol* **9**, R198-200 (1999).

67 Prasad, J., Colwill, K., Pawson, T. & Manley, J. L. The protein kinase Clk/Sty directly modulates SR protein activity: both hyper- and hypophosphorylation inhibit splicing. *Mol Cell Biol* **19**, 6991-7000 (1999).

68 Naro, C. & Sette, C. Phosphorylation-mediated regulation of alternative splicing in cancer. *Int J Cell Biol* **2013**, 151839 (2013).

69 Wang, E. T. *et al.* Alternative isoform regulation in human tissue transcriptomes. *Nature* **456**, 470-476 (2008).

70 Natua, S., Ashok, C. & Shukla, S. Hypoxia-induced alternative splicing in human diseases: the pledge, the turn, and the prestige. *Cell Mol Life Sci* **78**, 2729-2747 (2021).

71 Kanopka, A. Cell survival: Interplay between hypoxia and pre-mRNA splicing. *Exp Cell Res* **356**, 187-191 (2017).

72 Nakayama, K. & Kataoka, N. Regulation of Gene Expression under Hypoxic Conditions. *Int J Mol Sci* **20**, 3278 (2019).

73 Al-Ayoubi, A. M., Zheng, H., Liu, Y., Bai, T. & Eblen, S. T. Mitogen-activated protein kinase phosphorylation of splicing factor 45 (SPF45) regulates SPF45 alternative splicing site utilization, proliferation, and cell adhesion. *Mol Cell Biol* **32**, 2880-2893 (2012).

74 Bertocchi, C., Vaman Rao, M. & Zaidel-Bar, R. Regulation of adherens junction dynamics by phosphorylation switches. *J Signal Transduct* **2012**, 125295 (2012).

75 Martinez-Quiles, N., Ho, H. Y., Kirschner, M. W., Ramesh, N. & Geha, R. S. Erk/Src phosphorylation of cortactin acts as a switch on-switch off mechanism that controls its ability to activate N-WASP. *Mol Cell Biol* **24**, 5269-5280 (2004).

76 Kelley, L. C., Hayes, K. E., Ammer, A. G., Martin, K. H. & Weed, S. A. Cortactin phosphorylated by ERK1/2 localizes to sites of dynamic actin regulation and is required for carcinoma lamellipodia persistence. *PloS one* **5**, e13847 (2010).

77 Larsson, N., Marklund, U., Gradin, H. M., Brattsand, G. & Gullberg, M. Control of microtubule dynamics by oncoprotein 18: dissection of the regulatory role of multisite phosphorylation during mitosis. *Mol Cell Biol* **17**, 5530-5539 (1997).

78 Chang, M., Kistler, E. B. & Schmid-Schönbein, G. W. Disruption of the mucosal barrier during gut ischemia allows entry of digestive enzymes into the intestinal wall. *Shock* **37**, 297-305 (2012).

79 Chang, M., Alsaigh, T., Kistler, E. B. & Schmid-Schönbein, G. W. Breakdown of mucin as barrier to digestive enzymes in the ischemic rat small intestine. *PloS one* **7**, e40087 (2012).

SUPPLEMENTARY INFORMATION

Contents

Supplementary Figures

Supplementary Tables

Supplementary tables are available at https://pubs.acs.org/doi/10.1021/acs.jproteome.1c00447.

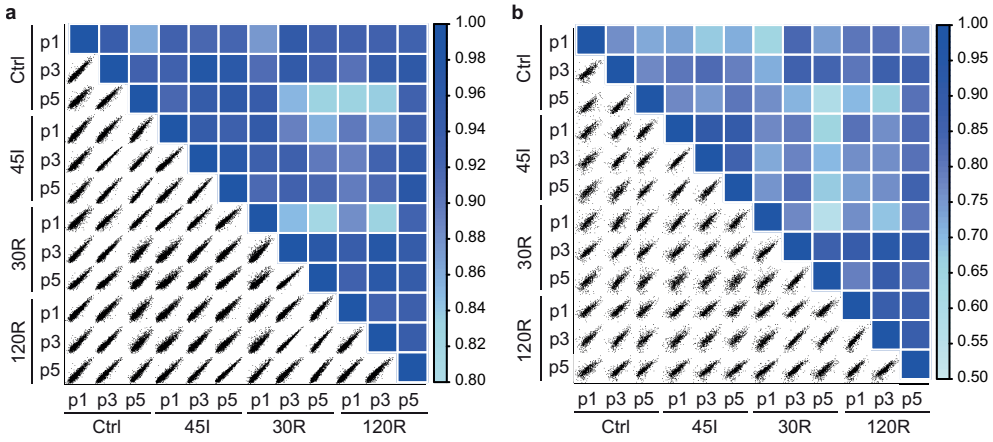

Figure S1. *Correlation plots between all samples for proteome (**a**) and phosphoproteome (**b**). Good correlation between biological replicates, except for 30R-p1, which was therefore excluded from analysis. Patient p1, p3 and p5 correspond to patient numbers in MSI data. Intensity scale indicates the correlation coefficient.*

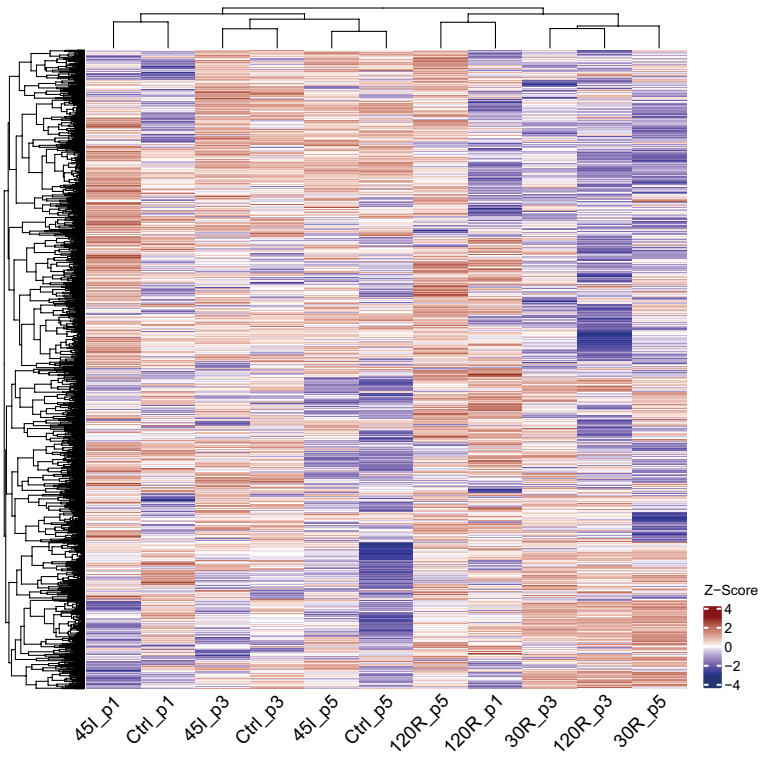

Figure S2. *Hierarchical clustering of the complete proteome. Heatmap visualizes Z-scored intensities, and was generated using a combination of k-means and hierarchical clustering (Complex Heatmap package in R). Two main clusters are Ctrl and 45I samples on the one hand and 30R and 120R on the other hand.*

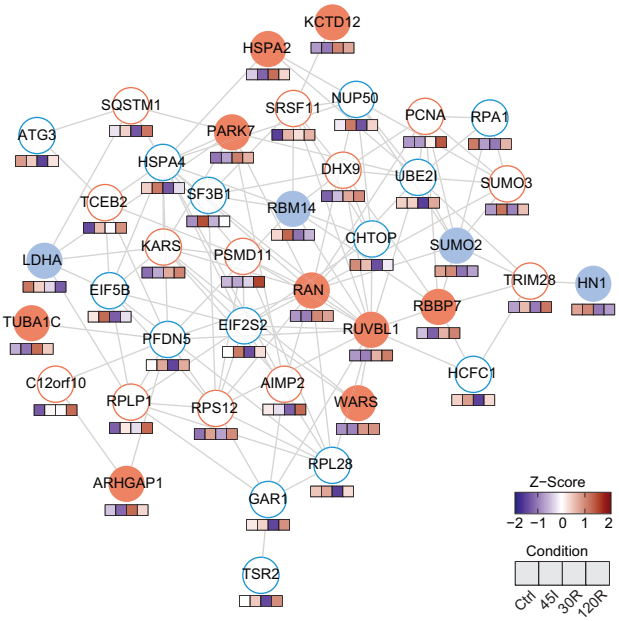

Figure S3. *Protein interaction network. Network is generated using STRING. Color of the circle indicates the temporal profile (cluster) of the protein. Blue line, cluster 1; Blue fill, cluster 2; Red fill, cluster 3, Red line, cluster 4. Color cubes below each protein indicates Z-score intensity in Ctrl, 45I, 30R and 120 R respectively. This network shows interactions between proteins located in all clusters, with a majority in cluster 1 and 4.*

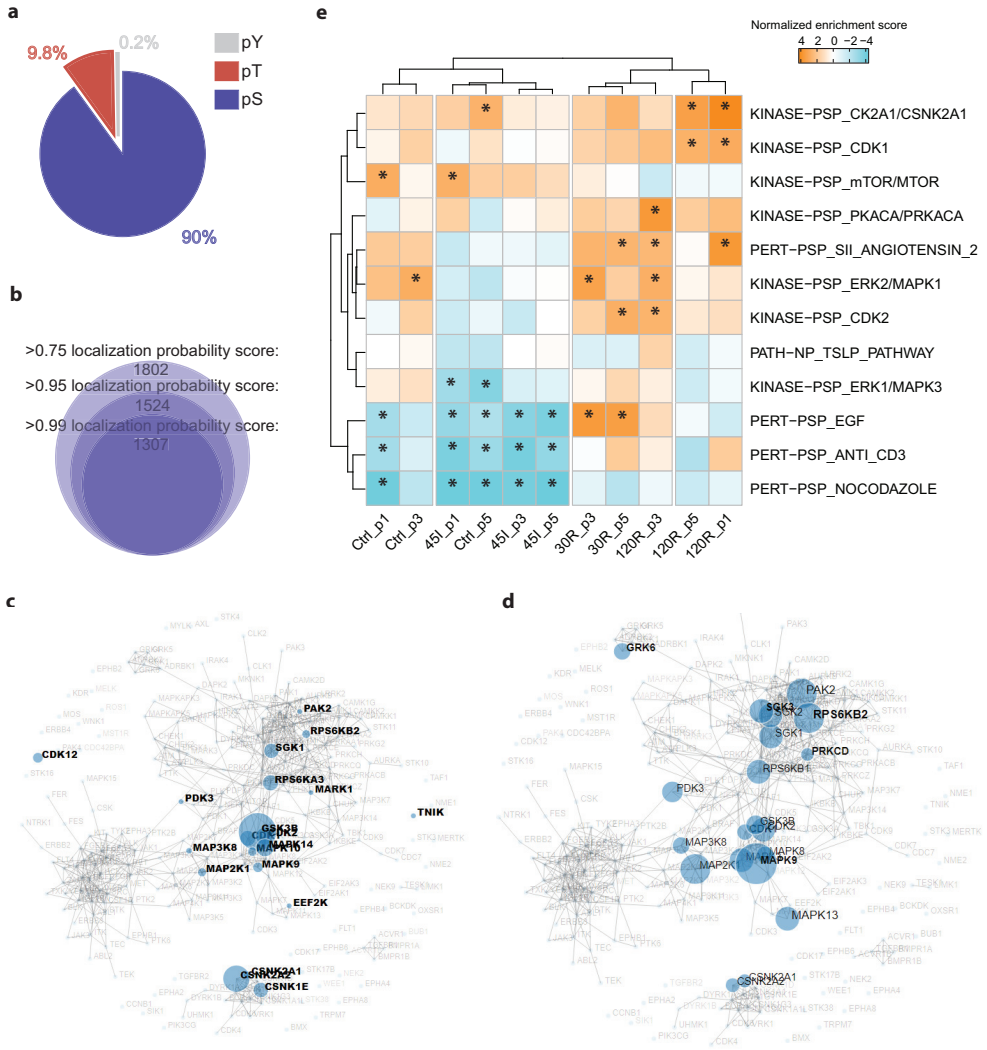

Figure S4. *Global overview of the phosphoproteome.* ***a****) Pie chart showing the proportion of phosphoserines, phosphothreonines and phosphotyrosines detected* ***b****) Concentric circles with proportional size corresponding to the number of phosphosites above the given localization probability scores.* ***c****) Kinase enrichment analysis using KEA2 tool, showing a kinase network highlighting those with targets overrepresented in the whole phosphoproteome and* ***d****) in the dynamic phosphoproteome (ANOVA, p<0.05). See also Table S4 and S5 for respective lists of kinases and their targets.* ***e****) Post-translational modification - signature enrichment (PTM-SEA) analysis. Heat map shows normalized enrichment scores of phosphorylation signatures detected in the whole dataset. Arterisks indicate enriched or depleted signatures enriched in the given sample (FDR<0.01).*

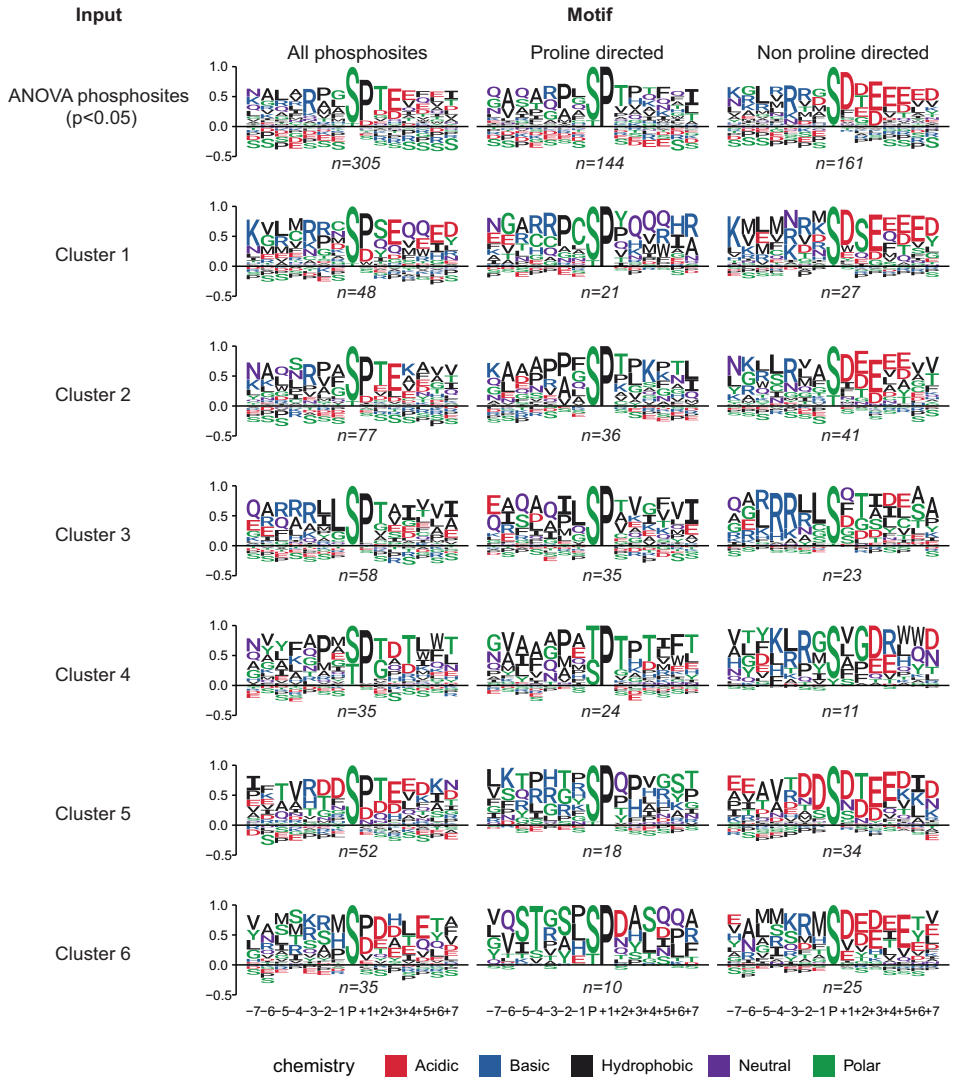

Figure S5. *Sequence motif logos for dynamic phosphosites overall and per cluster. Motifs for all phosphosites is shown per cluster on the left; separate motifs for proline and non-proline directed phosphosites are shown in the middle and to the right respectively. The number of phosphosites from which the motif logo was obtained, is indicated below the logo.*

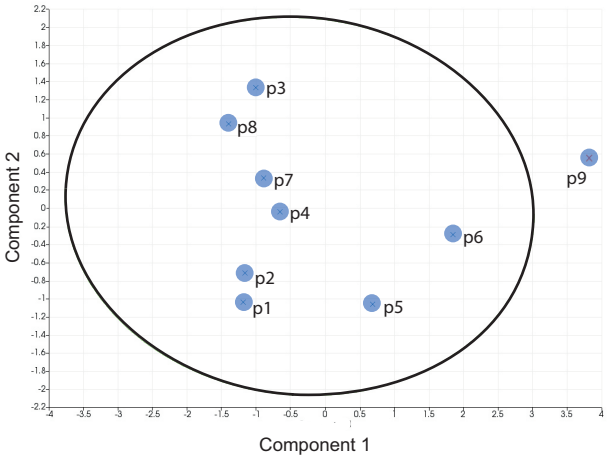

***Figure S6**. Principle component analysis of the average cytochrome c mass spectrum. Every dot represents the cytochrome c mass spectrum from one slide, and is thus used as a measure for digestion efficiency of the data sets from one patient. Respective patient numbers are indicated (p1 – p9). The ellipse indicates the 95% confidence interval. Any measurement outside the ellipse is considered an outlier.*

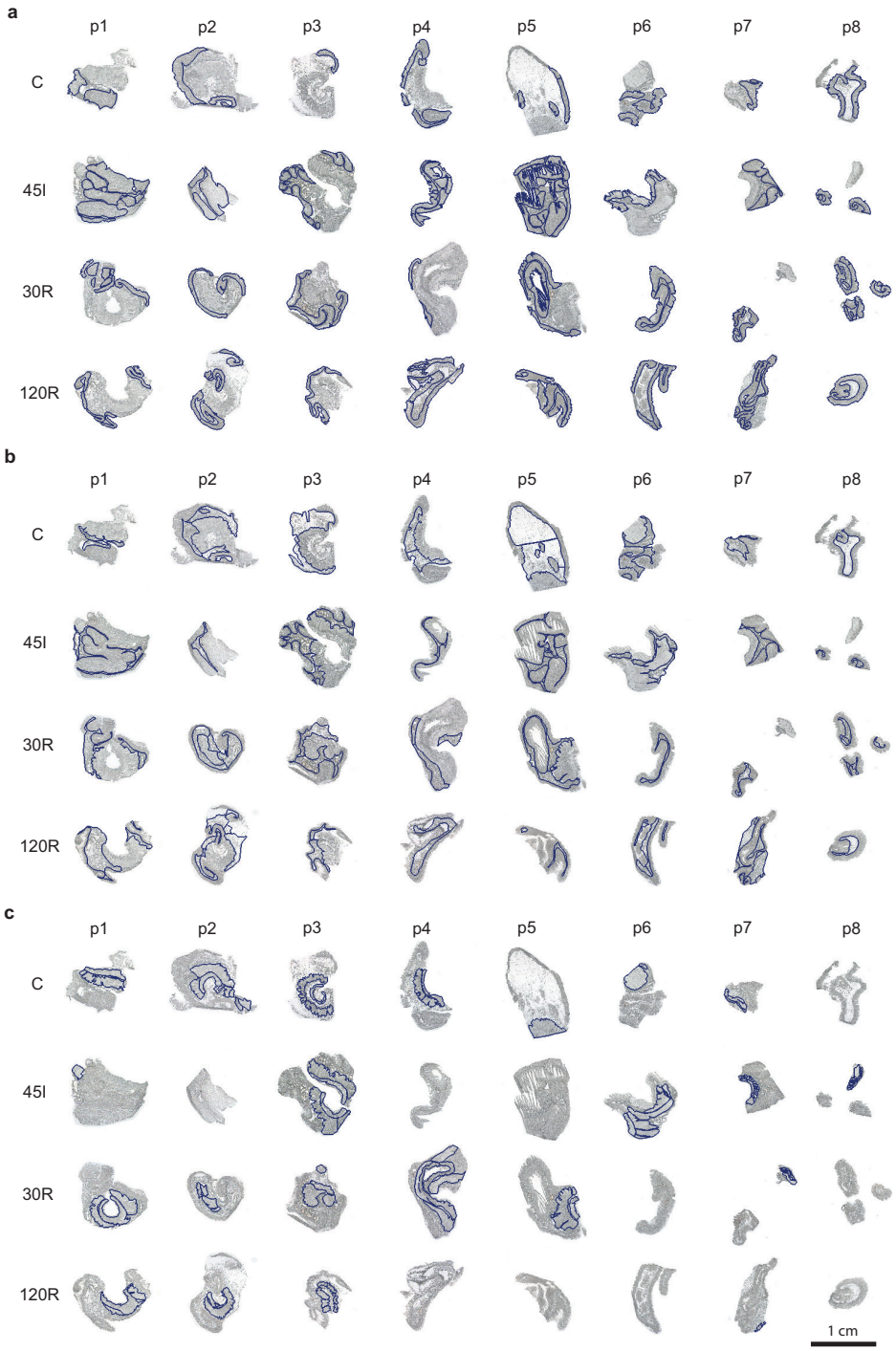

***Figure S7**. Annotation of histological regions in all MSI-analyzed tissue sections. **a**) Mucosa regions **b**) Submucosa regions **c**) Muscle regions*

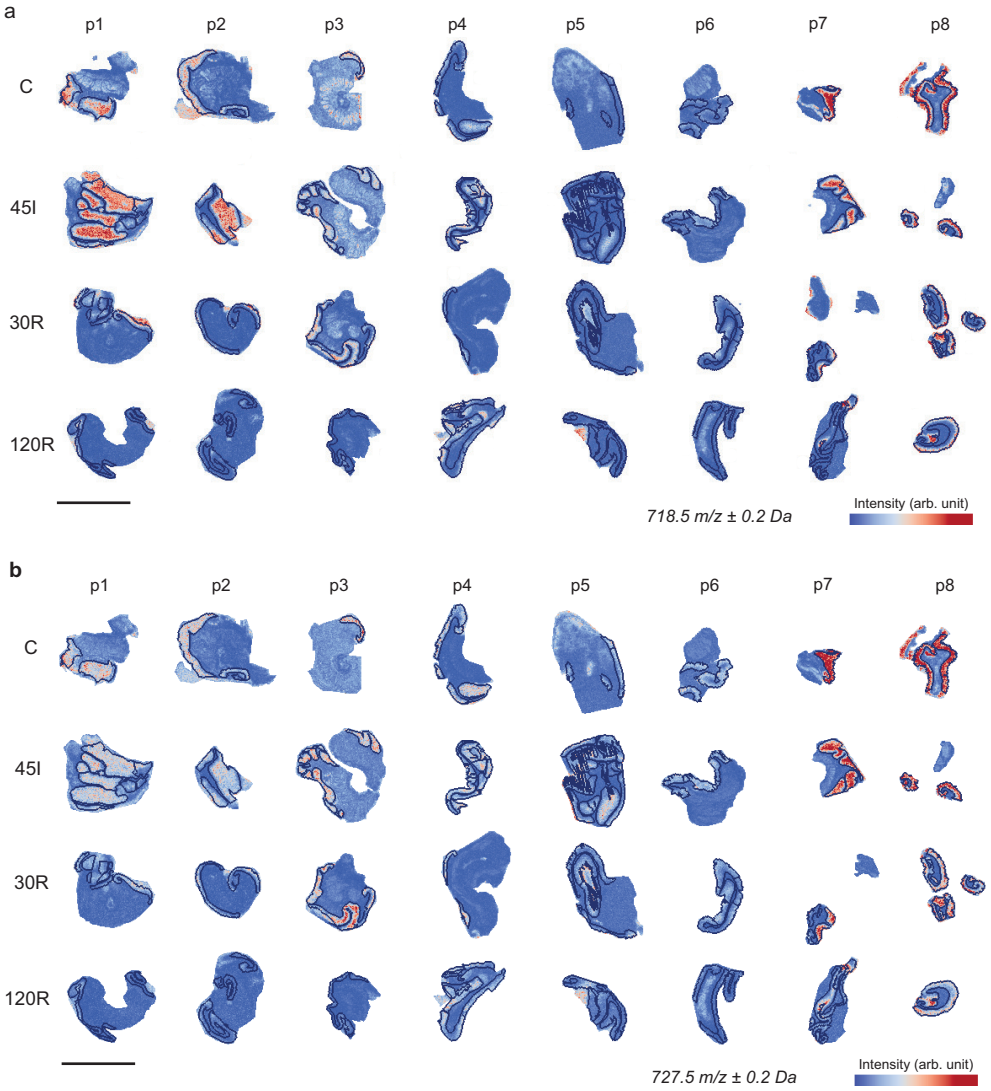

***Figure S8. a, b**) Individual peptide images showing examples of significantly changed m/z in mucosa layer with a high fold change (all examples in top 10 highest fold change).*

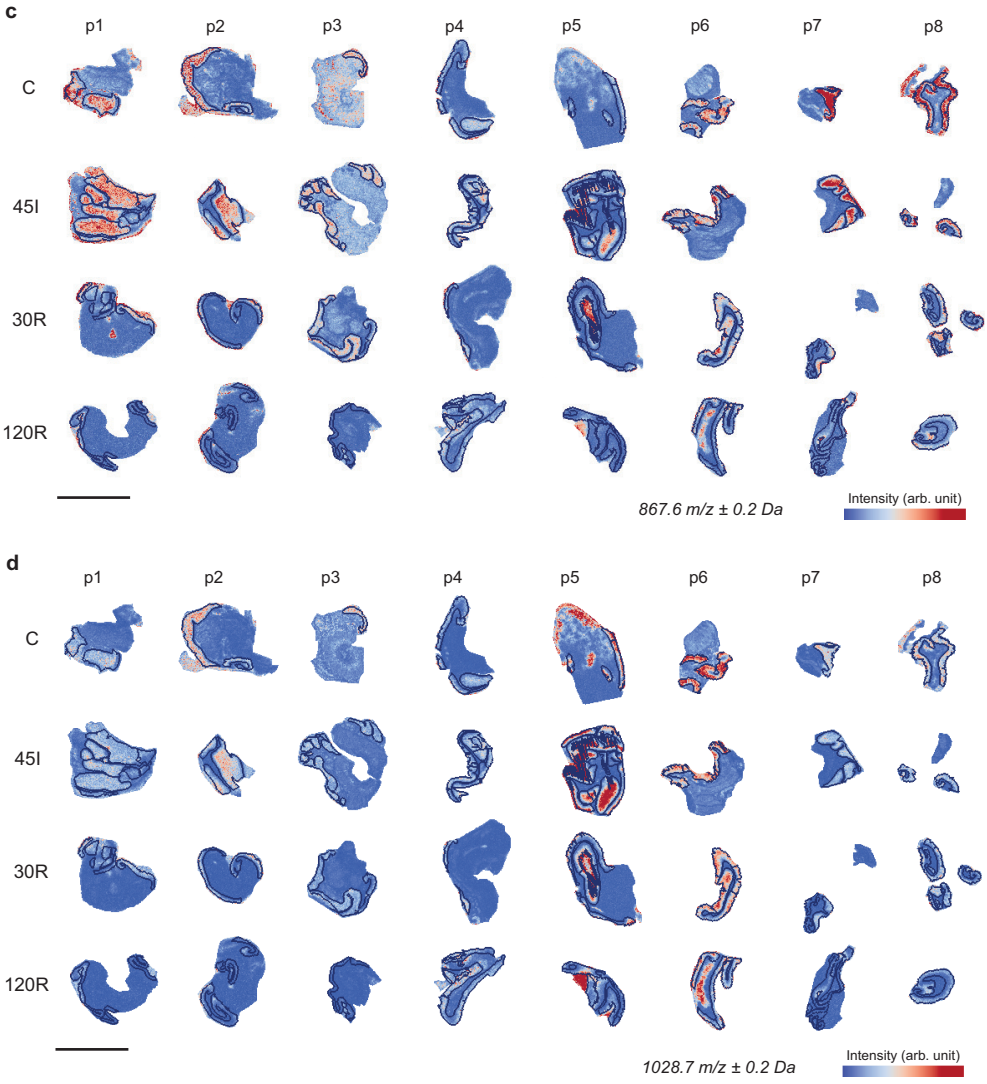

Figure S8. c, d*) Individual peptide images showing examples of significantly changed m/z in mucosa layer with a high fold change (all in top 10 highest fold change), and also among top 10 highest intensity m/z values.*

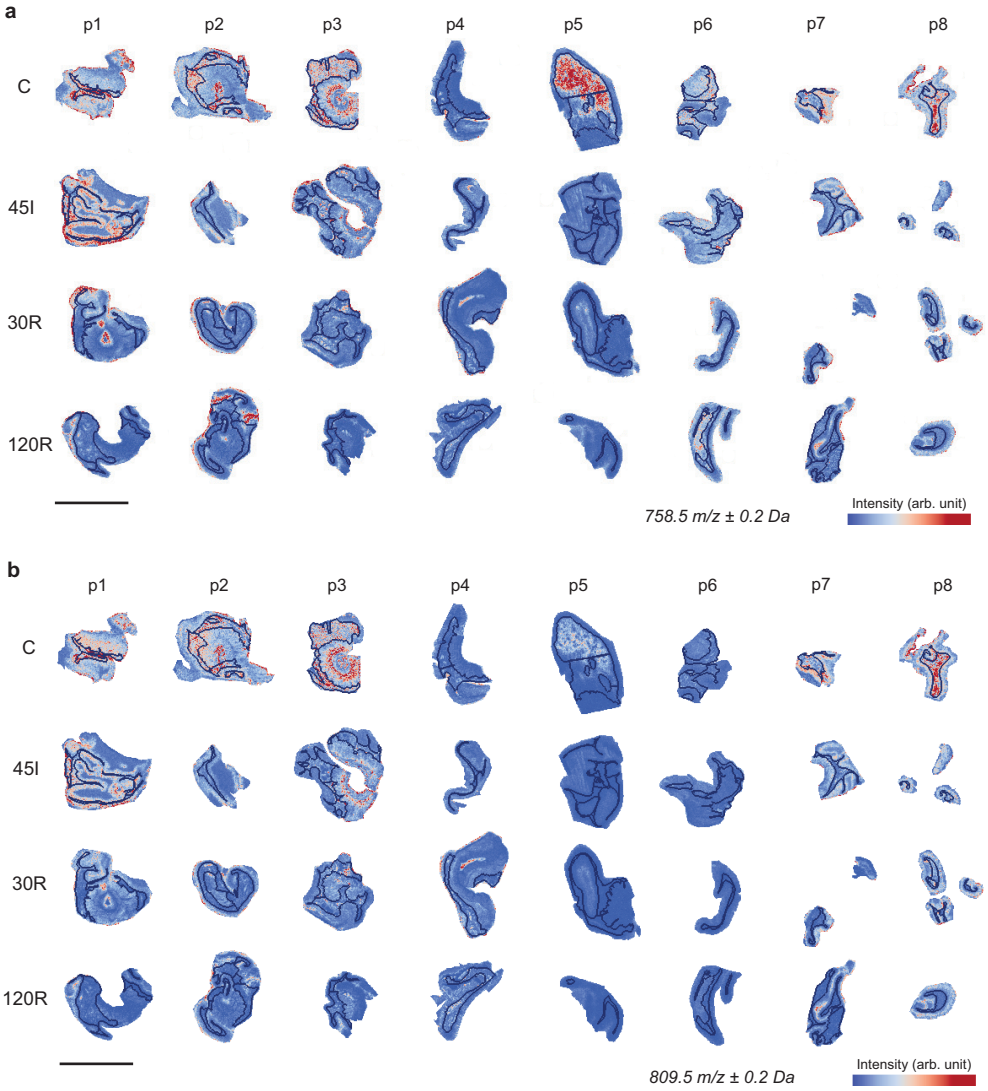

Figure S9. ***a, b***) *Individual peptide images showing examples of significantly changed m/z in submucosa layer with a high fold change (in top 10 highest fold change).*

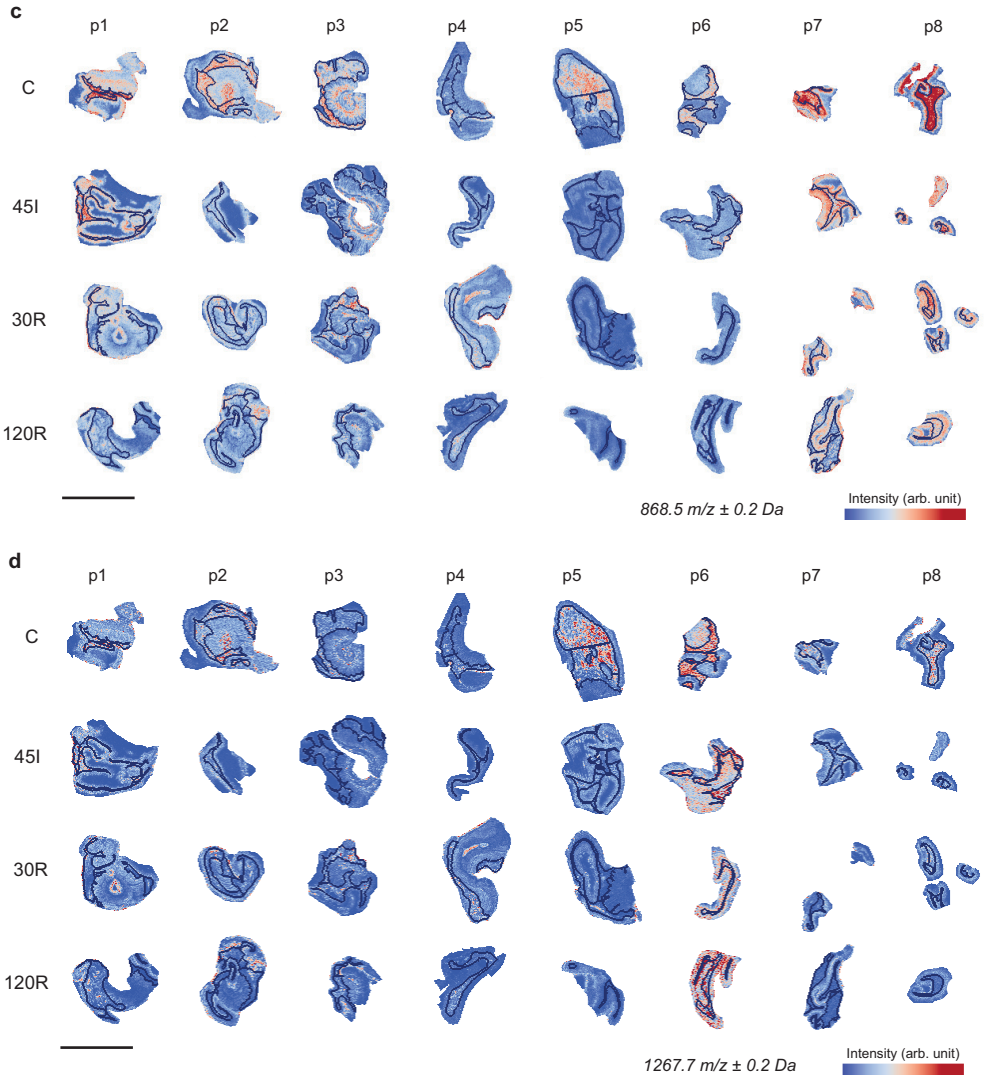

***Figure S9**. **c, d**) Individual peptide images showing examples of significantly changed m/z in submucosa layer with a high abundance (top 3 highest intensity in Ctrl sample among samples with a fold change >2).*

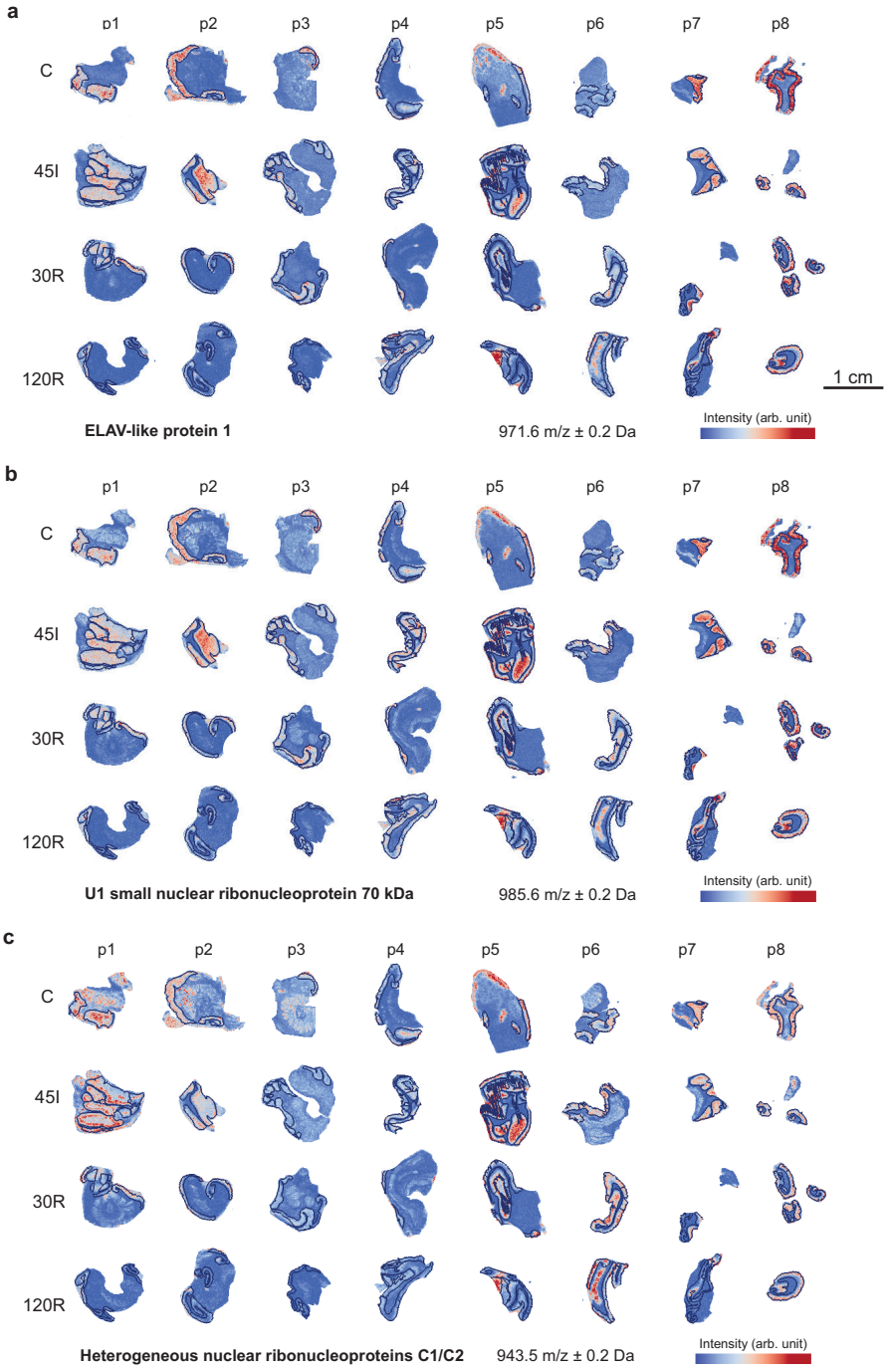

Figure S10. *Individual peptide images for a selection of annotated proteins using MALDI-TOF combined with FTICR and LC-MS/MS.* ***a, b, c****) Proteins related to RNA splicing and processing are located in the mucosa layer: ELAV like protein 1, ELAV1 (a), small nuclear ribonucleoprotein U1 subunit 70 (SNRNP70) (b), and heterogeneous nuclear*

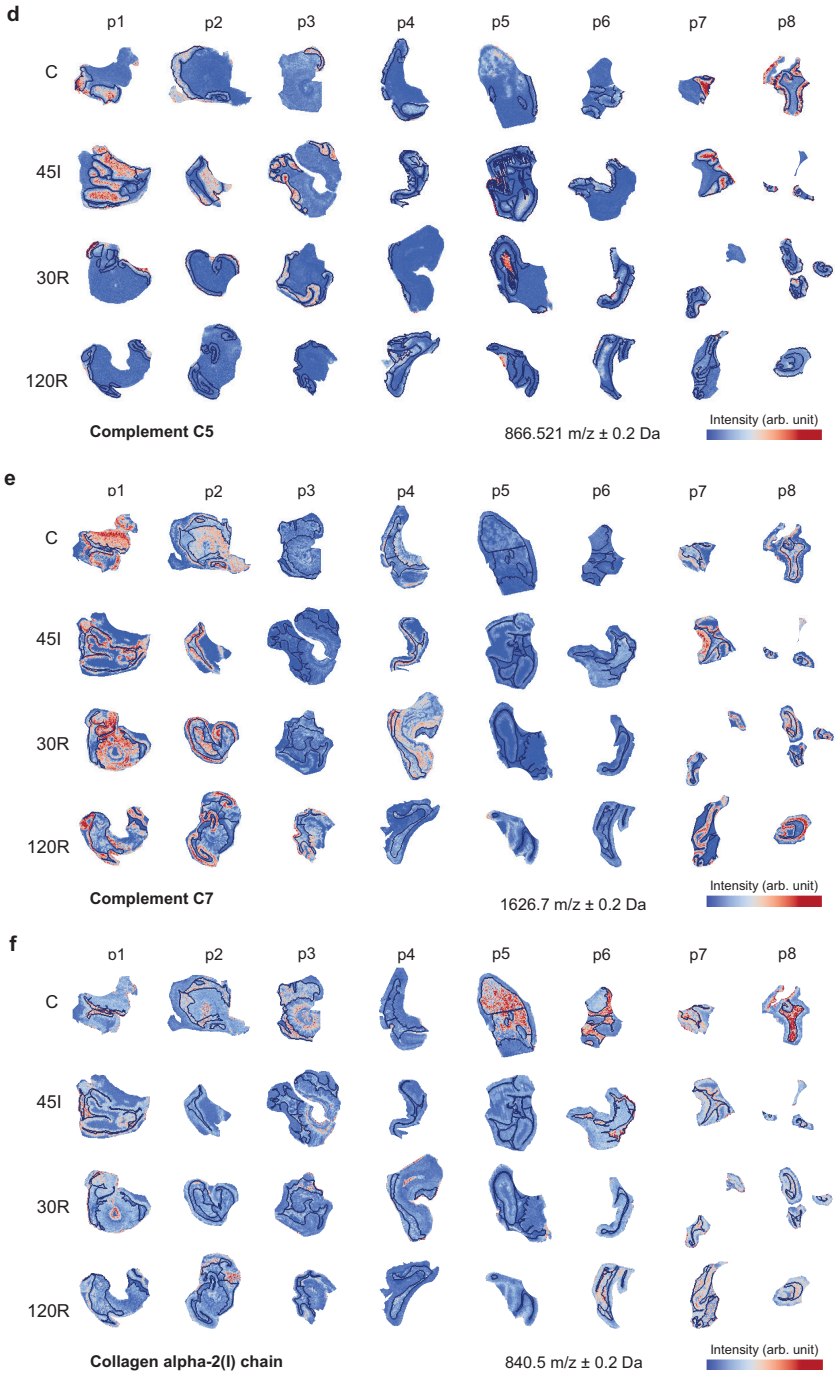

Figure S10. *ribonucleoprotein C (HNRNPC) (c).* ***d, e****) Complement factors C5 and C7 located in mucosa and submucosa layer, and* ***f****) collagen 1 alpha2 (I) chain (COL1A2) located in the submucosa layer*

CHAPTER 4

Proteomics analysis of human intestinal organoids during hypoxia and reoxygenation as a model to study ischemia-reperfusion injury

Anna M. Kip, Zita Soons, Ronny Mohren, Annet A.M. Duivenvoorden, Anjali AJ Röth, Berta Cillero-Pastor, Ulf P. Neumann, Cornelis H.C. Dejong, Ron M.A. Heeren, Steven W.M. Olde Damink, Kaatje Lenaerts

Cell Death Dis 12, 95 (2021)

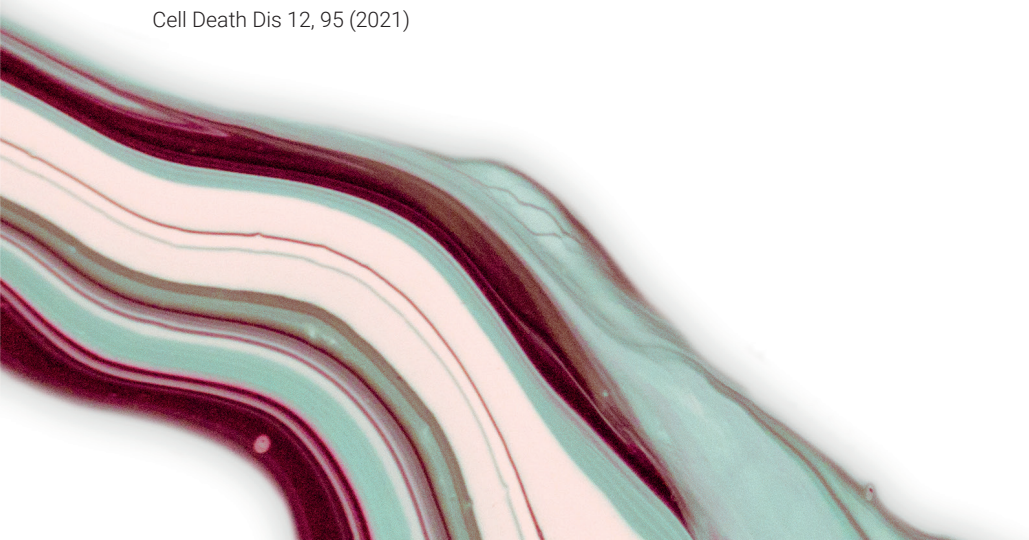

ABSTRACT

Intestinal ischemia-reperfusion (IR) injury is associated with high mortality rates, which have not improved in the past decades despite advanced insight in its pathophysiology using *in vivo* animal and human models. The inability to translate previous findings to effective therapies emphasizes the need for a physiologically relevant *in vitro* model to thoroughly investigate mechanisms of IR-induced epithelial injury and test potential therapies. In this study, we demonstrate the use of human small intestinal organoids to model IR injury by exposing organoids to hypoxia and reoxygenation (HR). A mass-spectrometry-based proteomics approach was applied to characterize organoid differentiation and decipher protein dynamics and molecular mechanisms of IR injury in crypt-like and villus-like human intestinal organoids. We showed successful separation of organoids exhibiting a crypt-like proliferative phenotype, and organoids exhibiting a villus-like phenotype, enriched for enterocytes and goblet cells. Functional enrichment analysis of significantly changing proteins during HR revealed that processes related to mitochondrial metabolism and organization, other metabolic processes, and the immune response were altered in both organoid phenotypes. Changes in protein metabolism, as well as mitophagy pathway and protection against oxidative stress were more pronounced in crypt-like organoids, whereas cellular stress and cell death associated protein changes were more pronounced in villus-like organoids. Profile analysis highlighted several interesting proteins showing a consistent temporal profile during HR in organoids from different origin, such as NDRG1, SDF4 or DMBT1. This study demonstrates that the HR response in human intestinal organoids recapitulates properties of the *in vivo* IR response. Our findings provide a framework for further investigations to elucidate underlying mechanisms of IR injury in crypt and/or villus separately, and a model to test therapeutics to prevent IR injury.

INTRODUCTION

Intestinal ischemia-reperfusion (IR) is a potentially life-threatening condition associated with a range of clinical conditions including acute mesenteric ischemia, shock and major surgery. Reperfusion of the ischemic intestine paradoxically aggravates tissue injury. Many biological processes are implicated in the complex pathophysiology of IR injury, including the oxidative stress response, cell death programs, epithelial barrier breach, innate and adaptive immune responses and the interplay with the luminal microenvironment[1,2]. Although previous work using animal IR models[3] and, in the last decade, human *in vivo* IR models[4,5] have provided important insights in understanding pathophysiological processes that occur during IR, the inability to translate findings to effective therapies contributes to continued high mortality rates of intestinal ischemia[6,7]. A physiologically relevant *in vitro* model is crucial to thoroughly investigate mechanisms of IR-induced epithelial injury and test potential therapies, and, hence, to eventually achieve an improved patient outcome.

IR-induced damage starts at the tip of the villi, and may, as the duration of ischemia increases, continue towards the crypt[8-10]. Reperfusion following prolonged ischemia resulted in apoptosis of Paneth cells in a human IR model[11]. Mature enterocytes at the villus tips are most susceptible to IR, which has been classically explained by the oxygen gradient along the crypt-villus axis with decreasing oxygen tension towards the villus tip[12]. In addition, mature enterocytes are physiologically in a pro-apoptotic state which makes them prone to be shed from the villus[13]. This mechanism is crucial for homeostasis, but may also contribute to increased susceptibility for IR-induced cell death compared to immature epithelial cells. These differences in IR response between crypt and villus, emphasizes the importance of a model that enables the study of both compartments.

Conventional two-dimensional cell lines do not reflect the complex intestinal architecture and composition and are far from translatable to the human setting. The recently established intestinal organoid model has attracted attention as an *in vitro* tool to study intestinal (patho)physiology. Intestinal organoids are three-dimensional epithelial structures that recapitulate the cellular diversity and many functions of the intestinal epithelium[14-16], which makes them closer to normal human physiology and thus superior to immortalized cell lines. Furthermore, organoids resemble the genetic signature of original tissues[15,17-19] and have been shown to exhibit a personalized proteome profile[20]. Next to the purpose of studying epithelial biology (e.g. tissue renewal and niche function), organoids have been used for disease modeling, e.g. cancer, hereditary diseases and infectious diseases[21-24] and as tools for personalized cancer therapy[25] and regenerative medicine[26].

In this study, we used human small intestinal organoids to model IR injury by exposing them to hypoxia-reoxygenation. As induction of a differentiated organoid phenotype allows for the separation of crypt and villus regions[22,23], the differences in molecular response to IR in the distinct regions could be investigated. We aimed to characterize the different organoid phenotypes, as well as decipher protein dynamics and molecular mechanisms of IR injury in crypt- and villus-like human intestinal organoids, by using a system-wide mass spectrometry (MS)-based proteomics approach.

METHODS

Human intestinal organoid culture

Human tissues and ethics

Tissue specimens of healthy small intestine were obtained from patients during pancreaticoduodenectomy at Maastricht University Medical Center+ or RWTH Aachen University Hospital. The ethics committee of both institutes approved this study (METC 16-4-185, EK 206/09) and written informed consent was obtained. Small intestinal organoid lines derived from 4 patients (average age 72 years; 3F/1M), of which 3 for proteomics analysis, were used for this study.

Organoid culture and differentiation

Crypts were isolated as described previously by Sato et al.[15], and embedded in basement membrane extract (BME, Geltrex LDEV-free reduced growth factor basement membrane matrix; Gibco, Carlsbad, CA). Organoids were maintained using growth medium (GM) which contained Advanced Dulbecco's Modified Eagle's medium F12 (Gibco) supplemented with Pen/Strep (50 units/ml penicillin and 50 µg/ml streptomycin) (Gibco), 10 mM HEPES (Gibco) and 1x Glutamax (Gibco), with 1x N2 (Gibco), 1x B27 (Gibco) and 50% v/v Wnt3a conditioned medium, 20% v/v Rspondin-1-conditioned medium, 10% v/v Noggin-conditioned medium, 10 mM Nicotinamide (Sigma-Aldrich, St. Louis, MO), 50 ng/ml murine EGF (Gibco), 1.25 mM *N*-acetyl cystein (Sigma-Aldrich), 10 mM Gastrin I (Sigma-Aldrich), 500 nM (TGFβ inhibitor) A83-01 (Sigma-Aldrich), and 10 µM (p38 MAPK inhibitor) SB202190 (Sigma-Aldrich). ROCK inhibitor Y-27632 10 µM (Abmole Bioscience, Houston, TX) was added to the medium only when organoids were generated, after passaging and thawing. Medium was changed every 2-3 days and organoids were passaged every 10 days using TrypLE™ Express Enzyme (Gibco) followed by mechanical disruption using a glass Pasteur pipette with a narrowed tip. Organoids were frozen 3-4 days after passaging using Recovery™ Cell Culture freezing medium (Gibco) and stored in liquid nitrogen. Cultures were regularly tested for mycoplasma contamination. Organoids used for experiments were passaged at least once after thawing. To induce differentiation, organoids were cultured in GM for 7 days followed by differentiation medium (VL) for 5 days. DM contained the same components as GM without addition of Wnt3a-conditioned medium, Nicotinamide and SB202190 as well as a 50% reduction of Rspondin-1- and Noggin-conditioned medium.

Exposure to hypoxia-reoxygenation

To mimic human intestinal ischemia-reperfusion injury, crypt-like (12 days GM-cultured) and villus-like (7 days GM- and 5 days DM-cultured) organoids were exposed to hypoxia (<1.0% O_2, 5% CO_2) using a O_2/CO_2 incubator (Panasonic), followed by reintroduction to 21% O_2, 5% CO_2 (reoxygenation phase). At the start of reoxygenation medium was changed. Different hypoxic periods, ranging from 2 to 24 h, were examined as it has been previously reported that it may take 4 to 24 h to reach adequately reduced O_2 levels in the medium after placing cells in hypoxic conditions[27,28]. The optimal duration of hypoxia was determined based on the stress response (HIF1A target VEGFA and unfolded protein stress signaling) and morphological changes (unpublished data). For the current study, organoids were harvested after 12 h of hypoxia (12H), after 30 and 120 minutes of reoxygenation (30R and 120R), and without hypoxic exposure (Ctrl).

Quantitative real-time PCR

Total RNA was isolated using TRI Reagent (Sigma-Aldrich) according to the manufacturer's instructions. RNA concentrations were measured with a DeNovix DS-11 spectrophotometer and 750 ng RNA was used for reverse transcription into cDNA using the SensiFast cDNA Synthesis kit (Bioline GmbH, Germany). Quantitative real-time PCR analysis was performed on the LightCycler480 (Roche) using a three-step program (40 cycles). SensiMix SYBR Hi-Rox kit (Bioline GmbH) was used for amplification. Data were processed using LinRegPCR software (version 2016.1). The geometric mean of reference genes beta-2-microglobulin (*B2MG*) and beta-actin (*ACTB*) was used for normalization. Primer sequences are listed in **Table 1**.

Table 1. Human primer sequences

Gene	Full name	Forward primer	Reverse primer
MUC2	Mucin 2	CTACTGGTGTGAGTCCAAGG	GGCACTTGGAGGAATAAACTG
OLFM4	Olfactomedin-4	TGGACAGAGTGGAACGCTTG	TCAGAGCCACGATTTCTCGG
LYZ	Lysozyme	GATAACATCGCTGATGCTGTAGCT	CATGCCACCCATGCTCTAATG
I-FABP	Intestinal fatty-acid binding protein	ACGGACAGACAATGGAAACGA	ACTGTGCGCCAAGAATAATGC
VEGF	Vascular endothelial growth factor	GGCCTCCGAAACCATGAACT	CTGGGACCACTTGGCATGG
B2MG	Beta-2-microglobulin	TCCATCCGACATTGAAGTTG	CGGCAGGCATACTCATCTT
ACTB	Beta-actin	GCTGTGCTACGTCGCCCTG	GGAGGAGCTGGAAGCAGCC

Immunohistochemistry

Organoids were collected in Cell Recovery Solution (Corning, New York, USA) to remove the BME. Then they were fixed in Unifix 4% paraformaldehyde (Klinipath, Duiven, The Netherlands) for 30 min and washed with PBS. Subsequently, organoids were first embedded in HistoGel (Thermo Scientific, Waltham, MA), followed by dehydration, paraffin embedding and sectioning (5 µm thickness, Leica microtome). Paraffin-embedded organoid sections were deparaffinized, and endogenous peroxidase activity was blocked using 0.6% hydrogen peroxide in methanol for 15 min. Antigen retrieval was performed in 10 mM citrate buffer (pH 6.0) at 90°C for 20 min. Non-specific antibody binding was blocked with 5% BSA in PBS, and sections were incubated with the primary antibodies for 1 h at room temperature. Next, sections were incubated with biotin-conjugated secondary antibodies for 30 min, followed by incubation with avidin-streptavidin complex (Vectorlabs, Burlingame, CA). Antibody binding was visualized with 3,3'-diaminobenzidine (DAB; Dako, Glostrup, Denmark) or HistoGreen (Linaris-Biologische Producte, Werheim-Bettingen, Germany). Sections were counterstained with hematoxylin and mounted using Entellan (Merck Millipore, Burlington, Massachusetts, USA). The following primary antibodies were used: lysozyme (Rabbit, 1:5000, Dako), Ki67 (Mouse, 1:200; Dako). Secondary antibodies rabbit anti-mouse (Dako) and swine anti-rabbit (Dako), both biotin-labelled, were used at a 1:500 dilution.

In addition, acidic mucins in goblet cells were stained with Alcian blue solution for 30 min at room temperature. To stain alkaline phosphatase, a brush border enzyme, sections were incubated with a mixture of 4-Nitro blue tetrazolium chloride, 4-toluidine salt and alkaline phosphate buffer in a humid chamber at 37°C for 30 min. Both histochemical stainings were counter-stained with Nuclear-fast red. All stainings were digitalized using Aperio CS2 scanner (Leica Microsystems) using a 20x magnification.

Western blot

Organoids were harvested in Cell Recovery Solution (Corning), followed by multiple ice-cold PBS washes to remove the BME. RIPA lysis buffer supplemented with protease inhibitors (Roche, Mannheim, Germany) and PhosSTOP (Roche), was added to the organoid pellet. Whole-cell lysates were incubated on ice for 20 min and vortexed every 5 min for 60 s. Then, the lysate was centrifuged at 16,000 g for 15 min at 4°C, and the supernatant was collected. Total protein concentrations were determined using the Pierce BCA Assay kit (Thermo Fisher, Rockford, IL).

Laemmli buffer was added to the lysate, and samples were heated for 5 min at 95°C. Equal amounts of protein were loaded on a 4-20% mini-PROTEAN TGX Stain-Free Gel (Bio-Rad, Hercules, CA) and separated by electrophoresis. Proteins were transferred to a Transblot Turbo PVDF membrane (Bio-Rad) using the Trans-Blot Turbo Blotting System (Bio-Rad). After blocking with 5% non-fat dry milk, membranes were incubated overnight at 4°C with primary antibodies against: IFABP (rabbit, 5 µg/ml, in-house antibody), Lysozyme (rabbit, 1:2000, Dako) and β-actin (mouse, 1:10000, Sigma-Aldrich). After washing with TBS-Tween 20 (0.1%), membranes were incubated for 1 h at room temperature with HRP-conjugated anti-mouse (1:15000; Jackson ImmunoResearch, West Grove, PA) or anti-rabbit (1:15000, Jackson ImmunoResearch) secondary antibodies. Signals were developed using SuperSignal West Pico chemiluminescent substrate (Thermo Fisher) or SuperSignal West Femto Maximum Sensitivity Substrate (Thermo Fisher), and a molecular imager (Amersham Imager 600, GE HealthcareLifeSciences) was used to obtain images. Band intensity was quantified with ImageQuant TL software (version 8.1, GE Healthcare Life Sciences), and normalized to β-actin control.

Proteomics sample preparation

Organoids were harvested using Cell Recovery Solution (Corning) and multiple ice-cold PBS washes to remove the BME. For protein extraction, a buffer containing 5 M Urea (GE Healthcare, Chicago, IL), 50 mM Ammonium bicarbonate (ABC) (Sigma-Aldrich) was added to the organoid pellet. Cell lysis was performed by three freeze-thaw cycles, using a -80°C freezer for freezing and sonication (40 s) in an ultrasonic bath for thawing. Protein concentrations were assessed using Bradford assay, and equal amounts of protein were used for analysis. Protein lysates were reduced with 20 mM Dithiothreitol (DTT) (Sigma-Aldrich) for 45 min, followed by alkylation with 40 mM Iodoacetamide (Sigma-Aldrich) for 45 min in the dark. The alkylation was terminated by 20 mM DDT to consume any excess Iodoacetamide. In solution digestion was performed with a Trypsin/LysC mixture (Promega, Madison, WI), added at a ratio of 1:25 (enzyme:protein), for two h at 37°C in a Thermo Shaker (Grant Instruments, Shepreth, UK) at 250 rpm. The lysate was then diluted to 1 M Urea using 50 mM ABC and further digested at 37°C at 250 rpm overnight. Addition of formic acid (Biosolve, Valkenswaard, The Netherlands) to a total of 1% terminated the digestion.

Liquid Chromatography Mass Spectrometry proteomics analysis

Peptide separation was performed on a Thermo Scientific (Dionex) Ultimate 3000 Rapid Separation ultrahigh-performance liquid-chromatography (UHPLC) system equipped with a PepSep C18 analytical column (15 cm, ID 75 µm, 1,9 µm Reprosil, 120Å). Prior to UHPLC separation, tryptic peptides were desalted on an online installed C18 trapping column. Peptides were separated on the

analytical column using a 90 min linear gradient of acetonitrile (5-35%) with 0.1% FA at a 300 nL/min flow rate. Mass spectra were collected on a Q-Exactive HF mass spectrometer (Thermo Scientific) using a data-dependent acquisition method. Raw mass spectra were processed in Proteome Discoverer software (PD, version 2.2, Thermo Scientific). Protein identification was performed using the SEQUEST search engine in combination with the SwissProt Human database (SwissProt TaxID=9606, v2017-10-25). For further analysis, results were filtered for proteins identified with high confidence (FDR <1%).

Statistical analysis

Data were obtained from three to four different organoid lines. Statistical analysis for gene expression (4 hSIO lines) and Western blot data (3 hSIO lines) was performed using Graphpad Prism (version 6.01). A Mann Whitney U-test was used to compare differences between groups (DM vs GM). A p-value <0.05 was considered statistically significant.

Proteome Discoverer software was used to assess the significance of differential protein expression. One-way ANOVA test was performed on abundance ratios between experimental conditions (6 biological replicates in 3 hSIO lines), and p-values were corrected using Benjamini-Hochberg (BH) method. A BH-adjusted p-value <0.05 was considered statistically significant. Proteins originating from Geltrex were excluded from further analysis. Functional enrichment analysis of GO biological processes and Reactome pathways was performed using METASCAPE with default settings[29].

Hierarchical clustering and temporal profile analysis were performed using R version 3.5.1. The hierarchical clustering used Ward's method and Pearson's correlation as the distance measure. The heatmap was created using the R package gplots (heatmap.2). For temporal profile analysis, proteins which were differentially expressed in at least one condition ($p<0.05$) were selected. In addition, proteins were excluded in case there were ≥1 missing values (ND values). For each significant protein, a regression fit was computed using the R package MaSigPro[30]. Linear, quadratic, third and fourth order profiles were used. Temporal profiles were considered statistically different from a 0-profile using an R-squared ≥0.5 and a BH-adjusted p-value <0.3.

Data availability

The mass spectrometry proteomics datasets generated and analyzed during the current study have been deposited to the ProteomeXchange Consortium via the PRIDE partner repository and are available with dataset identifier PXD022999.

RESULTS

Differentiation of human small intestinal organoids into crypt-like and villus-like organoids

Culture of human small intestinal organoids (hSIOs) in growth medium (GM) for 12 days resulted in either a multilobular or cystic organoid phenotype (**Figure 1a**, upper panel). To induce differentiation, organoids were cultured in differentiation medium (DM) for 5 days following 7 days GM, which resulted in a cystic phenotype either with or without a clear lumen (**Figure 1a**, lower panel). The differentiated state was demonstrated by higher gene expression of *I-FABP* and *MUC2* compared to undifferentiated hSIOs (**Figure 1b**). Alcian blue staining of mucus-containing goblet cells, a more intense staining of brush border enzyme alkaline phosphatase (**Figure 1c**) and higher protein expression of I-FABP (**Figure 1d**, **Figure S1**) confirmed the presence of goblet cells and enterocytes following differentiation. Interestingly, 20-40% of DM-cultured organoids showed villus-like structures pointing towards the lumen (**Figure 1c**, alkaline phosphatase staining). Downregulation of stem cell marker *OLFM4* (**Figure 1b**) and a lower number of Ki67-expressing cells (**Figure 1c**) was indicative for a reduced proliferative potential in DM-cultured organoids. Paneth cell marker *LYZ* was significantly higher (**Figure 1b**) and lysozyme staining appeared more pronounced in undifferentiated organoids (**Figure 1c**), however, lysozyme protein levels were not significantly different (**Figure 1d**, **Figure S1**). To further characterize undifferentiated (GM-cultured) and differentiated (DM-cultured) organoids, we implemented a quantitative proteomics approach. A total of 2182 unique proteins were identified across three different hSIO lines, of which 109 proteins were differentially expressed (75 upregulated, 32 downregulated) in DM compared to GM organoids (**Table S1**). Clustering analysis showed a clear separation between DM and GM with great similarity between different hSIO lines (**Figure 1e**). A list of known cell-type protein markers with their abundance ratios are shown in **Figure 1f**. Enterocyte and goblet cell markers were markedly increased in DM-cultured organoids (**Figure 1f**), whereas markers for enteroendocrine cells (CMGA, CHGB, SYP) and tuft cells (DLCK1) were not identified. Intestinal

***Figure 1. Characterization of crypt-like and villus-like human small intestinal organoids**. **a**) Brightfield images representing different phenotypes of hSIOs cultured in complete growth medium (GM) for 12 days (upper panel, scale bar = 200 µm) and differentiated hSIOs grown in GM for 7 days followed by 5 days in differentiation medium (DM) (lower panel, scale bar = 100 µm). **b**) mRNA expression of crypt cell markers OLFM4 (stem cells) and LYZ (Paneth cells) and villus cell markers I-FABP (absorptive enterocytes) and MUC2 (Goblet cells). Data were normalized to B2MG and ACTB reference genes, and reported as relative expression as compared to GM (set at 1). Results were obtained from 4 different hSIO lines (n=10-11, mean ±SD, ***p<0.001, ****p<0.0001, Mann Whitney U-test). OLFM4, Olfactomedin; LYZ, Lysozyme; I-FABP, Intestinal fatty acid-binding protein; MUC2, Mucin 2. **c**) Representative stainings for intestinal protein markers in sections of GM- and DM-cultured hSIO. Proliferation marker Ki67, lysozyme-containing Paneth cells, alcian blue-stained goblet cells, and alkaline phosphatase staining of the brushborder. Scale bar = 50 µm. **d**) Western blot analysis of lysozyme and IFABP. Band intensity was quantified and normalized using β-actin as loading control. Relative expression is shown as mean ±SD (n=5, obtained from 3 different hSIO lines; **p<0.01, Mann Whitney U-test). Full blots can be found in Figure S1. **e**) Heatmap showing relative change of differentially expressed proteins (p<0.05). Proteins with on/off expression are excluded from the heatmap and can be found in Table S1. n=6 from 3 different hSIO lines. **f**) List of known protein markers for intestinal cell-types, with respective abundance ratio (DM/GM) and adjusted p-value. AE, absorptive enterocytes; GC, goblet cells; SC, stem cells; PC, Paneth cells. **g**) Functional enrichment analysis showing GO biological processes significantly enriched (adjusted p-value <0.05) in DM organoids and GM organoids. Protein lists for enrichment analysis: upregulated in DM p-value <0.05; GM p-value <0.1. See also Table S1.*

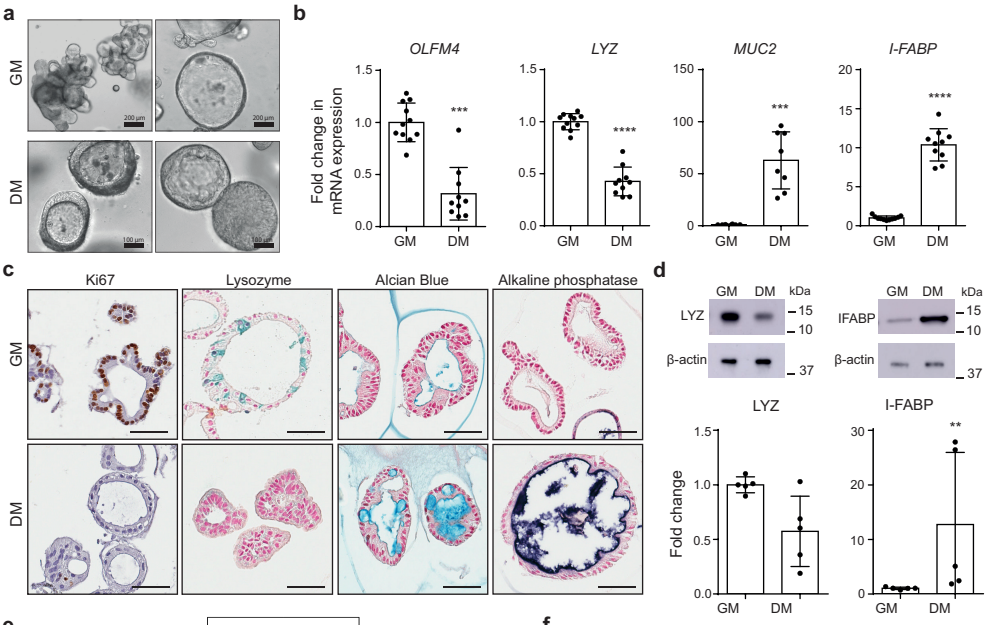

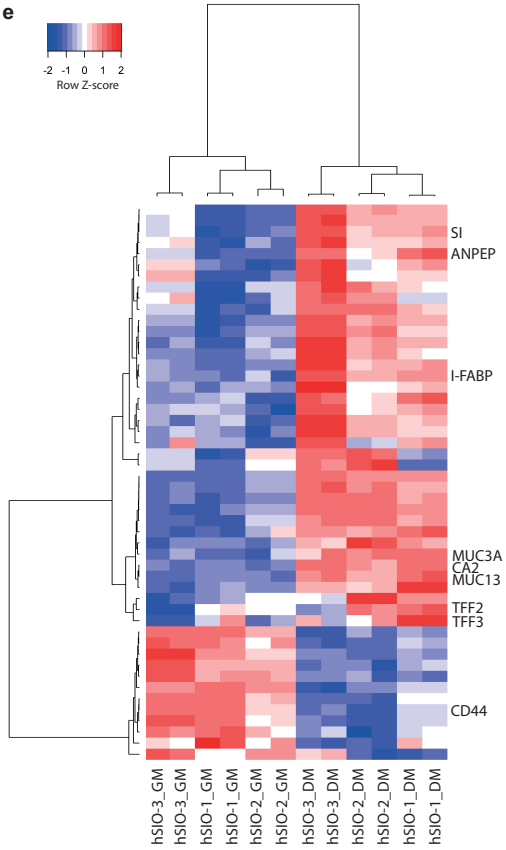

f

	Protein	Ratio DM/GM	Adj. P-value
AE	I-FABP	8.0	2.90E -09
AE	ANPEP	6.3	3.30E -06
AE	SI	5.5	1.58E -06
AE	ALPI	2.9	2.93E -02
AE	CA2	2.8	2.91E -02
AE	MGAM2	2.4	0.11
AE	VIL1	1.6	0.60
AE	VILL	1.5	0.70
GC	MUC13	4.3	9.73E -05
GC	MUC2	4.1	4.73E -04
GC	MUC3A	3.9	2.20E -03
GC	TFF3	2.9	2.56E -02
GC	TFF2	2.8	3.08E -02
GC	MUC1	1.6	0.44
SC	CD44	0.2	6.06E -04
PC	OLFM4	0.8	0.97
PC	LYZ	1.4	0.84

g

DM-enriched biological process	-Log(p-value)
Digestion	9.017
Retinoid metabolic process	5.879
Chylomicron assembly	4.806
Fructose catabolic process	3.709
Response to zinc ion	3.513
Cellular response to xenobiotic stimulus	2.536
Antibiotic catabolic process	2.240
Cofactor metabolic process	1.504
Negative regulation of immune effector process	1.309

GM-enriched biological process	-Log(p-value)
Pre-replicative complex assembly involved in nuclear cell cycle DNA replication	2.987

stem cell marker CD44 was reduced in DM-cultured organoids. Paneth cell marker LYZ showed no overall significant change. Next, functional differences between GM and DM-cultured organoids were evaluated by GO enrichment analysis. Enriched biological processes in differentiated organoids were predominantly related to digestion and metabolic processes (**Figure 1g**). Upregulated proteins in GM ($p<0.1$) were enriched for processes related to DNA replication (**Figure 1g**).

Overall, these data indicate that DM induced a villus-like (VL) organoid phenotype enriched for enterocytes and goblet cells, whereas GM-cultured organoids present a crypt-like (CL) phenotype enriched for proliferating cells. This allows for the separate investigation of the crypt- and villus response to hypoxia and reoxygenation.

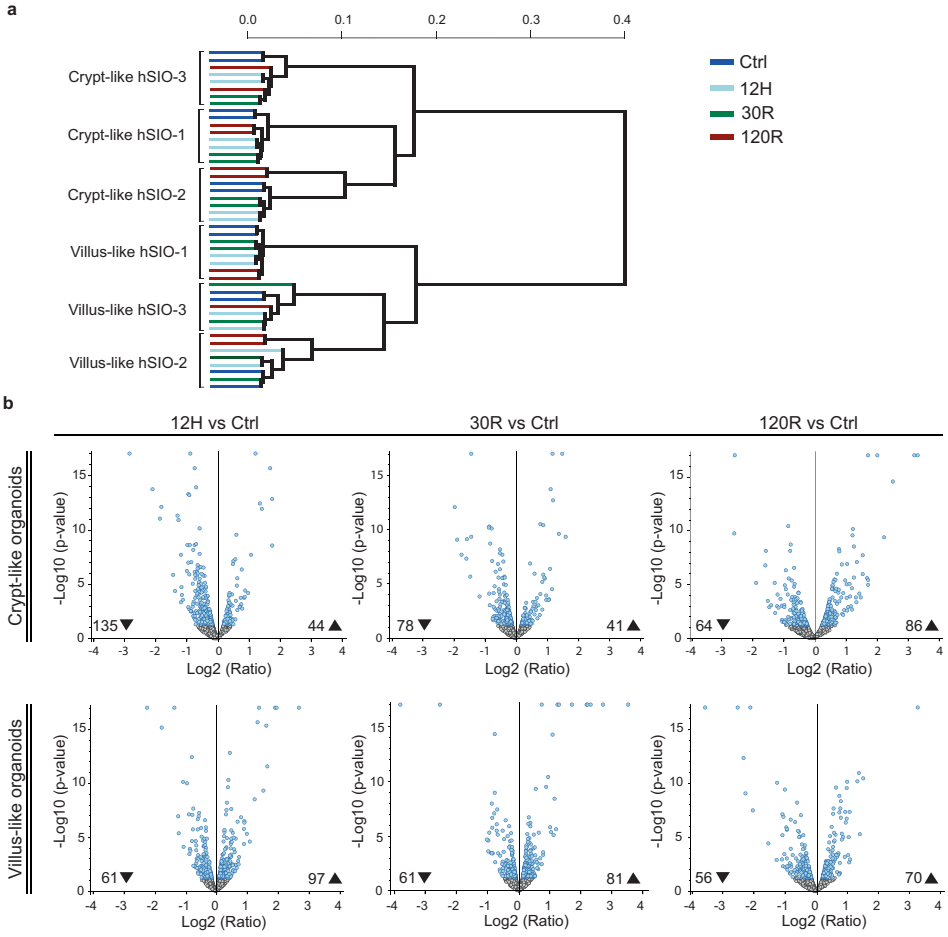

Figure 2. Proteomics analysis of the response to hypoxia-reoxygenation. a*) Hierarchical clustering of the complete proteomics dataset. 12H; 12 h of hypoxia, 30R; 30 min of reoxygenation, 120R; 120 min of reoxygenation.* ***b****) Vulcano plots for experimental conditions 12H, 30R and 120R compared to Ctrl in crypt-like and villus-like hSIOs, in which abundance ratio (Log2) is plotted against the p-value (-log10). The number upregulated and downregulated proteins are indicated in every plot (adjusted p-value <0.05). On/off proteins are not shown and can be found in Table S2. n=6 from 3 hSIO lines.*

Proteomic profiling of the response to hypoxia-reoxygenation in crypt and villus-like organoids

We next performed in-depth proteomics analysis of the response to hypoxia and reoxygenation (HR), mimicking ischemia and reperfusion, in both CL and VL organoids. The following experimental conditions were investigated: 12 h of hypoxia (12H), 30 and 120 min of reoxygenation (30R, 120R), and no HR (Ctrl). Hierarchical clustering analysis of the complete proteomics dataset revealed that the differentiation state of the organoids (CL versus VL) was responsible for the two main clusters (**Figure 2a**). Higher similarity was observed between samples derived from the same hSIO line than between samples in the same experimental HR condition. Biological replicates from all hSIO lines were combined to investigate robust HR-induced proteomic changes. Vulcano plots in **Figure 2b** show the number of up- and downregulated proteins at 12H, 30R and 120R compared to Ctrl in CL and VL organoids (see **Table S2** for lists of differentially expressed proteins).

Enrichment analysis of altered biological processes during hypoxia-reoxygenation

Functional enrichment analysis for the combined up- and downregulated proteins was performed to analyze biological processes that are changed in response to HR, and to determine the crypt- and villus response. Enriched processes at 12H, 30R and 120R compared to Ctrl are shown in **Figure 3** and abundance ratios of selected proteins can be found in **Figure S2**.

Mitochondrial metabolism and organization

The most significantly enriched biological process at 12H in both CL and VL organoids was related to energy production in the mitochondria. Additionally, the process 'mitochondrion organization' was enriched at 12H in both CL and VL organoids (**Figure 3**, light blue bars). Several subunits of the mitochondrial respiratory chain complexes were significantly changing, primarily at 12H. In VL organoids, we observed an upregulation of complex I subunits (NDUFB10 (**Figure S2a**), NDUFS5, NDUFV1), and subunits of complex IV (COX17) and V (ATP5PB) (**Figure S2a**). A downregulation of complex V subunits (ATP5PB (**Figure S2a**), ATP5ME, ATP5PD, ATP5MG) was found in CL organoids at 12H. With regard to mitochondrial structure, abundances of mitochondrial outer membrane proteins VDAC1 (**Figure S2b**), TOMM70 and TOMM22 (**Figure S2b**) were decreased in CL organoids. Interestingly, at 120R the mitophagy pathway was significantly enriched in CL organoids (**Figure 3**). An increased protein expression of autophagy receptor SQSTM1 (**Figure S2b**) and decreased abundances of mitochondrial proteins TOMM22, VDAC1 (**Figure S2b**) and SLC25A6, suggests occurrence of mitophagy following HR in CL organoids. No changes in mitophagy-related proteins were observed in VL organoids.

Protein metabolism

Enrichment analysis revealed regulation of various metabolic processes in both CL and VL organoids (**Figure 3**, dark blue). One of the top enriched processes in CL organoids ('SRP-dependent cotranslational protein targeting to membrane') is related to protein translation (**Figure 3**, vertical striped). Multiple 60S ribosomal proteins showed increased abundances in CL organoids following HR (e.g. RPL4, RPL6, RPL7a, RPL13, RPL35, RPL18) whereas in VL organoids we observed reduced abundances (e.g. RPL13, RPL4, **Figure S2c**) or no difference (e.g. RPL6, RPL18, **Figure S2c**). Furthermore, HR decreased expression of translation initiation factor EIF4G1 (**Figure S2c**),

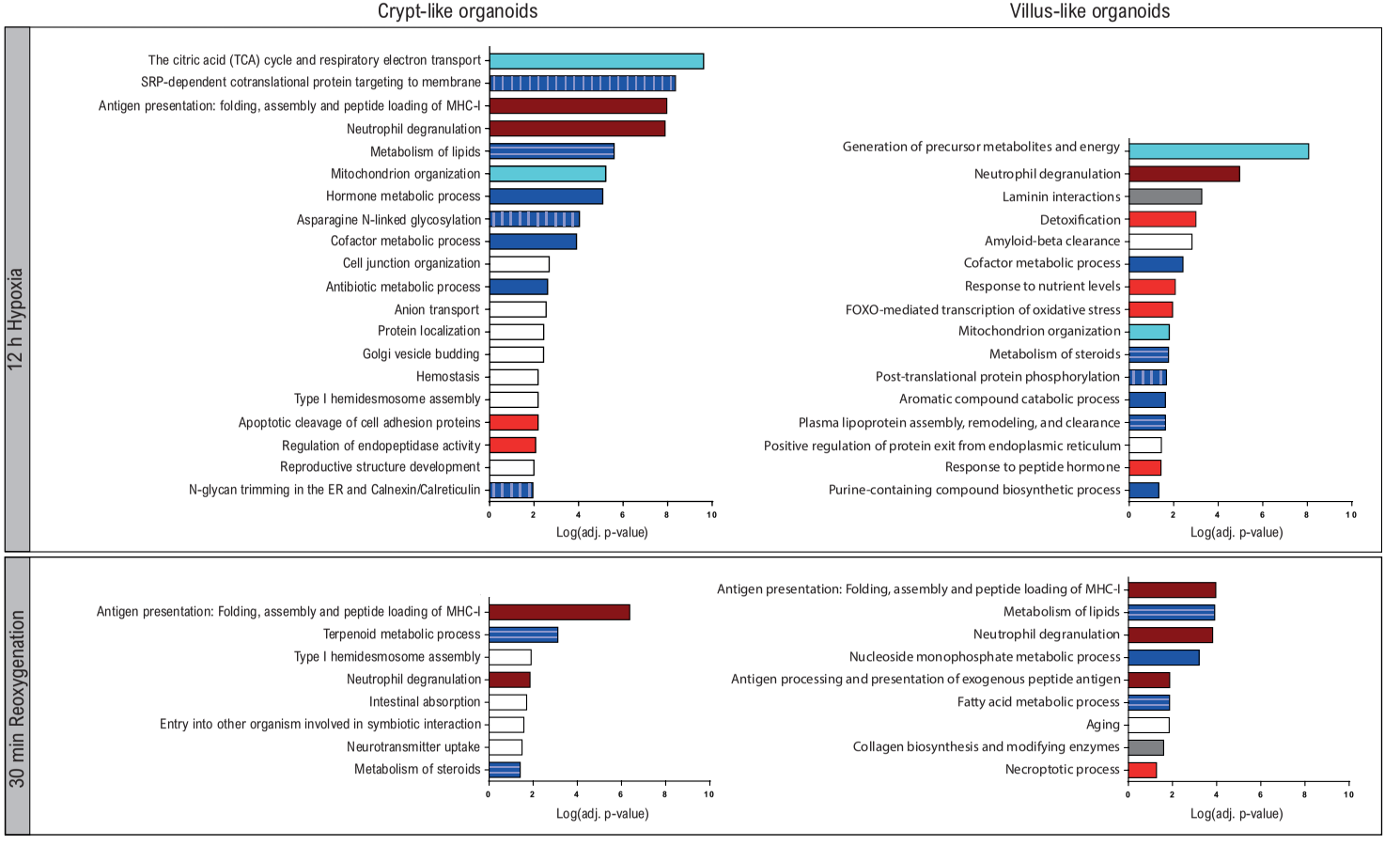
Crypt-like organoids
Villus-like organoids
12 h Hypoxia
The citric acid (TCA) cycle and respiratory electron transport
SRP-dependent cotranslational protein targeting to membrane
Antigen presentation: folding, assembly and peptide loading of MHC-I
Neutrophil degranulation
Metabolism of lipids
Mitochondrion organization
Hormone metabolic process
Asparagine N-linked glycosylation
Cofactor metabolic process
Cell junction organization
Antibiotic metabolic process
Anion transport
Protein localization
Golgi vesicle budding
Hemostasis
Type I hemidesmosome assembly
Apoptotic cleavage of cell adhesion proteins
Regulation of endopeptidase activity
Reproductive structure development
N-glycan trimming in the ER and Calnexin/Calreticulin
0 2 4 6 8 10
Log(adj. p-value)
Generation of precursor metabolites and energy
Neutrophil degranulation
Laminin interactions
Detoxification
Amyloid-beta clearance
Cofactor metabolic process
Response to nutrient levels
FOXO-mediated transcription of oxidative stress
Mitochondrion organization
Metabolism of steroids
Post-translational protein phosphorylation
Aromatic compound catabolic process
Plasma lipoprotein assembly, remodeling, and clearance
Positive regulation of protein exit from endoplasmic reticulum
Response to peptide hormone
Purine-containing compound biosynthetic process
0 2 4 6 8 10
Log(adj. p-value)
30 min Reoxygenation
Antigen presentation: Folding, assembly and peptide loading of MHC-I
Terpenoid metabolic process
Type I hemidesmosome assembly
Neutrophil degranulation
Intestinal absorption
Entry into other organism involved in symbiotic interaction
Neurotransmitter uptake
Metabolism of steroids
0 2 4 6 8 10
Log(adj. p-value)
Antigen presentation: Folding, assembly and peptide loading of MHC-I
Metabolism of lipids
Neutrophil degranulation
Nucleoside monophosphate metabolic process
Antigen processing and presentation of exogenous peptide antigen
Fatty acid metabolic process
Aging
Collagen biosynthesis and modifying enzymes
Necroptotic process
0 2 4 6 8 10
Log(adj. p-value)

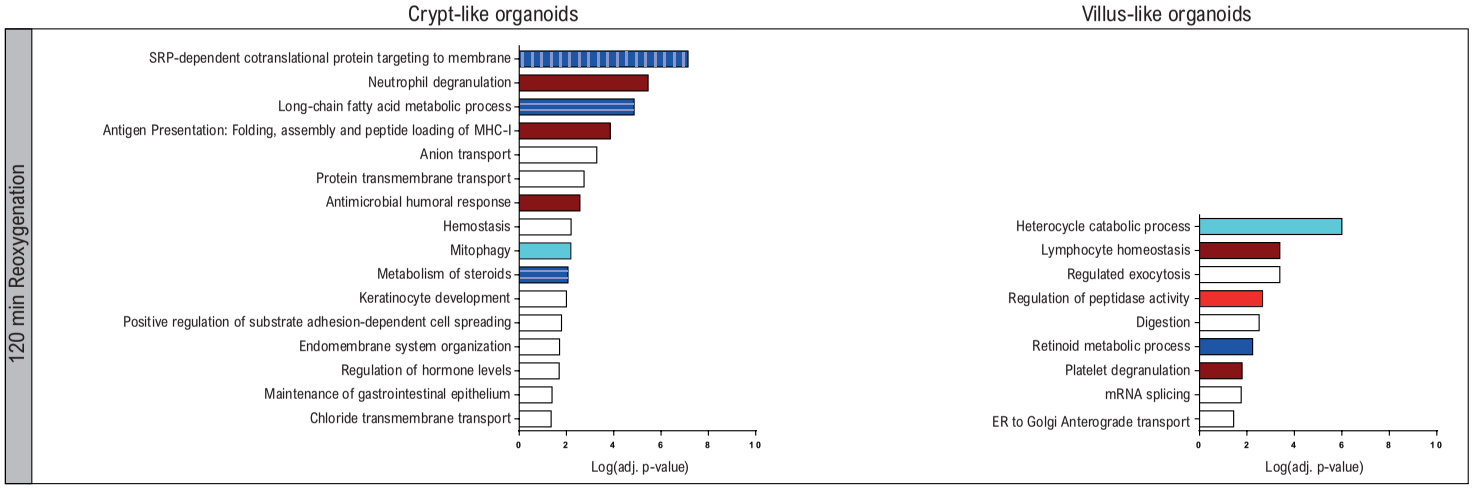

Figure 3. Functional enrichment analysis. *Enriched biological processes at 12H, 30R and 120R compared to Ctrl in CL organoids (left) and VL organoids (right) are shown. A combined list of significantly up- and downregulated proteins was used for analysis, and an adjusted p-value <0.05 was considered statistically significant. Enrichment analysis for GO biological processes and Reactome pathways was performed using METASCAPE. Bar colors indicate groups of selected processes. Processes related to mitochondrial structure and metabolism (light blue), enriched in both CL and VL organoids. Metabolic processes (dark blue): protein metabolism, enriched in CL organoids (vertical stripe); lipid metabolism, in CL and VL organoids (horizontal stripe). Processes related to stress response and apoptosis (red), more pronounced in VL organoids. Extracellular matrix interactions (grey), enriched in VL organoids. Immune response (dark red), enriched in both CL and VL organoids.*

proteins implicated in protein transport into the ER (SSR3, **Figure S2c**) and co-translational N-linked glycosylation (RPN1, RPN2 (**Figure S2c**), DDOST), as well as proteins involved in quality control of protein folding (CANX, **Figure S2c**) and transport of folded proteins (LMAN1).

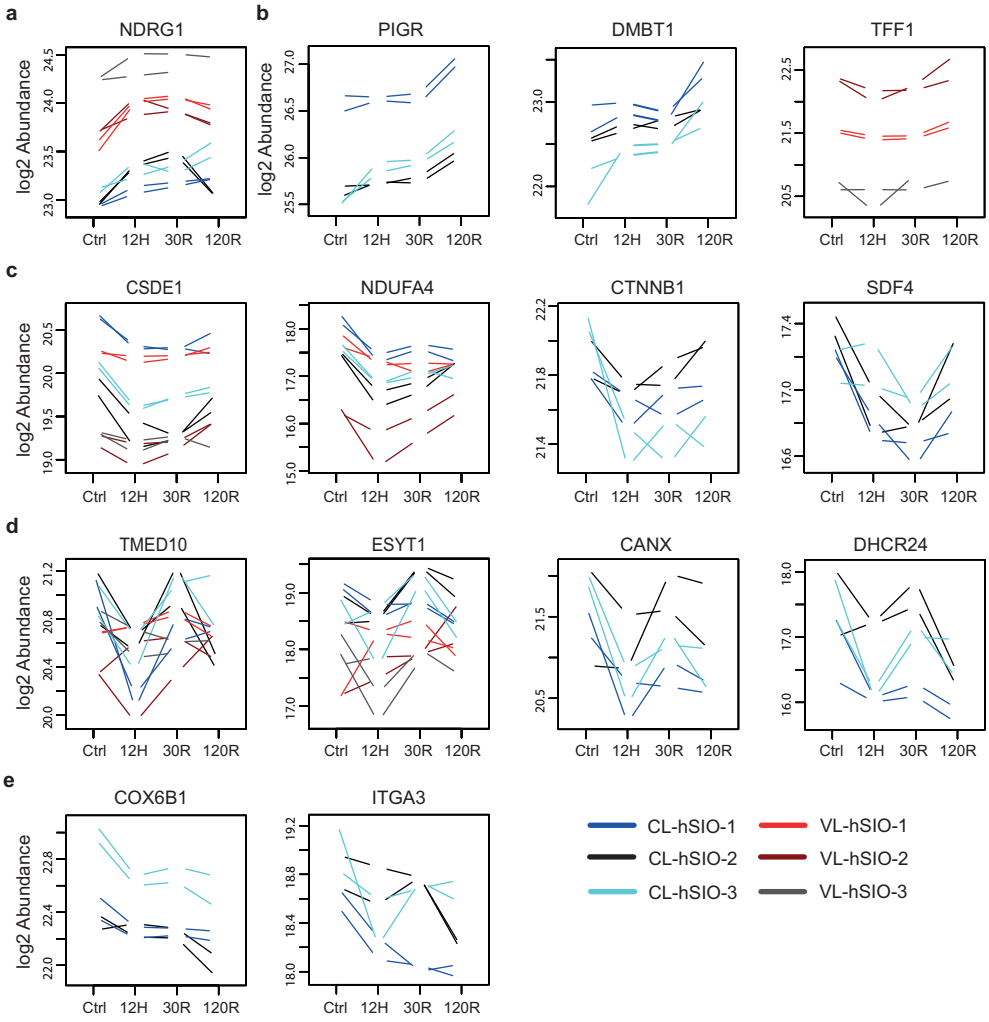

Figure 4. Temporal expression profiles. *Proteins showing a consistent temporal profile in both CL and VL organoids, or either CL or VL organoids are shown. Profiles are clustered in five groups which are presented in panels* ***a***, ***b***, ***c***, ***d*** *and* ***e***. *Temporal profile analysis was performed using R package MaSigPro, and temporal profiles were considered statistically different using an R-squared ≥0.5 and a adjusted p-value <0.3. See also Figure S4, in which all significant profiles can be found. NDRG1, N-Myc downstream regulated 1; PIGR, polymeric immunoglobulin receptor; DMBT1, deleted in malignant brain tumors 1; TFF1, trefoil factor 1; CSDE1, cold shock domain containing E1; NDUFA4, cytochrome c oxidase subunit; CTNNB1, B-catenin; SDF4, 45 kDa calcium-binding protein; TMED10, transmembrane emp24 domain-containing protein 10; ESYT1, extended synaptotagmin-1; CANX, calnexin; DHCR24, delta(24)-sterol reductase; COX6B1, cytochrome c oxidase subunit 6B1; ITGA3, integrin alpha-3.*

Lipid metabolism

Processes associated with lipid metabolism were enriched at all time points in CL and VL organoids (**Figure 3**, horizontal striped). Several proteins involved in fatty acid β-oxidation showed a decreased expression, and included CPT1A (CL; **Figure S2d**) and long-chain fatty acid-CoA ligases ACSL3, ACSL5 (CL) and ACSL4 (CL, VL; **Figure S2d**). In addition, we observed an upregulation of monoglyceride lipase (MGLL; CL), and fatty acid binding protein (FABP2; CL, VL). Changes in fatty acid synthesis included a reduced expression of fatty acid desaturase (FADS2, **Figure S2d**) (CL, VL), and enzymes playing a key role in fatty acid elongation (ELOVL1 (**Figure S2d**), HSD17B12, TECR) in CL organoids.

Cellular stress response

The processes 'response to hypoxia' and 'response to oxidative stress' were not significantly enriched, however, increased transcript levels of well-known HIF1A target VEGF confirmed hypoxic signaling (**Figure S3**). In addition, a closer inspection of protein abundances supports regulation of stress signaling. Hypoxic stress-responsive protein NDRG1 (**Figure S2e**) was significantly increased at all time points in both CL and VL organoids. Oxidative stress-related proteins (CHCHD2 (**Figure S2e**), ERO1A) were increased at 120R in VL organoids. In CL organoids, proteins involved in protection against oxidative stress (TXNRD2 (**Figure S2e**), PPIF) were increased at 120R, whereas in VL organoids a decrease in antioxidant protein SOD2 (12H, 30R) was observed. In addition, several processes associated with response to a stimulus (e.g. 'detoxification', 'response to nutrient levels') and cell death (e.g. 'FOXO-mediated transcription of oxidative stress', 'necroptotic process') were enriched in VL organoids (**Figure 3**, red bars). The number of cell death promoting proteins showing increased abundances was highest at 120R, and included among others DIABLO (**Figure S2e**), LCN2 (VL, CL), BCAP31 (**Figure S2e**) and ERO1A (VL). However, contradictory, the well-known apoptosis regulator BAX was decreased at 120R (VL).

Extracellular matrix

Processes related to the extracellular matrix (ECM) were exclusively enriched in VL organoids (**Figure 3**, grey bars), with increased expression of basement membrane components (COL4A1, COL4A2; **Figure S2f**), LAMB1, NID1, NID2 (**Figure S2f**), and enzymes that play a role in collagen crosslinking (PLOD1, PLOD2; **Figure S2f**). In contrast, a decreased expression of COL17A1 was observed.

Immune response

Finally, processes related to both innate and adaptive immune responses, including 'neutrophil degranulation' and 'antigen presentation' were enriched following HR in both CL and VL organoids (**Figure 3**, dark red bars).

Temporal protein profiles

We performed temporal profile analysis to examine which proteins exhibit consistent changes over the course of HR (**Figure S4**). We selected biologically interesting proteins showing consistent temporal profiles in all hSIO lines of CL and/or VL organoids by visual inspection (**Figure 4**). NDRG1 increased directly following hypoxia in CL and VL organoids with higher baseline expression in VL (**Figure 4a**). A profile characterized by increasing expression at 120R, was observed for PIGR and DMBT1

(CL; **Figure 4b**) and TFF1 and TFF2 (VL) (**Figure 4b**). B-catenin (CTNNB1), downstream effector of Wnt signaling, decreased following hypoxia and increased during reoxygenation in CL organoids. A similar profile was observed for SDF4 (CL), CSDE1 (CL, VL) and NDUF4a (CL, VL; **Figure 4c**). Different proteins involved in lipid metabolism (DHCR24 (**Figure 4d**), ACSL5, NSDHL) exhibit a down-up-down-profile in CL organoids. In addition, this profile was observed for vesicular trafficking protein TMED10, and proteins associated with ER structure and function, namely ESYT1 (CL, VL), CANX (CL; **Figure 4d**) and RPN1 (CL). A profile presenting a gradual decrease during HR was observed for cytochrome c oxidases (COX6B1, COX5a; **Figure 4e**), and integrin subunits ITGA6 and ITGA3 (**Figure 4e**) (CL).

DISCUSSION

Continued high mortality rates of intestinal ischemia emphasize the need to elucidate molecular mechanisms underlying IR injury. In this study, we demonstrate the use of the hSIO culture system to model IR injury. Proteomics analysis of CL and VL organoids separately has given us novel insights in the response to HR and potential differences between these distinct domains of the intestinal epithelium.

Successful separation of CL and VL organoids was shown by clustering and enrichment analysis of proteome data, as well as analysis of known cell-type specific markers. Consistent with previous hSIO studies[22,23], hSIOs cultured in GM exhibit a crypt-like proliferative phenotype, whereas DM induced a villus-like phenotype enriched for differentiated enterocytes and goblet cells. Even though we expected a lobular appearance of DM-treated organoids, cystic structures have been observed before in differentiated organoids from human origin[22,23]. Paneth cells, found in both organoid phenotypes, were likely present at the time differentiation was induced and DM did not further stimulate their differentiation.

The observed clustering per hSIO line rather than experimental HR condition implies that each hSIO line may hold a distinct proteome profile. This assumption is supported by a previous study in which patient-centric clustering of proteome profiles from healthy and tumor colon organoids was reported[20]. In addition, patient-derived tumor organoids resemble the original tumor and recapitulate diversity among patients[17]. The fact that hSIO lines are derived from genetically diverse individuals limits experimental reproducibility in comparison to traditional cell lines, but it is also considered a strength as this reflects interindividual differences.

Adaptation of the cellular metabolic program is required during HR, as is reflected in our functional analysis. Importantly, being major oxygen consumers for energy production, mitochondria and their metabolism are affected by hypoxia. Oxidative phosphorylation is known to adapt by repressing activity of the TCA cycle, and by remodeling protein composition of the electron transport chain[31]. Indeed, different subunits of the respiratory chain were modified after hypoxia. In CL organoids, mainly subunits of complex IV and V were downregulated, which suggests reduced ATP production. The increase in complex I subunits in VL organoids may point to higher ROS-producing capacity[32,33].

These differences between CL and VL organoid responses can be explained by the differences in energy metabolism between epithelial cell types. Proliferating cells rely mostly on aerobic glycolysis which is essential for efficient biosynthesis of macromolecular compounds. In contrast, differentiated cells primarily rely on oxidative phosphorylation[34-36]. In line, intestinal stem cell niche and differentiated cells have been shown to adapt their metabolism by different means in response to metabolic stress[36].

Next to adaptations in energy metabolism, we report a HR-induced decrease in structural mitochondrial proteins and enrichment of the mitophagy pathway in CL organoids. Mitophagy is a quality control mechanism that selectively removes damaged mitochondria by autophagy[37], and has been reported to have a protective role against renal and cardiac IR injury[38,39].

Protein synthesis and ribosome biosynthesis are energy-consuming processes that are suppressed during hypoxia to conserve cellular energy. Changed protein metabolism was observed exclusively in CL organoids, which can be explained by the fact that, in general, dividing cells have more ribosomes and a higher translational activity than non-dividing cells[40]. The increased expression of 60S ribosomal subunits following HR in combination with no changes in 40S subunits may be the result of an unbalanced production of 40S and 60S ribosomal subunits, as has been described in yeasts in response to stress[41]. The decreased expression of proteins playing a role in N-glycosylation suggests that this process is impaired, which may lead to defects in protein folding and degradation[42]. Unfolded protein stress, and subsequent activation of the unfolded protein response, plays an important role in hypoxic and IR injury[5,43-45]. In addition, our data suggests that protein transport into the ER and ER-to-Golgi are affected by HR. Our observations regarding changes in translation machinery, protein folding and trafficking in CL organoids imply suppression of protein synthesis which is a well-known adaptation mechanism of cells to cope with hypoxia and reoxygenation stress[46].

Many enzymes involved in lipid metabolic processes were changed during HR and changes were more pronounced in CL organoids. Fatty acids are normally used for oxidation and energy production as well as for synthesis of phospholipids and triacylglycerols[47]. The reduced expression of enzymes involved in fatty acid β-oxidation indicates impaired fatty acid catabolism, which may result in accumulation of free fatty acids and subsequent lipotoxicity and cell death[48].

Decreased abundances of enzymes catalyzing essential steps in fatty acid elongation and saturation likely affects synthesis and composition of (very) long-chain fatty acids, which are found as components of membrane lipids (glycerophospholipids and spingolipids)[49]. Changes in composition of membrane lipids as a result of altered fatty acid elongation metabolism, have been shown to change membrane properties and increase susceptibility to apoptosis[50].

Our data were indicative of higher ROS-producing capacity and cell death in VL organoids. Strikingly, proteins involved in protection against oxidative stress and IR injury[51,52], were exclusively increased in CL organoids. Together, this may indicate that CL organoids possess better protective mechanisms against HR-induced oxidative stress and cell death compared to VL organoids. This reflects the *in vivo* response in which villi have been shown to be affected first during IR, whereas crypts remain intact for a longer period of time[8].

Interestingly, in VL organoids, hypoxia induced the expression of various ECM proteins. Even though fibroblasts are the main source of extracellular matrix proteins, intestinal epithelial cells

can synthesize ECM proteins as well[53]. Hypoxia-induced collagen synthesis and ECM remodeling by fibroblasts has been reported[54-56]. However, to our knowledge, the effect of hypoxia on ECM remodeling by epithelial cells has not been investigated. Additionally, in CL organoids a gradually decreasing temporal profile was observed for integrins ITGA6 and ITGA3, which suggests that cell-matrix interactions are also affected in CL organoids. A decreased integrin expression may result in reduced adhesion and ECM changes.

Despite the lack of immune cells in our culture system, functional enrichment analysis revealed regulation of immune response related processes. This indicates that HR-induced stress responses interact with immune signaling, even in the absence of immune cells and microbes, which is in agreement with earlier reports[57,58]. Co-cultures of organoids with stromal cells or immune cells could be useful when aiming on specifically investigating the inflammatory response in IR or interactions between host and micro-organism. In this context, as well as for assessment of barrier function, self-organized epithelial monolayers may be a good alternative for 3D culture[59].

Temporal protein profile analysis highlighted consistent dynamic changes during HR. NDRG1 could be of particular interest in the context of IR injury as it has been shown to suppress pro-survival autophagy pathway and promote apoptosis via modulating ER stress responses[60,61], which plays an important role in IR injury. Several proteins with an upregulated profile during reoxygenation play a role in mucosal barrier integrity and defense, such as PIGR and DMBT1[62] in CL organoids, and trefoil factors in VL organoids. Temporal profiles for CTNNB1 and SDF4[63] reflect halted proliferation in CL organoids during hypoxia, which is resumed during reoxygenation. SDF4 has been shown to play a role in ER-stress induced apoptosis[64]. CSDE1 has not been specifically related with IR injury, but may be of interest considering its role in translational reprogramming[65]. Proteins involved in lipid metabolism (ASCL5, DHCR23, NSDHL) and protein metabolism and transport in the ER (TMED10, ESYT1, CANX, RPN1) showed a down-up-down profile during HR. This may be explained by hypoxic- and oxidative stress-induced metabolic changes at 12H and 120R, respectively.

In summary, we show that HR-induced protein changes in the hSIO model are involved in biological processes known to be regulated in response to IR. In addition, differences between crypt- and villus responses were highlighted. Most remarkably, cellular stress and cell death associated processes were more pronounced in VL organoids, whereas CL organoids are presumed to possess better protective mechanisms based on upregulation of proteins involved in protection against oxidative stress, and enrichment of the mitophagy pathway. In addition, protein metabolism was only enriched in CL organoids and HR-induced changes in ECM interaction were most prominent in VL organoids.

We established a model to study the epithelial response to hypoxia and reoxygenation in cultures enriched for crypt and villus cells separately. Our findings demonstrate that hSIO recapitulate *in vivo* properties of the response to IR and provide a framework for future investigations to decipher underlying mechanisms and test therapeutic targets to prevent or treat IR injury and promote regeneration. Of interest are the protective mitophagy pathway in CL organoids, or specific targets such as NDRG1, SDF4 or DMBT1 as highlighted by temporal profile analysis.

ACKNOWLEDGEMENTS

We thank Bas Boonen and Mo Hadfoune for their technical laboratory support. This work was supported by NUTRIM, Maastricht University Medical Center+ (NUTRIM Graduate Program grant to A.M. Kip); and NWO (Aspasia grant 015.010.046 to K. Lenaerts).

REFERENCES

1 Eltzschig, H. K. & Eckle, T. Ischemia and reperfusion--from mechanism to translation. *Nat Med* **17**, 1391-1401 (2011).

2 Lenaerts, K. *et al.* New insights in intestinal ischemia-reperfusion injury: implications for intestinal transplantation. *Curr Opin Organ Transplant* **18**, 298-303 (2013).

3 Gonzalez, L. M., Moeser, A. J. & Blikslager, A. T. Animal models of ischemia-reperfusion-induced intestinal injury: progress and promise for translational research. *Am J Physiol Gastrointest Liver Physiol* **308**, G63-75 (2015).

4 Derikx, J. P. *et al.* A new model to study intestinal ischemia-reperfusion damage in man. *The Journal of surgical research* **166**, 222-226 (2011).

5 Grootjans, J., Lenaerts, K., Buurman, W. A., Dejong, C. H. & Derikx, J. P. Life and death at the mucosal-luminal interface: New perspectives on human intestinal ischemia-reperfusion. *World J Gastroenterol* **22**, 2760-2770 (2016).

6 American Gastroenterological Association Medical Position Statement: guidelines on intestinal ischemia. *Gastroenterology* **118**, 951-953 (2000).

7 Kassahun, W. T., Schulz, T., Richter, O. & Hauss, J. Unchanged high mortality rates from acute occlusive intestinal ischemia: six year review. *Langenbeck's archives of surgery* **393**, 163-171 (2008).

8 Derikx, J. P. *et al.* Rapid reversal of human intestinal ischemia-reperfusion induced damage by shedding of injured enterocytes and reepithelialisation. *PloS one* **3**, e3428 (2008).

9 Chiu, C. J., McArdle, A. H., Brown, R., Scott, H. J. & Gurd, F. N. Intestinal mucosal lesion in low-flow states. I. A morphological, hemodynamic, and metabolic reappraisal. *Arch Surg* **101**, 478-483 (1970).

10 Park, P. O., Haglund, U., Bulkley, G. B. & Fält, K. The sequence of development of intestinal tissue injury after strangulation ischemia and reperfusion. *Surgery* **107**, 574-580 (1990).

11 Grootjans, J. *et al.* Level of activation of the unfolded protein response correlates with Paneth cell apoptosis in human small intestine exposed to ischemia/reperfusion. *Gastroenterology* **140**, 529-539. e523 (2011).

12 Blikslager, A. T. Life in the gut without oxygen: adaptive mechanisms and inflammatory bowel disease. *Gastroenterology* **134**, 346-348 (2008).

13 Bullen, T. F. *et al.* Characterization of epithelial cell shedding from human small intestine. *Lab Invest* **86**, 1052-1063 (2006).

14 Sato, T. *et al.* Single Lgr5 stem cells build crypt-villus structures in vitro without a mesenchymal niche. *Nature* **459**, 262-265 (2009).

15 Sato, T. *et al.* Long-term expansion of epithelial organoids from human colon, adenoma, adenocarcinoma, and Barrett's epithelium. *Gastroenterology* **141**, 1762-1772 (2011).

16 Sato, T. & Clevers, H. Growing self-organizing mini-guts from a single intestinal stem cell: mechanism and applications. *Science* **340**, 1190-1194 (2013).

17 van de Wetering, M. *et al.* Prospective derivation of a living organoid biobank of colorectal cancer patients. *Cell* **161**, 933-945 (2015).

18 Huch, M. *et al.* Long-term culture of genome-stable bipotent stem cells from adult human liver. *Cell* **160**, 299-312 (2015).

19 Georgakopoulos, N. *et al.* Long-term expansion, genomic stability and in vivo safety of adult human pancreas organoids. *BMC Dev Biol* **20**, 4 (2020).

20 Cristobal, A. *et al.* Personalized Proteome Profiles of Healthy and Tumor Human Colon Organoids Reveal Both Individual Diversity and Basic Features of Colorectal Cancer. *Cell Rep* **18**, 263-274 (2017).

21 Dutta, D., Heo, I. & Clevers, H. Disease Modeling in Stem Cell-Derived 3D Organoid Systems. *Trends Mol*

Med **23**, 393-410 (2017).
22 Foulke-Abel, J. *et al.* Human Enteroids as a Model of Upper Small Intestinal Ion Transport Physiology and Pathophysiology. *Gastroenterology* **150**, 638-649.e638 (2016).
23 Saxena, K. *et al.* Human Intestinal Enteroids: a New Model To Study Human Rotavirus Infection, Host Restriction, and Pathophysiology. *J Virol* **90**, 43-56 (2016).
24 Onozato, D. *et al.* Application of Human Induced Pluripotent Stem Cell-Derived Intestinal Organoids as a Model of Epithelial Damage and Fibrosis in Inflammatory Bowel Disease. *Biol Pharm Bull* **43**, 1088-1095 (2020).
25 Ooft, S. N. *et al.* Patient-derived organoids can predict response to chemotherapy in metastatic colorectal cancer patients. *Sci Transl Med* **11** (2019).
26 Leushacke, M. & Barker, N. Ex vivo culture of the intestinal epithelium: strategies and applications. *Gut* **63**, 1345-1354 (2014).
27 Newby, D., Marks, L. & Lyall, F. Dissolved oxygen concentration in culture medium: assumptions and pitfalls. *Placenta* **26**, 353-357 (2005).
28 Zhang, K. *et al.* Dissolved oxygen concentration in the medium during cell culture: Defects and improvements. *Cell Biol Int* **40**, 354-360 (2016).
29 Zhou, Y. *et al.* Metascape provides a biologist-oriented resource for the analysis of systems-level datasets. *Nat Commun* **10**, 1523 (2019).
30 Nueda, M. J., Tarazona, S. & Conesa, A. Next maSigPro: updating maSigPro bioconductor package for RNA-seq time series. *Bioinformatics* **30**, 2598-2602 (2014).
31 Fuhrmann, D. C. & Brüne, B. Mitochondrial composition and function under the control of hypoxia. *Redox Biol* **12**, 208-215 (2017).
32 Brand, M. D. The sites and topology of mitochondrial superoxide production. *Exp Gerontol* **45**, 466-472 (2010).
33 Dröse, S. & Brandt, U. Molecular mechanisms of superoxide production by the mitochondrial respiratory chain. *Adv Exp Med Biol* **748**, 145-169 (2012).
34 Stringari, C. *et al.* Metabolic trajectory of cellular differentiation in small intestine by Phasor Fluorescence Lifetime Microscopy of NADH. *Sci Rep* **2**, 568 (2012).
35 Schell, J. C. *et al.* Control of intestinal stem cell function and proliferation by mitochondrial pyruvate metabolism. *Nat Cell Biol* **19**, 1027-1036 (2017).
36 Okkelman, I. A., Neto, N., Papkovsky, D. B., Monaghan, M. G. & Dmitriev, R. I. A deeper understanding of intestinal organoid metabolism revealed by combining fluorescence lifetime imaging microscopy (FLIM) and extracellular flux analyses. *Redox Biol* **30**, 101420 (2020).
37 Anzell, A. R., Maizy, R., Przyklenk, K. & Sanderson, T. H. Mitochondrial Quality Control and Disease: Insights into Ischemia-Reperfusion Injury. *Mol Neurobiol* **55**, 2547-2564 (2018).
38 Tang, C. *et al.* PINK1-PRKN/PARK2 pathway of mitophagy is activated to protect against renal ischemia-reperfusion injury. *Autophagy* **14**, 880-897 (2018).
39 Zhou, H. *et al.* Pathogenesis of cardiac ischemia reperfusion injury is associated with CK2α-disturbed mitochondrial homeostasis via suppression of FUNDC1-related mitophagy. *Cell Death Differ* **25**, 1080-1093 (2018).
40 Buszczak, M., Signer, R. A. & Morrison, S. J. Cellular differences in protein synthesis regulate tissue homeostasis. *Cell* **159**, 242-251 (2014).
41 Albert, B. *et al.* A ribosome assembly stress response regulates transcription to maintain proteome homeostasis. *Elife* **8** (2019).
42 Harada, Y., Ohkawa, Y., Kizuka, Y. & Taniguchi, N. Oligosaccharyltransferase: A Gatekeeper of Health and Tumor Progression. *Int J Mol Sci* **20** (2019).

43 Bartoszewska, S. & Collawn, J. F. Unfolded protein response (UPR) integrated signaling networks determine cell fate during hypoxia. *Cell Mol Biol Lett* **25**, 18 (2020).

44 Badiola, N. *et al.* Induction of ER stress in response to oxygen-glucose deprivation of cortical cultures involves the activation of the PERK and IRE-1 pathways and of caspase-12. *Cell Death Dis* **2**, e149 (2011).

45 Thuerauf, D. J. *et al.* Activation of the unfolded protein response in infarcted mouse heart and hypoxic cultured cardiac myocytes. *Circ Res* **99**, 275-282 (2006).

46 Lee, P., Chandel, N. S. & Simon, M. C. Cellular adaptation to hypoxia through hypoxia inducible factors and beyond. *Nat Rev Mol Cell Biol* **21**, 268-283 (2020).

47 Ko, C. W., Qu, J., Black, D. D. & Tso, P. Regulation of intestinal lipid metabolism: current concepts and relevance to disease. *Nat Rev Gastroenterol Hepatol* **17**, 169-183 (2020).

48 Schaffer, J. E. Lipotoxicity: when tissues overeat. *Curr Opin Lipidol* **14**, 281-287 (2003).

49 Kihara, A. Very long-chain fatty acids: elongation, physiology and related disorders. *J Biochem* **152**, 387-395 (2012).

50 Sassa, T., Suto, S., Okayasu, Y. & Kihara, A. A shift in sphingolipid composition from C24 to C16 increases susceptibility to apoptosis in HeLa cells. *Biochim Biophys Acta* **1821**, 1031-1037 (2012).

51 Horstkotte, J. *et al.* Mitochondrial thioredoxin reductase is essential for early postischemic myocardial protection. *Circulation* **124**, 2892-2902 (2011).

52 Wang, Z. *et al.* Irisin Protects Heart Against Ischemia-Reperfusion Injury Through a SOD2-Dependent Mitochondria Mechanism. *J Cardiovasc Pharmacol* **72**, 259-269 (2018).

53 Hahn, U., Schuppan, D., Hahn, E. G., Merker, H. J. & Riecken, E. O. Intestinal cells produce basement membrane proteins in vitro. *Gut* **28 Suppl**, 143-151 (1987).

54 Liu, S. S., Wang, H. Y., Tang, J. M. & Zhou, X. M. Hypoxia-induced collagen synthesis of human lung fibroblasts by activating the angiotensin system. *Int J Mol Sci* **14**, 24029-24045 (2013).

55 Gilkes, D. M., Bajpai, S., Chaturvedi, P., Wirtz, D. & Semenza, G. L. Hypoxia-inducible factor 1 (HIF-1) promotes extracellular matrix remodeling under hypoxic conditions by inducing P4HA1, P4HA2, and PLOD2 expression in fibroblasts. *J Biol Chem* **288**, 10819-10829 (2013).

56 Tajima, R. *et al.* Hypoxic enhancement of type IV collagen secretion accelerates adipose conversion of 3T3-L1 fibroblasts. *Biochim Biophys Acta* **1540**, 179-187 (2001).

57 Muralidharan, S. & Mandrekar, P. Cellular stress response and innate immune signaling: integrating pathways in host defense and inflammation. *J Leukoc Biol* **94**, 1167-1184 (2013).

58 Chen, Y., Zhou, Z. & Min, W. Mitochondria, Oxidative Stress and Innate Immunity. *Front Physiol* **9**, 1487 (2018).

59 Altay, G. *et al.* Self-organized intestinal epithelial monolayers in crypt and villus-like domains show effective barrier function. *Sci Rep* **9**, 10140 (2019).

60 Merlot, A. M. *et al.* The metastasis suppressor, NDRG1, differentially modulates the endoplasmic reticulum stress response. *Biochim Biophys Acta Mol Basis Dis* **1865**, 2094-2110 (2019).

61 Sahni, S. *et al.* The metastasis suppressor, N-myc downstream-regulated gene 1 (NDRG1), inhibits stress-induced autophagy in cancer cells. *J Biol Chem* **289**, 9692-9709 (2014).

62 Kang, W. & Reid, K. B. DMBT1, a regulator of mucosal homeostasis through the linking of mucosal defense and regeneration? *FEBS Lett* **540**, 21-25 (2003).

63 Chen, L. *et al.* Cab45S promotes cell proliferation through SERCA2b inhibition and Ca2+ signaling. *Oncogene* **35**, 35-46 (2016).

64 Chen, L. *et al.* Cab45S inhibits the ER stress-induced IRE1-JNK pathway and apoptosis via GRP78/BiP. *Cell Death Dis* **5**, e1219 (2014).

65 Guo, A. X., Cui, J. J., Wang, L. Y. & Yin, J. Y. The role of CSDE1 in translational reprogramming and human diseases. *Cell Commun Signal* **18**, 14 (2020).

SUPPLEMENTARY INFORMATION

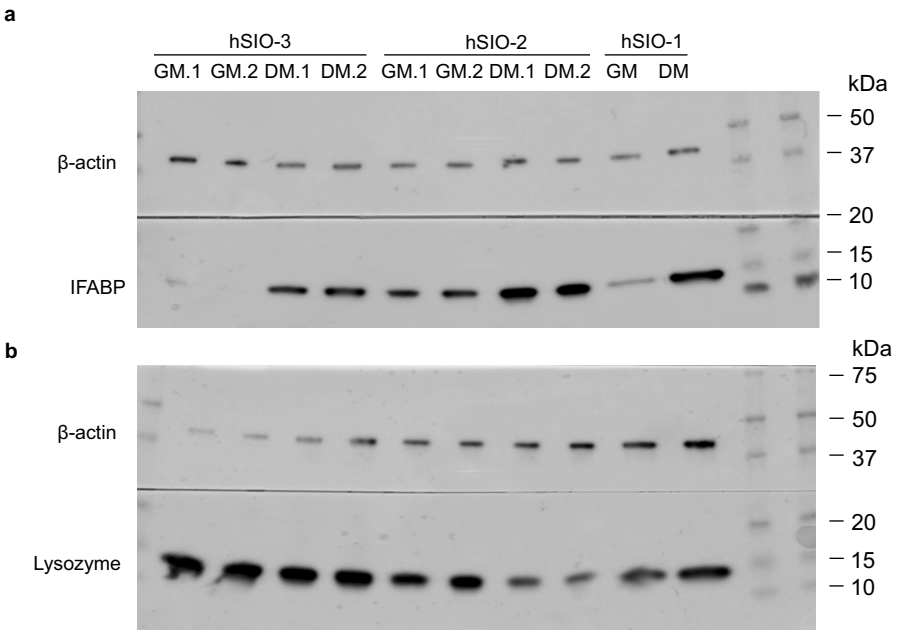

Figure S1. *Western blot data for* ***a****) IFABP (13-14 kDa) and* ***b****) lysozyme (14-15 kDa). β-actin was used as loading control. Precision Plus Protein Standards (Kaleidoscope), with a range 10-250 kDa was used.*

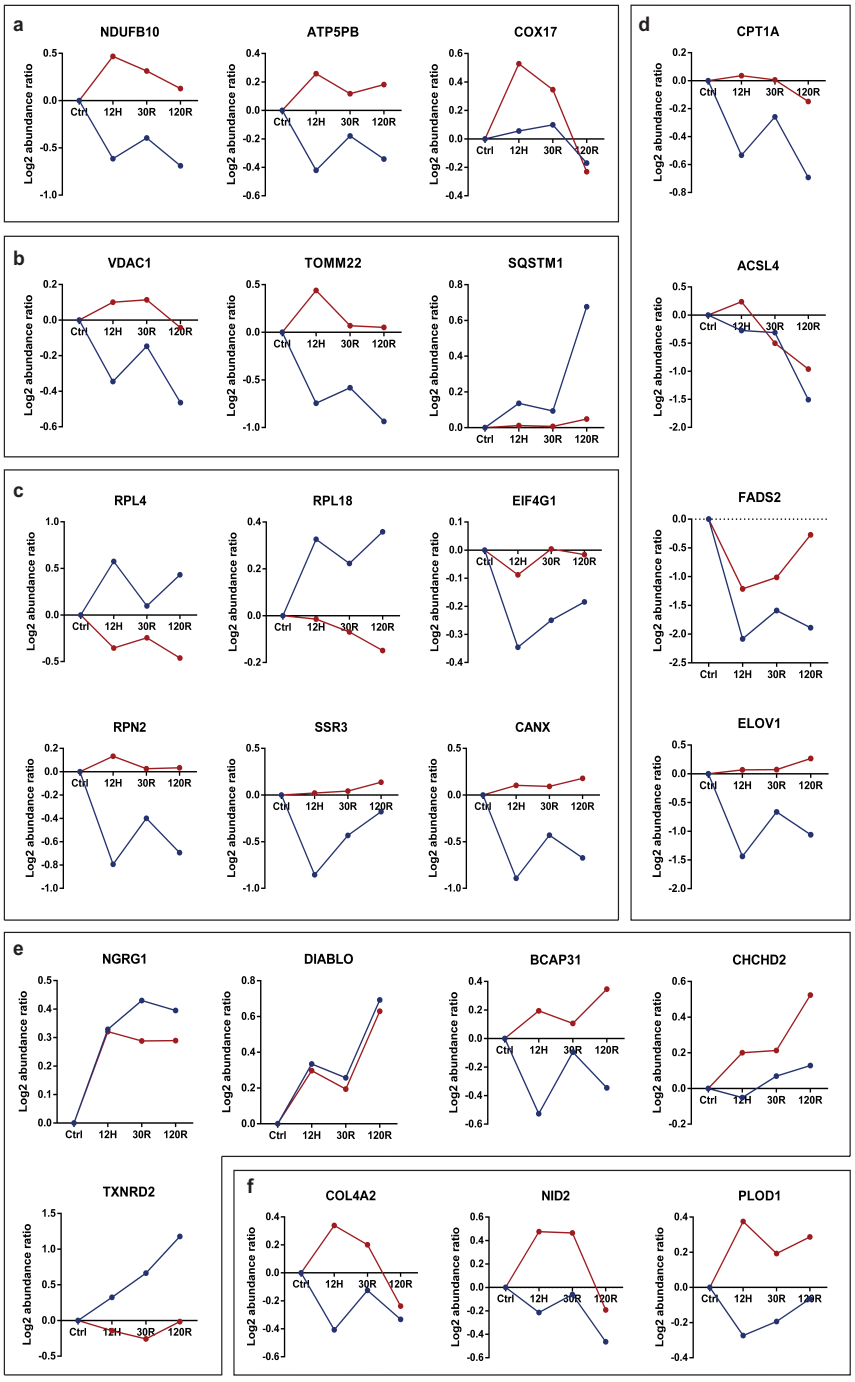

Figure S2. *Log2 abundance ratios for CL (blue) and VL (red) organoids. Selected proteins associated with* ***a****) mitochondrial respiratory chain,* ***b****) mitophagy,* ***c****) protein metabolism,* ***d****) lipid metabolism,* ***e****) stress response, apoptosis and anti-oxidant defense and* ***f****) extracellular matrix are shown.*

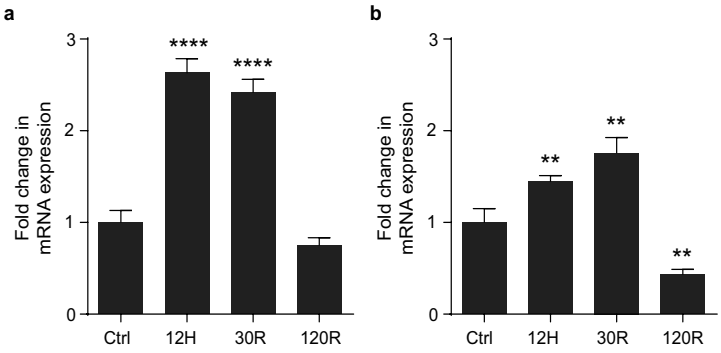

Figure S3. *mRNA expression of HIF1A target VEGF in CL organoids (**a**) and VL organoids (**b**). Data were normalized to B2MG and ACTN reference genes and reported as relative expression as compared to Ctrl. Results were obtained from 3 hSIO lines (mean ±SD) **** p<0.0001 ** p<0.01*

The following supplementary information is available at https://www.nature.com/articles/s41419-020-03379-9

Figure S4. Significant temporal protein profiles in crypt-like and villus-like organoids

Table S1. Differentially expressed proteins in growth medium- versus differentiation medium-cultured organoids

Table S2. Differentially expressed proteins during hypoxia-reoxygenation in crypt-like and villus-like organoids

CHAPTER 5

Temporal transcript profiling identifies a role for unfolded protein stress in human gut ischemia-reperfusion injury

Anna M. Kip, Joep Grootjans, Marco Manca, M'hamed Hadfoune, Bas Boonen, Joep P.M. Derikx, Erik A.L. Biessen, Steven W.M. Olde Damink, Cornelis H.C. Dejong, Wim A Buurman, Kaatje Lenaerts

Adapted from Cell Mol Gastroenterol Hepatol (2021), in press

ABSTRACT

Intestinal ischemia-reperfusion injury is a serious and life-threatening condition. A better understanding of molecular mechanisms related to intestinal ischemia-reperfusion injury in man is imperative in order to find therapeutic targets and improve patient outcome. First, the *in vivo* dynamic modulation of mucosal gene expression of the ischemia-reperfusion injured human small intestine was studied. Based on functional analysis of the changing transcriptome, one of the predominantly regulated pathways was selected for further investigation in an *in vitro* human intestinal organoid model. Ischemia-reperfusion massively changed the transcriptional landscape of the human small intestine. Functional analysis based on gene ontology and pathways pointed to the response to unfolded protein as a predominantly regulated process. In addition, regulatory network analysis identified hypoxia-inducing factor 1A (HIF1A) as one of the key mediators of ischemia-reperfusion induced changes, including the unfolded protein response (UPR). Differential expression of genes involved in the UPR was confirmed using quantitative PCR analysis. Electron microscopy showed signs of endoplasmic reticulum stress. Collectively, these findings point to a critical role for unfolded protein stress in intestinal ischemia-reperfusion injury in man. In a human intestinal organoid model exposed to hypoxia-reoxygenation, attenuation of UPR activation with integrated stress response inhibitor ISRIB strongly reduced pro-apoptotic ATF4-CHOP signaling. In conclusion, transcriptome analysis revealed a crucial role for unfolded protein stress in the response to ischemia-reperfusion in human small intestine. UPR inhibition during hypoxia-reoxygenation in an intestinal organoid model, suggests that downstream PERK signaling may be a promising target to reduce intestinal ischemia-reperfusion injury.

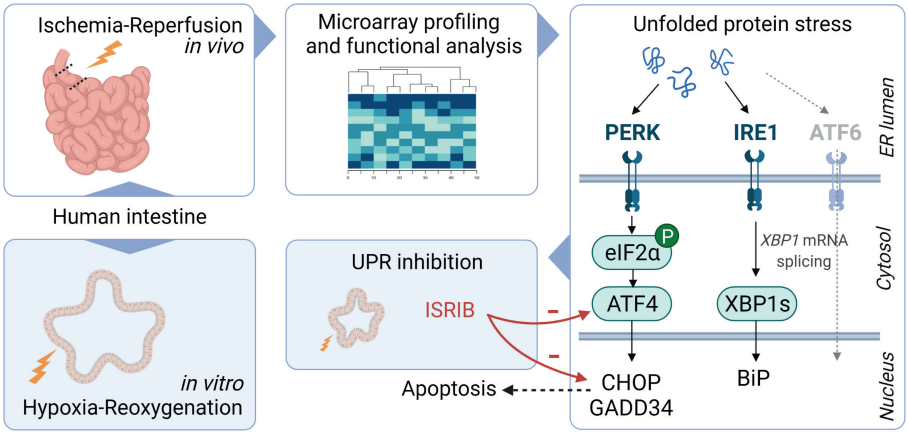

INTRODUCTION

The human intestine has an important role in nutrient and fluid uptake, while at the same time, it has to provide a protective barrier between the inner and outer milieu[1]. For both the absorptive and barrier function, the intestinal epithelium is dependent on sufficient oxygen supply[2]. Under physiologic conditions the intestinal mucosa experiences profound fluctuations in blood flow, e.g. intestinal perfusion is enhanced following meal ingestion and is considerably diminished during physical exercise[2,3]. In pathological conditions, more severe impairment of intestinal perfusion may lead to intestinal ischemia, for instance as a consequence of mesenteric thrombosis, shock, sepsis, vasculitis or major surgery[4,5]. In addition, it is well appreciated that epithelial hypoxia occurs secondary to inflammation, which plays a crucial role in the pathophysiology of inflammatory bowel disease[2,6]. During interruption of blood supply, metabolic disturbances with mitochondrial dysfunction and energy deficiency damage the enterocytes. Reperfusion of the ischemic tissue triggers an inflammatory response, with chemotactic recruitment of neutrophils, promoting an even more hypoxic environment[7], and further destruction of the intestinal mucosa, leading to barrier compromise[8].

Given the importance of ischemia-reperfusion injury as a pathophysiological phenomenon in a variety of diseases, it is imperative to understand the interactions between metabolic changes caused by ischemia-reperfusion, and the molecular mechanisms related to intestinal epithelial dysfunction and inflammation. Our knowledge on these interactions is derived mostly from studying animal models[9]. Although our knowledge on intestinal ischemia-reperfusion injury in man has improved in the last decade[10], the key players in its pathophysiology remain obscure.

In this study, we set out to investigate the molecular mechanisms driving intestinal ischemia-reperfusion-induced pathology, using a human experimental model[8]. The experimental framework enabled consecutive sampling of intestinal tissue specimens to monitor the temporal behavior of biological processes over a period of progressive injury and subsequent initiation of repair, through analysis of their transcriptional profiles. This led us to decipher the coordinated gene regulation events upon ischemia-reperfusion stress in the human intestine. The acquired knowledge provides a basis for the development of targeted interventions to diminish intestinal ischemia-reperfusion-induced mucosal injury and inflammation and restore intestinal homeostasis. Based on our analysis, we selected one of the predominantly regulated processes and further investigated its potential as a therapeutic target in ischemia-reperfusion injury, using a human intestinal organoid model[11].

MATERIALS AND METHODS

Ethics statement

Human studies were approved by the Medical Ethics Committee of Maastricht University Medical Center+ (METC 06-3-044, human ischemia-reperfusion model; METC 16-4-185, human intestinal organoid model) or Uniklinik RWTH Aachen (EK 206/09, human intestinal organoid model) and conducted according to the revised version of the Declaration of Helsinki (October 2008, Seoul). Written informed consent of all patients was obtained.

Experimental human IR model

The experimental protocol was performed as previously described[8]. In short, patients undergoing pancreatico-duodenectomy were included in this study. During pancreatico-duodenectomy, a variable length of jejunum is routinely resected in continuity with the head of the pancreas and duodenum as part of the surgical procedure. The terminal 6 cm of this jejunal segment was isolated and subjected to either 30 or 45 min of ischemia by placing two atraumatic vascular clamps across the mesentery. Meanwhile, surgery proceeded as planned. After ischemia, one third (2 cm) of the isolated ischemic jejunum was resected using a linear cutting stapler (0R). Next, clamps were removed to allow reperfusion, which was confirmed by regaining of normal pink color and restoration of gut motility. Another segment of the isolated jejunum (2 cm) was resected similarly after 30 min of reperfusion (30R). The last part was resected after 120 min of reperfusion (120R). In addition, a 2 cm segment of jejunum, which was not subjected to ischemia-reperfusion but underwent similar surgical handling as the isolated part of jejunum, was resected and served as internal control tissue (C). **Figure 1a** shows the experimental procedure that was followed to harvest tissue samples. Full-thickness tissue samples were immediately snap-frozen or formalin-fixed. Patients with obstructive jaundice underwent a stent procedure prior to surgery. All patients had normal bile flow at the time of surgery.

Human intestinal organoid model

Human tissue specimens of proximal jejunum, obtained from patients undergoing pancreatico-duodenectomy, were used for the generation of human small intestinal organoids[11]. Organoids were embedded in basement membrane extract (Geltrex, Gibco, Carlsbad, CA) and cultured in growth medium containing Advanced DMEM/F12 (Gibco), 50 units/ml penicillin and 50 µg/ml streptomycin (Gibco), 1x Glutamax (Gibco), 10 mM HEPES (Gibco), 1x B27 (Gibco), 1x N2 (Gibco), 50% v/v Wnt3a-conditioned medium, 20% v/v Rspondin-1-conditioned medium, 10% Noggin-conditioned medium, 50 ng/ml mEGF (Gibco), 10 mM Nicotinamide (Sigma-Aldrich, St. Louis, MO), 1.25 mM *N*-acetyl cystein (Sigma-Aldrich), 500 nM A83-01 (TGFβ inhibitor; Sigma-Aldrich), 10 mM Gastrin I (Sigma-Aldrich), and 10 µM SB202190 (p38 MAPK inhibitor, Sigma-Aldrich). ROCK inhibitor Y-27632 (10 µM, Abmole Bioscience, Houston, TX) was added to the medium when organoids were generated, after passaging, and thawing.

To mimic ischemia-reperfusion, organoids were exposed to 12 h of hypoxia (<1.0% O_2, 5% CO_2) and 2 h of reoxygenation (21% O_2, 5% CO_2) as described before[11]. Organoids were harvested for analysis immediately after 12 h of hypoxia without reoxygenation (0R), after 30 min of reoxygenation (30R) and 120 min of reoxygenation (120R), and without hypoxic exposure (C). Experiments were

performed in organoid lines derived from three patients. Integrated stress response inhibitor (ISRIB; Sigma) was used as inhibitor of the unfolded protein response. Organoids were exposed to hypoxia-reoxygenation (HR) with or without ISRIB, in concentrations 10 nM, 100 nM. ISRIB was added to the medium 2 h prior to HR.

Microarray analysis

RNA isolation

Total RNA was isolated from snap-frozen tissue samples using AllPrep DNA/RNA/Protein kit (Qiagen, Hilden, Germany). In short, jejunal samples were crushed with a pestle and mortar in liquid nitrogen. Disruption and homogenization of the tissue was performed using an Ultra Turrax Homogenizer (IKA Labortechnik, Staufen, Germany) in lysis buffer containing β-mercaptoethanol (Promega, Madison, WI). RNeasy spin columns were used to bind RNA. Columns were washed and RNA was eluted in RNase-free water. RNA samples were treated with DNase (Promega). RNA quantity and quality were measured using the NanoDrop spectrophotometer (NanoDrop, Wilmington, DE) and Agilent 2100 Bioanalyzer (Santa Clara, CA) respectively. All RNA samples included in the expression analysis had an RNA integrity number above 7.

Microarray analysis

Whole genome expression analysis was performed using Illumina Human HT-12_V3_expression arrays (Illumina, San Diego, CA) on material collected from seven patients (**Table S1**). Four tissue specimens per patient were analyzed, namely intestinal tissue exposed to 30 or 45 min of ischemia (0R), with 30 min (30R) and 120 min of reperfusion (120R), and a control sample (C). Per sample, 200 ng RNA was used for anti-sense RNA synthesis, amplification, purification, and labeling with the Illumina TotalPrep 96 RNA Amplification Kit (Applied Biosystems/Ambion, Austin, TX) according to the manufacturer's protocol. A total of 750 ng of complementary RNA was randomly hybridized to the Illumina arrays and scanned immediately on the Illumina BeadArray Reader. These microarrays contain 48,813 different probes targeting 37,812 different genes; some genes are targeted by more than one probe. The resulting data were quality-checked and extracted using Illumina GenomeStudio v1.1.1 software without normalization and background subtraction. Raw BeadStudio (Illumina) output text files were uploaded in R (http://www.R-project.org) statistical environment by the Bioconductor[12] software package lumi. Variance stabilizing transform and robust spline normalization were chosen as pre-processing methods; in order to minimize batch effects and provide an adequate statistical power, the whole dataset was simultaneously pre-processed as a whole. A filter was applied to the detection calls, excluding all probes which were negative (with a 0.01 confidence) in 3 individuals or more, in order to minimize the technical noise in the analysis and to restrict the statistical adjustment for repeated test to the informative data only.

Differential expression analysis

Time course differential analysis was performed using Bioconductor package limma with time points as factors, and corrections for patient-IDs effect. Statistical significance was corrected for repeated testing using a False Detection Rate method. The threshold for acceptance was set to

p≤0.05. Illumina IDs were translated into Entrez ID by lumiHumanAll.db, which is assembled on data from public repositories. Gene ontology (GO) enrichment analysis of the differentially expressed genes was performed with GeneAnswers querying GO biological process, GO molecular function and KEGG. Pathway enrichment analysis was performed with SPIA (Signaling pathway impact analysis) maintaining the standard scoring settings. All data were organized by patient IDs and time points using the R package longitudinal. Subsequently, Empirical Bayes Estimation of Dynamic Bayesian Networks (EbdbNet) was used to reverse engineer the expression regulation network linking the significantly differentially expressed genes. This was achieved by feeding IDs and expression values of those genes which had the words 'transcription factor' appearing in their GO information as the seed for the network architecture, and the same data from the remaining differentially expressed genes as the dataset from which to extract the network. Finally, the network was exported as comma-separated-values datasheets and imported to Cytoscape for visualization and comparative analysis of our inferred architecture against established biological pathways. Functional enrichment analysis was performed for GO biological process terms using METASCAPE[13].

Quantitative PCR

To validate observed transcriptional differences in microarray analysis, quantitative PCR analysis was performed. Tissue RNA samples were reverse transcribed into cDNA using iScript cDNA synthesis kit (Bio-Rad, Hercules, CA). Quantitative PCR reactions were performed using IQ SYBR Green Supermix (Bio-Rad). cDNA was amplified using a three-step program (40 cycles) with a MyiQ system (Bio-Rad). Gene expression levels were determined using iQ5 software using a ΔCt relative quantification model. The geometric mean of *RPLP0* and *CYPA* was used as a normalization factor.

For gene expression analysis in intestinal organoids, the cells in Geltrex were lysed using TRI Reagent (Sigma-Aldrich) and RNA was isolated according to manufacturer's instructions. Synthesis of cDNA was performed using the SensiFast cDNA Synthesis kit (Bioline GmbH, Germany). Quantitative PCR analysis was performed on the LightCycler480 (Roche, Mannheim, Germany) using SensiMix SYBR Hi-Rox kit (Bioline GmbH) for amplification. Data were processed using LinRegPCR software (version 2016.1). The geometric mean of reference genes *B2MG* and *ACTB* was used for normalization. All primer sequences are provided in Supplementary Material (**Table S2**).

Apoptosis assay

For apoptosis assays, organoids were plated in 10 µl Geltrex (20,000 cells/well) in a 96-well plate. Caspase-Glo 3/7 assay (Promega, Madison, USA) was performed according to manufacturer's protocol. Luminescence was measured on the Spark Microplate Reader (Tecan, Männedorf, Switzerland). Data were corrected for background luminescence.

Histology and transmission electron microscopy

Formalin-fixed tissue samples were embedded in paraffin and 4 µm sections were cut, deparaffinized in xylene, and rehydrated in graded ethanol to distilled water. Sections were stained with haematoxylin and eosin (H&E) for morphological analysis. Jejunal tissue exposed to ischemia-reperfusion from two additional patients was immersed in 3% glutaraldehyde fixative buffered in 0.09 M KH_2PO_4 at pH 7.4. Next, samples were washed in 0.09 M KH_2PO_4 buffer containing 7.5% sucrose and transferred

to a 1% OsO_4 fixative solution buffered with veronal acetate buffer (pH 7.4) plus 1.5% ferrocyanide. After washing in veronal acetate buffer plus 7% sucrose for 5 min at 4°C, dehydration was performed in graded ethanol series, followed by embedding in Epon (Burlington, VT). Tissue sections were examined with a Philips CM 100 electron microscope (Philips, Eindhoven, The Netherlands) at an accelerating voltage of 80 kV.

Statistical analysis

Statistical analysis of microarray data were performed in R as described in the paragraph *'Differential expression analysis'*. Statistical analysis of gene expression and apoptosis data was performed using Graphpad Prism (version 6.01). These data were analyzed using Kruskal–Wallis one-way analysis of variance test followed by Dunn's post hoc test. A p-value <0.05 was considered significant.

Data availability

Microarray data are available in GEO (http://www-ncbi.nlm.nih.gov, accession number GSE37013).

RESULTS

The progressively changing transcriptional landscape of the ischemically injured human intestine

To investigate the effect of disturbed blood supply on the human small intestine, we first performed histological assessment of ischemia-reperfusion-exposed tissue harvested according to the protocol depicted in **Figure 1a**. The extent of mucosal injury increased progressively with ischemia duration, i.e. 30 (30I) and 45 min of ischemia (45I) (**Figure 1b**). Most severe tissue damage was apparent after 30 min of reperfusion (30R), especially at the villi tips. Within 120 min of reperfusion (120R), damage was almost completely restored in 30I group, whereas in the 45I group, the epithelial lining was still interrupted.

To understand the molecular mechanisms underpinning the human intestinal response to ischemia-reperfusion, a microarray study was performed. Genome-wide expression profiles of consecutive specimens harvested during human intestinal ischemia-reperfusion were generated from 7 patients. Patient characteristics can be found in **Table S1**. Three tissue specimens harvested during ischemia-reperfusion at 0R, 30R and 120R as well as a normally perfused control sample (C) were profiled for each individual. Overall, the signal intensity of 1993 probe sets (representing 1847 unique genes) changed significantly (adjusted p-value ≤0.05) in response to ischemia-reperfusion. The number of differentially expressed transcripts increased steadily with reperfusion time (**Figure 1c**), which represents the highly dynamic nature of the response. **Figure 1d** depicts the top 20 differentially expressed genes in the human intestine in response to ischemia-reperfusion. The 50 most up- and downregulated genes per comparison are shown in **Table S3** of Supplementary Material. Hierarchical clustering based on the top 500 differentially expressed genes showed distinct clustering of the majority of control samples and samples exposed to different conditions of ischemia and reperfusion (**Figure 1e**). Moreover, two major clusters strictly divided the control and ischemic tissue from the tissue exposed to reperfusion, indicating that the most dramatic transcriptional changes occurred when perfusion is restored after an ischemic insult.

Figure 1. Transcriptional changes in the human intestine in response to ischemia-reperfusion. ***a****) Schematic overview of experimental protocol followed to harvest intestinal samples exposed to 30 min (30I) or 45 min (45I) of normothermic ischemia without reperfusion (0R, black bars), and with 30 min (30R, light blue bars) and 120 min of reperfusion (120R, dark blue bars). Control specimens (C) not exposed to ischemia-reperfusion stress were also collected from all patients (grey bar).* ***b****) Representative images of H&E staining of intestinal tissue harvested according to scheme depicted in a.* ***c****) Venn diagram of Boolean relationships between sets of differentially expressed genes in response to intestinal ischemia-reperfusion (N=7 patients). The total number of regulated genes is depicted per comparison (with number of up-regulated and down-regulated genes shown between parentheses).* ***d****) Top 20 differentially expressed genes in the human intestine in response to ischemia-reperfusion.* ***e****) The dendrogram depicts hierarchical clustering based on the top 500 significantly changed probe sets in response to ischemia-reperfusion injury. Probe sets for which the abundance was above the mean are shown in red, below the mean are shown in blue, and equivalent to the mean are in white.*

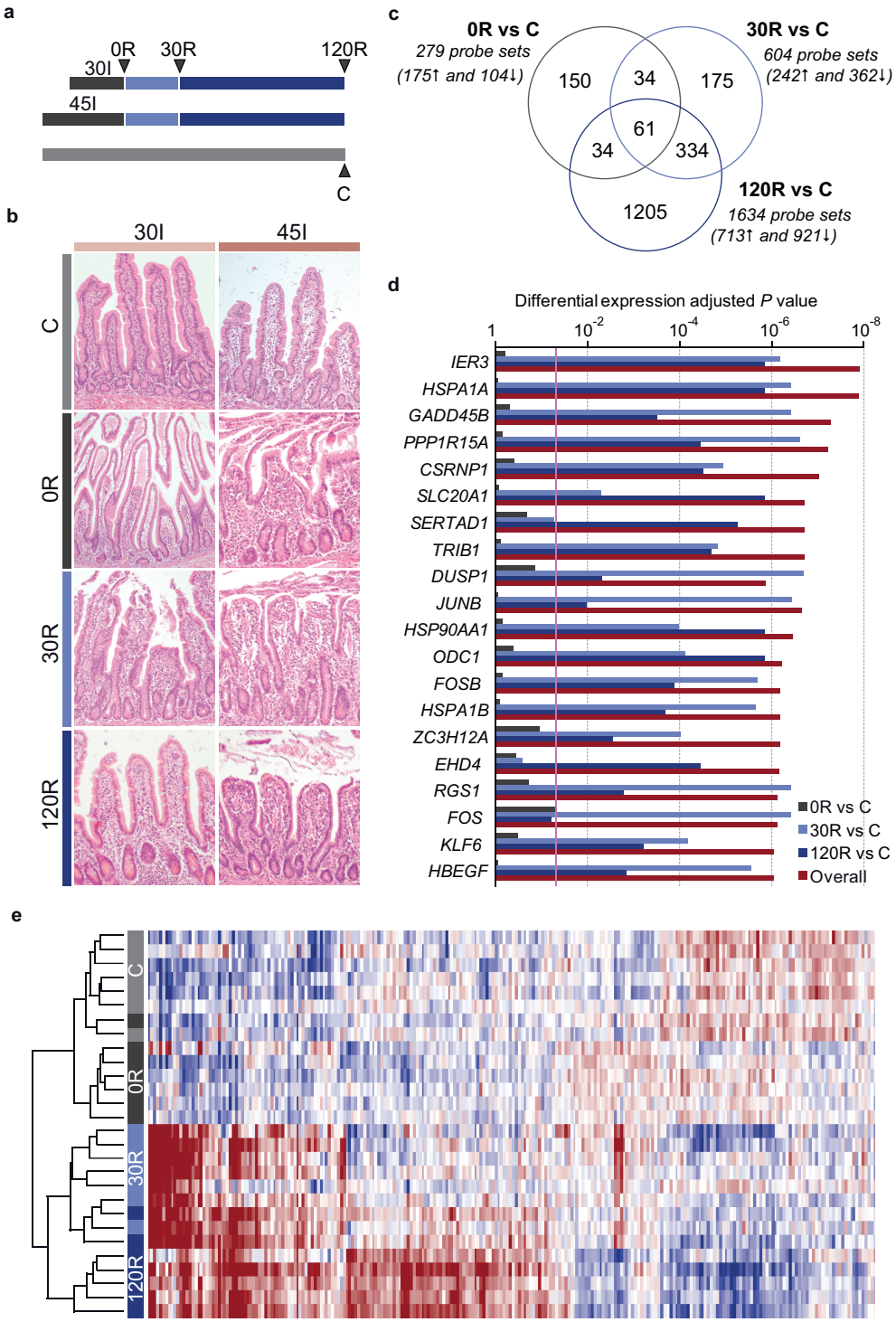
a
0R
30R
120R
30I
45I
C
b
30I
45I
C
0R
30R
120R
c
0R vs C
279 probe sets
(175↑ and 104↓)
30R vs C
604 probe sets
(242↑ and 362↓)
120R vs C
1634 probe sets
(713↑ and 921↓)
150
34
175
61
34
334
1205
d
Differential expression adjusted P value
1
10-2
10-4
10-6
10-8
IER3
HSPA1A
GADD45B
PPP1R15A
CSRNP1
SLC20A1
SERTAD1
TRIB1
DUSP1
JUNB
HSP90AA1
ODC1
FOSB
HSPA1B
ZC3H12A
EHD4
RGS1
FOS
KLF6
HBEGF
0R vs C
30R vs C
120R vs C
Overall
e
C
0R
30R
120R

Fundamental biological processes and pathways activated during human intestinal ischemia-reperfusion

To facilitate functional interpretation of genes influenced by ischemia-reperfusion in the human intestine, we first performed gene ontology (GO) term analysis in the categories biological process and molecular function (**Figure 2a**). In the first 30 min of reperfusion, functional categories were primarily associated with failure to properly fold and dispose damaged proteins. GO terms 'response to unfolded protein, 'response to stress', 'heat shock protein binding' and 'unfolded protein

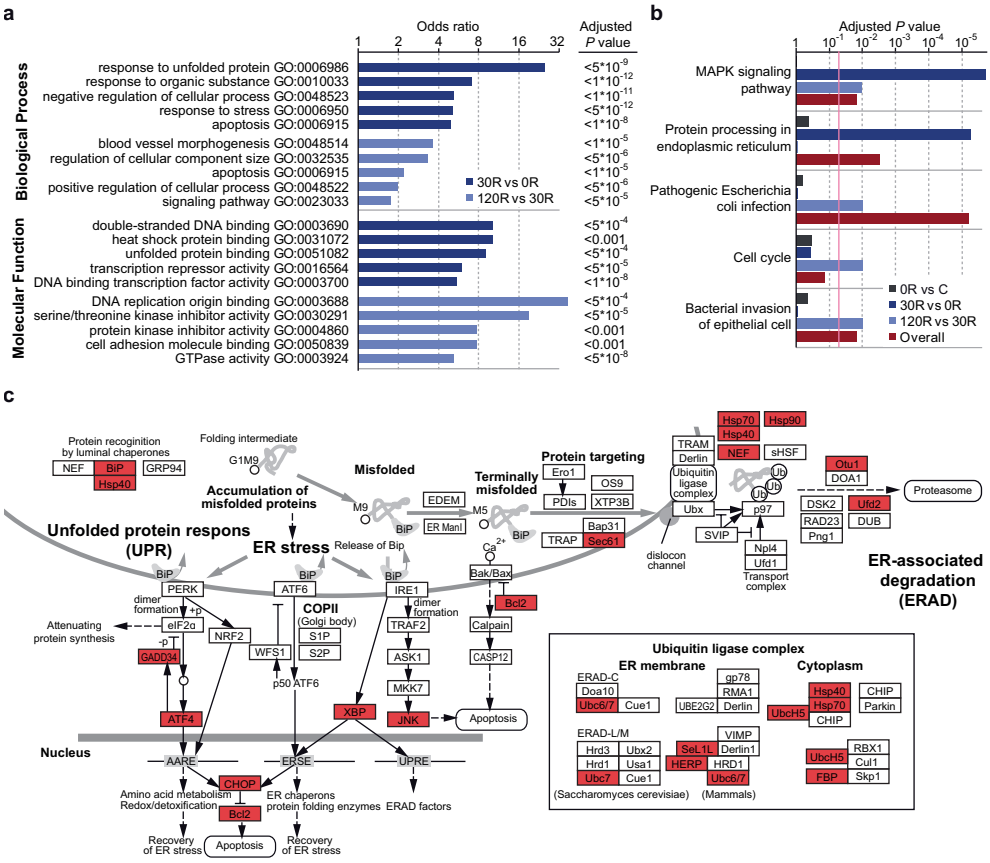

Figure 2. Mapping transcriptional changes to biological functions. ***a****) Top 5 of GO terms identified by enrichment analysis in the category of GO biological process and GO molecular function for significantly differentially expressed genes during reperfusion. The x-axis (log-scale) indicates the odds ratio that a GO term is enriched in the selected category. Several GO terms were excluded from the list due to overlap based on similar groups of genes. See Table S3 for the top 30 GO terms for biological processes (including overlapping terms) and all GO terms for molecular function.* ***b****) Top 5 of significantly overrepresented KEGG pathways in the human intestine in response to ischemia-reperfusion. All significantly overrepresented pathways (adjusted p-value <0.05) can be found in Table S4.* ***c****) Top perturbed pathway during reperfusion (30R) of ischemically injured intestine, namely 'protein processing in ER' (modified from KEGG pathway hsa04141). Significantly differentially expressed genes are indicated in red. Differential expression is evident in the regions of ER stress and ER-associated degradation, which is a process responsible for ubiquitination and degradation of terminally misfolded proteins through the proteasome.*

binding' were significantly enriched. Prolonged reperfusion was characterized by GO terms 'blood vessel morphogenesis', 'apoptosis', and 'cell adhesion molecule binding', which are all indicative of intestinal remodeling. In **Table S4** of Supplementary Material, the list of 30 most significantly enriched GO terms is depicted for biological process, and all GO terms with respect to molecular function. Functional enrichment analysis based on pathways in the KEGG database revealed most significant overrepresentation of genes involved in 'MAPK signaling pathway' and 'protein processing in endoplasmic reticulum' within the 0R to 30R time frame (**Figure 2b**, **Table S5**). The following time frame, i.e. between 30R and 120R, was characterized by signs of bacterial invasion and cell proliferation with overrepresentation of the pathways 'pathogenic Escherichia coli infection', 'cell cycle', and 'bacterial invasion of epithelial cells'.

In general, functional GO and KEGG pathway analyses strongly imply a response of the intestinal tissue towards unfolded protein in the ER during early reperfusion. Differentially expressed genes in the pathway 'protein processing in the ER' are depicted in **Figure 2c**. Co-activation of the ER stress pathway and MAPK signaling pathway, with altered gene expression particularly in the JNK and p38 MAPK cascade (**Figure S1**), during early reperfusion, provides a plausible link between ER stress on the one hand, and inflammation and apoptosis on the other hand. Indeed, ER-stress signaling molecules are known to trigger the inflammatory signaling components JNK and NF-κB[14]. Both factors and their downstream targets (e.g. c-Jun and c-fos, IκB-alpha, A20) were found to be induced in the human small intestine exposed to ischemia-reperfusion (**Figure S1**).

Dynamic gene regulatory network analysis reveals a key role for HIF1A in regulating the unfolded protein response during ischemia-reperfusion

Next, to further delineate molecular targets that primarily dictate the response to ischemia-reperfusion in the human intestine, we identified core networks essential for the adaptation of damaged intestinal tissue at the transcriptional level. Regulatory relationships among the differentially expressed genes were calculated, based on their temporal variation in transcript abundance in response to ischemia-reperfusion. We selected known transcription factors as network hubs. Of the 96 differentially expressed transcription factors in our set, 18 appeared in the network. Three transcription factors, HIF1A, NKX2-3, and ELF4 were identified as predominant regulators in our model (**Table S6**). The assembly of regulatory interactions is depicted in **Figure 3a**. Remarkably, functional enrichment analysis of HIF1A targets in the category biological process revealed highly significant enrichment of GO terms 'response to unfolded protein' ($p<2.6\times10^{-15}$), 'regulation of cellular response to stress' ($p<2.1\times10^{-13}$), and 'protein folding' ($p<3.0\times10^{-13}$) (**Figure 3b**, **Table S7**). These processes did not appear in the list of enriched GO terms for NKX2-3 and ELF4 targets (**Figure 3b**, **Table S7**). All genes annotated to the category 'response to unfolded protein' were marked red in the network and, interestingly, the majority was centered around HIF1A (**Figure 3a**). The genes involved and their relation to HIF1A and the other linked network hubs are depicted in **Figure 3c**. These data imply a key role for HIF1A in the response of the human intestine towards unfolded protein accumulation during ischemia-reperfusion.

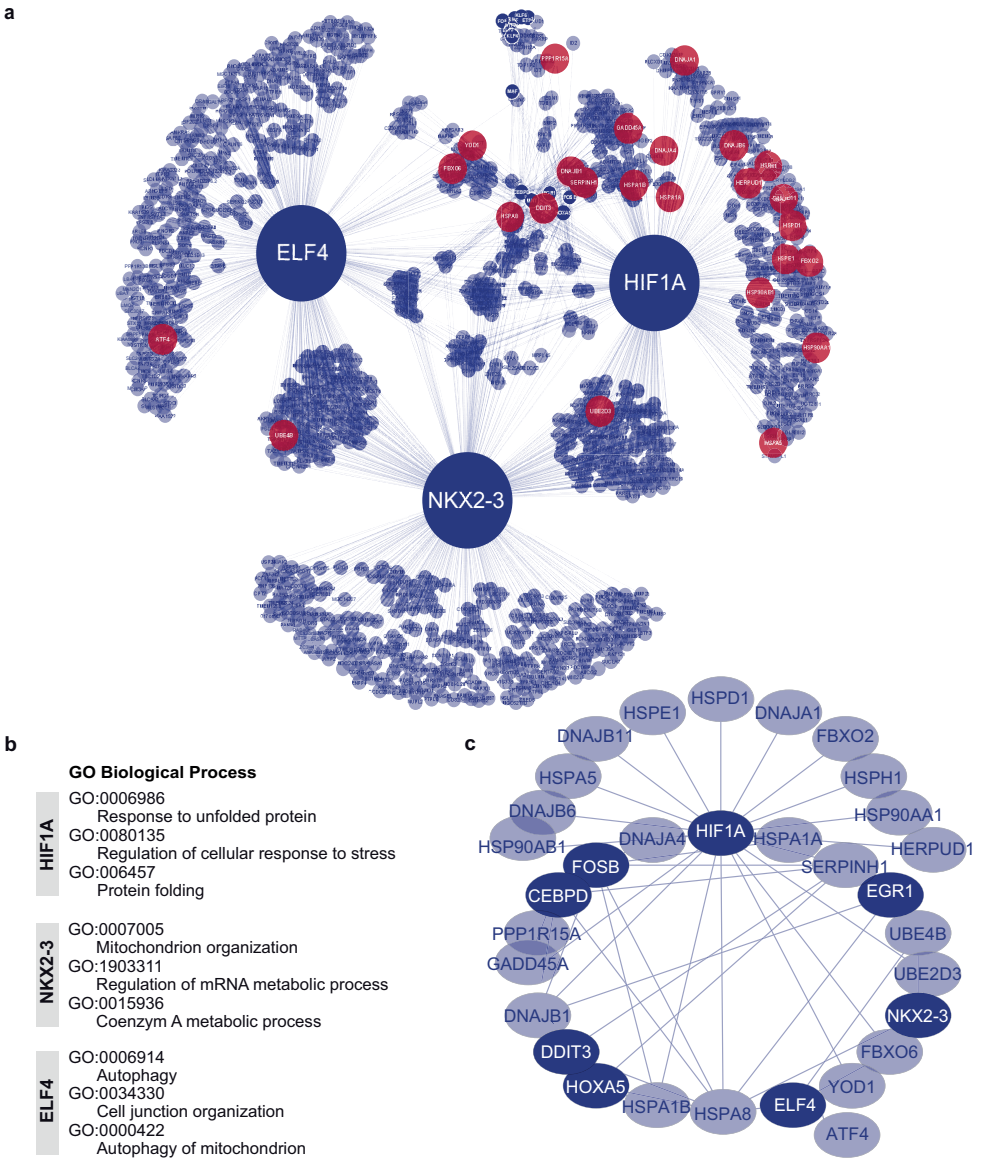

Figure 3. Dynamic network of regulatory interactions in the ischemia-reperfusion-exposed human intestine demonstrates a key role HIF1A in regulation of the response to unfolded protein. ***a****) Network of regulatory interactions involved in the response to ischemia and subsequent reperfusion in the human intestine. The nodes represent the regulators and their targets, and the regulatory interactions are the edges. All transcriptional regulators in the network are depicted in dark blue. See Table S5 for a list of transcription factors and the number of targets in the network. The three major transcriptional regulators in the network are HIF1A, NKX2-3 and ELF4. Genes annotated to the GO term 'response to unfolded protein' are marked in red.* ***b****) Top overrepresented biological processes are shown for HIF1A, NKX2-3 and ELF4 predicted targets in the network. Functional enrichment analysis for GO biological processes was performed using METASCAPE. In Table S6 the complete lists of enriched biological processes can be found.* ***c****) Genes in the category 'response to unfolded protein' in relation to HIF1A and the transcriptional regulators (dark blue).*

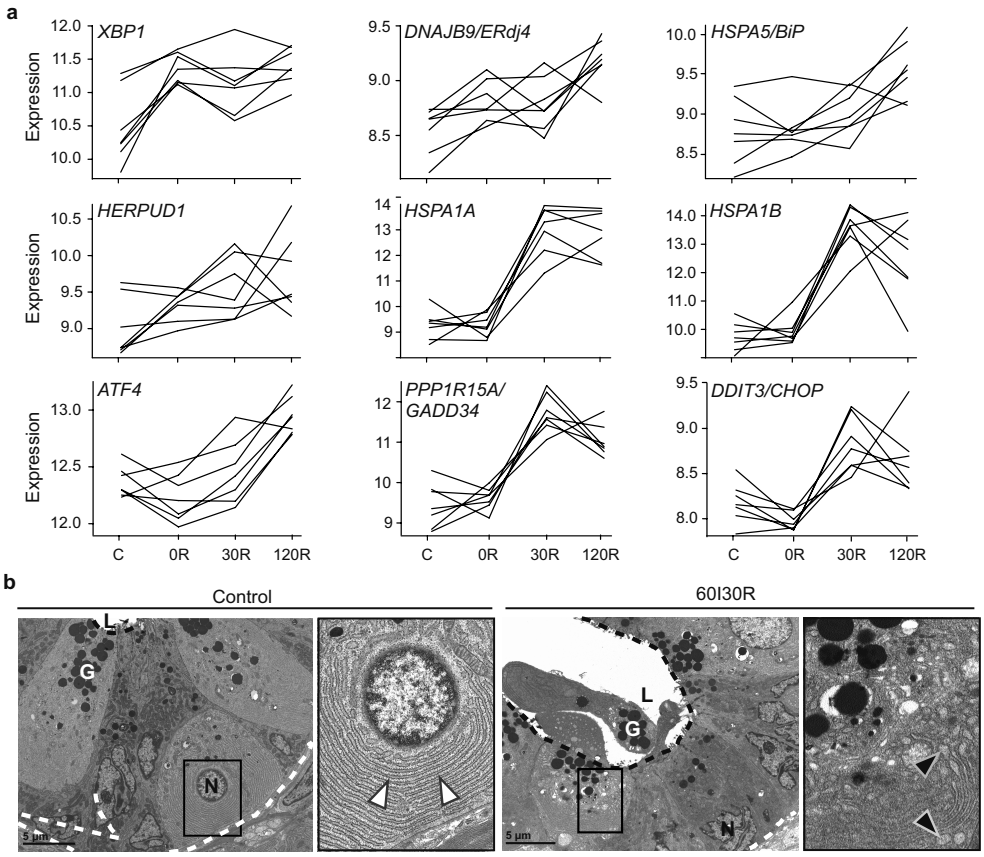

Figure 4. Signs of endoplasmic reticulum stress in the human small intestine exposed to ischemia-reperfusion. ***a****) A selection of genes involved in the response to unfolded protein is markedly upregulated in the intestine exposed to ischemia-reperfusion. The y-axis indicates the* Log_2 *normalized gene expression. The data reveal the temporal nature of gene expression and show the high degree of homogeneity between patients (N=7). Upper and middle panel represent genes involved in the IRE1 arm of the UPR, the lower panel represents PERK signaling* ***b****) EM images of control and ischemia-reperfusion-exposed (60I30R) jejunal crypt base epithelium. Higher-magnification views of the boxed regions are shown on the right. Paneth cells, characterized by cytoplasmic granules (G), are presented because of their extensive ER. Control tissue shows normally structured ER (white arrowheads). IR-exposed tissue displays vacuoles representing dilated ER lumina (black arrowheads). A white dashed line outlines the outer margin of the crypts; a black dashed line demarcates the luminal side. N, nucleus; L, lumen.*

Ischemia-reperfusion triggers endoplasmic reticulum stress in the human intestinal epithelium

As shown above, extensive analysis of transcriptional profiles at the level of pathways, functions and regulatory networks points to the relevance of protein folding stress in the ischemia-reperfusion-injured small intestine. Accumulation of unfolded proteins within the endoplasmic reticulum (ER) induces an adaptive stress response known as the unfolded protein response (UPR). Expression of XBP1, a critical effector of the UPR, was significantly upregulated after ischemia-reperfusion (**Figure 4a**). Upon UPR activation, IRE1 cleaves 26bp from XBP1 mRNA to yield spliced XBP1 (XBP1s), whose product transcriptionally activates major portions of the UPR[15]. In a previous study, we reported

elevated levels of XBP1s during human intestinal ischemia-reperfusion[16]. Here, known XBP1s targets were significantly upregulated and included BiP/GRP78 (encoded by *HSPA5*), ERdj4 (encoded by *DNAJB9*) and Herpud1 (**Figure 4a**, upper and middle panel)[15,17,18]. Increased XBP1 and BiP expression levels were confirmed by qPCR and were particularly enhanced at 120R (**Figure S2**). Hsp72 (encoded by *HSPA1A/B* in **Figure 4a**) is known to enhance IRE1-XBP1 signaling upon binding to IRE1, and hence promotes adaptation to ER stress and cell survival[19]. Hsp72 appeared in the top 20 list of differentially expressed genes (**Figure 1d**), and showed a huge induction of its expression at 30R and 120R, as validated by qPCR (**Figure S2**).

Next to IRE1 activation, upregulation of ATF4, CHOP (encoded by *DDIT3*) and GADD34 (encoded by *PPP1R15A*) (**Figure 4a**) are indicative of parallel activation of the PERK pathway in response to human intestinal ischemia-reperfusion. The induction of PERK signaling during reperfusion was also confirmed by qPCR analysis (**Figure S2**).

In addition to transcriptional activation of the UPR, we examined subcellular signs of ER stress using transmission electron microscopy. The intestine exposed to IR displays an enlarged ER with vacuoles in the Paneth cells which is indicative of ER stress, whereas control tissue exhibits normally structured ER (**Figure 4b**).

Inhibition of the UPR with ISRIB decreases pro-apoptotic UPR signaling in a human intestinal organoid model

Our data point to an important role of ER stress and UPR signaling in the pathophysiology of ischemia-reperfusion injury of the human intestine. The UPR is key to cell survival, however, UPR signaling can also promote apoptotic cell death and aggravate injury if ER stress is sustained[20]. To elucidate the functional role of the UPR in intestinal ischemia-reperfusion, we next investigated the effect of pharmacological UPR inhibition in a human small intestinal organoid model. Organoids were exposed to hypoxia-reoxygenation as depicted in **Figure 5a**, and treated with integrated stress response inhibitor ISRIB, which reverses the effects of eIF2α phosphorylation[21,22]. We hypothesized that inhibition of downstream PERK signaling with ISRIB is protective during hypoxia-reoxygenation by attenuating apoptosis.

A strong increase in gene expression of CHOP (7- to 10-fold), GADD34 (4- to 6-fold) and XBP1s (8-fold) (**Figure 5b**) was observed in organoids in response to hypoxia-reoxygenation at 0R and 30R compared to C, indicating activation of both PERK and IRE1 branches of the UPR. Also, in line with human IR data (**Figure S2**), Hsp72 was significantly increased at 120R (**Figure 5b**). Treatment with small molecule ISRIB resulted in significantly lower ATF4 and CHOP expression at 0R and 30R, with CHOP levels close to control conditions. In contrast, ISRIB did not significantly change GADD34 expression levels (**Figure 5b**). These data suggest pro-apoptotic ATF4-CHOP signaling was strongly reduced by ISRIB, whereas GADD34 expression remained intact. In addition, XBP1s expression at 30R was lower with ISRIB exposure (**Figure 5b**), which demonstrates the complex interaction between the different UPR branches.

To examine the effect of suppressed UPR signaling on epithelial cell death, caspase 3/7 activity was measured. A significant increase in apoptosis was observed in organoids at 0R, 30R and

120R, with the highest apoptosis levels during early reperfusion (3-fold compared to C) (**Figure 5c**). Although there seemed to be a downward trend in apoptosis with increasing concentrations of ISRIB at 30R, no statistical significance was reached (**Figure 5c**).

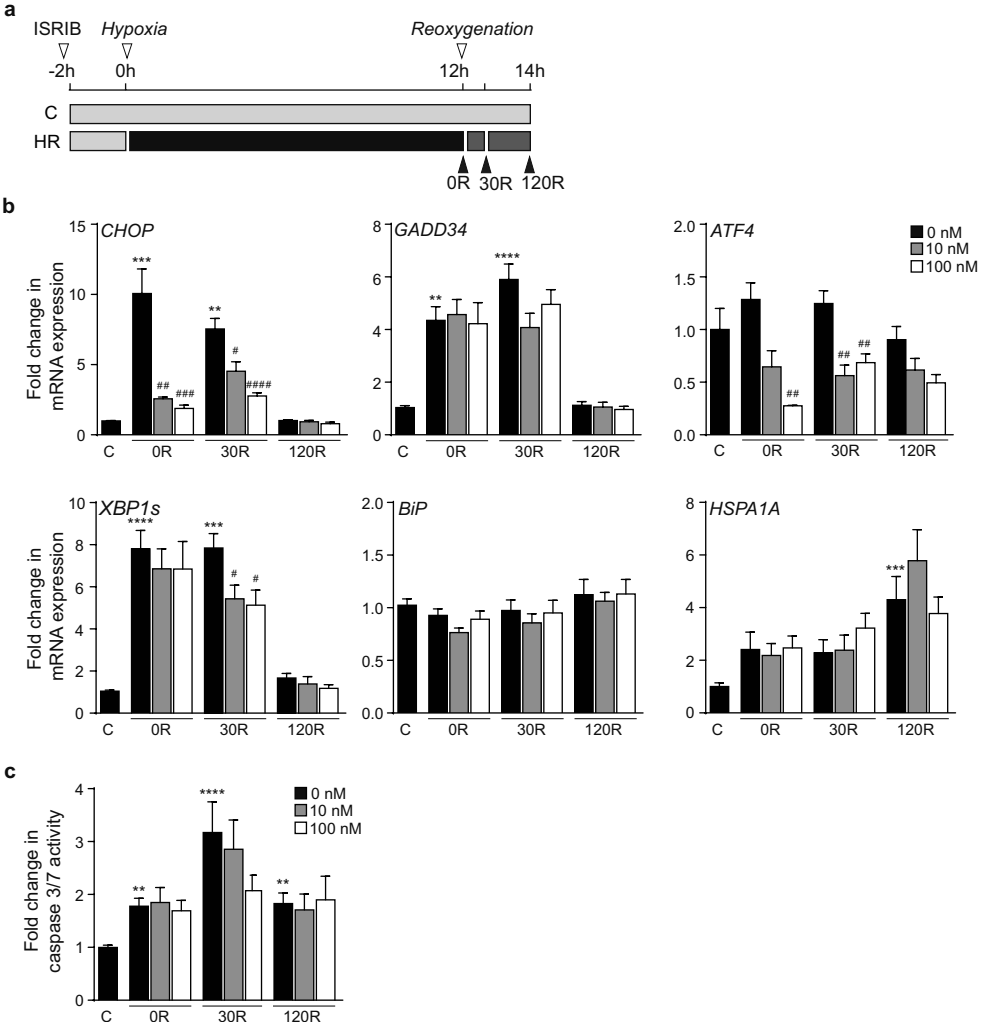

***Figure 5 Inhibition of the unfolded protein response decreases pro-apoptotic UPR signaling. a**) Experimental setup. Organoids were exposed to 12 h of hypoxia without reoxygenation (0R), 30 min of reoxygenation (30R) and 120 min of reoxygenation (120R). ISRIB (0, 10 or 100 nM) was added 2 h before the start of hypoxia. Control samples were not exposed to HR (C). **b**) mRNA expression of UPR-related genes CHOP, GADD34, ATF4, XBP1s, BiP and Hsp72. n=9 from 3 organoid lines. Data are presented as fold change compared to C (mean ±SEM). **c**) Apoptosis measurement using a Caspase 3/7 activity assay (Promega). Results are presented as fold change in luminescence (RLU) compared to C. n=12 from 3 organoid lines. Kruskal-Wallis with Dunn's multiple comparisons test was used to compare HR conditions to C (significance indicated with *), and per time point 10 and 100 nM ISRIB were compared to no ISRIB (significance indicated with #). *p<0.05, **p<0.01, ***p<0.001, ****p<0.0001, # p<0.05, ## p<0.01, ### p<0.001, #### p<0.0001.*

DISCUSSION

Systems biology tools are invaluable in deciphering the complexity of the tissue response to injury and in identifying novel targets for therapy. Through the transcriptomic profiling of consecutive stages of ischemia-reperfusion-exposed human intestinal tissue and comprehensive analyses of transcriptome changes at the level of functions, pathways and networks, we identified the key regulated biological processes activated during this tissue damage response.

Intriguingly, we found that, apart from expected regulated pathways involved in cell death, recovery, and inflammation, ischemia-reperfusion in the human intestine activates predominantly the cellular machinery to deal with unfolded protein stress. The sensitive protein-folding environment in the ER can be perturbed by various environmental factors, such as hypoxia, nutrient/energy depletion, oxidative stress, disturbances in ER Ca^{2+} balance and elevated secretory protein synthesis, which all occur during ischemia-reperfusion[23,24]. This disturbance of ER homeostasis results in the accumulation of unfolded proteins, called ER stress, which initiates a series of pro-survival mechanisms, known as the UPR. The UPR alters the cellular transcriptional and translational program to cope with stressful conditions and resolve the protein-folding defect. However, if ER stress is sustained, UPR signaling can promote apoptotic cell death[17,25]. Our data show crucial involvement of two principal UPR branches, namely IRE1 and PERK in UPR activation in the ischemia-reperfusion-exposed human intestine. The highly dynamic changes in these pathways are likely directed at restoring ER homeostasis by reducing the amount of new protein translocated into the ER lumen by increasing degradation of ER-localized proteins, and by augmenting the ER folding capacity. Pro-survival UPR mechanisms include IRE1-induced splicing of XBP1 and PERK-induced phosphorylation of eIF2α and subsequent translational block. In contrast, the observed increase in CHOP expression, also downstream target of PERK signaling, points to pro-apoptotic signaling[26].

Interestingly, network analysis of changed transcription factors and their targets revealed a key role for HIF1A in the intestinal response towards unfolded protein accumulation during ischemia-reperfusion. HIF1A (hypoxia-inducible factor 1-alpha) is a transcription regulator that plays a crucial role in metabolic adaptation and cellular survival under hypoxic conditions[27,28]. During ischemia, oxygen and nutrient insufficiency induces HIF1A signaling, which helps the intestine to adapt to these stressful conditions by inducing metabolic alterations, angiogenesis and barrier protection[29,30]. Activation of HIF1A has been reported in animal models of intestinal ischemia-reperfusion[31], and has been shown to be critical for cell survival in myocardial and renal ischemia-reperfusion injury[28,32,33]. As, in our model, HIF1A appears to be a central transcriptional regulator of numerous genes involved in the response to protein folding stress, it can be postulated that part of its protective properties is attributable to activation of the protein folding machinery. This is coherent with previous studies on the cross-talk between hypoxia and the UPR in cancer models - reviewed by Bartoszewska et al. - from which it was concluded that the required reduction in the cell's energy demand during hypoxia, is in part achieved via UPR-mediated suppression of translation[27]. Also, a link between HIF transcriptional activity and activation of PERK, ATF6 and IRE1 pathways in human endothelial cells,

independent of ER stress, has been reported[34]. Molecular chaperone Hsp72, one of the targets in the HIF1A-centered network of ischemia-reperfusion-damaged intestine, has been shown to be regulated by HIF1A before [35] and may provide another link with UPR activation[19]. Biological relevance of the inferred network was demonstrated by the presence of numerous known HIF1A target genes such as *VIM*, *ADAMTS1*, *PRNP* and *CD55*[36-39].

Analysis of transcriptional profiles revealed strong co-activation of the ER stress and MAPK signaling pathway. There is accumulating evidence on the extensive crosstalk between the ER stress response and the inflammatory response[14,40]. Also, ER stress and related UPR have been recognized to play a key role in intestinal pathology, such as inflammatory bowel disease [41,42]. The UPR and inflammatory response are interconnected through various mechanisms, including reactive oxygen species production, calcium release from the ER, activation of inflammatory NF-κB and MAPK signaling[14]. Activation of NF-κB has been shown to be mediated via IRE1[43], PERK[44] and ATF6[45] branches of the UPR. In addition, inflammatory response signaling via p38 and JNK MAPK pathways is known to be mediated by IRE1 and PERK signaling during ER stress[46-48]. The co-activation of UPR signaling and inflammatory signaling during ischemia-reperfusion, suggests that these processes cooperate during stress in the intestinal epithelium. Hence, besides exposure to luminal antigen as a consequence of the disrupted physical barrier[8], the ER stress response represents a plausible mechanism for exacerbation of inflammation in the ischemia-reperfusion-exposed human intestine.

In addition, ER stress can also indirectly be involved in inflammatory responses via its effects on Paneth cells, which are important players of the immunological intestinal barrier[49]. We have previously reported Paneth cell apoptosis during reperfusion, which strongly correlated with the level of UPR activation[16]. As Paneth cells are invaluable for host defense against microbial invasion, loss of these cells can induce bacterial translocation, thereby provoking an inflammatory response. In line, the current study reveals that during prolonged reperfusion, top regulated pathways were associated with signs of bacterial invasion, which is likely in part due to loss of this essential innate immune barrier.

Altogether, our data point to a prominent role of UPR signaling in ischemia-reperfusion injury of the human intestine. As UPR signaling is crucial in determining cell fate under ER stress, we explored the pharmacological modulation of UPR signaling and its potential to protect against intestinal ischemia-reperfusion injury. General UPR inhibition with chemical chaperones has been reported to improve survival during ischemia-reperfusion in other organs. The fact that all arms of the UPR have pro-survival and pro-death potential, makes it a challenging therapeutic target[50]. More specific inhibitors of the UPR, such as ISRIB, have enhanced therapeutic potential over general inhibitors as they are less likely to cause adverse effects. Moreover, ISRIB is known to effectively suppress the UPR within a certain window of activation[51]. The PERK-driven, ATF4-dependent induction of CHOP is considered to play a key role in UPR-related apoptotic cell death. We showed that inhibition of PERK signaling with its downstream inhibitor ISRIB, reduced ATF4 expression and almost completely prevented the huge induction in CHOP gene expression during hypoxia-reoxygenation in intestinal organoids. This indicates that ISRIB significantly reduced pro-apoptotic UPR signaling during hypoxia-reoxygenation. As ISRIB acts downstream of PERK signaling by selectively reversing the effects of eIF2α

phosphorylation, some of the protective effects of the UPR can be maintained[21,22,52]. This is supported by a recent study reporting that ISRIB, but not a direct PERK kinase inhibitor, improved neuronal cell survival[53]. Moreover, complete loss of PERK signaling has been shown to promote apoptosis[54].

Surprisingly, ISRIB treatment also led to a moderate reduction in XBP1s mRNA after reoxygenation, indicating that modulation of PERK signaling also affects IRE1 activity. The importance of the coordination between these two branches of the UPR in cell fate decisions has been reported recently by Chang er al., who demonstrated that PERK signaling attenuates IRE1s protective activity during the terminal UPR apoptotic signaling, and, opposite to our findings, that ISRIB treatment enhanced IRE1 activation upon ER stress[55]. This underlines the complexity of UPR dynamics, coordination between branches, and the effect of their modulation.

The heterogeneity of organoid cultures, as well as the fact that inhibition experiments were performed in human organoid lines derived from different individuals, likely accounts for the variation in functional outcome. Although the downward trend in apoptosis with increasing ISRIB concentration during reoxygenation did not reach statistical significance in the current experimental setting, these are promising results showing the potential of attenuating hypoxia-reoxygenation-induced cell death via a drastic decrease in pro-apoptotic ATF4/CHOP signaling. We believe that ISRIB has the potential to fine-tune the UPR in favor of survival, and to attenuate intestinal ischemia-reperfusion injury. However, thorough examination of the exact mechanisms and functional outcomes of ISRIB treatment during hypoxia-reoxygenation *in vitro* and ischemia-reperfusion *in vivo* is needed, as well as the effect on connected stress responses, such as MAPK, NFκb, and HIF1A signaling.

In this study, we captured the dynamic modulation of genes in the human intestine subjected to ischemia-reperfusion. We provided a pathway-based framework of the intestinal damage response to ischemia-reperfusion in man, which may advance the understanding of numerous pathophysiological conditions with reduced intestinal perfusion and hypoxic signaling. We can conclude that ischemia-reperfusion massively changes the transcriptional landscape of the human gut, and, apart from the expected pathways involved in cell death, restoration and inflammation, unfolded protein stress appeared to be of crucial importance among the regulated processes in human intestine exposed to ischemia-reperfusion. Therefore, we explored the potential of pharmacological modulation of UPR signaling in the protection against intestinal ischemia-reperfusion injury. We demonstrated that selective downstream PERK inhibition with ISRIB strongly reduced pro-apoptotic UPR signaling during hypoxia-reoxygenation in intestinal organoids. These findings suggest that downstream PERK targeting may be a promising strategy to treat ischemia-reperfusion-induced complications in the intestine, which is of utmost importance to reduce its high morbidity and mortality rates.

ACKNOWLEDGEMENTS

The authors thank Pieter van der Vlies and Bahram Sanjabi for their expertise on microarray analysis, Ronald van Dam for his surgical expertise with the human model, Fons Verheyen and Hans Duimel for their excellent expertise on electron microscopy imaging. We thank Anjali Röth for patient inclusion in Uniklinik RWTH Aachen for the generation of organoids, and Annet Duivenvoorden and Chantal van Heugten for their laboratory support. Graphical abstract was created with BioRender.com.

REFERENCES

1 Okumura, R. & Takeda, K. Roles of intestinal epithelial cells in the maintenance of gut homeostasis. *Exp Mol Med* **49**, e338 (2017).

2 Colgan, S. P. & Taylor, C. T. Hypoxia: an alarm signal during intestinal inflammation. *Nat Rev Gastroenterol Hepatol* **7**, 281-287 (2010).

3 van Wijck, K. *et al.* Exercise-induced splanchnic hypoperfusion results in gut dysfunction in healthy men. *PLoS One* **6**, e22366 (2011).

4 Brandt, L. J. & Boley, S. J. AGA technical review on intestinal ischemia. American Gastrointestinal Association. *Gastroenterology* **118**, 954-968 (2000).

5 Bala, M. *et al.* Acute mesenteric ischemia: guidelines of the World Society of Emergency Surgery. *World J Emerg Surg* **12**, 38 (2017).

6 Ibrahim, C. B., Aroniadis, O. C. & Brandt, L. J. On the role of ischemia in the pathogenesis of IBD: a review. *Inflamm Bowel Dis* **16**, 696-702 (2010).

7 Taylor, C. T. & Colgan, S. P. Hypoxia and gastrointestinal disease. *J Mol Med (Berl)* **85**, 1295-1300 (2007).

8 Grootjans, J. *et al.* Human intestinal ischemia-reperfusion-induced inflammation characterized: experiences from a new translational model. *Am J Pathol* **176**, 2283-2291 (2010).

9 Gonzalez, L. M., Moeser, A. J. & Blikslager, A. T. Animal models of ischemia-reperfusion-induced intestinal injury: progress and promise for translational research. *Am J Physiol Gastrointest Liver Physiol* **308**, G63-75 (2015).

10 Grootjans, J., Lenaerts, K., Buurman, W. A., Dejong, C. H. & Derikx, J. P. Life and death at the mucosal-luminal interface: New perspectives on human intestinal ischemia-reperfusion. *World J Gastroenterol* **22**, 2760-2770 (2016).

11 Kip, A. M. *et al.* Proteomics analysis of human intestinal organoids during hypoxia and reoxygenation as a model to study ischemia-reperfusion injury. *Cell Death Dis* **12**, 95 (2021).

12 Gentleman, R. C. *et al.* Bioconductor: open software development for computational biology and bioinformatics. *Genome Biol* **5**, R80 (2004).

13 Zhou, Y. *et al.* Metascape provides a biologist-oriented resource for the analysis of systems-level datasets. *Nat Commun* **10**, 1523 (2019).

14 Zhang, K. & Kaufman, R. J. From endoplasmic-reticulum stress to the inflammatory response. *Nature* **454**, 455-462 (2008).

15 Calfon, M. *et al.* IRE1 couples endoplasmic reticulum load to secretory capacity by processing the XBP-1 mRNA. *Nature* **415**, 92-96 (2002).

16 Grootjans, J. *et al.* Level of activation of the unfolded protein response correlates with Paneth cell apoptosis in human small intestine exposed to ischemia/reperfusion. *Gastroenterology* **140**, 529-539. e523 (2011).

17 Ron, D. & Walter, P. Signal integration in the endoplasmic reticulum unfolded protein response. *Nat Rev Mol Cell Biol* **8**, 519-529 (2007).

18 Acosta-Alvear, D. *et al.* XBP1 controls diverse cell type- and condition-specific transcriptional regulatory networks. *Mol Cell* **27**, 53-66 (2007).

19 Gupta, S. *et al.* HSP72 protects cells from ER stress-induced apoptosis via enhancement of IRE1alpha-XBP1 signaling through a physical interaction. *PLoS Biol* **8**, e1000410 (2010).

20 Hetz, C., Zhang, K. & Kaufman, R. J. Mechanisms, regulation and functions of the unfolded protein response. *Nat Rev Mol Cell Biol* **21**, 421-438 (2020).

21 Sidrauski, C. *et al.* Pharmacological brake-release of mRNA translation enhances cognitive memory. *Elife* **2**, e00498 (2013).

22 Sidrauski, C., McGeachy, A. M., Ingolia, N. T. & Walter, P. The small molecule ISRIB reverses the effects of eIF2α phosphorylation on translation and stress granule assembly. *Elife* **4** (2015).

23 Badiola, N. *et al.* Induction of ER stress in response to oxygen-glucose deprivation of cortical cultures involves the activation of the PERK and IRE-1 pathways and of caspase-12. *Cell Death Dis* **2**, e149 (2011).

24 Mallick, I. H., Yang, W., Winslet, M. C. & Seifalian, A. M. Ischemia-reperfusion injury of the intestine and protective strategies against injury. *Dig Dis Sci* **49**, 1359-1377 (2004).

25 Hetz, C. The unfolded protein response: controlling cell fate decisions under ER stress and beyond. *Nat Rev Mol Cell Biol* **13**, 89-102 (2012).

26 Szegezdi, E., Logue, S. E., Gorman, A. M. & Samali, A. Mediators of endoplasmic reticulum stress-induced apoptosis. *EMBO Rep* **7**, 880-885 (2006).

27 Bartoszewska, S. & Collawn, J. F. Unfolded protein response (UPR) integrated signaling networks determine cell fate during hypoxia. *Cell Mol Biol Lett* **25**, 18 (2020).

28 Loor, G. & Schumacker, P. T. Role of hypoxia-inducible factor in cell survival during myocardial ischemia-reperfusion. *Cell Death Differ* **15**, 686-690 (2008).

29 Karhausen, J. *et al.* Epithelial hypoxia-inducible factor-1 is protective in murine experimental colitis. *J Clin Invest* **114**, 1098-1106 (2004).

30 Chen, S. & Sang, N. Hypoxia-Inducible Factor-1: A Critical Player in the Survival Strategy of Stressed Cells. *J Cell Biochem* **117**, 267-278 (2016).

31 Koury, J. *et al.* Persistent HIF-1alpha activation in gut ischemia/reperfusion injury: potential role of bacteria and lipopolysaccharide. *Shock* **22**, 270-277 (2004).

32 Lee, J. W., Ko, J., Ju, C. & Eltzschig, H. K. Hypoxia signaling in human diseases and therapeutic targets. *Exp Mol Med* **51**, 1-13 (2019).

33 Conde, E. *et al.* Hypoxia inducible factor 1-alpha (HIF-1 alpha) is induced during reperfusion after renal ischemia and is critical for proximal tubule cell survival. *PLoS One* **7**, e33258 (2012).

34 Karali, E. *et al.* VEGF Signals through ATF6 and PERK to promote endothelial cell survival and angiogenesis in the absence of ER stress. *Mol Cell* **54**, 559-572 (2014).

35 Huang, W. J. *et al.* Transcriptional upregulation of HSP70-2 by HIF-1 in cancer cells in response to hypoxia. *Int J Cancer* **124**, 298-305 (2009).

36 Krishnamachary, B. *et al.* Regulation of colon carcinoma cell invasion by hypoxia-inducible factor 1. *Cancer Res* **63**, 1138-1143 (2003).

37 Hatipoglu, O. F. *et al.* ADAMTS1 is a unique hypoxic early response gene expressed by endothelial cells. *J Biol Chem* **284**, 16325-16333 (2009).

38 Jeong, J. K. *et al.* Hypoxia-inducible factor-1 α regulates prion protein expression to protect against neuron cell damage. *Neurobiol Aging* **33**, 1006.e1001-1010 (2012).

39 Louis, N. A., Hamilton, K. E., Kong, T. & Colgan, S. P. HIF-dependent induction of apical CD55 coordinates epithelial clearance of neutrophils. *Faseb j* **19**, 950-959 (2005).

40 Grootjans, J., Kaser, A., Kaufman, R. J. & Blumberg, R. S. The unfolded protein response in immunity and inflammation. *Nat Rev Immunol* **16**, 469-484 (2016).

41 Coleman, O. I. & Haller, D. ER Stress and the UPR in Shaping Intestinal Tissue Homeostasis and Immunity. *Front Immunol* **10**, 2825 (2019).

42 Ma, X. *et al.* Intestinal Epithelial Cell Endoplasmic Reticulum Stress and Inflammatory Bowel Disease Pathogenesis: An Update Review. *Front Immunol* **8**, 1271 (2017).

43 Hu, P., Han, Z., Couvillon, A. D., Kaufman, R. J. & Exton, J. H. Autocrine tumor necrosis factor alpha links endoplasmic reticulum stress to the membrane death receptor pathway through IRE1alpha-mediated NF-kappaB activation and down-regulation of TRAF2 expression. *Mol Cell Biol* **26**, 3071-3084 (2006).

44 Deng, J. *et al.* Translational repression mediates activation of nuclear factor kappa B by phosphorylated translation initiation factor 2. *Mol Cell Biol* **24**, 10161-10168 (2004).

45 Nakajima, S. *et al.* Selective abrogation of BiP/GRP78 blunts activation of NF-κB through the ATF6 branch of the UPR: involvement of C/EBPβ and mTOR-dependent dephosphorylation of Akt. *Mol Cell Biol* **31**, 1710-1718 (2011).

46 Urano, F. *et al.* Coupling of stress in the ER to activation of JNK protein kinases by transmembrane protein kinase IRE1. *Science* **287**, 664-666 (2000).

47 Darling, N. J. & Cook, S. J. The role of MAPK signalling pathways in the response to endoplasmic reticulum stress. *Biochim Biophys Acta* **1843**, 2150-2163 (2014).

48 Liang, S. H., Zhang, W., McGrath, B. C., Zhang, P. & Cavener, D. R. PERK (eIF2alpha kinase) is required to activate the stress-activated MAPKs and induce the expression of immediate-early genes upon disruption of ER calcium homoeostasis. *Biochem J* **393**, 201-209 (2006).

49 Bevins, C. L. & Salzman, N. H. Paneth cells, antimicrobial peptides and maintenance of intestinal homeostasis. *Nat Rev Microbiol* **9**, 356-368 (2011).

50 Maurel, M. *et al.* Controlling the unfolded protein response-mediated life and death decisions in cancer. *Semin Cancer Biol* **33**, 57-66 (2015).

51 Rabouw, H. H. *et al.* Small molecule ISRIB suppresses the integrated stress response within a defined window of activation. *Proc Natl Acad Sci U S A* **116**, 2097-2102 (2019).

52 Zyryanova, A. F. *et al.* Binding of ISRIB reveals a regulatory site in the nucleotide exchange factor eIF2B. *Science* **359**, 1533-1536 (2018).

53 Bugallo, R. *et al.* Fine tuning of the unfolded protein response by ISRIB improves neuronal survival in a model of amyotrophic lateral sclerosis. *Cell Death Dis* **11**, 397 (2020).

54 Guthrie, L. N. *et al.* Attenuation of PKR-like ER Kinase (PERK) Signaling Selectively Controls Endoplasmic Reticulum Stress-induced Inflammation Without Compromising Immunological Responses. *J Biol Chem* **291**, 15830-15840 (2016).

55 Chang, T. K. *et al.* Coordination between Two Branches of the Unfolded Protein Response Determines Apoptotic Cell Fate. *Mol Cell* **71**, 629-636.e625 (2018).

SUPPLEMENTARY INFORMATION

Contents

Supplementary figures

Supplementary tables

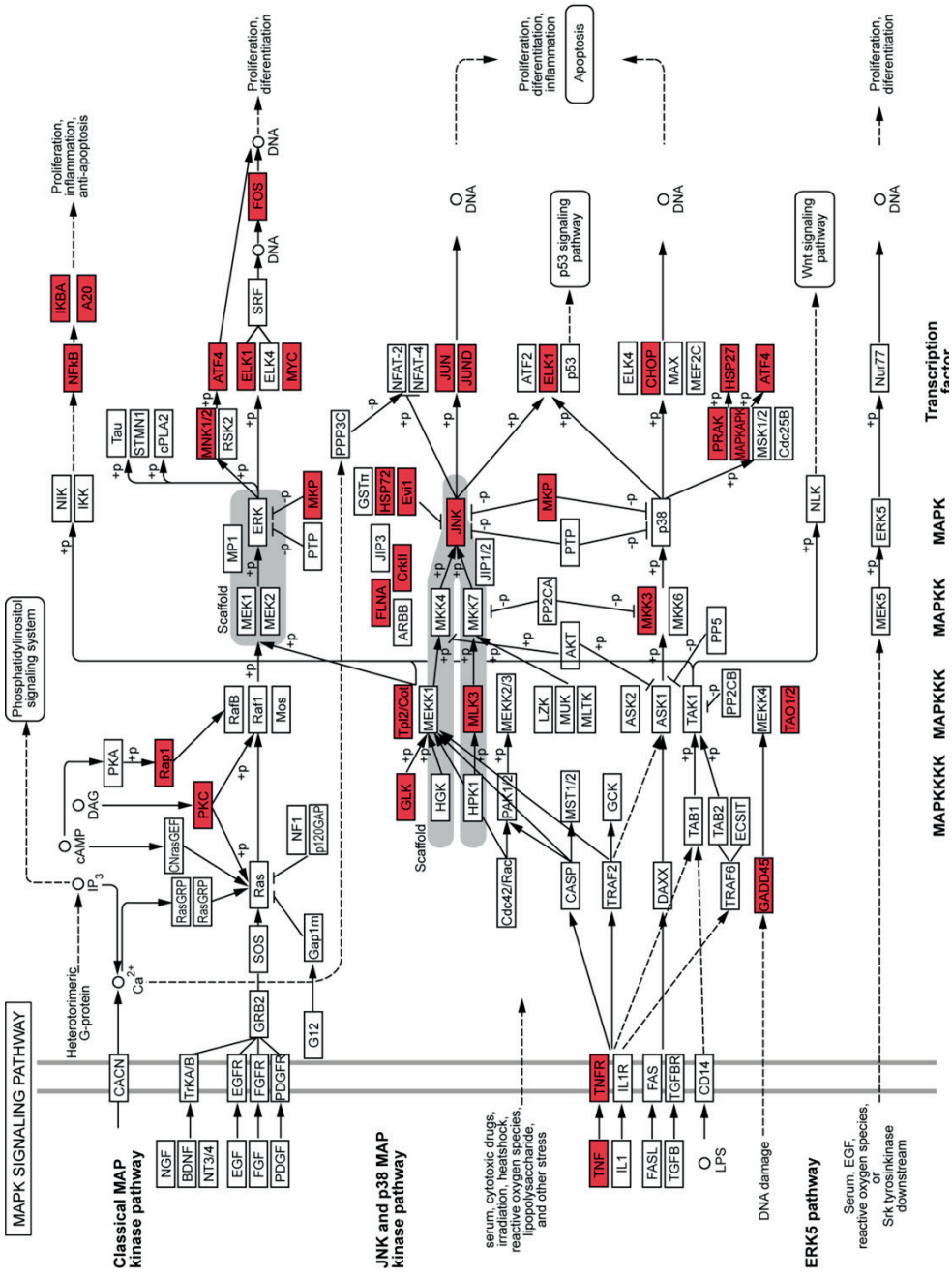

Figure S1. *Top perturbed pathway during reperfusion of ischemically injured intestine, namely MAPK signaling pathway (modified from KEGG pathway hsa04010). Changed genes are indicated in red. Differential expression is especially evident in JNK and p38 MAPK pathway and the classical MAPK pathway.*

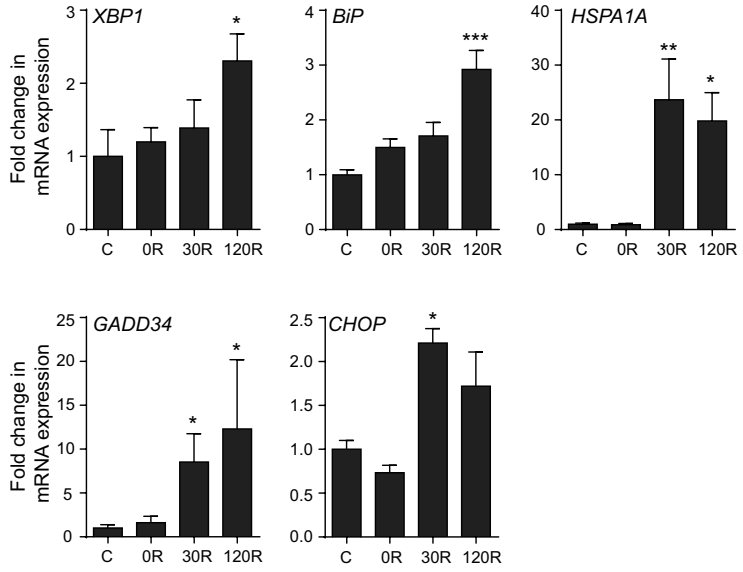

Figure S2. Quantitative PCR analysis of genes related to unfolded protein response in human ischemia-reperfusion. *Gene expression of XBP1, BiP, Hsp72 (encoded by HSPA1A), GADD34 and CHOP in control tissue (C), and tissue exposed to ischemia (0R), 30 minutes (30R) and 120 minutes of reperfusion (120R) (N=7 patients) *p<0.05 vs C, **p<0.01 vs C, ***p<0.001 vs C. Data are presented as fold change compared to C (mean ±SEM).*

Table S1. RNA samples included for gene expression analysis by Illumina Beadchips. Samples were randomized over three Beadchips.

Patient	Age	Sex	Condition	RIN	Chip	Array
1	72	male	30I/0R	8,6	4811636083	A
			30I/30R	8,2	4811636063	B
			30I/120R	8,8	4811636063	D
			C	7,3	4811636063	J
2	62	female	30I/0R	9,3	4811636083	D
			30I/30R	8,4	4811636083	H
			30I/120R	7,4	4811636083	I
			C	8,1	4811636083	K
3	73	male	30I/0R	9,2	4811636065	K
			30I/30R	8,8	4811636083	G
			30I/120R	7,3	4811636065	C
			C	8,1	4811636063	F
4	65	male	45I/0R	9,1	4811636065	I
			45I/30R	9,2	4811636063	A
			45I/120R	9,1	4811636083	C
			C	8,3	4811636065	A
5	54	female	45I/0R	9,4	4811636063	C
			45I/30R	9,6	4811636083	J
			45I/120R	8,5	4811636065	B
			C	7,1	4811636065	J
6	79	female	45I/0R	8,8	4811636065	L
			45I/30R	7,6	4811636083	L
			45I/120R	8,7	4811636063	L
			C	8,8	4811636065	H
7	76	female	45I/0R	8,9	4811636065	E
			45I/30R	8,4	4811636065	F
			45I/120R	7,8	4811636083	F
			C	8,7	4811636065	G

Table S2. Oligonucleotide primer sequences used for quantitative PCR

Gene	Forward primer sequence	Reverse primer sequence
IRE1	5'-CGAAACTTCCTTTTACCATCCC-3'	5'-CGATGACAAAGTCTGCTGCTT-3'
HSP72	5'-AAGATCACCATCACCAACGA-3'	5'-TCCTCCGCTTTGTACTTCTC-3'
LC3B	5'-AAGACCCTGGAGAAAGAGTG-3'	5'-TGCTTTCCGTAACAACACAG-3'
BIP	5'-CTGCTGTATCCTCTTCACCAGTTG- 3'	5'-TGACATTGAAGACTTCAAAGCTAAGA-3'
XBP1	5'-GGAGTTAAGACAGCGCTTGGGGA-3'	5'-TGTTCTGGAGGGGTGACAACTGGG-3'
XBP1s	5'-TGCTGAGTCCGCAGCAGGTG-3'	5'-GCTGGCAGGCTCTGGGGAAG-3'
CHOP	5'-GGAGCATCAGTCCCCCACTT-3'	5'-TGTGGGATTGAGGGTCACATC- 3'
GADD34	5'-CCCAGAAACCCCTACTCATGATC-3'	5'-GCCCAGACAGCCAGGAAAT-3'
ATF4	5'-CTCCGGGACAGATTGGATGTT-3'	5'-GGCTGCTTATTAGTCTCCTGGAC-3'
B2MG	5'-TCCATCCGACATTGAAGTTG-3'	5'-CGGCAGGCATACTCATCTT-3'
ACTB	5'-GCTGTGCTACGTCGCCCTG-3'	5'-GGAGGAGCTGGAAGCAGCC-3'
RPLP0	5'-GCAATGTTGCCAGTGTCTG-3'	5'-GCCTTGACCTTTTCAGCAA-3'
CYPA	5'-CTCGAATAAGTTTGACTTGTGTTT-3'	5'-CTAGGCATGGGAGGGAACA-3'

Table S3. Gene expression changes in the human intestine in response to ischemia-reperfusion. The 50 highest significantly up- and downregulated genes per condition (0R, 30R, and 120R vs C) are listed.

Entrez ID	Gene Symbol	Gene Name	Fold change	Adjusted p-value
0R vs C			**Up**	
4069	LYZ	lysozyme (renal amyloidosis)	4,11	0,0327
83998	REG4	regenerating islet-derived family, member 4	3,37	0,0233
2353	FOS	v-fos FBJ murine osteosarcoma viral oncogene homolog	2,96	0,0494
27299	ADAMDEC1	ADAM-like, decysin 1	2,06	0,0488
642817	LOC642817	hypothetical LOC642817	1,88	0,0322
7494	XBP1	X-box binding protein 1	1,86	0,0258
7494	XBP1	X-box binding protein 1	1,85	0,0328
71	ACTG1	actin, gamma 1	1,84	0,0448
6175	RPLP0	ribosomal protein, large, P0 pseudogene 2	1,81	0,0336
10935	PRDX3	peroxiredoxin 3	1,80	0,0407
58505	DC2	oligosaccharyltransferase complex subunit; similar to DC2	1,78	0,0181
64231	MS4A6A	membrane-spanning 4-domains, subfamily A, member 6A	1,69	0,0289
3150	HMGN1	high-mobility group nucleosome binding domain 1	1,64	0,0392
10175	CNIH	cornichon homolog (Drosophila)	1,63	0,0276
708	C1QBP	complement component 1, q subcomponent binding protein	1,63	0,0322
1109	AKR1C4	aldo-keto reductase family 1, member C4	1,63	0,0414
54504	CPVL	carboxypeptidase, vitellogenic-like	1,62	0,0407
114908	TMEM123	transmembrane protein 123	1,58	0,0335
10175	CNIH	cornichon homolog (Drosophila)	1,56	0,0182
6558	SLC12A2	solute carrier family 12 (sodium/potassium/chloride transporters), member 2	1,55	0,0276
6175	RPLP0	ribosomal protein, large, P0 pseudogene 2	1,55	0,0322
6613	SUMO2	SMT3 suppressor of mif two 3 homolog 2 (S. cerevisiae) pseudogene	1,54	0,0422
51522	TMEM14C	transmembrane protein 14C	1,53	0,0392
6218	RPS17	ribosomal protein S17	1,53	0,0182
2938	GSTA1	glutathione S-transferase alpha 1	1,53	0,0328
10252	SPRY1	sprouty homolog 1, antagonist of FGF signaling (Drosophila)	1,53	0,0442
2171	FABP5	fatty acid binding protein 5-like 2	1,53	0,0314
646567		oligosaccharyltransferase complex subunit; similar to DC2	1,52	0,0449
11222	MRPL3	mitochondrial ribosomal protein L3	1,52	0,0372
515	ATP5F1	ATP synthase, H+ transporting, mitochondrial F0 complex, subunit B1	1,51	0,0470
6636	SNRPF	small nuclear ribonucleoprotein polypeptide F	1,51	0,0244
9403	Sep-15	15 kDa selenoprotein	1,50	0,0130
7857	SCG2	secretogranin II (chromogranin C)	1,50	0,0375
51495	PTPLAD1	protein tyrosine phosphatase-like A domain containing 1	1,50	0,0068
10606	PAICS	phosphoribosylaminoimidazole carboxylase	1,50	0,0448
51192	CKLF	chemokine-like factor	1,50	0,0328
9204	ZMYM6	hypothetical LOC100130633; zinc finger, MYM-type 6	1,50	0,0103
52	ACP1	acid phosphatase 1, soluble	1,49	0,0392
84233	TMEM126A	transmembrane protein 126A	1,48	0,0182
6187	RPS2	ribosomal protein S2 pseudogene 8	1,47	0,0340
10412	TINP1	similar to TGF beta-inducible nuclear protein 1	1,47	0,0289
8804	CREG1	cellular repressor of E1A-stimulated genes 1	1,46	0,0197

8813	DPM1	dolichyl-phosphate mannosyltransferase polypeptide 1, catalytic subunit	1,46	0,0303
3094	HINT1	histidine triad nucleotide binding protein 1	1,45	0,0431
6727	SRP14	signal recognition particle 14kDa (homologous Alu RNA binding protein) pseudogene 1	1,45	0,0285
51014	TMED7	transmembrane emp24 protein transport domain containing 7	1,45	0,0197
6210	RPS15A	ribosomal protein S15a pseudogene 17	1,45	0,0289
54148	MRPL39	mitochondrial ribosomal protein L39	1,45	0,0182
86	ACTL6A	actin-like 6A	1,44	0,0233
9685	CLINT1	clathrin interactor 1	1,44	0,0499
0R vs C			**Down**	
126205	NLRP8	NLR family, pyrin domain containing 8	-1,88	0,0455
10299	MARCH6	membrane-associated ring finger (C3HC4) 6	-1,72	0,0328
729603	LOC729603	calcium binding protein P22 pseudogene	-1,68	0,0494
1577	CYP3A5	cytochrome P450, family 3, subfamily A, polypeptide 5	-1,63	0,0372
136051	ZNF786	zinc finger protein 786	-1,61	0,0427
8566	PDXK	pyridoxal (pyridoxine, vitamin B6) kinase	-1,59	0,0431
9679	FAM53B	family with sequence similarity 53, member B	-1,57	0,0276
79784	MYH14	myosin, heavy chain 14	-1,55	0,0292
7430	EZR	ezrin	-1,53	0,0499
4967	OGDH	oxoglutarate (alpha-ketoglutarate) dehydrogenase (lipoamide)	-1,53	0,0335
3691	ITGB4	integrin, beta 4	-1,51	0,0322
55667	DENND4C	DENN/MADD domain containing 4C	-1,51	0,0182
192683	SCAMP5	secretory carrier membrane protein 5	-1,48	0,0442
10908	PNPLA6	patatin-like phospholipase domain containing 6	-1,46	0,0322
5119	CHMP1A	chromatin modifying protein 1A	-1,45	0,0182
11282	MGAT4B	mannosyl (alpha-1,3-)-glycoprotein beta-1,4-N-acetylglucosaminyltransferase, isozyme B	-1,45	0,0328
8073	PTP4A2	protein tyrosine phosphatase type IVA, member 2	-1,45	0,0053
4296	MAP3K11	mitogen-activated protein kinase kinase kinase 11	-1,45	0,0133
23140	ZZEF1	zinc finger, ZZ-type with EF-hand domain 1	-1,44	0,0096
79157	MFSD11	major facilitator superfamily domain containing 11	-1,44	0,0289
5753	PTK6	PTK6 protein tyrosine kinase 6	-1,43	0,0455
90007	MIDN	midnolin	-1,43	0,0328
23277	KIAA0664	KIAA0664	-1,42	0,0276
9600	PITPNM1	phosphatidylinositol transfer protein, membrane-associated 1	-1,42	0,0392
728294	D2HGDH	D-2-hydroxyglutarate dehydrogenase	-1,41	0,0444
25920	COBRA1	cofactor of BRCA1	-1,41	0,0258
9927	MFN2	mitofusin 2	-1,41	0,0278
6687	SPG7	spastic paraplegia 7 (pure and complicated autosomal recessive)	-1,40	0,0328
10163	WASF2	WAS protein family, member 2	-1,40	0,0289
64780	MICAL1	microtubule associated monoxygenase, calponin and LIM domain containing 1	-1,40	0,0440
4248	MGAT3	mannosyl (beta-1,4-)-glycoprotein beta-1,4-N-acetylglucosaminyltransferase	-1,40	0,0372
3609	ILF3	interleukin enhancer binding factor 3, 90kDa	-1,39	0,0289
90639	COX19	COX19 cytochrome c oxidase assembly homolog (S. cerevisiae)	-1,39	0,0293
440704	LOC440704	hypothetical gene supported by BC042042	-1,39	0,0444
57464	FAM40B	family with sequence similarity 40, member B	-1,39	0,0412
3636	INPPL1	inositol polyphosphate phosphatase-like 1	-1,38	0,0289
64761	PARP12	poly (ADP-ribose) polymerase family, member 12	-1,38	0,0448

317762	C14orf65	coiled-coil domain containing 85C	-1,38	0,0236
79720	VPS37B	vacuolar protein sorting 37 homolog B (S. cerevisiae)	-1,38	0,0303
8408	ULK1	unc-51-like kinase 1 (C. elegans)	-1,38	0,0289
9807	IHPK1	inositol hexakisphosphate kinase 1	-1,37	0,0258
23352	UBR4	ubiquitin protein ligase E3 component n-recognin 4	-1,37	0,0372
83734	ATG10	ATG10 autophagy related 10 homolog (S. cerevisiae)	-1,36	0,0182
5917	RARS	arginyl-tRNA synthetase	-1,36	0,0448
27072	VPS41	vacuolar protein sorting 41 homolog (S. cerevisiae)	-1,36	0,0375
140628	GATA5	GATA binding protein 5	-1,34	0,0462
2017	CTTN	cortactin	-1,34	0,0181
6829	SUPT5H	suppressor of Ty 5 homolog (S. cerevisiae)	-1,34	0,0292
22906	TRAK1	trafficking protein, kinesin binding 1	-1,34	0,0328
79784	MYH14	myosin, heavy chain 14	-1,33	0,0289
30R vs C			**Up**	
2353	FOS	v-fos FBJ murine osteosarcoma viral oncogene homolog	20,89	0,0000
2354	FOSB	FBJ murine osteosarcoma viral oncogene homolog B	16,64	0,0000
3304	HSPA1B	heat shock 70kDa protein 1A; heat shock 70kDa protein 1B	14,33	0,0000
3303	HSPA1A	heat shock 70kDa protein 1A; heat shock 70kDa protein 1B	13,53	0,0000
1843	DUSP1	dual specificity phosphatase 1	10,40	0,0000
3725	JUN	jun oncogene	9,53	0,0000
467	ATF3	activating transcription factor 3	9,44	0,0000
1958	EGR1	early growth response 1	9,04	0,0000
7832	BTG2	BTG family, member 2	7,51	0,0000
3337	DNAJB1	DnaJ (Hsp40) homolog, subfamily B, member 1	6,97	0,0001
1839	HBEGF	heparin-binding EGF-like growth factor	6,66	0,0000
5996	RGS1	regulator of G-protein signaling 1	5,45	0,0000
4929	NR4A2	nuclear receptor subfamily 4, group A, member 2	5,07	0,0000
7538	ZFP36	zinc finger protein 36, C3H type, homolog (mouse)	4,92	0,0000
23645	PPP1R15A	protein phosphatase 1, regulatory (inhibitor) subunit 15A	4,88	0,0000
10365	KLF2	Kruppel-like factor 2 (lung)	4,86	0,0001
3491	CYR61	cysteine-rich, angiogenic inducer, 61	3,92	0,0000
1490	CTGF	connective tissue growth factor	3,35	0,0013
3320	HSP90AA1	heat shock protein 90kDa alpha (cytosolic), class A member 2	3,22	0,0000
414062	CCL3L3	chemokine (C-C motif) ligand 3-like 3	3,19	0,0001
64651	AXUD1	cysteine-serine-rich nuclear protein 1	3,17	0,0000
1490	CTGF	connective tissue growth factor	3,15	0,0023
6515	SLC2A3	solute carrier family 2 (facilitated glucose transporter), member 3	3,01	0,0001
1316	KLF6	Kruppel-like factor 6	2,95	0,0001
8870	IER3	immediate early response 3	2,91	0,0000
388	RHOB	ras homolog gene family, member B	2,90	0,0001
10808	HSPH1	heat shock 105kDa/110kDa protein 1	2,84	0,0064
90637	ZFAND2A	zinc finger, AN1-type domain 2A	2,84	0,0209
969	CD69	CD69 molecule	2,79	0,0001
5743	PTGS2	prostaglandin-endoperoxide synthase 2 (prostaglandin G/H synthase and cyclooxygenase)	2,70	0,0165
10221	TRIB1	tribbles homolog 1 (Drosophila)	2,68	0,0000
9314	KLF4	Kruppel-like factor 4 (gut)	2,68	0,0002
9531	BAG3	BCL2-associated athanogene 3	2,66	0,0053
9023	CH25H	cholesterol 25-hydroxylase	2,63	0,0002
56892	C8orf4	chromosome 8 open reading frame 4	2,60	0,0027
5552	SRGN	serglycin	2,55	0,0113

8553	BHLHB2	basic helix-loop-helix family, member e40	2,55	0,0000
6355	CCL8	chemokine (C-C motif) ligand 8	2,53	0,0019
1164	CKS2	CDC28 protein kinase regulatory subunit 2	2,53	0,0268
3399	ID3	inhibitor of DNA binding 3, dominant negative helix-loop-helix protein	2,51	0,0007
3726	JUNB	jun B proto-oncogene	2,50	0,0000
3336	HSPE1	heat shock 10kDa protein 1 (chaperonin 10)	2,42	0,0014
1847	DUSP5	dual specificity phosphatase 5	2,38	0,0019
8848	TSC22D1	TSC22 domain family, member 1	2,36	0,0015
3315	HSPB1	heat shock 27kDa protein-like 2 pseudogene; heat shock 27kDa protein 1	2,31	0,0113
3490	IGFBP7	insulin-like growth factor binding protein 7	2,26	0,0299
10124	ARL4A	ADP-ribosylation factor-like 4A	2,23	0,0053
3301	DNAJA1	DnaJ (Hsp40) homolog, subfamily A, member 1	2,17	0,0027
4953	ODC1	ornithine decarboxylase 1	2,16	0,0001
114789	SLC25A25	solute carrier family 25 (mitochondrial carrier; phosphate carrier), member 25	2,12	0,0005
30R vs C			**Down**	
89872	AQP10	aquaporin 10	-3,37	0,0424
4680	CEACAM6	carcinoembryonic antigen-related cell adhesion molecule 6 (non-specific cross reacting antigen)	-3,32	0,0148
1510	CTSE	cathepsin E	-2,56	0,0245
5265	SERPINA1	serpin peptidase inhibitor, clade A (alpha-1 antiproteinase, antitrypsin), member 1	-2,41	0,0304
8566	PDXK	pyridoxal (pyridoxine, vitamin B6) kinase	-2,28	0,0001
54825	PCLKC	protocadherin 24	-2,23	0,0063
1687	DFNA5	deafness, autosomal dominant 5	-2,16	0,0165
29881	NPC1L1	NPC1 (Niemann-Pick disease, type C1, gene)-like 1	-2,00	0,0223
6564	SLC15A1	solute carrier family 15 (oligopeptide transporter), member 1	-1,93	0,0099
1308	COL17A1	collagen, type XVII, alpha 1	-1,90	0,0030
59272	ACE2	angiotensin I converting enzyme (peptidyl-dipeptidase A) 2	-1,87	0,0165
4967	OGDH	oxoglutarate (alpha-ketoglutarate) dehydrogenase (lipoamide)	-1,83	0,0012
629	CFB	complement factor B	-1,83	0,0154
733	C8G	complement component 8, gamma polypeptide	-1,81	0,0469
3914	LAMB3	laminin, beta 3	-1,81	0,0304
6337	SCNN1A	sodium channel, nonvoltage-gated 1 alpha	-1,80	0,0100
5243	ABCB1	ATP-binding cassette, sub-family B (MDR/TAP), member 1	-1,79	0,0272
246181	AFAR3	aldo-keto reductase family 7-like	-1,78	0,0227
2875	GPT	glutamic-pyruvate transaminase (alanine aminotransferase)	-1,78	0,0053
338	APOB	apolipoprotein B (including Ag(x) antigen)	-1,78	0,0289
55715	DOK4	docking protein 4	-1,77	0,0038
347741	OTOP3	otopetrin 3	-1,76	0,0196
192683	SCAMP5	secretory carrier membrane protein 5	-1,76	0,0019
79762	C1orf115	chromosome 1 open reading frame 115	-1,74	0,0255
25845	LOC25845	hypothetical LOC25845	-1,74	0,0427
11181	TREH	trehalase (brush-border membrane glycoprotein)	-1,71	0,0185
164091	PAQR7	progestin and adipoQ receptor family member VII	-1,70	0,0219
3938	LCT	lactase	-1,70	0,0368
11282	MGAT4B	mannosyl (alpha-1,3-)-glycoprotein beta-1,4-N-acetylglucosaminyltransferase, isozyme B	-1,69	0,0012
535	ATP6V0A1	ATPase, H+ transporting, lysosomal V0 subunit a1	-1,69	0,0055

53841	MUPCDH	mucin-like protocadherin	-1,68	0,0434
7430	EZR	hypothetical protein LOC100129652; ezrin	-1,68	0,0122
4248	MGAT3	mannosyl (beta-1,4-)-glycoprotein beta-1,4-N-acetylglucosaminyltransferase	-1,67	0,0005
399665	FAM102A	family with sequence similarity 102, member A	-1,67	0,0278
54566	EPB41L4B	erythrocyte membrane protein band 4.1 like 4B	-1,66	0,0190
6462	SHBG	sex hormone-binding globulin	-1,66	0,0370
6813	STXBP2	syntaxin binding protein 2	-1,66	0,0025
9679	FAM53B	family with sequence similarity 53, member B	-1,65	0,0038
3691	ITGB4	integrin, beta 4	-1,65	0,0038
83715	ESPN	espin	-1,65	0,0240
10223	GPA33	glycoprotein A33 (transmembrane)	-1,64	0,0304
7512	XPNPEP2	X-prolyl aminopeptidase (aminopeptidase P) 2, membrane-bound	-1,62	0,0490
10908	PNPLA6	patatin-like phospholipase domain containing 6	-1,61	0,0031
79065	ATG9A	ATG9 autophagy related 9 homolog A (S. cerevisiae)	-1,60	0,0095
4354	MPP1	membrane protein, palmitoylated 1, 55kDa	-1,60	0,0271
55884	WSB2	WD repeat and SOCS box-containing 2	-1,60	0,0041
6523	SLC5A1	solute carrier family 5 (sodium/glucose cotransporter), member 1	-1,58	0,0171
6653	SORL1	sortilin-related receptor, L(DLR class) A repeats-containing	-1,57	0,0239
11148	HHLA2	HERV-H LTR-associating 2	-1,56	0,0370
4311	MME	membrane metallo-endopeptidase	-1,56	0,0304
120R vs C			**Up**	
3303	HSPA1A	heat shock 70kDa protein 1A; heat shock 70kDa protein 1B	12,19	0,0000
2354	FOSB	FBJ murine osteosarcoma viral oncogene homolog B	7,93	0,0001
10808	HSPH1	heat shock 105kDa/110kDa protein 1	7,12	0,0000
3304	HSPA1B	heat shock 70kDa protein 1A; heat shock 70kDa protein 1B	6,73	0,0002
1604	CD55	CD55 molecule, decay accelerating factor for complement (Cromer blood group)	5,73	0,0000
3320	HSP90AA1	heat shock protein 90kDa alpha (cytosolic), class A member 2; heat shock protein 90kDa alpha (cytosolic), class A member 1	4,45	0,0000
9531	BAG3	BCL2-associated athanogene 3	4,12	0,0001
3337	DNAJB1	DnaJ (Hsp40) homolog, subfamily B, member 1	4,06	0,0013
1958	EGR1	early growth response 1	4,06	0,0003
3949	LDLR	low density lipoprotein receptor	3,98	0,0001
6280	S100A9	S100 calcium binding protein A9	3,93	0,0250
6279	S100A8	S100 calcium binding protein A8	3,86	0,0225
2810	SFN	stratifin	3,64	0,0001
90637	ZFAND2A	zinc finger, AN1-type domain 2A	3,46	0,0027
5552	SRGN	serglycin	3,30	0,0006
1847	DUSP5	dual specificity phosphatase 5	3,26	0,0000
3336	HSPE1	heat shock 10kDa protein 1 (chaperonin 10)	3,19	0,0000
3301	DNAJA1	DnaJ (Hsp40) homolog, subfamily A, member 1	3,16	0,0000
1839	HBEGF	heparin-binding EGF-like growth factor	3,11	0,0014
5209	PFKFB3	6-phosphofructo-2-kinase/fructose-2,6-biphosphatase 3	3,06	0,0016
6574	SLC20A1	solute carrier family 20 (phosphate transporter), member 1	3,02	0,0000
8870	IER3	immediate early response 3	3,02	0,0000
23645	PPP1R15A	protein phosphatase 1, regulatory (inhibitor) subunit 15A	3,01	0,0000
64651	AXUD1	cysteine-serine-rich nuclear protein 1	3,01	0,0000
467	ATF3	activating transcription factor 3	3,00	0,0122
3329	HSPD1	heat shock 60kDa protein 1 (chaperonin) pseudogene 5	2,99	0,0001
3638	INSIG1	insulin induced gene 1	2,92	0,0033

6515	SLC2A3	solute carrier family 2 (facilitated glucose transporter), member 3	2,91	0,0001
6347	CCL2	chemokine (C-C motif) ligand 2	2,88	0,0225
4953	ODC1	ornithine decarboxylase 1	2,78	0,0000
4929	NR4A2	nuclear receptor subfamily 4, group A, member 2	2,76	0,0021
5743	PTGS2	prostaglandin-endoperoxide synthase 2 (prostaglandin G/H synthase and cyclooxygenase)	2,76	0,0065
83716	CRISPLD2	cysteine-rich secretory protein LCCL domain containing 2	2,71	0,0014
1051	CEBPB	CCAAT/enhancer binding protein (C/EBP), beta	2,71	0,0000
10221	TRIB1	tribbles homolog 1 (Drosophila)	2,71	0,0000
55466	DNAJA4	DnaJ (Hsp40) homolog, subfamily A, member 4	2,71	0,0006
7538	ZFP36	zinc finger protein 36, C3H type, homolog (mouse)	2,69	0,0021
2012	EMP1	epithelial membrane protein 1	2,69	0,0001
3320	HSP90AA1	heat shock protein 90kDa alpha (cytosolic), class A member 2; heat shock protein 90kDa alpha (cytosolic), class A member 1	2,68	0,0000
3315	HSPB1	heat shock 27kDa protein-like 2 pseudogene	2,66	0,0014
10365	KLF2	Kruppel-like factor 2 (lung)	2,65	0,0058
5552	SRGN	serglycin	2,59	0,0023
1843	DUSP1	dual specificity phosphatase 1	2,57	0,0047
301	ANXA1	annexin A1	2,53	0,0012
3336	HSPE1	heat shock 10kDa protein 1 (chaperonin 10)	2,50	0,0001
27314	RAB30	RAB30, member RAS oncogene family	2,50	0,0001
29950	SERTAD1	SERTA domain containing 1	2,49	0,0000
4071	TM4SF1	transmembrane 4 L six family member 1	2,47	0,0001
3725	JUN	jun oncogene	2,45	0,0118
5328	PLAU	plasminogen activator, urokinase	2,43	0,0001
120R vs C			**Down**	
89872	AQP10	aquaporin 10	-4,38	0,0071
1510	CTSE	cathepsin E	-3,12	0,0028
2981	GUCA2B	guanylate cyclase activator 2B (uroguanylin)	-2,81	0,0267
4680	CEACAM6	carcinoembryonic antigen-related cell adhesion molecule 6 (non-specific cross reacting antigen)	-2,77	0,0163
5265	SERPINA1	serpin peptidase inhibitor, clade A (alpha-1 antiproteinase, antitrypsin), member 1	-2,67	0,0076
345	APOC3	apolipoprotein C-III	-2,62	0,0135
5265	SERPINA1	serpin peptidase inhibitor, clade A (alpha-1 antiproteinase, antitrypsin), member 2	-2,57	0,0117
1687	DFNA5	deafness, autosomal dominant 5	-2,55	0,0016
79170	ATAD4	ATPase family, AAA domain containing 4	-2,53	0,0009
339221	ENPP7	ectonucleotide pyrophosphatase/phosphodiesterase 7	-2,41	0,0222
79762	C1orf115	chromosome 1 open reading frame 115	-2,37	0,0003
51471	NAT8B	N-acetyltransferase 8 (GCN5-related, putative); N-acetyltransferase 8B (GCN5-related, putative, gene/pseudogene)	-2,36	0,0108
339221	ENPP7	ectonucleotide pyrophosphatase/phosphodiesterase 7	-2,31	0,0307
1576	CYP3A4	cytochrome P450, family 3, subfamily A, polypeptide 4	-2,29	0,0082
1510	CTSE	cathepsin E	-2,21	0,0131
5169	ENPP3	ectonucleotide pyrophosphatase/phosphodiesterase 3	-2,14	0,0096
5210	PFKFB4	6-phosphofructo-2-kinase/fructose-2,6-biphosphatase 4	-2,12	0,0019
1559	CYP2C9	cytochrome P450, family 2, subfamily C, polypeptide 9	-2,08	0,0218
53354	PANK1	pantothenate kinase 1	-2,07	0,0020
1124	CHN2	chimerin (chimaerin) 2	-2,02	0,0015
8566	PDXK	pyridoxal (pyridoxine, vitamin B6) kinase	-2,02	0,0006

733	C8G	complement component 8, gamma polypeptide	-2,00	0,0109
4094	MAF	v-maf musculoaponeurotic fibrosarcoma oncogene homolog (avian)	-2,00	0,0098
140803	TRPM6	transient receptor potential cation channel, subfamily M, member 6	-1,99	0,0002
10	NAT2	N-acetyltransferase 2 (arylamine N-acetyltransferase)	-1,98	0,0019
54825	PCLKC	protocadherin 24	-1,97	0,0095
1030	CDKN2B	cyclin-dependent kinase inhibitor 2B (p15, inhibits CDK4)	-1,97	0,0005
1308	COL17A1	collagen, type XVII, alpha 1	-1,96	0,0009
5651	PRSS7	protease, serine, 7 (enterokinase)	-1,95	0,0369
25845	LOC25845	hypothetical LOC25845	-1,94	0,0078
948	CD36	CD36 molecule (thrombospondin receptor)	-1,93	0,0238
6564	SLC15A1	solute carrier family 15 (oligopeptide transporter), member 1	-1,92	0,0045
2065	ERBB3	v-erb-b2 erythroblastic leukemia viral oncogene homolog 3 (avian)	-1,92	0,0002
4225	MEP1B	meprin A, beta	-1,92	0,0148
2064	ERBB2	v-erb-b2 erythroblastic leukemia viral oncogene homolog 2, neuro/glioblastoma derived oncogene homolog (avian)	-1,90	0,0003
56241	SUSD2	sushi domain containing 2	-1,89	0,0432
10720	UGT2B11	UDP glucuronosyltransferase 2 family, polypeptide B11	-1,89	0,0491
8743	TNFSF10	tumor necrosis factor (ligand) superfamily, member 10	-1,88	0,0004
164091	PAQR7	progestin and adipoQ receptor family member VII	-1,86	0,0033
246181	AFAR3	aldo-keto reductase family 7-like	-1,85	0,0067
6505	SLC1A1	solute carrier family 1 (neuronal/epithelial high affinity glutamate transporter, system Xag), member 1	-1,85	0,0014
7512	XPNPEP2	X-prolyl aminopeptidase (aminopeptidase P) 2, membrane-bound	-1,83	0,0074
192683	SCAMP5	secretory carrier membrane protein 5	-1,82	0,0005
59272	ACE2	angiotensin I converting enzyme (peptidyl-dipeptidase A) 2	-1,82	0,0096
11181	TREH	trehalase (brush-border membrane glycoprotein)	-1,80	0,0042
55715	DOK4	docking protein 4	-1,80	0,0014
4311	MME	membrane metallo-endopeptidase	-1,80	0,0021
3938	LCT	lactase	-1,80	0,0107
338	APOB	apolipoprotein B (including Ag(x) antigen)	-1,80	0,0127
29881	NPC1L1	NPC1 (Niemann-Pick disease, type C1, gene)-like 1	-1,80	0,0251

Table S4. Enrichment analysis of Gene Ontology terms for genes differentially expressed during human intestinal ischemia-reperfusion

GOBPID	p-value	Odds Ratio	Exp Count	Count	Size	Term
0R to 30R						
GO:0006986	4,9E-09	25,36	0,39	8	65	response to unfolded protein
GO:0051789	1,9E-13	24,36	0,70	13	116	response to protein stimulus
GO:0006916	1,6E-07	9,13	1,42	11	235	anti-apoptosis
GO:0009607	9,1E-08	6,54	2,78	15	459	response to biotic stimulus
GO:0010033	9,0E-13	7,13	5,39	27	889	response to organic substance
GO:0009628	4,4E-06	5,82	2,40	12	396	response to abiotic stimulus
GO:0051726	2,8E-06	5,60	2,73	13	450	regulation of cell cycle
GO:0009605	1,7E-06	4,82	3,99	16	658	response to external stimulus
GO:0006915	5,2E-09	4,94	6,78	25	1118	apoptosis
GO:0012501	6,0E-09	4,90	6,82	25	1126	programmed cell death
GO:0042127	2,3E-06	4,28	5,12	18	845	regulation of cell proliferation
GO:0008283	4,7E-08	4,49	6,99	24	1154	cell proliferation
GO:0042981	4,4E-06	4,08	5,36	18	884	regulation of apoptosis
GO:0008219	3,7E-08	4,43	7,47	25	1233	cell death
GO:0016265	3,9E-08	4,41	7,49	25	1236	death
GO:0043067	5,0E-06	4,04	5,41	18	892	regulation of programmed cell death
GO:0042221	1,0E-09	4,71	9,03	30	1490	response to chemical stimulus
GO:0010941	5,6E-06	4,00	5,45	18	899	regulation of cell death
GO:0006950	4,4E-12	5,24	11,21	37	1849	response to stress
GO:0048523	5,8E-12	5,18	11,31	37	1866	negative regulation of cellular process
GO:0048519	1,6E-11	4,92	12,32	38	2033	negative regulation of biological process
GO:0048522	3,2E-07	3,48	12,24	31	2020	positive regulation of cellular process
GO:0048518	2,2E-07	3,45	13,45	33	2219	positive regulation of biological process
GO:0048513	3,7E-06	3,18	11,55	28	1906	organ development
GO:0050896	7,2E-11	4,29	21,84	50	3604	response to stimulus
GO:0048856	8,2E-06	2,82	16,49	34	2720	anatomical structure development
GO:0031323	1,8E-06	2,90	21,80	42	3597	regulation of cellular metabolic process
GO:0050794	1,5E-07	3,35	36,48	60	6018	regulation of cellular process
GO:0050789	4,7E-07	3,22	38,53	61	6357	regulation of biological process
GO:0065007	5,7E-06	2,87	40,91	61	6749	biological regulation
30R to 120R						
GO:0048514	5,5E-06	3,64	5,76	19	276	blood vessel morphogenesis
GO:0001525	1,1E-04	3,36	4,85	15	232	angiogenesis
GO:0032535	3,8E-06	3,35	7,25	22	347	regulation of cellular component size
GO:0001944	7,3E-06	3,32	6,98	21	334	vasculature development
GO:0001568	1,6E-05	3,24	6,77	20	324	blood vessel development
GO:0007264	2,9E-05	2,84	8,86	23	424	small GTPase mediated signal transduction
GO:0090066	5,3E-05	2,79	8,58	22	411	regulation of anatomical structure size
GO:0051128	2,1E-05	2,47	13,81	31	661	regulation of cellular component organization
GO:0006366	3,3E-05	2,20	19,01	38	910	transcription from RNA polymerase II promoter
GO:0006915	6,4E-06	2,21	23,35	46	1118	apoptosis
GO:0012501	7,7E-06	2,19	23,52	46	1126	programmed cell death
GO:0008219	7,9E-06	2,13	25,75	49	1233	cell death
GO:0016265	8,4E-06	2,13	25,81	49	1236	death
GO:0048518	5,7E-09	2,23	46,34	85	2219	positive regulation of biological process

GO:0042221	3,5E-05	1,94	31,12	54	1490	response to chemical stimulus
GO:0048522	1,0E-06	2,02	42,19	73	2020	positive regulation of cellular process
GO:0007165	3,8E-05	1,79	45,80	72	2193	signal transduction
GO:0023060	2,5E-05	1,77	52,76	81	2526	signal transmission
GO:0023033	3,0E-05	1,76	52,19	80	2499	signaling pathway
GO:0023046	2,7E-05	1,77	52,88	81	2532	signaling process
GO:0051171	5,0E-05	1,70	60,71	89	2907	regulation of nitrogen compound metabolic process
GO:0019219	6,2E-05	1,69	60,19	88	2882	regulation of nucleobase, nucleoside, nucleotide and nucleic acid metabolic process
GO:0050794	4,5E-12	2,31	125,69	183	6018	regulation of cellular process
GO:0031323	1,9E-05	1,70	75,12	107	3597	regulation of cellular metabolic process
GO:0050789	1,0E-11	2,29	132,77	189	6357	regulation of biological process
GO:0023052	2,9E-05	1,68	73,14	104	3502	signaling
GO:0080090	5,1E-05	1,66	71,36	101	3417	regulation of primary metabolic process
GO:0060255	9,6E-05	1,64	67,98	96	3255	regulation of macromolecule metabolic process
GO:0065007	5,1E-11	2,24	140,95	195	6749	biological regulation
GO:0019222	4,6E-05	1,64	81,16	112	3886	regulation of metabolic process
0R to 30R						
GO:0003690	2,1E-04	10,24	0,54	5	96	double-stranded DNA binding
GO:0031072	8,9E-04	10,23	0,43	4	76	heat shock protein binding
GO:0051082	3,6E-04	9,04	0,61	5	108	unfolded protein binding
GO:0016564	1,8E-05	6,03	1,89	10	335	transcription repressor activity
GO:0003700	5,0E-09	5,48	5,22	22	925	sequence-specific DNA binding transcription factor activity
GO:0016563	2,7E-05	5,21	2,42	11	428	transcription activator activity
GO:0043565	1,5E-06	5,17	3,46	15	613	sequence-specific DNA binding
GO:0008134	3,1E-05	4,74	2,91	12	516	transcription factor binding
GO:0030528	7,4E-07	4,47	5,25	19	930	transcription regulator activity
GO:0046983	9,6E-05	4,18	3,28	12	581	protein dimerization activity
GO:0005515	3,0E-05	2,70	44,83	63	7945	protein binding
30R to 120R						
GO:0003688	2,6E-04	37,01	0,14	3	7	DNA replication origin binding
GO:0030291	2,2E-05	19,10	0,36	5	18	protein serine/threonine kinase inhibitor activity
GO:0004860	8,1E-04	7,75	0,74	5	37	protein kinase inhibitor activity
GO:0050839	8,1E-04	7,75	0,74	5	37	cell adhesion molecule binding
GO:0003924	3,7E-08	5,21	4,15	19	207	GTPase activity
GO:0003714	1,5E-04	4,19	2,87	11	143	transcription corepressor activity
GO:0005525	6,0E-08	3,93	7,16	25	357	GTP binding
GO:0019001	1,1E-07	3,79	7,40	25	369	guanyl nucleotide binding
GO:0032561	1,1E-07	3,79	7,40	25	369	guanyl ribonucleotide binding
GO:0016564	1,5E-04	2,89	6,72	18	335	transcription repressor activity
GO:0003712	9,3E-04	2,52	7,18	17	358	transcription cofactor activity
GO:0030528	5,1E-05	2,17	18,65	37	930	transcription regulator activity
GO:0005515	2,6E-06	1,76	159,34	198	7945	protein binding

GOBPID, Gene Ontology Biological Process Identification number; GOMFID, Gene Ontology Molecular Function Identification number; p-value, p value given by the hypergeometric test (p<0.01); Odds Ratio, ratio of odds that a GO term is enriched in the selected category; ExpCount, expected number of transcripts found associated with the GO term for enrichment; Count, real number of transcripts found associated with the GO term; Size, population size of transcripts found associated with the GO term within the analysis; Term, Gene Ontology description term

Table S5. KEGG pathway analysis for genes differentially expressed during human ischemia-reperfusion

KEGG ID	Pathway name	Adjusted p-value	Size	Count	Status
30R vs 0R					
4010	MAPK signaling pathway	1,92E-6	263	12	Inhibited
4141	Protein processing in endoplasmic reticulum	5,43E-6	161	8	Inhibited
5140	Leishmaniasis	3,34E-2	71	4	Inhibited
5120	Epithelial cell signaling in Helicobacter pylori infection	3,34E-2	67	3	Activated
4621	NOD-like receptor signaling pathway	4,67E-2	62	3	Inhibited
4912	GnRH signaling pathway	4,67E-2	98	2	Activated
5210	Colorectal cancer	4,67E-2	62	2	Activated
5142	Chagas disease	4,67E-2	104	4	Inhibited
120R vs 30R					
5130	Pathogenic Escherichia coli infection	1,01E-2	57	7	Activated
4110	Cell cycle	1,01E-2	124	9	Inhibited
5100	Bacterial invasion of epithelial cells	1,01E-2	71	7	Activated
5210	Colorectal cancer	1,01E-2	62	4	Inhibited
4010	MAPK signaling pathway	1,01E-2	263	14	Activated
4350	TGF-beta signaling pathway	1,29E-2	84	8	Activated
4920	Adipocytokine signaling pathway	1,76E-2	67	5	Activated
5222	Small cell lung cancer	1,76E-2	84	7	Activated
5416	Viral myocarditis	2,89E-2	70	3	Activated
5014	Amyotrophic lateral sclerosis	2,89E-2	53	4	Activated
4810	Regulation of actin cytoskeleton	2,89E-2	210	10	Activated
5131	Shigellosis	4,24E-2	62	5	Activated
Overall					
5130	Pathogenic Escherichia coli infection	6,43E-6	57	21	Activated
4141	Protein processing in endoplasmic reticulum	2,95E-3	161	32	Inhibited
4012	ErbB signaling pathway	3,59E-3	87	19	Inhibited
5223	Non-small cell lung cancer	4,88E-3	54	13	Inhibited
3320	PPAR signaling pathway	4,88E-3	69	17	Inhibited
5211	Renal cell carcinoma	9,57E-3	70	13	Inhibited
4722	Neurotrophin signaling pathway	1,37E-2	126	24	Activated
5219	Bladder cancer	1,37E-2	42	11	Inhibited
4350	TGF-beta signaling pathway	1,54E-2	84	18	Inhibited
5020	Prion disease	1,54E-2	35	9	Inhibited
4010	MAPK signaling pathway	1,54E-2	263	40	Inhibited
5110	Vibrio cholerae infection	1,54E-2	53	12	Activated
5100	Bacterial invasion of epithelial cells	1,54E-2	71	15	Inhibited
4510	Focal adhesion	1,59E-2	198	28	Inhibited
5131	Shigellosis	1,59E-2	62	14	Inhibited
4370	VEGF signaling pathway	1,68E-2	74	13	Inhibited
4666	Fc gamma R-mediated phagocytosis	2,67E-2	93	17	Inhibited
4912	GnRH signaling pathway	2,80E-2	98	15	Inhibited
5210	Colorectal cancer	2,94E-2	62	10	Activated
4910	Insulin signaling pathway	2,94E-2	137	22	Inhibited
4142	Lysosome	4,37E-2	118	21	Inhibited

**No significant enrichment of KEGG pathways in the 0RvsC time-frame*

Count, Number of differentially expressed genes in the KEGG pathway; Size, Total number of genes in the KEGG pathway

Table S6. Transcription factors and corresponding number of up- and downregulated targets in the regulatory network

Entrez ID	Gene Symbol	Gene Name	Number of targets Up	Down
64651	CSRNP1	cysteine-serine-rich nuclear protein 1	1	0
159296	NKX2-3	NK2 homeobox 3	594	0
2000	ELF4	E74-like factor 4 (ets domain transcription factor)	489	0
3091	HIF1A	hypoxia inducible factor 1, alpha subunit (basic helix-loop-helix transcription factor)	353	148
4335	MNT	MAX binding protein	99	20
1052	CEBPD	CCAAT/enhancer binding protein (C/EBP), delta	76	0
2354	FOSB	FBJ murine osteosarcoma viral oncogene homolog B	67	0
3202	HOXA5	homeobox A5	64	6
1649	DDIT3	DNA-damage-inducible transcript 3	38	0
1958	EGR1	early growth response 1	26	0
9314	KLF4	Kruppel-like factor 4 (gut)	3	0
4094	MAF	v-maf musculoaponeurotic fibrosarcoma oncogene homolog (avian)	3	0
64651	CSRNP1	cysteine-serine-rich nuclear protein 1	1	0
2353	FOS	FBJ murine osteosarcoma viral oncogene homolog	1	0
1316	KLF6	Kruppel-like factor 6	1	0
467	ATF3	activating transcription factor 3	1	0
2114	ETS2	v-ets erythroblastosis virus E26 oncogene homolog 2 (avian)	1	0
6722	SRF	serum response factor (c-fos serum response element-binding transcription factor)	1	0
1999	ELF3	E74-like factor 3 (ets domain transcription factor, epithelial-specific)	1	0

CHAPTER 6

Mitochondria are better protected from hypoxia-reoxygenation injury in the crypts compared to villi in human intestinal organoids: a role for mitophagy?

Anna M. Kip, Annet A.M. Duivenvoorden, Anja Alićehajić, M'hamed Hadfoune, Steven W.M. Olde Damink, Kaatje Lenaerts

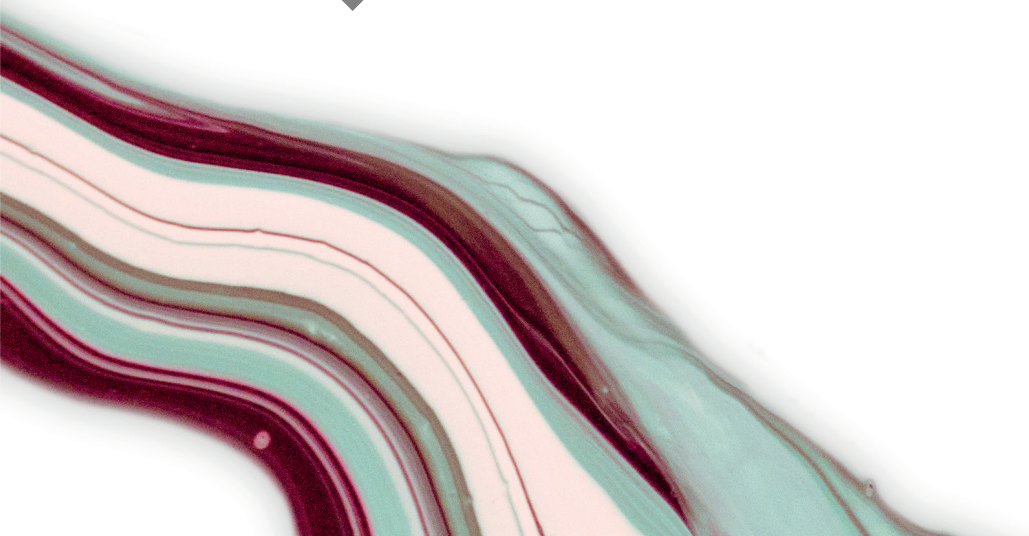

CHAPTER 7

General discussion

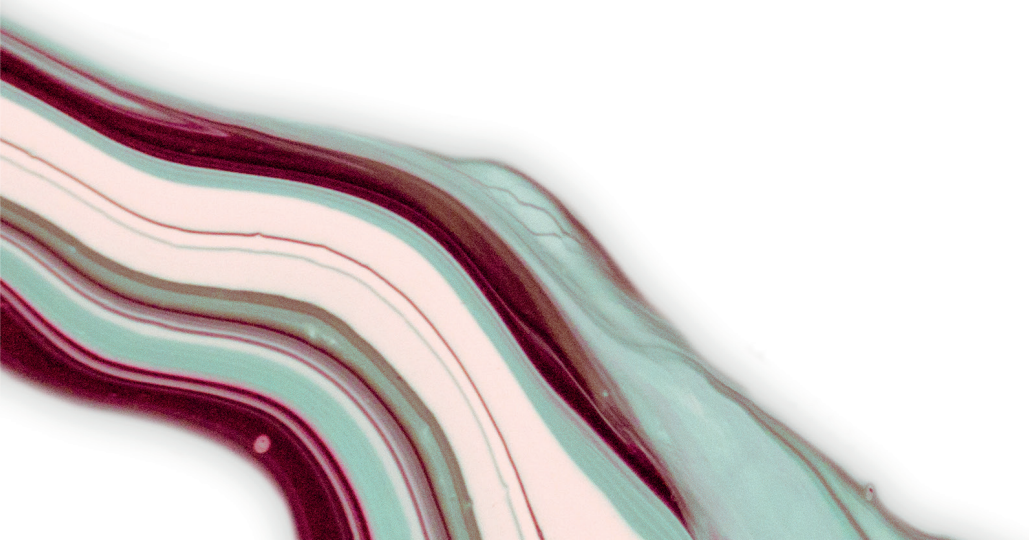

GENERAL DISCUSSION

Intestinal ischemia-reperfusion (IR) is a phenomenon that occurs in a variety of clinical conditions, including intestinal transplantation, mesenteric thrombosis or embolism, and shock. Acute mesenteric ischemia is a life-threatening condition. Delayed diagnosis and limited therapeutic options account for the persistent high mortality rates of 60-80%[1,2]. To be able to identify novel therapeutic strategies and improve patient survival, it is imperative to understand the molecular mechanisms underlying ischemia and reperfusion of the human intestine. In this thesis, we performed omics analyses to study the intestinal response to IR in an *in vivo* human experimental model. For in-depth investigation and testing of potential therapeutic targets, there is an urgent need for an *in vitro* model that offers improved translation to *in vivo* IR. To this end, we modeled IR in human small intestinal organoids.

THE RESPONSE TO ISCHEMIA-REPERFUSION IN HUMAN INTESTINE

The experimental framework of our *in vivo* human experimental model enabled monitoring of the temporal changes during progressive intestinal IR injury and initiation of repair. In this thesis, we mapped temporal transcription profiles (**chapter 5**) as well as the dynamic proteome and phosphoproteome (**chapter 3**) during ischemia and reperfusion of the human intestine. The main findings of these studies are discussed below.

Transcriptional profiling reveals a crucial role for unfolded protein stress in human intestinal IR

Under stressful conditions, reprogramming of transcription is needed for the cell to survive the stressor and restore homeostasis. Transcriptional reprogramming upon stress is characterized by induction of pro-survival genes as well as a wide-spread repression of genes involved in transcription, translation and cell cycle[3]. Distinct stress responses can be activated, depending on the type of stress. During IR, several stress responses could play a role including the hypoxia response, controlled by hypoxia-inducible factors (HIFs), and the oxidative stress response, in which ROS production activates Nrf2 signaling. In addition, aggregation of misfolded proteins causes proteotoxic stress, which triggers the heat shock response, and when unfolded or misfolded proteins accumulate inside the endoplasmic reticulum (ER) or mitochondria, the unfolded protein response (UPR) is activated. Our analysis of the changing transcriptome in response to IR in the human intestine revealed a crucial role for the response to unfolded protein (**chapter 5**). Moreover, we observed signs of ER stress following IR and strong regulation of the IRE1 and PERK branches of the UPR. Interestingly, gene regulatory network analysis identified HIF1A as the predominant regulator of the response to unfolded protein during IR. This suggests an important connection between hypoxia-induced HIF signaling and the UPR, which recently has also been reviewed by Bartoszewska et al.[4].

The UPR initiates a series of pro-survival mechanisms directed at restoring homeostasis in the ER, but can eventually promote apoptosis if ER stress is sustained. Pro-survival mechanisms include degradation of ER-localized proteins and certain mRNAs, enhancing ER folding capacity, and repression of protein translation, aimed at reducing the amount of newly synthesized protein that needs to be folded in the ER[5]. In concordance with transcriptional observations, proteome analysis showed a reduction in expression of translation initiation factors in response to IR of the

human intestine, as well as alterations in protein phosphorylations that are known to regulate protein translation (**chapter 3**), which both point to inhibition of translation during IR.

Link between UPR and inflammatory signaling

Accumulating evidence has shown that the UPR plays a significant role in regulating immunity and inflammation, and it is well appreciated that ER stress and the UPR contribute to the pathogenesis of inflammatory bowel disease[6-8]. The UPR has been linked to inflammation via activation of stress pathways NF-κB[9-11] and p38 and JNK MAPK signaling[12-14], which mediate the production of pro-inflammatory cytokines and chemokines. Interestingly, we found induced transcription of NF-κB and MAP kinases in response to intestinal IR, and, moreover, MAPK signaling appeared as top regulated pathway during early reperfusion (**chapter 5**). Crosstalk between the UPR and MAPKs has been described in several pathologies including diabetes, atherosclerosis, ischemia, and cancer (reviewed in [13]). The simultaneous activation of the ER stress response and MAPK signaling pathway, suggests that these pathways cooperate during IR-induced stress in the human intestine and provides a possible link of ER stress with inflammation and apoptosis.

In general, MAPK families play a pivotal role in several cellular programs including regulation of cell proliferation, differentiation, development, stress response, apoptosis, and inflammation. In addition to stress-responsive JNK and p38 MAPK pathways, the classical MAPK pathway (known as ERK) was activated during IR as well (**chapter 5**) and plays a crucial role in proliferation and survival. The importance of MAPK signaling during IR in the human intestine is supported by phosphoproteome analysis in **chapter 3**. The drastic increase in phosphosite alterations of MAP kinase targets during reperfusion suggested activity of both stress-responsive JNK and p38, and classical ERK MAP kinases.

ER stress and the immune barrier: Paneth cell loss and its implications in intestinal transplantation

In addition to the interconnection between the UPR and inflammatory signaling, ER stress can indirectly lead to intestinal inflammation via its effect on Paneth cells, which function as important players in innate epithelial immunity[15]. Paneth cells are equipped with an extensive ER which enables them to produce the antimicrobial peptides and stem cell supporting factors, yet their secretory function also makes these cells highly susceptible to ER stress. Apoptosis of Paneth cells during reperfusion of the human ischemic intestine was shown to strongly correlate with the level of UPR activation[16].

Loss of Paneth cells leads to a reduction in the continuous secretion of antimicrobials as well as secretion in response to sensing bacterial threats[15,17], and consequently compromises the immunological barrier and increases the risk of bacterial invasion. Indeed, our transcriptome analysis showed overrepresentation of the pathway 'bacterial invasion of epithelial cells' after prolonged reperfusion of human ischemic intestine (**chapter 5**). Also, Paneth cell loss has been associated with bacterial translocation and intestinal inflammation in human intestinal IR[16]. Given the crucial role of Paneth cells in preventing bacterial invasion and considering their susceptibility to IR injury, we speculated that Paneth cell loss may also have a share in bacterial translocation after intestinal transplantation (ITx). This led us to study Paneth cell numbers and antimicrobial lysozyme intensity

in ITx patients shortly after reperfusion of the graft and regularly up until 5 years post-ITx (**chapter 2**). Surprisingly, no apoptotic Paneth cells were detected shortly after reperfusion of the intestinal graft. However, we did observe a significant reduction in Paneth cell numbers in the first follow-up biopsy (3-7 days post-ITx), indicating loss of Paneth cells in the days after transplantation which was most likely not directly related to IR. Other post-operative factors, including immunosuppression, antibiotic use, ICU stay, and immune factors may also have affected Paneth cells in the days following transplantation. Interestingly, Paneth cell numbers gradually restored in the first months, whereas lysozyme intensity was continuously reduced in biopsies of ITx patients.

Loss of Paneth cells and antimicrobial defense in ITx patients may have the following consequences on graft function: (1) facilitate pathogen colonization and increase susceptibility of the graft to infectious enteritis, and (2) enable invasion of luminal microbes, which may stimulate innate immune activation which indirectly increases the vulnerability to graft rejection. Studies in experimental models indicate that local innate immune activation – triggered for example by IR injury, microbial exposure or infections – can enhance the alloimmune response, thereby promoting rejection[18,19]. Therefore, we next explored a potential relation between Paneth cell impairment in the early post-ITx period and functional outcomes of the graft. Unfortunately, the patient groups studied were small, which impeded statistical analysis. Nevertheless, a tendency was observed towards a larger reduction in Paneth cell number and lysozyme in the first days after ITx in patients who developed rejection in a later stage compared to patients without rejection. Therefore, it would be worthwhile investigating this link between Paneth cell impairment and graft outcome in a larger patient cohort in future studies.

The UPR as a therapeutic target

The prominent role for ER stress and UPR activation in the pathophysiology of intestinal IR provides a potential target to prevent and/or treat intestinal IR injury. While the UPR is crucial for cell survival in conditions causing ER stress, it can also promote apoptotic cell death and aggravate injury if sustained. As a pivotal player in immunity and inflammation, targeting the UPR has also been recognized as a potential therapeutic strategy for various immune-mediated and inflammatory pathologies such as inflammatory bowel disease, non-alcoholic steatohepatitis, diabetes mellitus and cancer[7,20]. In **chapter 5**, we investigated the therapeutic potential of UPR inhibition in attenuating IR injury in intestinal organoids, which will be discussed later.

The integrated analysis of IR-induced changes in protein expression, phosphorylation and localization

In **chapter 3** we adopted a multidimensional proteomics approach to study the molecular mechanisms related to ischemia and reperfusion of the human intestine. Liquid chromatography-mass spectrometry (LC-MS) proteomics, LC-MS-based phosphoproteomics, and matrix-assisted laser desorption/ionization-mass spectrometry imaging (MALDI MSI) provided different layers of protein information, respectively: protein abundance, post-translational phosphorylation of proteins, and spatial information of proteins. The key findings are discussed below.

Innate immune activation during reperfusion: a prominent role of the complement system

Innate immune activation is a well-known consequence of IR-induced injury and disruption of the intestinal epithelial barrier. Key players in innate immune activation include innate inflammatory cells, including neutrophils, mast cells, dendritic cells and platelets, and innate immune proteins such as toll-like receptors and complement proteins[21]. Analysis of the dynamic proteome during intestinal IR strongly indicated immune activation upon reperfusion, and suggested that the complement system has a key role in the intestinal immune response to IR (**chapter 3**). In addition to an increased abundance of the majority of complement proteins, MS imaging analysis showed an interesting localization shift of complement factor towards the villus tips. Although our analysis could not distinguish between native and active complement factors, we speculate that the observed altered distribution might reflect the accumulation of activated complement protein in damaged epithelial cells in the villi tips and luminal debris, as was reported previously for active C3 after IR[22]. These findings emphasize the importance of the complement system in human intestinal IR. Considering several reports on the protective effects of complement inhibition in animal IR models[23-25], future studies should focus on the potential of the complement system as a therapeutic target in human intestinal IR.

Loss of villus tips as a consequence of IR injury

Analysis of the changing proteome during IR demonstrated overrepresentation of proteins related to digestion and absorption, brush border and microvillus (**chapter 3**). The decreased abundance of structural proteins of intestinal microvilli, brush border enzymes and transporters for nutrient absorption likely reflects the loss of villus tips, another hallmark of intestinal IR injury. Two of these proteins, intestinal fatty acid binding protein (IFABP) and villin-1, have been shown to be serological markers for intestinal IR in man[26,27], suggesting that other proteins that were related to shortening of the villus tips may have diagnostic implications as well. Schellekens et al. reported that IR-induced epithelial damage results in leakage of IFABP in the intestinal lumen as well as in the subepithelial space[26]. Subsequent release of IFABP into the plasma was demonstrated by an increase in arteriovenous (V-A) concentration difference, where the venous plasma was derived from the vein draining the isolated intestinal segment exposed to IR. To explore diagnostic potential of other biomarker candidates, the next steps would be to investigate protein leakage into the plasma by measuring arteriovenous concentrations in the experimental IR model, followed by validation in a clinical study.

Cell junction organization

Both proteome and phosphoproteome analysis pointed to significant regulation of the cytoskeleton and cell junction during intestinal IR (**chapter 3**). Cell junction complexes and their tight connection to the actin cytoskeleton are crucial for epithelial barrier integrity, and changes in their organization may contribute to barrier disruption[28]. While the abundance of proteins related to cell junction and cytoskeleton consistently decreased after reperfusion, alterations in phosphorylation of these proteins showed distinct dynamics during the course of ischemia and reperfusion. The phosphorylation status of cell junction and cytoskeletal proteins regulates their organization and

integrity[29], suggesting that observed protein phosphorylations may play an important role in the reorganization of the cytoskeleton and subsequent zipper-like constriction of the epithelium during IR of human intestine[30]. This protective mechanism enables restoration of the epithelial lining before shedding of the villus tips, which limits exposure to the harmful intestinal lumen.

mRNA splicing

Functional enrichment analysis of the dynamic phosphoproteome revealed strong regulation of mRNA splicing during IR (**chapter 3**). In addition, as shown by MSI analysis, mucosal expression of several proteins related to RNA splicing was found to be decreased (**chapter 3**). The phosphorylation state of splicing factors is important in regulating function and organization of the spliceosome[31]. The temporal behavior of dynamic phosphosites on RNA splicing-related proteins demonstrated that ischemia and reperfusion induced phosphorylation and dephosphorylation events, which are both crucial during the splicing reaction[31,32]. Phosphorylation acts as a major player in regulation of both constitutive mRNA splicing and alternative splicing. The latter is an important mechanism in regulating the stress response, for example during hypoxic stress[33-35] and ER stress[36]. A well-known example is alternative splicing of UPR-related XBP1 upon ER stress. We have shown increased expression of this spliced variant in response to IR in human intestine (**chapter 5**).

Phosphosite dynamics and predicted kinase activity

Protein phosphorylation is important in the regulation of cellular functions and the response to cellular stress. In addition to functional analysis of the dynamic phosphoproteome during IR, which demonstrated that phosphorylation is crucial in the regulation of RNA splicing and cell junction organization during IR stress, phosphosite-centric analyses predicted which kinases were most likely responsible for the detected IR-induced changes in protein phosphorylation. Among dynamic phosphosites, many were potential targets of MAPKs and cyclin-dependent kinases (CDKs), suggesting activity of these kinases during IR (**chapter 3**). More specifically, these potential targets were decreased after ischemia followed by a strong increase during reperfusion. MAPK signaling during intestinal IR has also been evidenced by transcriptome analysis (**chapter 5)** as discussed before. CDKs are essential in cell cycle regulation, a process that was shown to be overrepresented after prolonged reperfusion based on the transcriptional response to IR (**chapter 5**), but these kinases are also involved in the regulation of transcription and mRNA splicing.

Mass spectrometry imaging

State of the art LC-MS/MS (phospho)proteomics enabled identification and quantification of thousands of proteins which gave valuable insights in the intestinal tissue response to IR. In addition to that, MSI can give information on localization of proteins and their spatiotemporal alterations and is considered to be powerful yet still evolving technology. MSI analysis is particularly useful in the context of intestinal IR injury, because the intestinal wall is a heterogeneous tissue composed of three tissue layers, i.e. mucosa, submucosa and muscle layer, which have distinct cell populations that respond differently to stressors. IR injury starts in the mucosa with loss of the villus tips followed by crypt damage, and progresses towards the muscle layer in severe cases.

In our study, we were particularly interested in the mucosa region because a mild IR model was used. As the crypt and villus compartment contain distinct epithelial cell types that perform different functions, visualization of protein changes within mucosa may reveal region- or cell-specific changes that could be missed in proteomics analysis of whole tissue homogenates. These region-specific peptide alterations could give pathophysiological insights of IR injury, as, for instance, the integrity of the crypt region is crucial for regeneration and tissue repair. In addition, information on the localization of peptide alterations could also lead to the discovery of potential biomarker candidates for mild injury, restricted to the mucosa, or severe transmural damage. A decrease in protein expression in tissue might be accompanied by leakage into the systemic circulation, as has been demonstrated for IFABP[26] and SM22[37], markers for mild intestinal IR injury and transmural damage respectively.

Our MSI analysis detected many peptides with specific localization in distinct intestinal tissue structures (**chapter 3**). Interestingly, some peptides showed a distribution shift during the various stages of IR. Statistical analysis of peptide dynamics within mucosa and submucosa resulted in many differentially expressed peptides, however, only a relatively small number of these peptides could be identified. Our MSI findings were supported by (phospho)proteome data, presenting temporal alterations in proteins related to overrepresented processes in the dynamic (phospho)proteome. However, comprehensive functional analysis was limited because of the difficulty to match tryptic peptides to corresponding proteins.

Recent advances in MSI sample preparation and instrumentation have greatly improved reproducibility, mass resolution, spatial resolution and acquisition time[38], however, protein identification remains a challenge. Several protein identification strategies have been proposed[39-42]. In our approach, increased confidence of protein identification was obtained by matching high-speed TOF MSI data first with high-mass resolution FTICR MSI data before matching with the LC-MS/MS proteomics dataset. An alternative method to identify and quantify more proteins in a specific tissue area would be the use of laser capture micro-dissection (LCM) followed by LC-MS/MS proteomics analysis[43]. This can be performed either in an MSI-guided manner, in which the spatial molecular information is obtained with MSI, or in a histology-guided manner. The latter would be a useful approach to study, for instance, the crypt-specific dynamic proteome to get insight in the regenerative response following IR. Drawbacks of the LCM approach would be the loss of information on temporal distribution shifts and the fact that it is rather labor-intensive.

Concluding note

Altogether, several complementary technologies were used to study the dynamic response to intestinal IR in man. They provided insight in the transcriptional response, and different layers of protein information, i.e. protein expression, phosphorylation and localization. These findings gave rise to a wide range of directions for future research. To further study the processes that were found to be regulated in human intestinal IR, and their potential as a therapeutic target in IR injury, we developed a human intestinal organoids to model IR *in vitro*.

A HUMAN INTESTINAL ORGANOID MODEL TO STUDY ISCHEMIA-REPERFUSION

The human small intestinal organoid model

Organoid technology is a rapidly expanding field. Organoids better represent the tissue of origin with respect to architecture and functionality when compared to traditional cell lines, and offer reduced complexity and easy manipulation when compared to *in vivo* models. In the past decade, numerous organoid models for different organs and tissues have arisen with applications ranging from studying epithelial biology and disease modeling to personalized (cancer) therapy, regenerative medicine and gene therapy[44-49]. Specifically, small intestinal organoids have been shown to be a valuable model to study stem cell niche functions[50], intestinal nutrient transport[45,51], hormone secretion[51], and infectious disease[46].

Murine intestinal crypts grow into organoids comprising crypt and villus structures, which contain the cellular diversity of the intestinal epithelium while maintaining the ability to indefinitely expand[52]. As to intestinal organoids from human origin, the maintenance of cellular diversity has been challenging. The growth factor cocktail that is required for establishment, expansion and long-term culture[53] also suppresses differentiation into mature epithelial cell types. In this thesis we characterized this proliferative phenotype as crypt-like organoids, which were shown to be enriched for proliferating cells (i.e. stem cells and transit-amplifying cells) and Paneth cells. Removal of several growth factors (i.e. Wnt3A, nicotinamide, p38 inhibitor, and 50% reductions in R-spondin-1 and Noggin) induced a villus-like organoid phenotype that was enriched for absorptive enterocytes and goblet cells (**chapter 4**). The separate investigation of the crypt and villus response is of interest given the differences in function and IR susceptibility: while the villus is more susceptible to IR injury, protection of crypt integrity is crucial for repair of the epithelial lining.

Interestingly, Fujii et al. recently succeeded to modify culture conditions that allow human intestinal organoids to undergo multi-differentiation and concurrently maintain self-renewal capacity[54]. On the other hand, recent studies demonstrated how small molecule treatments skewed differentiation of murine intestinal organoids towards Paneth cell or goblet cell lineages[55-57], providing cell-type enriched organoids. Moreover, Maed et al. reported that the Paneth cells in these enriched organoids better resemble their *in vivo* counterparts when compared to Paneth cells in conventional organoids[58]. Whether these small molecules are able to skew differentiation in human organoids, and whether they provide improved physiological representation of specialized cells, remains to be investigated. Because of their crucial roles in maintaining epithelial barrier integrity, these cell type-enriched organoids might be a useful tool to study Paneth cell or goblet cell specific function/dysfunction during IR injury and repair.

Modeling IR in human intestinal organoids

Intestinal organoids were subjected to hypoxia and reoxygenation to mimic IR. In **chapter 4**, we performed proteomics analysis to explore the molecular response to hypoxia-reoxygenation (HR) in human intestinal organoids enriched for crypt and villus cells separately.

The dynamic proteome during HR in intestinal organoids was found to be predominantly related to metabolic processes (**chapter 4**). Cellular metabolic adaptations that are required under hypoxic

conditions, include changes in mitochondrial energy metabolism and respiration, lipid metabolism, and protein synthesis[59]. Our data, showing alterations in abundance of proteins related to these processes, likely reflect these metabolic adaptations. In the first place, mitochondrial metabolism was affected by hypoxia in both crypt- and villus-like organoids. In **chapter 6**, we confirmed impaired mitochondrial function following HR by the loss of mitochondrial membrane potential, a key indicator of mitochondrial activity. Here, mitochondria appeared to be more severely affected in villus-like compared to crypt-like organoids. As to mitochondrial metabolism-related proteins alterations (**chapter 4**), we observed differences between the phenotypes as well, which was to be expected given the known differences in energy metabolism between epithelial cell types: proliferating cells rely primarily on anaerobic glycolysis, whereas differentiated cells rely on oxidative phosphorylation[60-62]. Second, the reduced expression of many enzymes involved in lipid metabolic processes, suggested that fatty acid catabolism was impaired during HR. This might lead to accumulation of free fatty acids and thus lipotoxicity. Future studies are required to determine the implications of modified fatty acid metabolism during HR, and its contribution to the pathophysiology of intestinal IR injury. Third, the differential expression of proteins related to the translational machinery, protein folding and trafficking in crypt-like organoids pointed to suppression of protein synthesis. In addition to the metabolic processes, functional enrichment analysis of the dynamic proteome revealed regulation of immune response related processes during HR in organoids. This suggests that the organoid model offers a reductionist approach to study the interaction between the cellular stress response and epithelial immunity following HR.

Interestingly, proteome analysis suggested that crypt-like organoids were better protected against oxidative stress and cell death when compared to villus-like organoids. Cellular stress and cell death-associated protein changes were more pronounced in villus-like organoids, while crypt-like organoids demonstrated increased levels of antioxidant proteins. With this we showed that the organoid phenotypes reflect *in vivo* differences between crypt and villus in the susceptibility to IR injury. Intriguingly, the mitophagy pathway was found to be enriched in crypt-like organoids only, which led to further investigate the role of this protective mechanism in **chapter 6**.

Comparing the organoid HR model with intestinal IR in vivo

While alterations in the proteome during HR in organoids were mostly associated with metabolic processes, the dynamic proteome in human IR was dominated by proteins related to the immune response and inflammation, and to microvillus and cytoskeleton which most likely reflects loss of differentiated cells in the villus tips (**chapter 5)**. Processes that were found to be regulated in both the human IR model as well as the organoid HR model were protein synthesis, extracellular matrix organization, and to some extent, the immune response (**chapter 4** and **5**).

The discrepancy in protein alterations and related processes between the models could partly be explained by the cellular diversity of the human intestine as opposed to organoids that consist of epithelial cells only. The MS-identified proteomes of the human intestine and the intestinal organoid showed an overlap of 57%. The other 43% of proteins, which were detected in the human intestine only, were enriched for immune response- and inflammation-related processes. The proteins that were detected in intestinal organoids only, showed an enrichment for various metabolic processes.

Furthermore, structural changes in the human intestine, such as shortening of the villus, greatly impact the protein profile, whereas such changes are less likely to be detected in organoids that have either a crypt-or a villus phenotype. Another important explanation for differences between the models is the lack of environmental factors in the intestinal organoids and will be discussed next.

Organoids to study intestinal epithelial immunity and interaction with the environment

Although the immune response appeared to be regulated to some extent in the organoid model, it is obvious that a stronger immune response is induced in response to IR *in vivo*, especially during reperfusion which allows migration of immune cells (e.g. neutrophils) and proteins (complement factors, cytokines) into the IR-damaged tissue[22]. This immunological aspect of the IR damage response as well as the role of luminal microbiota are eliminated in the organoid model. To study the specific interaction of the epithelium with the environment, it could be useful to co-culture organoids and immune cells[63], or luminal factors, for instance bacteria[64]. In this context, it should be taken into account that the epithelial cell polarity is retained in organoids, with the apical side facing the organoid lumen under normal culture conditions. To study intestinal microbiota for instance, luminal exposure can be achieved by means of microinjection into the organoid lumen[65,66]. Alternatively, organoid-derived epithelial monolayers in a transwell system may be a good alternative for co-culture studies[67].

The immune regulation in the organoid HR model, in the absence of microbiota and immune cells, represented damage-induced epithelial immune signaling. Besides afore-mentioned specialized epithelial cells with an innate immune function (Paneth cells), all intestinal epithelial cell types act as active participants in directing the mucosal immune response via expression of pattern recognition receptors (PRRs). PRRs sense damage-associated molecular patterns (DAMPs) and microbe-associated molecular patterns (MAMPs), which consequently induces inflammatory signaling to regulate immune cells[68,69]. Recently, Kayisoglu et al. mapped the expression of innate immune signaling genes along the gastrointestinal tract by using murine and human organoids derived from different gastrointestinal (GI) segments[70]. They found that expression and function of immune related genes were both GI segment specific and species specific. The latter stresses the importance of using human organoids to study disease pathology and test potential therapies.

Diversity among human intestinal organoid lines

In general, organoids resemble the genetic signature of the tissue they originated from[53,71-73] and have been shown to express a personalized proteome profile[74]. Likewise, the different organoid lines hold distinct proteome profiles as was shown in our proteome study. The diversity among the organoid lines derived from different individuals is a strength of the model as it reflects the interindividual differences. This, in combination with the heterogeneity of intestinal organoid cultures – i.e. the cellular diversity within a culture – makes the model more representative and at the same time less standardized than conventional cell cultures. When performing experiments with different organoid lines, this should be taken into account, and it may be considered to apply a larger sample size than the generally accepted three independent experiments for *in vitro* cell culture experiments.

Altogether, proteomics analysis demonstrated that the HR response in human intestinal organoids recapitulates properties of the *in vivo* response to intestinal IR. The model enabled to study the human epithelial response to IR injury without confounding environmental factors. On the other hand, it should be considered that the interaction with luminal (microbial) content and immune cells are significant elements of the pathophysiology of IR injury.

The use of the organoid HR model to study potential therapeutic targets

In this thesis, the organoid HR model was used to study two potential therapeutic targets in intestinal IR: UPR signaling and mitophagy. The selective targeting of pro-apoptotic UPR signaling was aimed at inhibition of a damaging process, whereas targeting mitophagy would aim for stimulation of a protective mechanism.

Fine-tuning the UPR to alleviate IR injury

Our finding that the UPR was strongly regulated in IR of the human intestine (**chapter 5**), led us to further investigate this pathway in the organoid model. After confirming that HR activated the IRE1 and PERK branches of the UPR in human intestinal organoids, we next explored whether targeting UPR signaling may be protective against HR/IR injury. Several studies in experimental models of renal, hepatic and myocardial IR reported beneficial effects of general UPR inhibition with chemical chaperones, such as tauroursodeoxycholic acid (TUDCA) or 4-phenyl butyrate acid (4-PBA)[75-79]. The fact that the UPR can promote both cell survival and cell death, makes fine-tuning of this pathway in favor of survival challenging[80]. Even though all branches of the UPR have pro-survival and pro-apoptotic potential, IRE1-induced splicing of XBP1 is crucial in survival, whereas ATF4-CHOP signaling (downstream of PERK) is considered to have a key role in UPR-induced cell death. Therefore, ISRIB – a more specific inhibitor acting downstream of PERK by selectively reversing the effects of eIF2α phosphorylation – is believed to have enhanced therapeutic potential as this inhibitor is less likely to cause adverse effects from repressing the beneficial effects of the UPR[81,82]. We showed that pharmacological UPR inhibition with ISRIB strongly reduced pro-apoptotic ATF4-CHOP signaling during HR in intestinal organoids, while pro-survival XBP1 splicing was largely maintained (**chapter 5**). These results suggested that ISRIB may be a promising strategy to balance the UPR, reduce apoptosis and attenuate injury in intestinal IR.

In addition to potential inhibition of apoptosis, we speculate that ISRIB may have beneficial effects by attenuating ER stress-induced inflammatory signaling during IR, given that ER stress-induced CHOP expression has been linked to inflammatory responses[83]. Moreover, ISRIB has been shown to suppress inflammation during thapsigargin-induced ER stress[84]. Investigating whether ISRIB treatment will result in a reduction in cell death and decreased inflammatory signaling in intestinal HR, and eventually in improved barrier integrity and reduced inflammation in IR *in vivo,* are important directions for future research.

Cross-talk UPR, autophagy and mitochondria during ER stress

In response to ER stress, the UPR interacts with other important processes including autophagy and mitochondrial function. Both IRE1 and PERK pathways have been implicated in autophagy induction under ER stress[85,86]. Although ATF4 and CHOP are mostly associated with cell death, they

have also been shown to transcriptionally regulate autophagy[87]. Autophagy has been recognized as a crucial survival mechanism under ER stress[85,88], yet severe ER stress has also been reported to induce autophagy-dependent cell death mechanisms[89]. Furthermore, ATF4 controls the expression of ubiquitin ligase Parkin[90], which is a crucial regulator of mitophagy[91], mitochondrial dynamics[92], and mitochondrial bioenergetics via modulation of the mitochondrial-associated ER membranes (MAMs)[93]. Interestingly, these MAMs have been associated with a variety of processes including bioenergetics, ER stress, autophagy, apoptosis, and inflammasome signaling[94,95]. It is of great importance to understand how these processes interact, and to define the effect of fine-tuning the UPR on different cellular outcomes, including cell death, autophagy and inflammation.

A protective role for mitophagy in IR?

The apparent interaction between the UPR and mitophagy, in combination with our proteomics analysis of the HR response in organoids, which revealed an overrepresentation of the mitophagy pathway in crypt-like organoids (**chapter 4**), stimulated us to study this pathway. The difference in activation of this protective pathway between crypt and villus caught our interest. In addition, the question was raised whether mitophagy might be a potential therapeutic target in intestinal IR injury. As damaged mitochondria release cytotoxic molecules, their removal via mitophagy is important for cellular survival[96-99]. In **chapter 6**, we assessed HR-induced mitochondrial damage and evaluated signs of mitophagy in crypt- and villus-like intestinal organoids. Here, we demonstrated that the mitochondrial membrane potential was more severely affected during HR in crypt-like compared to villus-like organoids, and, interestingly, we observed changes in expression of autophagy and mitophagy markers, particularly in crypt-like organoids, that may point to occurrence of mitophagy. Based on these preliminary results we speculate that mitophagy in intestinal crypts may contribute to a better protection from IR injury compared to villi. While mitochondrial damage initially induces mitophagy, it is likely that a certain threshold of mitochondrial injury was reached in the villi that induced signaling to promote apoptosis[100]. In this ongoing study, analyses that will be performed next include assessment of autophagic flux and colocalization of mitochondria and autophagosomes to confirm occurrence of mitophagy in the organoid HR model. Future studies should be directed at investigating the protective effect of mitophagy against intestinal IR injury, and the therapeutic potential of stimulating mitophagy. In addition, considering its essential role in stem cell maintenance[101] and stem cell protection during stressful conditions[102], stimulation of mitophagy may also be beneficial for regeneration of the injured epithelium.

CONCLUDING REMARKS

The comprehensive analysis of the dynamic transcriptome, proteome and phosphoproteome, and of spatiotemporal protein changes in human intestinal IR 1) showed the complementary nature of the different technologies, 2) provided a system-wide understanding of the human intestinal response to IR, 3) supported existing knowledge and gave novel insights of IR in a human experimental setting, and 4) provided directions for future research into therapeutic targets as well as diagnostic markers. In addition, we demonstrated that the human intestinal organoid model provides a useful tool to study IR *in vitro*. This model was used to show that balancing the UPR may be a promising strategy

to attenuate intestinal IR injury. In addition, we identified differences in mitochondrial damage and mitophagy after HR in the crypt and villus. Whether fine-tuning of the UPR and stimulation of mitophagy could serve as therapeutic target to protect against intestinal IR injury and promote intestinal regeneration and repair, for example in the context of intestinal transplantation, remains subject for future studies. Furthermore, our model lays a foundation for more advanced models in the future, for instance organoid co-culture systems to study the interaction of the epithelium with environmental factors.

REFERENCES

1 Bala, M. *et al.* Acute mesenteric ischemia: guidelines of the World Society of Emergency Surgery. *World journal of emergency surgery : WJES* **12**, 38 (2017).

2 American Gastroenterological Association Medical Position Statement: guidelines on intestinal ischemia. *Gastroenterology* **118**, 951-953 (2000).

3 Himanen, S. V. & Sistonen, L. New insights into transcriptional reprogramming during cellular stress. *J Cell Sci* **132** (2019).

4 Bartoszewska, S. & Collawn, J. F. Unfolded protein response (UPR) integrated signaling networks determine cell fate during hypoxia. *Cell Mol Biol Lett* **25**, 18 (2020).

5 Ron, D. & Walter, P. Signal integration in the endoplasmic reticulum unfolded protein response. *Nat Rev Mol Cell Biol* **8**, 519-529 (2007).

6 Ma, X. *et al.* Intestinal Epithelial Cell Endoplasmic Reticulum Stress and Inflammatory Bowel Disease Pathogenesis: An Update Review. *Front Immunol* **8**, 1271 (2017).

7 Coleman, O. I. & Haller, D. ER Stress and the UPR in Shaping Intestinal Tissue Homeostasis and Immunity. *Front Immunol* **10**, 2825 (2019).

8 Kaser, A. & Blumberg, R. S. Endoplasmic reticulum stress and intestinal inflammation. *Mucosal Immunol* **3**, 11-16 (2010).

9 Hu, P., Han, Z., Couvillon, A. D., Kaufman, R. J. & Exton, J. H. Autocrine tumor necrosis factor alpha links endoplasmic reticulum stress to the membrane death receptor pathway through IRE1alpha-mediated NF-kappaB activation and down-regulation of TRAF2 expression. *Mol Cell Biol* **26**, 3071-3084 (2006).

10 Deng, J. *et al.* Translational repression mediates activation of nuclear factor kappa B by phosphorylated translation initiation factor 2. *Mol Cell Biol* **24**, 10161-10168 (2004).

11 Nakajima, S. *et al.* Selective abrogation of BiP/GRP78 blunts activation of NF-κB through the ATF6 branch of the UPR: involvement of C/EBPβ and mTOR-dependent dephosphorylation of Akt. *Mol Cell Biol* **31**, 1710-1718 (2011).

12 Urano, F. *et al.* Coupling of stress in the ER to activation of JNK protein kinases by transmembrane protein kinase IRE1. *Science* **287**, 664-666 (2000).

13 Darling, N. J. & Cook, S. J. The role of MAPK signalling pathways in the response to endoplasmic reticulum stress. *Biochim Biophys Acta* **1843**, 2150-2163 (2014).

14 Liang, S. H., Zhang, W., McGrath, B. C., Zhang, P. & Cavener, D. R. PERK (eIF2alpha kinase) is required to activate the stress-activated MAPKs and induce the expression of immediate-early genes upon disruption of ER calcium homoeostasis. *Biochem J* **393**, 201-209 (2006).

15 Bevins, C. L. & Salzman, N. H. Paneth cells, antimicrobial peptides and maintenance of intestinal homeostasis. *Nature reviews. Microbiology* **9**, 356-368 (2011).

16 Grootjans, J. *et al.* Level of Activation of the Unfolded Protein Response Correlates With Paneth Cell Apoptosis in Human Small Intestine Exposed to Ischemia/Reperfusion. *Gastroenterology* **140**, 529-539000 (2011).

17 Vaishnava, S., Behrendt, C. L., Ismail, A. S., Eckmann, L. & Hooper, L. V. Paneth cells directly sense gut commensals and maintain homeostasis at the intestinal host-microbial interface. *Proceedings of the National Academy of Sciences of the United States of America* **105**, 20858-20863 (2008).

18 Chong, A. S. & Alegre, M.-L. The impact of infection and tissue damage in solid-organ transplantation. *Nature Reviews Immunology* **12** (2012).

19 Kawai, M., Kitade, H., Koshiba, T., Waer, M. & Pirenne, J. Intestinal Ischemia Reperfusion and Lipopolysaccharide Transform a Tolerogenic Signal into a Sensitizing Signal and Trigger Rejection. *Transplantation* **87**, 1464 (2009).

20 Grootjans, J., Kaser, A., Kaufman, R. J. & Blumberg, R. S. The unfolded protein response in immunity and inflammation. *Nat Rev Immunol* **16**, 469-484 (2016).

21 Lenaerts, K. *et al.* New insights in intestinal ischemia–reperfusion injury: implications for intestinal transplantation. *Current Opinion in Organ Transplantation* **18**, 298 (2013).

22 Grootjans, J. *et al.* Human intestinal ischemia-reperfusion-induced inflammation characterized: experiences from a new translational model. *Am J Pathol* **176**, 2283-2291 (2010).

23 Wada, K., Montalto, M. C. & Stahl, G. L. Inhibition of complement C5 reduces local and remote organ injury after intestinal ischemia/reperfusion in the rat. *Gastroenterology* **120**, 126-133 (2001).

24 Fleming, S. D. *et al.* C5a causes limited, polymorphonuclear cell-independent, mesenteric ischemia/reperfusion-induced injury. *Clin Immunol* **108**, 263-273 (2003).

25 Arumugam, T. V. *et al.* Protective effect of a new C5a receptor antagonist against ischemia-reperfusion injury in the rat small intestine. *The Journal of surgical research* **103**, 260-267 (2002).

26 Schellekens, D. H. *et al.* Plasma intestinal fatty acid-binding protein levels correlate with morphologic epithelial intestinal damage in a human translational ischemia-reperfusion model. *J Clin Gastroenterol* **48**, 253-260 (2014).

27 Ceulemans, L. *et al.* Villin-1 Is a Novel Serological Biomarker for Intestinal Ischemia and Reperfusion Injury in Rats and Humans. *Transplantation* **101**, S91 (2017).

28 Delacour, D., Salomon, J., Robine, S. & Louvard, D. Plasticity of the brush border - the yin and yang of intestinal homeostasis. *Nat Rev Gastroenterol Hepatol* **13**, 161-174 (2016).

29 Bertocchi, C., Vaman Rao, M. & Zaidel-Bar, R. Regulation of adherens junction dynamics by phosphorylation switches. *J Signal Transduct* **2012**, 125295 (2012).

30 Grootjans, J. *et al.* Rapid lamina propria retraction and zipper-like constriction of the epithelium preserves the epithelial lining in human small intestine exposed to ischaemia-reperfusion. *The Journal of pathology* **224**, 411-419 (2011).

31 Misteli, T. RNA splicing: What has phosphorylation got to do with it? *Curr Biol* **9**, R198-200 (1999).

32 Prasad, J., Colwill, K., Pawson, T. & Manley, J. L. The protein kinase Clk/Sty directly modulates SR protein activity: both hyper- and hypophosphorylation inhibit splicing. *Mol Cell Biol* **19**, 6991-7000 (1999).

33 Natua, S., Ashok, C. & Shukla, S. Hypoxia-induced alternative splicing in human diseases: the pledge, the turn, and the prestige. *Cell Mol Life Sci* (2021).

34 Kanopka, A. Cell survival: Interplay between hypoxia and pre-mRNA splicing. *Exp Cell Res* **356**, 187-191 (2017).

35 Nakayama, K. & Kataoka, N. Regulation of Gene Expression under Hypoxic Conditions. *Int J Mol Sci* **20** (2019).

36 Tsalikis, J. *et al.* The transcriptional and splicing landscape of intestinal organoids undergoing nutrient starvation or endoplasmic reticulum stress. *BMC Genomics* **17**, 680 (2016).

37 Schellekens, D. *et al.* SM22 a Plasma Biomarker for Human Transmural Intestinal Ischemia. *Ann Surg* **268**, 120-126 (2018).

38 Buchberger, A. R., DeLaney, K., Johnson, J. & Li, L. Mass Spectrometry Imaging: A Review of Emerging Advancements and Future Insights. *Anal Chem* **90**, 240-265 (2018).

39 Rauser, S. *et al.* Classification of HER2 receptor status in breast cancer tissues by MALDI imaging mass spectrometry. *Journal of proteome research* **9**, 1854-1863 (2010).

40 Stauber, J. *et al.* MALDI imaging of formalin-fixed paraffin-embedded tissues: application to model animals of Parkinson disease for biomarker hunting. *Journal of proteome research* **7**, 969-978 (2008).

41 Schober, Y., Schramm, T., Spengler, B. & Rompp, A. Protein identification by accurate mass matrix-assisted laser desorption/ionization imaging of tryptic peptides. *Rapid communications in mass spectrometry : RCM* **25**, 2475-2483 (2011).

42 Huber, K. *et al.* Approaching cellular resolution and reliable identification in mass spectrometry imaging of tryptic peptides. *Analytical and bioanalytical chemistry* **410**, 5825-5837 (2018).

43 Eveque-Mourroux, M. R., Rocha, B., Barré, F. P. Y., Heeren, R. M. A. & Cillero-Pastor, B. Spatially resolved proteomics in osteoarthritis: State of the art and new perspectives. *J Proteomics* **215**, 103637 (2020).

44 Clevers, H. Modeling Development and Disease with Organoids. *Cell* **165**, 1586-1597 (2016).

45 Foulke-Abel, J. *et al.* Human Enteroids as a Model of Upper Small Intestinal Ion Transport Physiology and Pathophysiology. *Gastroenterology* **150**, 638-649.e638 (2016).

46 Saxena, K. *et al.* Human Intestinal Enteroids: a New Model To Study Human Rotavirus Infection, Host Restriction, and Pathophysiology. *J Virol* **90**, 43-56 (2016).

47 Onozato, D. *et al.* Application of Human Induced Pluripotent Stem Cell-Derived Intestinal Organoids as a Model of Epithelial Damage and Fibrosis in Inflammatory Bowel Disease. *Biol Pharm Bull* **43**, 1088-1095 (2020).

48 Ooft, S. N. *et al.* Patient-derived organoids can predict response to chemotherapy in metastatic colorectal cancer patients. *Sci Transl Med* **11** (2019).

49 Leushacke, M. & Barker, N. Ex vivo culture of the intestinal epithelium: strategies and applications. *Gut* **63**, 1345-1354 (2014).

50 Farin, H. F., Van Es, J. H. & Clevers, H. Redundant sources of Wnt regulate intestinal stem cells and promote formation of Paneth cells. *Gastroenterology* **143**, 1518-1529.e1517 (2012).

51 Zietek, T., Rath, E., Haller, D. & Daniel, H. Intestinal organoids for assessing nutrient transport, sensing and incretin secretion. *Sci Rep* **5**, 16831 (2015).

52 Sato, T. *et al.* Single Lgr5 stem cells build crypt-villus structures in vitro without a mesenchymal niche. *Nature* **459**, 262-265 (2009).

53 Sato, T. *et al.* Long-term expansion of epithelial organoids from human colon, adenoma, adenocarcinoma, and Barrett's epithelium. *Gastroenterology* **141**, 1762-1772 (2011).

54 Fujii, M. *et al.* Human Intestinal Organoids Maintain Self-Renewal Capacity and Cellular Diversity in Niche-Inspired Culture Condition. *Cell Stem Cell* **23**, 787-793.e786 (2018).

55 Luu, L. *et al.* Proteomic Profiling of Enteroid Cultures Skewed toward Development of Specific Epithelial Lineages. *Proteomics* **18**, e1800132 (2018).

56 Treveil, A. *et al.* Regulatory network analysis of Paneth cell and goblet cell enriched gut organoids using transcriptomics approaches. *Mol Omics* **16**, 39-58 (2020).

57 Yin, X. *et al.* Niche-independent high-purity cultures of Lgr5+ intestinal stem cells and their progeny. *Nat Methods* **11**, 106-112 (2014).

58 Mead, B. E. *et al.* Harnessing single-cell genomics to improve the physiological fidelity of organoid-derived cell types. *BMC Biol* **16**, 62 (2018).

59 Lee, P., Chandel, N. S. & Simon, M. C. Cellular adaptation to hypoxia through hypoxia inducible factors and beyond. *Nat Rev Mol Cell Biol* **21**, 268-283 (2020).

60 Stringari, C. *et al.* Metabolic trajectory of cellular differentiation in small intestine by Phasor Fluorescence Lifetime Microscopy of NADH. *Sci Rep* **2**, 568 (2012).

61 Schell, J. C. *et al.* Control of intestinal stem cell function and proliferation by mitochondrial pyruvate metabolism. *Nat Cell Biol* **19**, 1027-1036 (2017).

62 Okkelman, I. A., Neto, N., Papkovsky, D. B., Monaghan, M. G. & Dmitriev, R. I. A deeper understanding of intestinal organoid metabolism revealed by combining fluorescence lifetime imaging microscopy (FLIM) and extracellular flux analyses. *Redox Biol* **30**, 101420 (2020).

63 Bar-Ephraim, Y. E., Kretzschmar, K. & Clevers, H. Organoids in immunological research. *Nat Rev Immunol* **20**, 279-293 (2020).

64 Pompaiah, M. & Bartfeld, S. Gastric Organoids: An Emerging Model System to Study Helicobacter pylori Pathogenesis. *Curr Top Microbiol Immunol* **400**, 149-168 (2017).

65 Bartfeld, S. & Clevers, H. Organoids as Model for Infectious Diseases: Culture of Human and Murine Stomach Organoids and Microinjection of Helicobacter Pylori. *J Vis Exp* (2015).

66 Williamson, I. A. *et al.* A High-Throughput Organoid Microinjection Platform to Study Gastrointestinal Microbiota and Luminal Physiology. *Cell Mol Gastroenterol Hepatol* **6**, 301-319 (2018).

67 Altay, G. *et al.* Self-organized intestinal epithelial monolayers in crypt and villus-like domains show effective barrier function. *Sci Rep* **9**, 10140 (2019).

68 Peterson, L. W. & Artis, D. Intestinal epithelial cells: regulators of barrier function and immune homeostasis. *Nat Rev Immunol* **14**, 141-153 (2014).

69 Pott, J. & Hornef, M. Innate immune signalling at the intestinal epithelium in homeostasis and disease. *EMBO Rep* **13**, 684-698 (2012).

70 Kayisoglu, O. *et al.* Location-specific cell identity rather than exposure to GI microbiota defines many innate immune signalling cascades in the gut epithelium. *Gut* **70**, 687-697 (2021).

71 Sato, T. & Clevers, H. Growing self-organizing mini-guts from a single intestinal stem cell: mechanism and applications. *Science* **340**, 1190-1194 (2013).

72 van de Wetering, M. *et al.* Prospective derivation of a living organoid biobank of colorectal cancer patients. *Cell* **161**, 933-945 (2015).

73 Georgakopoulos, N. *et al.* Long-term expansion, genomic stability and in vivo safety of adult human pancreas organoids. *BMC Dev Biol* **20**, 4 (2020).

74 Cristobal, A. *et al.* Personalized Proteome Profiles of Healthy and Tumor Human Colon Organoids Reveal Both Individual Diversity and Basic Features of Colorectal Cancer. *Cell Rep* **18**, 263-274 (2017).

75 Xie, Y. *et al.* Tauroursodeoxycholic acid inhibits endoplasmic reticulum stress, blocks mitochondrial permeability transition pore opening, and suppresses reperfusion injury through GSK-3ß in cardiac H9c2 cells. *Am J Transl Res* **8**, 4586-4597 (2016).

76 Gupta, S. *et al.* Prevention of acute kidney injury by tauroursodeoxycholic acid in rat and cell culture models. *PloS one* **7**, e48950 (2012).

77 Zhang, C. *et al.* Unfolded protein response plays a critical role in heart damage after myocardial ischemia/reperfusion in rats. *PloS one* **12**, e0179042 (2017).

78 Gu, Y. *et al.* Connexin32 plays a crucial role in ROS-mediated endoplasmic reticulum stress apoptosis signaling pathway in ischemia reperfusion-induced acute kidney injury. *J Transl Med* **16**, 117 (2018).

79 Vilatoba, M. *et al.* Sodium 4-phenylbutyrate protects against liver ischemia reperfusion injury by inhibition of endoplasmic reticulum-stress mediated apoptosis. *Surgery* **138**, 342-351 (2005).

80 Maurel, M. *et al.* Controlling the unfolded protein response-mediated life and death decisions in cancer. *Semin Cancer Biol* **33**, 57-66 (2015).

81 Sidrauski, C., McGeachy, A. M., Ingolia, N. T. & Walter, P. The small molecule ISRIB reverses the effects of eIF2α phosphorylation on translation and stress granule assembly. *Elife* **4** (2015).

82 Zyryanova, A. F. *et al.* Binding of ISRIB reveals a regulatory site in the nucleotide exchange factor eIF2B. *Science* **359**, 1533-1536 (2018).

83 Park, S. H. *et al.* Endoplasmic reticulum stress-activated C/EBP homologous protein enhances nuclear factor-kappaB signals via repression of peroxisome proliferator-activated receptor gamma. *J Biol Chem* **285**, 35330-35339 (2010).

84 Guthrie, L. N. *et al.* Attenuation of PKR-like ER Kinase (PERK) Signaling Selectively Controls Endoplasmic Reticulum Stress-induced Inflammation Without Compromising Immunological Responses. *J Biol Chem* **291**, 15830-15840 (2016).

85 Ogata, M. *et al.* Autophagy is activated for cell survival after endoplasmic reticulum stress. *Mol Cell Biol* **26**, 9220-9231 (2006).

86 Rouschop, K. M. *et al.* The unfolded protein response protects human tumor cells during hypoxia through regulation of the autophagy genes MAP1LC3B and ATG5. *J Clin Invest* **120**, 127-141 (2010).

87 B'Chir, W. *et al.* The eIF2α/ATF4 pathway is essential for stress-induced autophagy gene expression. *Nucleic Acids Res* **41**, 7683-7699 (2013).

88 Chandrika, B. B. *et al.* Endoplasmic Reticulum Stress-Induced Autophagy Provides Cytoprotection from Chemical Hypoxia and Oxidant Injury and Ameliorates Renal Ischemia-Reperfusion Injury. *PloS one* **10**, e0140025 (2015).

89 Tomar, D. *et al.* TRIM13 regulates caspase-8 ubiquitination, translocation to autophagosomes and activation during ER stress induced cell death. *Biochim Biophys Acta* **1833**, 3134-3144 (2013).

90 Bouman, L. *et al.* Parkin is transcriptionally regulated by ATF4: evidence for an interconnection between mitochondrial stress and ER stress. *Cell Death Differ* **18**, 769-782 (2011).

91 Narendra, D., Tanaka, A., Suen, D. F. & Youle, R. J. Parkin is recruited selectively to impaired mitochondria and promotes their autophagy. *J Cell Biol* **183**, 795-803 (2008).

92 Deng, H., Dodson, M. W., Huang, H. & Guo, M. The Parkinson's disease genes pink1 and parkin promote mitochondrial fission and/or inhibit fusion in Drosophila. *Proceedings of the National Academy of Sciences of the United States of America* **105**, 14503-14508 (2008).

93 Calì, T., Ottolini, D., Negro, A. & Brini, M. Enhanced parkin levels favor ER-mitochondria crosstalk and guarantee Ca(2+) transfer to sustain cell bioenergetics. *Biochim Biophys Acta* **1832**, 495-508 (2013).

94 Thoudam, T., Jeon, J. H., Ha, C. M. & Lee, I. K. Role of Mitochondria-Associated Endoplasmic Reticulum Membrane in Inflammation-Mediated Metabolic Diseases. *Mediators Inflamm* **2016**, 1851420 (2016).

95 van Vliet, A. R., Verfaillie, T. & Agostinis, P. New functions of mitochondria associated membranes in cellular signaling. *Biochim Biophys Acta* **1843**, 2253-2262 (2014).

96 Hu, Q. *et al.* Released Mitochondrial DNA Following Intestinal Ischemia Reperfusion Induces the Inflammatory Response and Gut Barrier Dysfunction. *Sci Rep* **8**, 7350 (2018).

97 Grazioli, S. & Pugin, J. Mitochondrial Damage-Associated Molecular Patterns: From Inflammatory Signaling to Human Diseases. *Front Immunol* **9**, 832 (2018).

98 Jassem, W. & Heaton, N. D. The role of mitochondria in ischemia/reperfusion injury in organ transplantation. *Kidney Int* **66**, 514-517 (2004).

99 Stotland, A. & Gottlieb, R. A. Mitochondrial quality control: Easy come, easy go. *Biochim Biophys Acta* **1853**, 2802-2811 (2015).

100 Bloemberg, D. & Quadrilatero, J. Autophagy, apoptosis, and mitochondria: molecular integration and physiological relevance in skeletal muscle. *Am J Physiol Cell Physiol* **317**, C111-c130 (2019).

101 Asano, J. *et al.* Intrinsic Autophagy Is Required for the Maintenance of Intestinal Stem Cells and for Irradiation-Induced Intestinal Regeneration. *Cell Rep* **20**, 1050-1060 (2017).

102 Levy, A. *et al.* Innate immune receptor NOD2 mediates LGR5(+) intestinal stem cell protection against ROS cytotoxicity via mitophagy stimulation. *Proceedings of the National Academy of Sciences of the United States of America* **117**, 1994-2003 (2020).

ADDENDUM

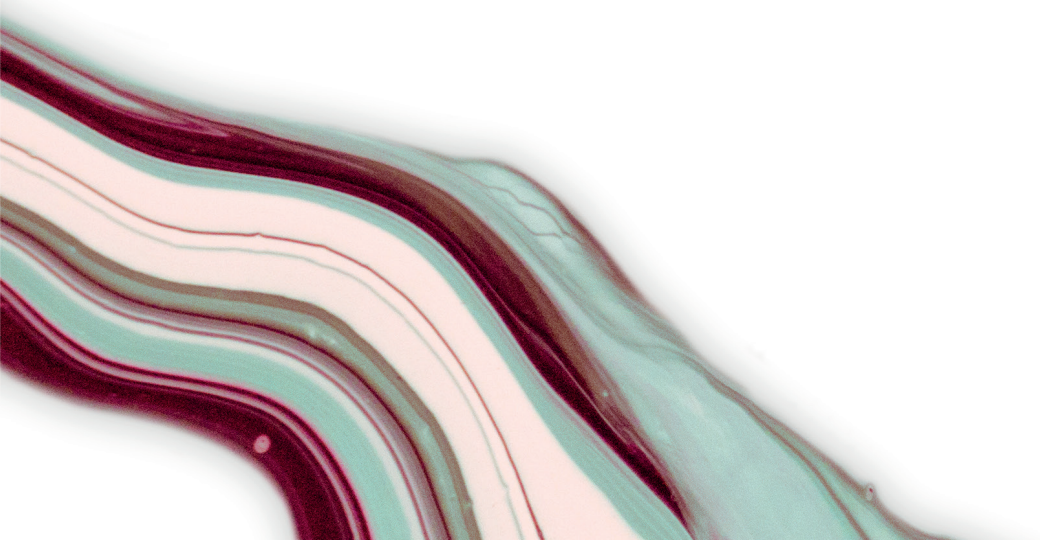

SUMMARY

Intestinal ischemia is the result of impaired perfusion to the intestine, and can occur in a variety of clinical conditions. Intestinal perfusion can be obstructed for instance by occlusion with a thrombus, or due to twisting of the bowel (volvulus). It can also be caused by hypovolemia secondary to shock, trauma or major surgery. In addition, intestinal transplantation is associated with a temporary interruption of the blood flow. Acute mesenteric ischemia is a potentially life-threatening condition occurring in about 13 per 100,000 people per year in the Netherlands. Mortality rates are persistently high (60-80%), which could be attributed to both the difficulty to diagnose intestinal ischemia at an early stage, and lack of therapeutic options. Prompt intervention to restore the blood flow is crucial for patient survival, however, reperfusion of the ischemic intestine initially exacerbates tissue injury, known as reperfusion injury. Therefore, the development of therapeutic strategies aiming at reducing reperfusion injury is urgently needed in order to improve patient outcome.

Intestinal ischemia and reperfusion initiate a cascade of events that can lead to cell death, disruption of the epithelial barrier and an inflammatory response. Previous observations during ischemia-reperfusion (IR) of the human intestine revealed that damage initially occurs at the villus tips and progresses towards the crypt with increasing duration of the ischemic period. Prolonged IR triggered apoptosis of Paneth cells, which are crucial for innate immune defense and stem cell support. This finding stimulated us to study the effect of IR on Paneth cells in a clinical setting, during intestinal transplantation, in **chapter 2**. Organ transplantation is inevitably accompanied by IR and can have a negative impact on transplant outcome. As producers of antimicrobial peptides (e.g. lysozyme), Paneth cells are considered important players in epithelial immunity, and hence their loss may enhance vulnerability of the graft to rejection. In a retrospective study we investigated alterations in Paneth cell numbers and lysozyme abundance in intestinal transplantation patients after reperfusion of the graft, during follow-up (up to 5 years) and during graft rejection. Unexpectedly, no apoptotic Paneth cells were detected shortly after graft reperfusion. However, our data showed a decreased number of Paneth cell and reduced lysozyme abundance within the first week after transplantation. Follow-up biopsies revealed gradual restoration of Paneth cell numbers within months, yet lysozyme abundance remained reduced in these patients. We speculate that the concomitant immune defect may contribute to the vulnerability of the intestinal transplant to rejection and infection. Altogether, in this study we revealed a transient fall in Paneth cell numbers in the early post-transplantation period, which was most likely not directly related to IR injury, and a permanent reduction in lysozyme abundance following transplantation. The potential link between Paneth cell impairment and graft outcome on the longer term, remains to be investigated in a larger patient cohort.

Intestinal IR injury is a complex problem whose pathophysiology has not been completely elucidated. In order to identify potential therapeutic targets, it is imperative to improve our understanding of the molecular mechanisms underlying ischemia and reperfusion of the human intestine. In this thesis, an *in* vivo experimental model was used to study the sequential stages of ischemia and reperfusion injury and repair in the human intestine.

In **chapter 3,** we described the dynamics of the proteome and phosphoproteome during IR in human intestine, using this *in vivo* model. Three complementary approaches were used to study changes in protein abundance, protein phosphorylation status and protein localization in the tissue during IR. With liquid chromatography-mass spectrometry (LC-MS/MS) proteomics and phosphoproteomics analysis, we obtained quantitative information of thousands of proteins and phosphosites. In addition, matrix-assisted laser desorption/ionization mass spectrometry imaging (MALDI MSI) analysis provided spatial information and presented peptide alterations in abundance and distribution. Functional enrichment analysis of the dynamic proteome during IR revealed a decreased abundance of structural proteins of intestinal microvilli, brush border enzymes and transporters for nutrient absorption, which most likely reflects the loss of villus tips, a hallmark of intestinal IR injury. Furthermore, proteome analysis strongly indicated immune activation upon reperfusion, in particular the complement system. In addition to increased abundances of complement factors after IR, MSI revealed alterations in their distribution in the tissue. Many cellular functions are regulated by the phosphorylation and dephosphorylation of proteins. Alterations in the phosphorylation status of proteins during IR, revealed strong regulation of the cytoskeleton and cell junction organization, and mRNA splicing events. Further analysis into the specific phosphosites predicted activity of mitogen-activated protein kinase (MAPK, i.a. regulating the stress response) and cyclin-dependent kinase (CDK, essential in cell cycle regulation) families during IR. Altogether, this study expanded our understanding of the molecular changes that occur during IR in human intestine.

The *in vivo* model for intestinal IR is incredibly useful to study its pathophysiology, however, it is not suitable for in-depth mechanistic studies and testing of therapeutic targets. For that, an *in vitro* model that offers improved translation to *in vivo* IR when compared to conventional cell culture systems, is urgently needed. The intestinal organoid model has recently attracted a lot of attention as an *in vitro* tool to study epithelial biology and to model diseases. Organoids are three-dimensional near-physiological, self-renewing cultures that are derived from primary tissue and exhibit similar architecture and functionality as the tissue of origin.

In **chapter 4**, we demonstrated the use of human small intestinal organoids to model IR injury *in vitro* by exposure to hypoxia and reoxygenation (HR). A mass spectrometry-based proteomics approach was applied to characterize organoid differentiation and decipher protein dynamics and molecular mechanisms of IR injury in human intestinal organoids. First, we showed successful generation of organoids with a crypt-like phenotype, enriched for proliferating cells and Paneth cells, and a villus-like phenotype, enriched for enterocytes and goblet cells. This allowed for separate investigation of the molecular response to hypoxia-reoxygenation in crypt and villus regions. Functional enrichment analysis of differentially expressed proteins during HR showed an overrepresentation of a variety of metabolic processes, i.e. related to mitochondrial metabolism, lipid and protein metabolism. The most prominent difference between the crypt-like and villus-like organoid response is that cellular stress and cell death associated processes were more pronounced in villus-like organoids, whereas overrepresentation of mitophagy and protection against oxidative stress was shown in crypt-like organoids during HR, presuming that the latter possess better protective mechanisms. To conclude, this study demonstrated that the HR response in human intestinal organoids recapitulates properties

of the *in vivo* IR response. Our findings provide a framework for further investigations to elucidate underlying mechanisms of IR injury in crypt and/or villus separately, and a model to test therapeutics to prevent IR injury.

In **chapter 5,** we mapped the transcriptional landscape of the human intestinal response to IR. Transcriptomic profiling was performed at the sequential stages of ischemia and reperfusion using the *in vivo* experimental model. Comprehensive analysis of transcriptomic changes at the level of functions, pathways and networks is described in this chapter, and revealed key regulated biological processes that are activated during IR. We identified the response to unfolded protein as one of the top regulated processes during reperfusion of the ischemic intestine. The unfolded protein response is a pro-survival mechanism that is activated in response to endoplasmic reticulum stress, yet overactivation can promote cell death. Considering its crucial role in determining cell fate during stress, we next explored pharmacological inhibition of the unfolded protein response and its potential to protect against ischemia-reperfusion injury, using the human intestinal organoid model. Here we showed that selective downstream inhibition of the unfolded protein response, strongly reduced pro-apoptotic signaling during hypoxia and reoxygenation in intestinal organoids while pro-survival signaling was largely maintained. These results suggest that targeting the unfolded protein response may be a promising strategy to reduce IR injury.

In **chapter 6**, we studied mitochondrial injury and evaluated signs of mitophagy in response to hypoxia-reoxygenation in crypt-like and villus-like human intestinal organoids. Mitochondria are sensitive to IR injury, and release cytotoxic molecules if they are damaged, which can aggravate injury. Clearance of damaged mitochondria via autophagy, known as mitophagy, is therefore essential for cellular survival. Interestingly, in chapter 4 we identified mitophagy as a regulated process in crypt-like organoids, whereas no indications of mitophagy were found in villus-like organoids in response to HR. This difference between the phenotypes was supported in chapter 6. We showed that mitochondria were damaged in both crypt-like and villus-like organoids following HR, however, mitochondrial function appeared to be more severely affected during reoxygenation in the villus-like phenotype. Interestingly, changes in expression of autophagy and mitophagy markers were more pronounced in crypt-like organoids and may point to activation of mitophagy. Additional analyses need to be performed to confirm occurrence of mitophagy. Future studies should focus on the protective effect of mitophagy in ischemia-reperfusion and the potential of mitophagy-based therapies.

Finally, in **chapter 7** the main findings of this thesis are discussed as well as implications for future research. Altogether, our comprehensive analysis of the dynamic transcriptome, proteome and phosphoproteome, and of spatiotemporal protein changes in the *in vivo* IR model improved our understanding of the human intestinal response to IR and provided directions for future research into therapeutic targets. In addition, we demonstrated that the human intestinal organoid model provides a useful tool to study IR *in vitro*, and identified balancing the UPR as a promising strategy to attenuate intestinal IR injury.

NEDERLANDSE SAMENVATTING

Darmischemie is het gevolg van een verstoorde bloedvoorziening van de darm, waardoor deze onvoldoende zuurstof en voedingstoffen krijgt. Er zijn verschillende oorzaken van darmischemie. Er kan een onderscheid gemaakt worden tussen oorzaken waarbij een bloedvat is afgesloten (occlusieve ischemie), bijvoorbeeld door een bloedprop, en oorzaken waarbij er verminderde bloedtoevoer is zonder dat het bloedvat is afgesloten (niet-occlusieve ischemie). De laatstgenoemde vorm kan het gevolg zijn van een algemene daling van de hoeveelheid bloed in het lichaam, ook wel systemische hypovolemie genoemd, bijvoorbeeld door bloedverlies ten gevolge van een ongeluk of grote operatie. Een apart geval van darmischemie treedt op tijdens darmtransplantatie, een procedure die vanzelfsprekend gepaard gaat met een tijdelijke onderbreking van de bloedtoevoer.

Acute darmischemie is een potentieel levensbedreigende aandoening die in Nederland bij ongeveer 13 per 100.000 mensen per jaar voorkomt. Het sterftecijfer is hoog (60-80%), wat zowel kan worden toegeschreven aan de moeilijkheid om darmischemie in een vroeg stadium te diagnosticeren, alsook aan een gebrek aan effectieve behandelingsopties. Een snelle interventie, gericht op het herstellen van de bloedstroom, is essentieel voor de overleving van de patiënt. De aanvoer van bloed naar de ischemische darm (reperfusie) zal echter in eerste instantie leiden tot een verergering van de weefselschade, wat reperfusieschade wordt genoemd. De ontwikkeling van behandelingsopties, gericht op het verminderen van de reperfusieschade, is daarom dringend nodig om de uitkomst voor de patiënt te verbeteren.

Ischemie en reperfusie van de darm brengt een cascade van gebeurtenissen op gang die kan leiden tot celdood, een ontstekingsreactie en een verstoring van de darmbarrière die het lichaam beschermt tegen schadelijke stoffen in de darm. Eerdere studies van onze groep, waarbij de humane darm werd blootgesteld aan ischemie-reperfusie (IR), onthulden dat de schade aanvankelijk optreedt in de uiteinden van de villi, de vingervormige uitstulpingen van de darmwand. Naarmate de duur van de blootstelling aan ischemie toeneemt, breidt de schade zich uit richting de crypten (instulpingen). Ook zagen we dat langdurige IR leidt tot apoptose van Panethcellen, gespecialiseerde cryptcellen die cruciaal zijn voor de aangeboren afweer en de ondersteuning van de stamcellen. Deze bevinding stimuleerde ons om het effect van IR op Panethcellen te bestuderen in een klinische setting, namelijk tijdens darmtransplantatie (**hoofdstuk 2**). IR is onvermijdelijk tijdens de procedure van orgaantransplantatie en kan een negatief effect hebben op de uitkomst van transplantatie. Panethcellen produceren antimicrobiële peptiden (bijvoorbeeld lysozym) en hebben daarmee een belangrijke rol in de immuniteit van het darmepitheel. Verlies van Panethcellen kan daarom de kwetsbaarheid van de getransplanteerde darm voor afstoting vergroten. In een retrospectieve studie onderzochten we de veranderingen in het aantal Panethcellen en de hoeveelheid lysozym in biopten van darmtransplantatiepatiënten op verschillende tijdspunten: kort na reperfusie van het transplantaat, op vaste tijdstippen tijdens de follow-up periode (tot 5 jaar) en wanneer er afstotingsverschijnselen van de getransplanteerde darm optraden. Tegen onze verwachting in werden er geen Panethcellen gedetecteerd die geprogrammeerde celdood (apoptose) ondergingen kort na reperfusie van het transplantaat. Desondanks stelden we wel een vermindering vast van het aantal Panethcellen en

hoeveelheid lysozym in de eerste week na transplantatie. Follow-up biopten lieten een geleidelijk herstel zien van het aantal Panethcellen gedurende de eerste maanden na transplantatie, terwijl de hoeveelheid lysozym verlaagd bleef gedurende de follow-up periode. We speculeren dat de daarmee gepaard gaande verminderde lokale afweer kan bijdragen aan de kwetsbaarheid van het darmtransplantaat voor afstoting en infectie. Samenvattend toonde deze studie een tijdelijke daling aan van het aantal Panethcellen in de vroege periode na transplantatie, die hoogstwaarschijnlijk niet direct gerelateerd was aan IR-schade, en een permanente vermindering van de hoeveelheid lysozym na transplantatie. Het mogelijke verband tussen de mate waarin Panethcellen zijn aangetast en de uitkomst van transplantatie op de langere termijn moet nog worden onderzocht in een groter patiëntencohort.

Darm IR-schade is een complex probleem waarvan de pathofysiologie nog niet volledig opgehelderd is. Om een veelbelovend doelwit voor therapie te identificeren, is het noodzakelijk om onze kennis van de moleculaire mechanismen die ten grondslag liggen aan ischemie en reperfusie van de humane darm te verbeteren. In dit proefschrift werd een humaan *in vivo* experimenteel model gebruikt om de opeenvolgende stadia van ischemie- en reperfusieschade en daaropvolgend herstel in de menselijke darm te bestuderen.

Hoofdstuk 3 beschrijft eiwitveranderingen die optreden in de darm bij blootstelling aan IR, gebruik makend van dit model. Verschillende complementaire benaderingen werden toegepast om (1) de aanwezige eiwitten in het weefsel te identificeren en kwantificeren (proteoom), (2) de status van fosforylering van deze eiwitten te bestuderen (fosfoproteoom) en (3) de verdeling van eiwitten in het weefsel te visualiseren. Voor de analyse van het proteoom en fosfoproteoom werd gebruik gemaakt van vloeistofchromatografie-massaspectrometrie. Deze analyse leverde kwantitatieve informatie op van duizenden eiwitten en gefosforyleerde eiwitten in de verschillende stadia van ischemie en reperfusie. Daarnaast werd beeldvormende massaspectrometrie gebruikt om de ruimtelijke verdeling van eiwitten in het weefsel te visualiseren en veranderingen daarin te bestuderen.

Om inzicht te krijgen in de biologische betekenis van deze eiwitveranderingen, hebben we functionele verrijkingsanalyses uitgevoerd van de eiwitten die kwantitatieve veranderingen tijdens IR lieten zien. Deze analyse geeft informatie over welke functies van genen/eiwitten meer vertegenwoordigd zijn in bepaalde datasets. De eiwitten die afnamen in hoeveelheid na reperfusie waren veelal structuureiwitten van de microvilli, enzymen in de borstelrand en transporters voor de opname van voedingsstoffen. De afname van deze eiwitten weerspiegelt waarschijnlijk het verlies van villus tips, wat een bekend kenmerk is van darmschade als gevolg van IR. Verder duidde de proteoomanalyse op activatie van een immuunrespons na reperfusie; met name het complementsysteem bleek sterk opgereguleerd te zijn. Het complementsysteem is een belangrijk onderdeel van de aangeboren afweer. Naast een kwantitatieve toename van complementfactoren toonde de beeldvormende massaspectrometrie-analyse veranderingen in complementfactor distributie in het weefsel gedurende IR.

De fosforylering en defosforylering van eiwitten reguleert veel cellulaire functies. Veranderingen in eiwitfosforylering tijdens IR wezen op een sterkte regulatie van mRNA splitsing en de organisatie

van het cytoskelet en celverbindingen. Verdere analyse van eiwitfosforylering voorspelde activiteit van de enzymfamilies mitogeen-geactiveerde proteïnekinase (MAPK, o.a. het reguleren van de stressrespons) en cycline-afhankelijke kinase (CDK, essentieel in celcyclusregulatie) tijdens IR. Samenvattend heeft deze studie ons begrip van de moleculaire veranderingen die in de humane darm optreden als gevolg van IR uitgebreid.

Het experimentele humane *in vivo* IR-model is bijzonder nuttig gebleken voor het bestuderen van de pathofysiologie van darm-IR in de mens, maar het is niet zo geschikt voor grondige mechanistische studies en het testen van potentiële therapeutische doelwitten. Voor dit doeleinde is het noodzakelijk om een *in vitro* IR-model te ontwikkelen dat de processen in de darm beter nabootst dan traditionele *in vitro* modellen, zodat de bevindingen beter vertaalbaar zijn naar de mens. Recente inzichten hebben geleid tot het ontwikkelen van zogenaamde organoïden: driedimensionale zelf-organiserende structuren die gekweekt worden vanuit weefsel van de patiënt. Deze gekweekte mini-orgaantjes behouden belangrijke structurele en functionele eigenschappen van het weefsel van oorsprong, waardoor ze de darmfysiologie beter nabootsen dan traditionele tweedimensionale celkweeksystemen met cellijnen die vaak afstammen van tumorcellen. Darmorganoïden worden dan ook steeds vaker ingezet voor het bestuderen van biologische processen en voor het modelleren van darmaandoeningen.

In **hoofdstuk 4** beschrijven we het gebruik van humane dunne darm-organoïden om IR-schade *in vitro* te modelleren door middel van blootstelling aan hypoxie en reoxygenatie (HR). Massaspectrometrische proteoomanalyse werd toegepast om de organoïden te karakteriseren, als ook de eiwitveranderingen die optreden tijdens HR. Door gebruik te maken van kweekmedia met een verschillende samenstelling waren we in staat om twee verschillende fenotypen van darmorganoïden te genereren: het crypte-achtig fenotype dat met name prolifererende cellen en Panethcellen bevat en het villus-achtige fenotype dat met name absorptieve enterocyten en slijmbekercellen bevat. Dit maakte het mogelijk om de HR-respons van de crypte en de villus afzonderlijk van elkaar te onderzoeken. Statistische kwantitatieve analyse van het proteoom resulteerde in een set van differentieel tot expressie komende eiwitten op verschillende tijdstippen tijdens HR in vergelijking met de controleconditie (organoïden die niet werden blootgesteld aan HR). Functionele verrijkingsanalyse van deze eiwitten toonde een oververtegenwoordiging van verschillende metabole processen, waaronder processen gerelateerd aan energiemetabolisme in de mitochondriën, vet- en eiwitmetabolisme. Het meest opvallende verschil in respons op HR tussen de crypte-achtige en villus-achtige organoïden was dat de cellulaire stressreactie en processen gerelateerd aan celdood meer uitgesproken waren in villus-achtige organoïden, terwijl een verrijking van beschermende mechanismen – zoals mitofagie en bescherming tegen oxidatieve stress – enkel in crypte-achtige organoïden werd gezien. We concludeerden dat de respons van humane darmorganoïden op HR typische eigenschappen van de *in vivo* respons op IR nabootst. Verder bieden onze bevindingen een kader voor vervolgonderzoek naar de onderliggende mechanismen van IR-schade in de crypte en/of villus en kan het model gebruikt worden om potentiële therapieën te testen ter voorkoming van IR-schade.

In **hoofdstuk 5** hebben we het transcriptionele landschap van de humane darmrespons op IR in kaart gebracht. Transcriptoomanalyse meet alle genen die op dat moment tot expressie komen, oftewel al het aanwezige mRNA en hun relatieve hoeveelheid. Met behulp van het humane *in vivo* experimentele model hebben we transcriptoom-profilering van de verschillende stadia van ischemie en reperfusie uitgevoerd. We beschrijven in dit hoofdstuk verschillende functionele verrijkings- en netwerkanalyses van de transcriptionele veranderingen. Uit deze analyses kwam de 'respons op ongevouwen eiwit' naar voren als één van de sterkst gereguleerde processen na reperfusie van de ischemische darm. De ongevouwen eiwitrespons wordt geactiveerd wanneer een ophoping van ongevouwen eiwit in het endoplasmatisch reticulum (ER) leidt tot ER-stress. De ongevouwen eiwitrespons is een mechanisme dat er in eerste instantie op gericht is celoverleving te bevorderen. Echter bij overactivering of langdurige ER-stress worden celdood-mechanismen geactiveerd. Gezien de cruciale rol van de ongevouwen eiwitrespons in het bepalen van het lot van de cel tijdens stress, onderzochten we of farmacologische remming van deze respons de cel kan beschermen tegen IR-schade. Hiervoor maakten we gebruik van het HR-model in humane darmorganoïden. We lieten zien dat een selectieve remming van een deel van de ongevouwen eiwitrespons resulteerde in een sterk verminderde pro-apoptotische signalering na HR in darmorganoïden, terwijl pro-overleving signalering grotendeels behouden bleef. Deze resultaten suggereren dat de ongevouwen eiwitrespons een veelbelovend therapeutisch doelwit zou kunnen zijn om IR-schade te reduceren.

In **hoofdstuk 6** bestudeerden we mitochondriële schade en tekenen van mitofagie in reactie op hypoxie en reoxygenatie in crypte-achtige en villus-achtige humane darmorganoïden. Mitochondriën fungeren als de energieproducenten van de cel – een proces dat veel zuurstof verbruikt – en zijn daarom erg gevoelig voor IR- en HR-schade. Als mitochondriën beschadigd raken komen er moleculen vrij die toxisch zijn voor de cel en die daarmee de schade kunnen verergeren. Het is daarom essentieel dat beschadigde mitochondriën worden opgeruimd. Het proces van de selectieve opruiming van mitochondriën via autofagie wordt mitofagie genoemd. Proteoomanalyse in hoofdstuk 4 duidde op regulatie van de mitofagie-route in crypte-achtige organoïden tijdens HR, terwijl er geen aanwijzingen waren voor mitofagie-regulatie in villus-achtige organoïden. Dit verschil tussen de fenotypes werd ondersteund door onze bevindingen in hoofdstuk 6. We toonden aan dat HR de mitochondriën beschadigde zowel in crypt-achtige als villus-achtige organoïden. De functionaliteit van de mitochondriën bleek echter sterker achteruit te gaan tijdens reoxygenatie in de villus-achtige organoïden. De veranderingen in expressie van autofagie- en mitofagiemarkers waren meer uitgesproken in crypte-achtige organoïden en zouden kunnen wijzen op activering van mitofagie met mogelijk een bescherming tot gevolg. Er zullen aanvullende analyses moeten worden uitgevoerd om het optreden van mitofagie te bevestigen. Toekomstige studies zouden zich moeten richten op het beschermende effect van mitofagie na IR van de darm en de mogelijkheden voor mitofagie modulatie als therapeutische strategie.

Ten slotte werden in **hoofdstuk 7** de belangrijkste bevindingen van dit proefschrift bediscussieerd, evenals de implicaties voor toekomstig onderzoek. Samenvattend hebben onze uitgebreide analyses van veranderingen in het transcriptoom en het (fosfo)proteoom in het experimentele *in vivo*

model ons begrip van de darmrespons op IR in de mens verbeterd en aanwijzingen gegeven voor toekomstig onderzoek naar therapeutische doelwitten. Daarnaast hebben we aangetoond dat het humane darmorganoïden-model een zeer waardevol model is om IR-schade *in vitro* te bestuderen. Ook identificeerden we de ongevouwen eiwitrespons als een veelbelovend therapeutisch doelwit voor het reduceren van darm IR schade.

IMPACT PARAGRAPH

Relevance

Intestinal ischemia is a reduced blood flow to the intestine resulting in decreased oxygen and nutrient supply. The blood flow to the intestine can be severely obstructed for example by a blood clot, a process that is similar to what happens in the heart during a heart attack. Besides blockage by a blood clot, blood flow can be diminished in several conditions including mechanical obstruction due to twisting of the bowel or due to low blood pressure secondary to shock, trauma or major surgery. In addition, intestinal transplantation is a procedure that requires temporary interruption of the blood flow and is therefore also associated with ischemia. While the intestine can tolerate brief fluctuations in the blood flow, a severe reduction results in tissue injury.

Acute intestinal ischemia is a devastating condition that occurs in about 13 per 100,000 people every year in the Netherlands. This number is expected to increase due to ageing of the population. In 60 to 80% of cases the patient dies, accounting for 1400 to 1800 deaths a year in the Netherlands only. For comparison, a heart attack is much more common - 1450 per 100,000 people had a heart attack in the Netherlands in 2019 - but a relatively low percentage (2%) died from it, accounting for nearly 5000 deaths in 2019. The mortality of intestinal ischemia has barely declined in recent decades. Early diagnosis and prompt surgical intervention to restore the blood flow are essential for patient survival. However, restoring blood flow – called reperfusion – to the intestine, for instance by removing the blood clot, initially exacerbates tissue injury, which is known as reperfusion injury. Therefore, the development of therapeutic strategies aiming at reducing reperfusion injury is urgently needed to improve patient outcome. In most cases ischemic damage has already occurred at the time of diagnosis, so it cannot be prevented by therapeutic intervention. However, in some cases preventive therapy can be initiated before the start of ischemia, for instance in organ transplantation. Intestinal ischemia-reperfusion injury is a highly complex problem, and a better understanding of the underlying molecular mechanisms is crucial to identify potential targets for the prevention or treatment of ischemia-reperfusion injury in the human intestine. To subsequently study these mechanisms and test their therapeutic potential, there is an urgent need for an experimental human model that (1) allows modulation of specific mechanisms in a controlled setting, and (2) recapitulates human intestinal physiology and pathophysiological aspects of ischemia-reperfusion injury as closely as possible. The latter will improve the translation of mechanistic findings in experimental models to effective treatment of human disease.

Scientific impact

Novel insight in ischemia-reperfusion injury of the human intestine

The research described in this thesis significantly contributes to our understanding of the mechanisms underlying ischemia and reperfusion injury in the human intestine. The unique Maastricht experimental model in human intestine enabled investigation of the sequential stages of progressive ischemic injury, reperfusion injury and initiation of repair mechanisms. Comprehensive analysis of alterations in thousands of genes and proteins provided insight in regulated biological processes during human intestinal ischemia-reperfusion. These results give rise to further investigations into

potential therapeutic targets, aimed at suppressing damaging processes, promoting protective mechanisms or advancing regeneration and recovery of the injured tissue. Obtained insights may also be relevant to other intestinal pathologies that are associated with intestinal damage, inflammation and disruption of the intestinal barrier function, for instance Crohn's disease or ulcerative colitis. Hence, although the cause of these inflammatory bowel diseases differs from ischemia-reperfusion, similar therapeutic strategies may be valuable.

Our big datasets on human intestinal ischemia-reperfusion have been deposited in open-source databases and made publicly available after publication. This offers the opportunity for wider evaluation by the scientific community and allows other researchers to build their research on our results. In addition, our data on the intestinal response to ischemia-reperfusion can be used for comparison with, for instance, the response to infection or Crohn's disease. This may contribute to a better understanding of the distinctive features of these responses, and may lead to identification of specific candidate diagnostic markers that can distinguish between the conditions.

Intestinal organoids as a model to study ischemia-reperfusion

In this thesis we presented a model for ischemia-reperfusion in intestinal organoids from human origin. Organoids represent an important bridge between widely used traditional cell culture systems and animal/human models. On the one hand, they are easier to manipulate than human models. On the other hand, the organoid model offers improved translation to the human setting compared to traditional cell culture models, because they better mimic the original tissue in terms of cellular diversity, structure and function.

We showed that exposure of intestinal organoids to hypoxia and reoxygenation mimicked the response of the human intestine to ischemia-reperfusion. The model enables the study of the epithelial component of ischemia-reperfusion, and will be useful for future studies into mechanisms of injury and regeneration. Importantly, the model allows isolated investigation of the intestinal crypt, which harbors the stem cells and is crucial for regeneration of the epithelium, and the intestinal villus, which contains mature cells that are more susceptible to injury. However, it should be noted that the interaction of the epithelium with microbes in the intestinal lumen and with immune cells are important elements of the pathophysiology of ischemia-reperfusion injury in the intestine. To investigate this interaction of the epithelium with the environment, it could be useful to co-culture organoids with immune cells or luminal factors in future studies. Hence, our organoid model lays the foundation for more advanced and complex models.

One of the potential therapeutic targets that we studied in the organoid model, was the unfolded protein response, a regulatory pathway initially crucial for survival, yet eventually promoting cell death. Targeting this pathway is aimed at balancing the response in favor of survival. We demonstrated that fine-tuning of the unfolded protein response considerably reduced pro-death signaling in the organoid model, suggesting it would be a promising therapeutic strategy that needs to be further exploited.

The biobank of established human intestinal organoid lines can be used for future mechanistic studies. In this thesis we primarily focused on the injury-aspect of ischemia-reperfusion. In addition, as organoids have been demonstrated to recapitulate stem cell function and tissue renewal, the established human intestinal organoids provide an excellent model to study tissue regeneration

after hypoxia-reoxygenation. Besides the application to mimic and study ischemia-reperfusion injury, hypoxic exposure of organoids can be used as a general damage model.

Knowledge transfer

The results in this thesis were disseminated via conferences, publications and open-source databases. The obtained knowledge is relevant for scientists and physicians in various fields including surgery, organ transplantation, critical care and gastroenterology. Results were and will be presented at relevant national and international scientific conferences on digestive diseases, i.e. Dutch Digestive Disease Days and United European Gastroenterology (UEG) congress, conferences on organ transplantation, i.e. Congress of the Intestinal Rehabilitation & Transplant Association (CIRTA) and International Meeting on Ischemia Reperfusion injury in Transplantation (IMIRT), and the world congress of Tissue Engineering and Regenerative Medicine International Society (TERMIS). Furthermore, our work has been published in international peer-reviewed journals, i.e. *Cell Death & Disease, Cellular and Molecular Gastroenterology and Hepatology, Transplantation*, and *Journal of Proteome Research.* With publication in these journals a broad audience of basic scientists and clinicians are reached.

Societal impact

The research described in this thesis advanced our understanding of ischemia-reperfusion injury of human intestine and provided a useful model to test potential therapeutic targets, which are both critical steps towards novel treatment options of patients with intestinal ischemia. In the long term, the development of an effective treatment is expected to reduce the risk of developing life-threatening complications of intestinal ischemia, improve patient survival and reduce health care costs.

DANKWOORD | ACKNOWLEDGEMENTS

Het zit erop, mijn proefschrift is af! Het was een periode vol pieken en dalen en zonder de hulp, steun en gezelligheid van velen was dit eindresultaat niet mogelijk geweest. Bedankt allemaal! Een aantal mensen wil ik graag persoonlijk bedanken.

Mijn promotieteam | **Kaatje** en **Steven**, bedankt voor de mogelijkheid om mijn promotieonderzoek bij de chirurgie onder jullie supervisie te mogen doen. Jullie hebben me altijd het vertrouwen gegeven om in vrijheid mijn onderzoeksprojecten op te zetten en uit te voeren. **Kaatje**, ik heb erg veel van je geleerd de afgelopen jaren en ik ben je ontzettend dankbaar voor je begeleiding en inhoudelijke ondersteuning. Jouw bijdrage en constructieve feedback zijn absoluut onmisbaar geweest voor het bereiken van dit eindresultaat. Veel dank ook voor jouw positieve kijk als ik te pessimistisch was, voor je motiverende woorden als het even tegenzat, voor je rust als het in mijn hoofd een chaos was. Ik mocht altijd bij je aankloppen: of het nu was voor je advies, om een mooi resultaat met je te delen, om even gezellig te kletsen of om mijn hart te luchten. Dat waardeer ik enorm. Dankjewel voor alles! **Steven**, ik heb bewondering voor hoe jij altijd vol enthousiasme je onderzoek, je werk in de kliniek en het opzetten van nieuwe bedrijven combineert. Ook al was 'de darm' niet jouw primaire onderzoekslijn, je maakte altijd tijd om mijn stukken door te nemen (op soms onmenselijke tijden) en om mee te denken over de opzet van een artikel of de langetermijnplanning. Dankjewel daarvoor. Daarnaast had je ook oog voor mijn ontwikkeling als persoon en dacht je mee over mijn vervolgcarrière. Dat heb ik erg gewaardeerd. Bedankt voor je hulp en je advies. Dank ook voor je gastvrijheid en de gezelligheid tijdens de jaarlijkse barbecues bij jou thuis.

Prof. Dejong, beste **Kees**, u was de bedenker van het experimentele model voor ischemie-reperfusie in de mens. Vele mooie studies volgden en ook ik heb in dit proefschrift van het model gebruik mogen maken. Bedankt voor uw wijze raad en uw klinische blik.

Mijn paranimfen | **Rianne**, vanaf dag één was jij mijn maatje. Vier jaar lang zaten we tegenover elkaar op kantoor en maakten we elkaars frustraties, successen en overwinningen van heel dichtbij mee. Ik ben blij dat jij op deze belangrijke dag als paranimf aan mijn zijde wil staan. Het was erg fijn dat wij alles met elkaar konden delen, zowel werk als privé. Dankjewel voor je gezelligheid, je luisterend oor en de mentale support. **Annet**, ik was erg blij toen jij het darm IR team kwam versterken. Je bent enthousiast, behulpzaam en reuzegezellig. Bedankt voor de fijne samenwerking, je vriendschap en al je hulp: niet alleen op het lab, maar ook als ik weer eens ruzie had met mijn computer. En niet te vergeten, dank voor de lekkere theetjes, koekjes en vooral de vele chocolade wanneer dat nodig was (en ook wanneer niet).

Beoordelingscommissie | **Prof. dr. Jonkers**, beste Daisy, tijdens mijn masterstage onder jouw begeleiding deed ik mijn eerste ervaring op met labonderzoek. Dit was een erg leuke periode, waarin ik veel heb geleerd, dank daarvoor. Wat speciaal dat je nu de voorzitter bent van de beoordelingscommissie. Ik wil Prof. dr. Jonkers, **Prof. dr. Cramer**, **Prof. dr. Libert**, **Prof. dr. Mariman**

en **Prof. Dr. Peters** allen hartelijk danken voor het beoordelen van mijn proefschrift en voor de bereidheid om zitting te nemen in de promotiecommissie.

The office | **Merel** en **Sara**, in mijn laatste jaar kwamen jullie **Annet** en mij vergezellen op kantoor en wat was het daar fijn en gezellig! Er werd hard gewerkt en daar beloonden we onszelf voor: kleine overwinningen, significante resultaten en publicaties werden gevierd met lekker eten en wijn. Ons kantoor was ook de plek voor de plank challenge, wallsits en yoga at your desk. Merel, jij weet goed wat je wil en blijft dicht bij jezelf. Saar, ik waardeer jouw positieve en rustgevende energie. Meiden, veel dank voor jullie steun, adviezen en gezellige momenten, die me altijd weer energie gaven en die de weg naar de eindstreep een stuk leuker hebben gemaakt. Gelukkig kan ik ook nu nog altijd even binnenwandelen in mijn oude kantoor. Op naar nog vele gezellige etentjes, wijntjes, koffies en (als Saar niet kan) spelletjesavonden.

Analisten | **Bas, Mo, Annemarie, Hans, Chantal** en **Cathy**, veel dank voor jullie hulp in het lab en voor alles wat ik van jullie geleerd heb. **Bas**, omdat het niet echt je meest favoriete bezigheid was, extra dank voor al die coupes die je gesneden hebt. Jij was de enige die die darmweefsels fatsoenlijk (en vliegensvlug) kon snijden. Fijn ook dat ik altijd binnen kon lopen met vragen of voor een gezellig praatje. Bedankt dat je ook altijd aanvoelde wanneer het even niet zo goed ging. **Mo**, bedankt voor al die perfecte RNA isolaties en qPCRs (en sorry voor de soms ingewikkelde plaatopzet). Samen werkten we aan het lanthanide project, dat helaas vastliep (en nu weer tot leven lijkt te komen: wie had dat gedacht?). Ik wil je bedanken voor de prettige samenwerking, voor je tips en adviezen en je mooie verhalen. Je bulderende lach zal me bijblijven. **Annemarie**, dank voor je hulp, je interesse en de gezellige momenten bij de koffieautomaat en in het lab. **Hans**, je was altijd bereid om mee te denken en jouw massaspectrometriekennis te delen, bedankt voor je kritische blik. **Chantal**, officieel werkte je niet voor het lab, maar als je wat tijd over had hielp je altijd graag of bedacht je zelf projectjes. Je vertrek was een gemis voor het lab. Naast dat het erg fijn was om met je samen te werken, was het ook altijd reuzegezellig op het werk maar ook daarbuiten. Leuk dat we elkaar ondanks de afstand nog steeds blijven zien. **Cathy**, jij kon met iedereen goed overweg zowel in het lab als in het ziekenhuis. Naast het verzamelen van de vele weefsels, haren en nagels op de OK, hielp je ook met analyses in het lab. Dankjewel voor je hulp en de leuke tijd.

Collega's chirurgie | **Livia**, de plank-challenge winnares, veel dank voor al je administratieve hulp en de gezelligheid. **Sander** en **Frank**, bedankt voor jullie feedback en kritische vragen tijdens de labchats. **Anjali**, thank you so much for all the effort and help with including patients in Aachen for my organoid studies. **Zita**, veel dank voor de prettige samenwerking en de analyses die je gedaan hebt, ook nadat je niet meer bij ons werkzaam was. **Tessa**, we brachten veel tijd samen door op het celkweek lab en wat hebben we veel lol gehad. Je typische Tessa-uitspraken, organoïde grappen ('the threeling') en kattenpraat, het was leuk! **Loes**, bedankt voor alle gezellige koffiepauzes en lunches. Leuk dat je af en toe nog naar het zuiden afreist voor een reünie. **Jorne**, als je langskwam op kantoor ging dat altijd gepaard met een grap of een goed verhaal. Bedankt voor je humor en alle gezelligheid. **Rob** (awkard-silence krekelgeluid) bedankt voor de leuke tijd en voor al die keren dat ik achterop

je fiets mocht. **David**, dank voor je adviezen en bedankt dat je me vaak kon overhalen om mee te gaan naar Thembi. Ik wil graag alle collega's bedanken voor de gezellige vlaai-momenten, borrels, lab-uitjes, sinterklaasvieringen, kerstdiners, pizza's en ambtenarencarnavals: **Ilse, Romy, Cathelijne, Lin, Xinwei, Jacqueline, Marjolein, Ralph, Caitlin, Kim, Evie, Anne, Aurelia, Min, Renee, Sebastiaan, Kees, Jos, Tom, Janine, Gloria, Hong, Kiran, Kim, Frans, Claire** en **Junfang**.

Stagiaires | **Anja**, bedankt voor je toewijding, je interesse, je ideeën en niet te vergeten al die blotjes die je gedaan hebt. Jouw bijdrage is essentieel geweest voor mijn laatste hoofdstuk. **Naima**, bedankt voor je hulp, het gezelschap en de lol die we hadden tijdens die ellenlange hypoxie-experimenten tot laat in de avond (wie bedenkt dat?). Ook de zorg voor 'onze baby's' nam jij graag op je en ik wist dat ze bij jou in goede handen waren. Veel dank voor je enthousiasme, betrokkenheid en harde werk. **Ado**, **Blaz**, **Bryan**, **Kayleigh** en **Betzabel** ook jullie wil ik bedanken voor jullie bijdrage en inzet in het lab.

Tijdens mijn PhD heb ik voor verschillende projecten samengewerkt met onderzoeksgroepen binnen en buiten de UM, waarvan ik een aantal mensen in het bijzonder wil bedanken.

M4I | **Ron**, ik ben onder de indruk van jouw gedrevenheid en passie voor onderzoek. Met amper kennis van massaspectrometrie begon ik aan het begin van mijn PhD ook een MS imaging project bij M4I. Dankjewel voor deze mogelijkheid en voor alles wat ik sindsdien van je geleerd heb. Ik heb het enorm gewaardeerd dat je altijd de tijd nam om samen met mij naar de resultaten te kijken; deze meetings hebben me erg geholpen en gemotiveerd. Veel dank voor je begeleiding, interesse en ideeën. **Benjamin**, thanks a lot for your help and support in navigating through these large piles of MSI data. I would also like to thank you for the fruitful discussions. I really appreciated your constructive feedback on the manuscript (which has just been accepted for publication!). **Ronny**, dank voor de prettige samenwerking en de gezelligheid op de gang. **Berta**, thank you for the collaboration and your input. Colleagues at M4I, thanks for your help in the lab and with the instruments.

Nanoscopy | **Kevin**, **Hans**, **Carmen**, **Prof. Dr. Peters**, thank you for sharing your expertise on electron microscopy. Kevin, veel dank voor je hulp met live-cell imaging van de organoïden en je ondersteuning bij de data-analyses.

Utrecht University | A special thanks to **Juan Manuel** and **Dr. Maarten Altelaar** for the fruitful collaboration described in chapter 3. Juan Manuel, I really appreciate your efforts for this project and your contribution in the writing of the manuscript.

Leuven | **Prof. Dr. Pirenne**, **Laurens** en **Emilio**, bedankt voor de fijne samenwerking voor het SPIRIT project. De projectbesprekingen, jullie ideeën en constructieve feedback op het manuscript hebben enorm geholpen.

Intestinal organoid collega's UM | **Daisy, Montserrat, Pan,** and **Ilse**, although we were working with different intestinal organoid models, sharing our experiences with organoid culture has been very helpful for me, thank you.

MERLN | **Lorenzo** and **Stefan**, thank you for the great opportunity to start my post-doc project at MERLN under your supervision. **Daniel** and **Mirco**, thank you for the warm welcome in the SCREENED team, it has been a great time so far!

Vrienden | **Astrid,** 'vriendinnen sinds de peuterspeelzaal' vertellen we altijd trots. Op school, tijdens de studie en een promotietraject in dezelfde stad: jij was altijd dichtbij. Jij hebt de pieken en dalen tijdens mijn promotietijd, vooral de afgelopen twee jaar (lockdown buddies!), allemaal meegemaakt. Dankjewel voor het aanhoren van mijn frustraties en beklag, dank dat je me geleerd hebt soms iets meer aan mezelf te denken en dat je ook boos werd als ik dat niet deed. Ook veel dank natuurlijk voor de gezellig avondjes (en dat de wijn altijd koud stond), lange kooksessies, al die uren die we op jouw dakterras hebben doorgebracht en de welverdiende vakantie naar Zákynthos. Lieve Ad, wat ben ik blij met een vriendin als jij. **Meriam**, 'Hoi ik heet ook Meriam': het begin van een mooie vriendschap, die nog sterker werd in de maanden dat we met onze Chubby camper door Australië en Nieuw-Zeeland reisden. Inmiddels woon je helaas al heel wat jaren niet meer in de buurt, maar gelukkig blijven we mede dankzij de ellenlange telefoongesprekken wel op de hoogte van elkaars leven. Lieve Merie, dankjewel dat ik jou alles kan vertellen en dat ik altijd bij je terecht kan voor steun of advies. Ik ben ontzettend dankbaar voor onze vriendschap en hoop dat we nog veel mooie avonturen gaan beleven en nieuwe herinneringen blijven maken. **Suzanne,** lieve Suus, ook voor jou is Limburg nog steeds je thuis. Dat vind ik fijn. Ik waardeer je eerlijkheid, de manier waarop jij verhalen tot in detail vertelt en je lekkere kookkunsten. Dankjewel voor alle lol en gezelligheid, maar ook voor de goede gesprekken en je steun. **Tessa**, **Rosa, Gonneke,** Ad, Merie en Suus, lieve jaarclub, ik kijk met veel plezier terug op onze studententijd en vind het mooi om te zien wat voor sterke vrouwen jullie geworden zijn. Het is altijd weer een feest als we samen zijn. Ik hoop nog lang van onze vriendschap te mogen genieten.

Zsa Zsa, niet lang na onze eerste ontmoeting op station Roermond werden we huisgenoten op de Louis Loyens. Wat een gezellig huis hadden we en wat een mooie tijd was dat! Tijdens mijn promotietijd lag jouw kantoor op een steenworp afstand van de mijne. Zo maakten we elkaars promotie van dichtbij mee. We zijn zelfs nog samen naar een congres geweest. Lieve Zsas, bedankt voor je eerlijkheid, voor je vrienschap en dat je altijd voor me klaarstaat. **Lisa**, als stagiaire mocht ik tijdelijk intrekken in jullie IBS kantoor, erg gezellig. Gelukkig kon ik ook na mijn 'overloop' naar de Chirurgie nog regelmatig binnenwippen. Het wordt tijd dat we dat stapavondje eens kunnen laten doorgaan! **Karlijn** en **Liyanne**, ik weet nog goed dat we elkaar ontmoetten tijdens de eerste onderwijsgroep op de uni. Liyanne, wij zijn ook nog collega's geweest tijdens mijn eerste jaar bij de Chirurgie. Bedankt voor de leuke tijd. Karlijn, veel dank voor je steun en de fijne vriendschap door de jaren heen.

Jeff, jij was mijn steun voor een groot deel van mijn promotietijd en daar wil ik je graag voor bedanken.

Lotte, als kinderen liepen we bij elkaar de deur plat. Ik vind het ontzettend fijn dat het altijd weer zo vertrouwd is als we elkaar zien. Uiteindelijk zijn we allebei gaan promoveren en ben ik zelfs nog bij jou langs geweest op het Hubrecht om mee te kijken met de organoïdenkweek, zo leuk! Bedankt voor je interesse, de gesprekken over ons onderzoek en je hulp met InDesign. **Michelle**, ook al zien we elkaar niet zo vaak, het is altijd als vanouds gezellig. Bedankt voor je vriendschap.

Familie | Lieve **opa** en **oma**, bedankt voor uw interesse in mijn onderzoek en promotietraject. Ik vind het erg bijzonder dat u mijn promotie kan meemaken.

Lieve **Anke** en **Nelleke**, wat ben ik enorm blij met zussen zoals jullie. Jullie wonen helaas niet om de hoek, maar ik weet dat jullie altijd voor me klaar staan. Ik kan jullie alles vertellen, zonder oordeel, zó fijn. Ank, jij begrijpt hoe zwaar deze laatste loodjes zijn, dankjewel dat je zo meeleeft en meedenkt en voor je hulp in deze voor jou ook hectische periode. Nel, ik waardeer jouw nuchterheid en vermogen te relativeren. Zusjes, ik wil jullie bedanken voor jullie betrokkenheid, steun en alle fijne zussenweekenden die voor de nodige ontspanning zorgden.

Lieve **pap** en **mam**, zonder jullie was het me niet gelukt. Ik besef hoeveel geluk ik heb dat ik in zo'n fijn gezin ben opgegroeid en ik ben heel dankbaar voor de band die we met elkaar hebben. Jullie hebben mij alle kansen gegeven om te doen wat ik wilde en hebben mijn keuzes in het leven altijd gesteund. Ik waardeer jullie adviezen en vind het fijn dat ik altijd bij jullie terecht kan. Bedankt voor jullie liefde en onvoorwaardelijke steun. Dank voor wie jullie voor mij zijn als ouders.

AFFILIATIONS

A. Alićehajić	Department of Surgery, NUTRIM School of Nutrition and Translational Research in Metabolism, Maastricht University, Maastricht, the Netherlands
M. Altelaar	Biomolecular Mass Spectrometry and Proteomics, Bijvoet Center for Biomolecular Research and Utrecht Institute for Pharmaceutical Sciences, Utrecht University, Utrecht, Netherlands
B. Balluff	Maastricht Multimodal Molecular Imaging institute (M4i), Maastricht University, Maastricht, The Netherlands
E.A.L. Biessen	Department of Pathology, CARIM School for Cardiovascular Diseases, Maastricht University Medical Centre, Maastricht, the Netherlands, Institute for Molecular Cardiovascular Research, RWTH Aachen University Hospital, Aachen, Germany
B. Boonen	Department of Surgery, NUTRIM School of Nutrition and Translational Research in Metabolism, Maastricht University, Maastricht, the Netherlands
R.M. Brown	Birmingham Children's Hospital and University Hospitals Birmingham, Birmingham, United Kingdom
W.A. Buurman	Department of Surgery, NUTRIM School of Nutrition and Translational Research in Metabolism, Maastricht University, Maastricht, the Netherlands
E. Canovai	Leuven Intestinal Failure and Transplantation (LIFT), Department of Abdominal Transplant Surgery, University Hospitals Leuven, Leuven, Belgium; Department of Microbiology and Immunology, KULeuven, Leuven, Belgium
L.J. Ceulemans	Leuven Intestinal Failure and Transplantation (LIFT), Department of Abdominal Transplant Surgery, University Hospitals Leuven, Leuven, Belgium; and Department of Microbiology and Immunology, KULeuven, Leuven, Belgium
B. Cillero-Pastor	Maastricht Multimodal Molecular Imaging institute (M4i), Maastricht University, Maastricht, The Netherlands
O. Corcos	Beaujon Hospitals, Paris, France
C.H.C. Dejong	Department of Surgery, NUTRIM School of Nutrition and Translational Research in Metabolism, Maastricht University Medical Centre, Maastricht, The Netherlands; Department of General, Visceral- and Transplantation Surgery, RWTH Aachen University Hospital, Aachen, Germany
J.P.M. Derikx	Department of Surgery, NUTRIM School of Nutrition and Translational Research in Metabolism, Maastricht University, Maastricht, the Netherlands; Department of Pediatric Surgery, Emma Children's Hospital, Amsterdam UMC, University of Amsterdam and Vrije Universiteit Amsterdam, Amsterdam, the Netherlands
A.M.A. Duivenvoorden	Department of Surgery, NUTRIM School of Nutrition and Translational Research in Metabolism, Maastricht University, Maastricht, the Netherlands
J. Grootjans	Department of Surgery, NUTRIM School of Nutrition and Translational Research in Metabolism, Maastricht University, Maastricht, the Netherlands
G. Gupte	Birmingham Children's Hospital and University Hospitals Birmingham, Birmingham, United Kingdom
M. Hadfoune	Department of Surgery, NUTRIM School of Nutrition and Translational Research in Metabolism, Maastricht University, Maastricht, the Netherlands

H. Hartog	Birmingham Children's Hospital and University Hospitals Birmingham, Birmingham, United Kingdom; Department of Surgery, Division of Hepato-Pancreato-Biliary and Transplant Surgery, Erasmus Medical Centre, Rotterdam, The Netherlands
R.M.A. Heeren	Maastricht Multimodal Molecular Imaging institute (M4i), Maastricht University, Maastricht, The Netherlands
G. de Hertogh	Leuven Intestinal Failure and Transplantation (LIFT), Department of Abdominal Transplant Surgery, University Hospitals Leuven, Leuven, Belgium and Department of Microbiology and Immunology, KULeuven, Leuven, Belgium
I.H.R. Hundscheid	Department of Surgery, NUTRIM School of Nutrition and Translational Research in Metabolism, Maastricht University Medical Centre, Maastricht, The Netherlands
F. Joly	Beaujon Hospitals, Paris, France
A.M. Kip	Department of Surgery, NUTRIM School of Nutrition and Translational Research in Metabolism, Maastricht University, Maastricht, The Netherlands
K. Lenaerts	Department of Surgery, NUTRIM School of Nutrition and Translational Research in Metabolism, Maastricht University Medical Centre, Maastricht, The Netherlands
M. Manca	Department of Pathology, CARIM School for Cardiovascular Diseases, Maastricht University Medical Centre, Maastricht, the Netherlands
D. Mirza	Birmingham Children's Hospital and University Hospitals Birmingham, Birmingham, United Kingdom
R. Mohren	Maastricht Multimodal Molecular Imaging institute (M4i), Maastricht University, Maastricht, The Netherlands
U.P. Neuman	Department of Surgery, NUTRIM School of Nutrition and Translational Research in Metabolism, Maastricht University, Maastricht, the Netherlands; Department of General, Visceral and Transplantation Surgery, RWTH Aachen University Hospital, Aachen, Germany
S.M.W. Olde Damink	Department of Surgery, NUTRIM School of Nutrition and Translational Research in Metabolism, Maastricht University Medical Centre, Maastricht, The Netherlands; Department of General, Visceral- and Transplantation Surgery, RWTH Aachen University Hospital, Aachen, Germany
J. Pirenne	Leuven Intestinal Failure and Transplantation (LIFT), Department of Abdominal Transplant Surgery, University Hospitals Leuven, Leuven, Belgium and Department of Microbiology and Immunology, KULeuven, Leuven, Belgium
A.J.A. Röth	Department of Surgery, NUTRIM School of Nutrition and Translational Research in Metabolism, Maastricht University, Maastricht, the Netherlands; Department of General, Visceral and Transplantation Surgery, RWTH Aachen University Hospital, Aachen, Germany
Z. Soons	Department of Surgery, NUTRIM School of Nutrition and Translational Research in Metabolism, Maastricht University, Maastricht, the Netherlands
J.M. Valverde	Biomolecular Mass Spectrometry and Proteomics, Bijvoet Center for Biomolecular Research and Utrecht Institute for Pharmaceutical Sciences, Utrecht University, Utrecht, Netherlands

LIST OF PUBLICATIONS

Kip AM, Valverde JM, Altelaar M, Heeren RMA, Hundscheid IHR, Dejong CHC, Olde Damink SWM, Balluff B, Lenaerts K. Combined quantitative (phospho)proteomics and mass spectrometry imaging reveal temporal and spatial protein changes in human intestinal ischemia-reperfusion. *J Proteome Res.* (2021) In press

Kip AM, Grootjans J, Manca M, Hadfoune M, Boonen B, Derikx JPM, Biessen EAL, Olde Damink SWM, Dejong CHC, Buurman WA, Lenaerts K. Temporal transcript profiling identifies a role for unfolded protein stress in human gut ischemia-reperfusion injury. *Cell Mol Gastroenterol Hepatol. (*2021) In press

Kip AM, Soons Z, Mohren R, Duivenvoorden AAM, Röth AAJ, Cillero-Pastor B, Neumann UP, Dejong CHC, Heeren RMA, Olde Damink SWM, Lenaerts K. Proteomics analysis of human intestinal organoids during hypoxia and reoxygenation as a model to study ischemia-reperfusion injury. *Cell Death Dis. 12, 95 (*2021)

Kip AM, Ceulemans LJ, Hundscheid IHR, Canovai E, Hartog H, Brown RM, Corcos O, Joly F, de Hertogh G, Gupte G, Dejong CHC, Olde Damink SWM, Pirenne J, Mirza D, Lenaerts K. Paneth Cell Alterations During Ischemia-reperfusion, Follow-up, and Graft Rejection After Intestinal Transplantation. *Transplantation.* 104, 1952-1958 *(*2020)

van der Beek CM, Canfora EE, **Kip AM**, Gorissen SHM, Olde Damink SWM, van Eijk HM, Holst JJ, Blaak EE, Dejong CHC, Lenaerts K. The prebiotic inulin improves substrate metabolism and promotes short-chain fatty acid production in overweight to obese men. *Metabolism.* 87, 25-35 *(*2018)

CURRICULUM VITAE

Mirjam Kip was born on December 20th 1989 in Limbricht, the Netherlands. After graduating cum laude from secondary school at Trevianum school group in 2008, she started medical school at Maastricht University and obtained her bachelor's degree in 2011. During her master she did an internship at Landspitali University Hospital in Reykjavik, Iceland. Following one year in the medicine master program she continued her education in biomedical research. She started the Biomedical Sciences master at Maastricht University in 2013. As part of this master program, Mirjam did her first research internship in the department of Surgery under supervision of dr. K. Lenaerts. Next, she completed her senior research internship in the division of gastroenterology-hepatology under supervision of prof. dr. D. Jonkers. During this 9-month period she studied barrier disruption in inflammatory bowel disease using a three-dimensional intestinal cell culture model. Mirjam obtained her master's degree cum laude in 2015. After working as a researcher in the department of Surgery at Maastricht University for one year, she started working as a PhD candidate in this department. The research was performed within NUTRIM School of Nutrition and Translational Research in Metabolism under the supervision of prof. dr. S. Olde Damink, and dr. K. Lenaerts. Mirjam was awarded with the NUTRIM graduate program grant, which funded her PhD trajectory. The results obtained during her PhD research are described in this thesis. In July 2021, Mirjam continued her career as a postdoctoral researcher in the department of Complex Tissue Regeneration at MERLN Institute for Technology-Inspired Regenerative Medicine, Maastricht University, under the supervision of prof. dr. L. Moroni and dr. S. Giselbrecht. Her research focuses on the use of novel *in vitro* models of the thyroid gland for the screening of endocrine disrupting compounds.